Copyright

by

Chirayus Viyanant

2006

The Dissertation Committee for Chirayus Viyanant
certifies that this is the approved version of the following dissertation:

Potential Use of Recycled Asphalt Pavement and Crushed Concrete as Backfill for Mechanically Stabilized Earth Walls

Committee:

_____
Ellen M. Rathje, Supervisor

_____
Stephen G. Wright

_____
Kevin J. Folliard

_____
Jon E. Olson

_____
David Trejo

Potential Use of Recycled Asphalt Pavement and Crushed Concrete as Backfill for Mechanically Stabilized Earth Walls

by

Chirayus Viyanant, B.Eng.; M.S.

Dissertation

Presented to the Faculty of the Graduate School of

The University of Texas at Austin

in Partial Fulfillment

of the Requirements

for the Degree of

Doctor of Philosophy

The University of Texas at Austin

August, 2006

Dedicated to my parents and grandparents

for their unconditional love, support, and encouragement

Acknowledgements

The completion of this research would not have been possible without the encouragement and support from many individuals who have been part of my life throughout my doctoral work in Austin. First and foremost, I would like to express my most sincere appreciation and gratitude to my advisor Professor Ellen M. Rathje for her continued guidance, encouragement, and support. There were times during the course of this research when I felt that things in life were overwhelming. She was always there for me and gave me the inspiration I needed to go on. I am, and always will be, grateful for the opportunity and time I have had working with her.

I would also like to extend my thanks to my Advisory Committee, Professor Stephen G. Wright, Kevin J. Folliard, Jon E. Olson, David Trejo, and Alan F. Rauch, for their invaluable suggestions and comments that became many of the integral parts in this study. I also thank my fellow graduate students at UT for their friendship and for lending me their help in many occasions. Without them my life in Austin would not have been this much enjoyable. Special thanks are given to The Texas Department of Transportation for providing financial support for this work.

My family will always be the inspirational strength of my life. In particular my beloved parents and my dazzling sister who are the three most influential people in my life. I am deeply indebted for their unconditional love and support, and for their patience during all my years spent in the U.S. And finally to Ms. Napat Nantavechsanti, I am thankful for having you in my life.

Chirayus Viyanant

The University of Texas at Austin
August 2006

Potential Use of Recycled Asphalt Pavement and Crushed Concrete as Backfill for Mechanically Stabilized Earth Walls

Publication No._____

Chirayus Viyanant, Ph.D.

The University of Texas at Austin, 2006

Supervisor: Ellen M. Rathje

Increasing demands for construction aggregates have raised concerns within the highway-related government agencies and the industrial community for the past twenty years. Although yearly production of recycled asphalt pavement (RAP) and crushed concrete (CC) has significantly increased over the past few decades, many state agencies and jurisdictions have limited experience using these materials as an MSE wall backfill. The use of more locally available RAP or CC not only minimizes the cost of transporting select materials from remote areas but also alleviates the cost of disposing these materials in a commercial landfill.

This dissertation presents results from comprehensive experimental studies that focus primarily on the intrinsic geotechnical properties of RAP and CC. The preliminary testing involves determining the general index properties of RAP and CC. Subsequent

testing includes laboratory and field investigations to evaluate compaction characteristics, shear strength properties, hydraulic conductivity, and collapse potential of the study materials. Test results obtained on RAP and CC specimens are analyzed and compared with the results obtained from the conventional fill material (CFM) to further evaluate comparatively their suitability as MSE wall backfill.

The last part of this study covers two detailed investigations on the most significant potential problems for RAP and CC backfill. Creep becomes a major concern for RAP because of its viscoelastic properties. The creep potential of RAP is investigated through a series of constant stress, drained triaxial creep tests. The experimental data were fit with an empirical-based model developed by Singh and Mitchell (1968) to describe the creep behavior of RAP with respect to confining pressure and stress level. Empirical expressions to predict creep rupture were investigated. The laboratory data were also used to identify the upper yield strength, below which creep rupture does not occur. For CC, the most significant concern is the potential for calcium carbonate ($CaCO_3$) precipitation. In this study, laboratory measurement of calcium ion concentration of CC-water mixtures were conducted on a wide range of CC grain sizes to determine the threshold particle size that may exacerbate the $CaCO_3$ formation of a CC backfill.

Table of Contents

List of Tables xii
List of Figures xiv
Chapter 1. Introduction 1
1.1 Problem statement and research significance 1
1.2 Objective and scope of research 4
1.3 Organization of dissertation 6
Chapter 2. Potential Use of RAP and CC as MSE Wall Backfill 9
2.1 Introduction 9
2.2 Description of RAP and CC 9
2.3 Current geotechnical uses of RAP 12
2.4 Current geotechnical uses of CC 17
2.5 Mechanically stabilized earth walls 24
2.5.1 MSE wall design 30
2.5.2 Critical backfill properties 35
2.6 MSE wall backfill specifications 40
2.6.1 Gradation 40
2.6.2 Compaction 41
2.6.3 Hydraulic conductivity 46
2.6.4 Settlement 47
2.6.5 Shear strength 48
2.6.6 Creep characteristics 49
2.6.7 Summary of backfill requirements 50
2.7 Summary 52
Chapter 3. Test Materials and Index Properties 53
3.1 Introduction 53
3.2 State-wide survey 54

3.3 Identifying sources of test materials 58
3.4 Index properties of the bulk samples 62
3.4.1 Grain size distribution 63
3.4.2 pH 68
3.4.3 Atterberg limits 68
3.4.4 Specific gravity 70
3.5 Summary 73
Chapter 4. Compaction Characteristics 75
4.1 Introduction 75
4.2 Laboratory compaction 76
4.3 Field compaction control 83
4.3.1 Field density measurement methods 84
4.3.2 Field testing program 90
4.3.3 Test results and discussions 96
4.4.4 Conclusions from field compaction control tests 105
4.5 Summary 106
Chapter 5. Shear Strength, Hydraulic Conductivity, and
Collapse Potential of RAP and CC 107
5.1 Introduction 107
5.2 Test equipment 108
5.2.1 Triaxial system 108
5.2.2 Large-scale direct shear machine 111
5.3 Shear strength characteristics 116
5.3.1 Consolidated-drained triaxial tests 116
5.3.2 Large-scale drained direct shear tests 132
5.3.3 Integration of shear strength results 143
5.4 Hydraulic conductivity measurements 150
5.4.1 Sample preparation and testing program 150
5.4.2 Test results and discussion 152

5.5 Collapse potential....156
5.5.1 Sample preparation and testing program....157
5.5.2 Test results and discussion....157
5.6 Summary....161
Chapter 6. Creep Potential of RAP....163
6.1 Introduction....163
6.2 Theoretical background....164
6.3 Experimental program....172
6.4 Test results and discussions....175
6.4.1 Creep tests at σ'3 = 20 psi....176
6.4.2 Creep tests at σ'3 = 40 psi....183
6.4.3 Effect of Stress History on Creep Behavior....190
6.4.4 RAP creep rupture....197
6.5 Conclusion....211
Chapter 7 Tufa Precipitation Potential of Crushed Concrete....213
7.1 Introduction....213
7.2 Background on tufa precipitation....213
7.2.1 Previous studies....213
7.2.2 Indicators used for predicting tufa potential....217
7.3 Experimental program....221
7.4 Test results and discussions....226
7.5 Conclusion....236
Chapter 8. Summary and Conclusions....237
8.1 Summary....237
8.1.1 Assessment of index properties and compaction characteristics....238
8.1.2 Assessment of shear strength, hydraulic conductivity, and collapse potential....238
8.1.3 Assessment of potential problematic properties....239
8.2 Conclusions....241

8.2.1 Index Properties and Compaction Characteristics 241
8.2.2 Shear Strength, Hydraulic Conductivity, and Collapse Potential 242
8.2.3 RAP Creep Behavior.....243
8.2.4 Tufa Precipitation of CC 245
8.3 Recommendations for future research 246
References.....248
Vita.....264

List of Tables

Table 2-1 TxDOT experience with RAP backfill [after TxDOT (1999)].....13
Table 2-2 Categorization of waste recycled materials as roadbase construction aggregate [after Saeed et al. (1996)].....15
Table 2-3 Physical properties of crushed concrete material [after ACPA (1993)].....19
Table 2-4 TxDOT's projects using CC as backfill material [after TxDOT (1999)].....22
Table 2-5 Backfill gradation limits by TxDOT (2004) and FHWA (2004) 42
Table 2-6 Compaction test methods using by TxDOT and FHWA.....43
Table 2-7 MSE wall backfill specifications from TxDOT and FHWA in 2004.....51
Table 3-1 Survey results from TxDOT districts [after Rathje et al. (2001)] 56
Table 3-2 Survey results from Texas commercial producers [after Rathje, et al. (2001)].....57
Table 3-3 Summary of test results from the initial characterization [Ogolla (2002)] 61
Table 3-4 Atterberg limits of RAP and CC 70
Table 3-5 Specific gravity of test materials.....73
Table 4-1 Recommended specimen water contents and dry unit weights.....80
Table 4-2 Ratio of moist densities measured by nuclear gauge ($\gamma_{m,NG}$) and rubber balloon method ($\gamma_{m,BAL}$) 98
Table 4-3 Ratio of moisture contents measured by nuclear gauge (w_{NG}) and oven drying (w_{oven})..... 104
Table 5-1 Theoretical B values for typical soils at and near full saturation [after Black and Lee (1973)] 122
Table 5-2 Drained shear strength parameters of the tested materials based on the triaxial test results 132
Table 5-3 Summary of hydraulic conductivity of the test materials.....154
Table 5-4 ASTM classification of collapse index.....160
Table 6-1 Activation energies of typical materials.....173

Table 6-2 Typical *a* and *b* values for materials subject to creep stress.....201
Table 7-1 Dry material-water mixing proportions of the test samples 223
Table 7-2 Sample calculation for the expected total calcium ions
release from CC backfill 231

List of Figures

Figure 2-1 Bulk sample of RAP....10
Figure 2-2 Bulk sample of CC....11
Figure 2-3 Influence of dry density on peak direct shear angle of friction [O'Mahony and Milligan (1991)]....20
Figure 2-4 Influence of vertical stress on peak direct shear angle of friction [O'Mahony and Milligan (1991)]....20
Figure 2-5 Schematic view of a reinforced earth wall [after Schlosser and Delage (1988)]....25
Figure 2-6 Stress transfer mechanism of soil particles when subjected to vertical loading [Lambe and Whitman (1979)]....26
Figure 2-7 Mohr circles of unreinforced and reinforced soil samples under triaxial test..27
Figure 2-8 Tensile stress in the reinforcement and maximum tensile force line....28
Figure 2-9 Stress transfer mechanisms mobilized on reinforcement [after Morris and Delphia (1999)]....30
Figure 2-10 External stability mechanisms of failure [Elias and Christopher 1996)]....31
Figure 2-11 Internal failure (a) tension failure (b) pullout failure....34
Figure 2-12 MSE wall failures due to poorly compacted backfill settlement....38
Figure 3-1 RAP gradations from the initial characterization....60
Figure 3-2 CC gradations from the initial characterization....60
Figure 3-3 Grain size distribution of the RAP stockpile....64
Figure 3-4 Grain size distribution of the CC stockpile....65
Figure 3-5 Grain size distribution of the CFM stockpile....66
Figure 3-6 Proposed reference gradation for future tests....67
Figure 3-7 Liquid limits of RAP and CC using multipoint method....69
Figure 4-1 Compaction curve for RAP based on the Tex-113-E test method....77
Figure 4-2 Compaction curve for CC based on the Tex-113-E test method....79

Figure 4-3 Compaction curve for CFM based on the Tex-113-E test method 80
Figure 4-4 Comparison of compaction curves between test materials 81
Figure 4-5 Grain size distribution of materials after compaction 82
Figure 4-6 Nuclear gauge testing for field compaction control 84
Figure 4-7 Nuclear gauge setup: (a) direct transmission method and
(b) backscatter method [from Troxler (2001)] 88
Figure 4-8 Test material stockpiles at Pickle Research Center, Austin, TX.....91
Figure 4-9 Light compaction of the test site using a front-end loader.....91
Figure 4-10 RAP stockpile and test locations.....92
Figure 4-11 CC stockpile and test locations 92
Figure 4-12 CFM stockpile and test locations 93
Figure 4-13 Nuclear gauge testing on material stockpile 94
Figure 4-14 Hole excavation for rubber balloon test and its location.....95
Figure 4-15 Rubber balloon test performed on material stockpile 96
Figure 4-16 Comparison of moist densities measured by rubber balloon
and nuclear gauge methods in all three material stockpiles.....97
Figure 4-17 Test pit performed over a previously rubber balloon-tested location 100
Figure 4-18 Comparison of moist densities measured by rubber balloon
and test pit methods 101
Figure 4-19 Comparison of moist densities measured by test pit and nuclear gauge.....102
Figure 4-20 Comparison of the moisture contents measured
with the nuclear gauge and oven drying 103
Figure 5-1 GCTS triaxial test system.....109
Figure 5-2 Triaxial cell and loading components 110
Figure 5-3 Large-scale (20 in x 20 in) direct shear machine during testing 113
Figure 5-4 Cross section of the large-scale direct shear machine.....114
Figure 5-5 Grain size distribution of reference gradation and triaxial test specimens 118
Figure 5-6 Details of the complete triaxial test specimen setup 120
Figure 5-7 Drained shear triaxial test results from four CFM specimens.....125

Figure 5-8 Drained shear triaxial test results from four CC specimens.....126
Figure 5-9 Drained shear triaxial test results from five RAP specimens.....127
Figure 5-10 Mohr failure envelopes based on the triaxial test results 131
Figure 5-11 Results from large-scale drained direct shear tests
on washed mortar sand.....135
Figure 5-12 Comparison of small-scale vs. large-scale direct shear tests
on washed mortar sand.....136
Figure 5-13 Large-scale, load-controlled direct shear tests on RAP specimens.....138
Figure 5-14 Results from large-scale direct shear tests on CFM.....140
Figure 5-15 Results from large-scale direct shear tests on CC.....141
Figure 5-16 Best-fit Coulomb envelopes for large-scale drained direct shear tests
on CFM and CC specimens 143
Figure 5-17 Diagram showing Mohr circles' closest coordinates
to the strength envelope 145
Figure 5-18 Combined direct shear and triaxial shear strength data for CFM 146
Figure 5-19 Combined direct shear and triaxial shear strength data for CC 147
Figure 5-20 Secant friction angles vs. log (σ'_3/P_a) [or (σ'_n/P_a)] 148
Figure 5-21 Schematic drawing of the test setup for hydraulic conductivity
measurement [after ASTM D 5084] 151
Figure 5-22 Hydraulic conductivity of test materials at different confining pressures ...155
Figure 5-23 Compression curves from collapse potential tests 158
Figure 5-24 Collapse indexes of test materials at different normal stresses.....160
Figure 6-1 Time-dependent creep deformation under a constant stress level 164
Figure 6-2 Strain rate vs. time relationships during undrained creep
of Osaka alluvial clay [after Murayama and Shibata (1958)].....168
Figure 6-3 Typical plot between strain rate and stress level at any given time
after stress application [after Febres-Cordero and Mesri (1974)] 169
Figure 6-4 Effect of *m* values on predicted creep strains [after Mitchell (1993)] 171
Figure 6-5 Stress paths applied to creep test specimens at σ'3 = 20 psi 174

Figure 6-6 Axial strain vs. time for RAP specimens tested at σ'3 = 20 psi 177
Figure 6-7 Axial strain rate vs. time for RAP specimens tested at σ'3 = 20 psi 178
Figure 6-8 Sample plots used to develop best-fit *m*-values for creep tests
σ'_3 = 20 psi (a) $\bar{D}$ = 0.40; (b) $\bar{D}$ = 0.62; (c) $\bar{D}$ = 0.70; (d) $\bar{D}$ = 0.80 180
Figure 6-9 Best-fit *m* values vs. stress levels for creep tests at σ'_3 = 20 psi 181
Figure 6-10 Axial strain rates vs. stress levels at select times for tests at σ'_3 = 20 psi 183
Figure 6-11 Axial strain vs. time for RAP specimens tested at σ'3 = 40 psi 184
Figure 6-12 Axial strain rate vs. time for RAP specimens tested at σ'3 = 40 psi 186
Figure 6-13 Sample best-fitting plots of appropriate *m* values for creep tests
at σ'_3 = 40 (a) $\bar{D}$ = 0.50; (b) $\bar{D}$ = 0.70; (c) $\bar{D}$ = 0.80; (d) $\bar{D}$ = 0.88 187
Figure 6-14 Best-fit *m* values vs. stress levels for creep tests at σ'_3 = 40 psi 188
Figure 6-15 Axial strain rates vs. stress levels at select times for tests at σ'3 = 40 psi....188
Figure 6-16 Effect of consolidation pressure and overconsolidation ratio on A
and $\bar{\alpha}$ for an undisturbed San Francisco Bay mud
[after Singh and Mitchell (1968)] 189
Figure 6-17 Combined plot from two set of tests at σ'_3 = 20 and 40 psi
after 5 minute of stress application 190
Figure 6-18 Axial creep strain vs. time performed at different σ'_3 192
Figure 6-19 Axial strain rate vs. time performed with same $\bar{D}$ = 0.8 at various σ'_3 193
Figure 6-20 Axial strain rates vs. stress levels after 5 minute of stress application 196
Figure 6-21 Effect of the confining pressure on m parameter 197
Figure 6-22 Typical comparison between predicted and measured creep strains 198
Figure 6-23 Plot of creep rupture life vs. minimum strain rate
[Saito and Uezawa (1961)] 199
Figure 6-24 Plots between time to creep rupture (tr) and minimum strain rate ($\dot{\varepsilon}_{min}$) 202
Figure 6-25 (a) log (t_r) vs. σ'_c-normalized creep stress level for Haney clay
[Campanella and Vaid (1974)], (b) log ($\dot{\varepsilon}_{min}$) vs. creep shear stress
for Ohya stone [Adachi and Takase (1981)].....204
Figure 6-26 Time to rupture vs. stress level 204

Figure 6-27 Minimum strain rate vs. stress level.....205
Figure 6-28 Upper yield stress for Haney clay tested with constant stress creep under isotropic triaxial test condition [Vaid and Campanella (1977)] 207
Figure 6-29 Creep stress normalized with σ'1c versus log (time to rupture).....208
Figure 6-30 Stress level versus log(time to rupture).....209
Figure 6-31 Determination of upper yield strength 210
Figure 7-1 Tufa totally blocking an 8-in diameter drain [Feldmann (1981)] 214
Figure 7-2 Tufa forming at the mouth of a 6-in diameter drain [Feldmann (1981)] 215
Figure 7-3 Picture of a CC-water mixture sample for the Ca2+ ion measurement 222
Figure 7-4 Calcium ion concentrations in the test samples vs. time.....227
Figure 7-5 Calcium ion concentration per weight of dry material vs. time.....228
Figure 7-6 Weight of dissolved calcium ions per weight of dry material vs. time.....229
Figure 7-7 Calcium ions per dry material vs. particle sizes.....232
Figure 7-8 Percent contribution of calcium ions from different CC particle sizes.....234
Figure 7-9 Calcium ion dissolution vs. time for washed and unwashed CC particles.....235

Chapter 1. Introduction

1.1 PROBLEM STATEMENT AND RESEARCH SIGNIFICANCE

Over the past twenty years, increasing demands for construction aggregates have raised concerns within highway-related government agencies and the industrial community, particularly for highly populated areas around the U.S. With an estimate of 2 billion tons of natural aggregates produced annually and a projected production of 2.5 billion tons per year by the year 2020 [FHWA (2004)], the growing need for alternative materials to replace natural aggregates is undeniably required for the construction community. Many states in the U.S. are using economic incentives for the use of recycled products, such as increasing landfill disposal fees for waste materials and enacting more stringent environmental regulations and land use policies [FHWA (2004)]. Therefore, using recycled materials for construction purposes in the future will serve not only as an economical solution for construction, but also as a positive impact on the natural environment.

The National Asphalt Paving Association reported in April 2000 that nearly 91 million tons of asphalt pavements are removed each year. Of that amount, 73 million tons were reused as part of new pavements or as backfill in embankments. Also, as of the year 2001, more than 45 states were already using recycled asphalt pavement (RAP) in construction applications [Eighmy and Magee (2001)]. A 1998 study by the Portland Cement Association estimated that 105 million tons of crushed concrete (CC) are used

each year. Although yearly production of RAP and CC has significantly increased over the past few decades, many state agencies and jurisdictions have limited experience using these materials as backfill material. It appears that RAP and CC are most frequently used as aggregate substitutes for roadway construction, while utilizing RAP and CC as backfill has received the least interest.

There are many types of earth retaining structures that require backfill material. Of all potential earth retaining structures, mechanically stabilized earth (MSE) walls have gained much popularity over the past twenty years. MSE walls have been constructed in every State in the U.S., with the majority in Texas, Georgia, Florida, Pennsylvania, New York, and California [Elias and Christopher (1996)]. The major advantages of MSE walls compared to other retaining structures are their flexibility, aesthetic appeal, ease of installation, and low cost [Morris and Delphia (1999)]. To ensure long-term integrity of the wall, conventional backfills consisting predominantly of granular soils have been recommended and used in the past. This material limitation can significantly increase the cost of construction on some projects due to the cost of hauling select backfill material to the construction site.

Texas, for example, is one of the largest MSE wall builders in the nation. However, many parts of Texas do not have backfill materials that meet the current material specifications required by the Texas Department of Transportation (TxDOT). In these cases, transporting select material from other parts of the state is inevitable, and this option has become more and more costly. The problem with select backfill availability could keep MSE walls from being an economically attractive option over conventional

retaining walls. One possible solution is to use RAP or CC, which are more locally available, as alternative backfills. The use of RAP or CC not only minimizes the cost of material transportation but also alleviates the cost of disposing these materials in a landfill. Hence, if RAP and CC were used as backfill for MSE walls, transportation and disposal costs for these materials could be greatly reduced, translating into significant savings.

The concept of using RAP and CC for new constructions began to gain more attention during the past twenty years when the fees for landfill disposal of construction debris were purposely increased by states' environmental agencies as an economic incentive to use recycled materials for construction [FHWA (2000)]. In many cases, RAP and CC are discarded by-products from pavement resurfacing or reconstruction and belong to state Departments of Transportation. These recycled materials often end up being disposed and stockpiled along highway rights of way. These temporary stockpiles may eventually raise public concerns because of their unsightly appearance and undesired dust blowing into nearby residential areas [Ahmad (1991)]. Thus, there is a real need to deal with these stockpiles of materials currently owned by states DOT.

Utilization of RAP and CC as backfill material for MSE walls has not been studied extensively in the past. This is most likely because RAP and CC have been used predominantly in pavement construction, and thus, the majority of the previous studies have put their emphasis on characterization of these materials for pavement applications. Due to the lack of any comprehensive studies regarding the use of RAP and CC as MSE wall backfill, this research study was initiated to extensively characterize the geotechnical

properties of RAP and CC. The experimental results obtained from this study will be used to assess whether RAP and CC can be confidently used as MSE wall backfill..

1.2 OBJECTIVE AND SCOPE OF RESEARCH

This dissertation is part of a joint research program sponsored by the TxDOT under project No. 4177, "*Use of Recycled Asphalt Pavement and Crushed Concrete as Backfill for Mechanically Stabilized Earth Retaining Walls"*. The work performed under the entire research program was divided among several research groups based on the expertise of each group. This dissertation presents results from extensive experimental studies that are part of the complete geotechnical investigation. The studies conducted for this research and presented in this dissertation are focused primarily on the intrinsic geotechnical properties of RAP and CC. Separate investigations were performed to study the material-reinforcement interaction [Jain (2004)], and the durability [Ogalla (2002)] and corrositivity [Esfeller (2006)] of the materials. The durability tests were performed under the direction of Dr. Kevin Folliard of the University of Texas, and the corrosion tests were performed under the direction of Dr. David Trejo at Texas A&M University.

This dissertation is aimed to evaluate the potential use of RAP and CC as a backfill material for MSE walls through a series of geotechnical tests. The scope of the work contained in this dissertation can be divided into three main parts: (1) literature review on MSE wall design, the critical properties for MSE wall backfill, the current uses of RAP and CC, and the identification of possible problems when using RAP or CC as an MSE wall backfill; (2) an evaluation of the geotechnical properties of RAP and CC as

compared to a conventional fill material; and (3) detailed studies on the most significant potential problems for RAP and CC.

The first part of the dissertation (Chapter 2) introduces RAP and CC materials in their general terms, and discusses engineering findings for the materials reported in the literature. The current geotechnical applications of RAP and CC in the U.S. are presented along with past experience with the materials. A general background on MSE walls, the soil-reinforcement interface mechanism, and typical backfill requirements are provided along with a broad overview of the current design criteria for MSE walls. Critical backfill properties and current MSE wall backfill specifications from TxDOT and FHWA are reviewed.

The second part of the dissertation (Chapter 3 through 5) focuses on a series of laboratory and field studies to compare the geotechnical properties of RAP and CC with those of a conventional fill material (CFM) used in central Texas. The initial laboratory experiments assess the index properties (i.e. grain-size distribution, pH, Atterberg limits, and specific gravity) of RAP, CC, and CFM. Subsequent testing includes laboratory and field investigations regarding the compaction characteristics, the drained shear strength (as measured in a triaxial apparatus and a force-controlled, large-scale direct shear box), the material hydraulic conductivity, and the collapse potential of three test materials. Test results obtained on RAP and CC specimens are analyzed and compared with the results obtained from CFM samples to evaluate comparatively their suitability as backfill materials.

The third part of the dissertation covers two detailed investigations regarding the most significant potential problems when using RAP and CC as backfill. For RAP, the most significant concern is creep behavior. Creep becomes a major concern for RAP because of the viscoelastic behavior of the bitumen coating that surrounds the aggregate particles. The RAP creep potential is investigated through a series of constant stress, drained triaxial creep tests. For CC, the most significant concern is the potential for tufa (calcium carbonate, $CaCO_3$) precipitation. The calcium ion concentration on a wide range of CC particle sizes to determine the threshold particle size that may exacerbate the tufa formation of a CC backfill.

1.3 ORGANIZATION OF DISSERTATION

This dissertation focuses on the presentation and evaluation of experimental test results aimed at assessing the potential use of RAP and CC as backfill material for MSE walls. The dissertation consists of eight chapters.

Chapter 1 briefly discusses the significance of utilizing RAP and CC backfill as a replacement for conventional backfill, the objectives and scope of the research, as well as the organizational description of the dissertation.

Chapter 2 serves as a comprehensive literature review on RAP and CC. A general description of RAP and CC, and how they are produced, is provided. The current geotechnical uses of RAP and CC are summarized and a number of performance evaluations reported in Texas are included. An overview of MSE wall design and the importance of the backfill material on MSE wall performance are also discussed.

Chapter 3 presents the result from a state-wide survey of RAP and CC producers and used to select the sources of material for this study. The responses received from the survey are presented and summarized as a database of the RAP and CC production in Texas. Index properties of the final bulk materials are presented in comparison with the values from CFM.

Chapter 4 describes an experimental program that incorporates laboratory and field investigations to study the compaction characteristics of the test materials. Laboratory studies were carried out to obtain compaction curves of the test materials, and to study their potential for particle breakdown during compaction. The field investigation assessed the ability of the nuclear gauge device to measure accurately the in-place dry unit weight and water content.

Chapter 5 presents a laboratory program that measures the shear strength properties, hydraulic conductivity, and collapse potential of the test materials. Discussion of the test equipment (triaxial and large-scale direct shear apparatuses), test procedures, and test results are presented.

Chapter 6 describes the triaxial creep testing program used to study the creep potential of RAP. A theoretical background on soil creep and the constitutive model used to investigate creep of soils are presented. Creep test results and the translation of the measured data to fit the creep model are discussed. The effect of stress history and stress level on the creep behavior of RAP is also presented.

Chapter 7 describes an experimental investigation initiated to evaluate the potential for tufa precipitation of CC material. The basic chemical reactions required to

form tufa are discussed, along with several thermodynamic parameters that control the rate and quantity of tufa formation.

Chapter 8 presents a summary of this research, recommendations for future investigations, and concluding remarks of the research. The final recommendations regarding the use of RAP and CC as backfill materials are also included.

Chapter 2. Potential Use of RAP and CC as MSE Wall Backfill

2.1 INTRODUCTION

This chapter serves as a comprehensive literature review on RAP and CC materials based on studies previously reported in the literature. A general description of RAP and CC, and how they are produced, is briefly described. The current geotechnical applications of RAP and CC are summarized and a number of performance evaluations reported in Texas are included. An overview of MSE wall design and the importance of the backfill material on MSE wall performance are also discussed.

2.2 DESCRIPTION OF RAP AND CC

RAP is a removed and/or reprocessed pavement material containing asphalt and aggregates. Asphalt pavement generally is removed either by milling or full-depth removal. Milling involves removal of the pavement surface using a milling machine, which can remove up to 2 in. of pavement in a single pass. Full-depth removal is usually achieved with a pneumatic pavement breaker or a rhino horn on a bulldozer. The broken materials are transferred to a central facility for a series of recycling processes including crushing, screening, conveying and stacking. Asphalt pavement can also be pulverized in place and incorporated into granular or stabilized base courses using a self-propelled pulverizing machine [FHWA (2000)]. In-place recycling eliminates the cost of

transporting material to and from the processing facility. Figure 2-1 illustrates a bulk sample of RAP that was taken from a TxDOT stockpile in Corpus Christi, Texas.

Figure 2-1 Bulk sample of RAP

CC is generated through the demolition of Portland cement concrete elements from roads, airport runways, and concrete structures. CC is generally removed by a backhoe and loaded into dump trucks for removal from the source site. In cases where CC is secured from demolished pavements, soil and small quantities of bituminous concrete are expected in the excavated materials. Generally, the reclaimed concrete materials are hauled to a central processing plant where crushing, screening, and ferrous metal recovery are performed before stockpiling. However, on-site recycling and processing can alternatively be performed with a mobile plant [Halm (1980)].

At the central processing plant, reclaimed CC is subjected to primary and secondary crushers. The primary crusher breaks the reinforcing elements from the concrete debris and breaks down the rubble to particle sizes of about 3 to 4 in. Removal of reinforcing steel by an electromagnetic separator occurs while conveying the materials to the secondary crusher. The secondary crusher further breaks down the particle sizes to the desired gradation [Halm (1980)]. Stockpiling of CC is usually done through the separation of coarse and fine particles to avoid inadvertent commingling of materials. Figure 2-2 shows a bulk sample of CC that was produced by a commercial producer in Dallas, Texas.

Figure 2-2 Bulk sample of CC

Over the past several years, there has been an increasing use of RAP and CC in highway construction throughout the United States. However, utilizing RAP and CC as a

backfill material has gained the least interest compared to other highway applications. RAP and CC are most frequently used as an aggregate substitute for pavement construction and good performance has been reported [TxDOT (1999)]. The following sections discuss previous uses of RAP and CC by TxDOT in highway-related construction, along with recent TxDOT research studies on both materials.

2.3 CURRENT GEOTECHNICAL USES OF RAP

The recycling of asphalt pavements is not a new concept and can be dated back as far as 1915 [FHWA (2004)]. In the U.S., a large increase in price of asphalt brought about through the oil crisis of the mid-1970s made the recycling of asphalt pavements an attractive option for reducing highway construction costs [Ahmad (1991,1992)]. It is estimated that as much as 36 million ton per year, or 80 percent of the annual excess asphalt, is being used either as a portion of recycled hot mix asphalt, in cold mixes, or as aggregate in granular or stabilized base materials [FHWA (2004)]. Estakhri and Button (1992) indicated that TxDOT has successfully used untreated RAP in many highway applications. These applications include paving driveway and country road approaches, paving mailbox and litter barrel turnouts, and repairing pavement edges.

TxDOT (1999) reported that more than 90% of RAP construction projects in Texas used RAP for paving purposes. The other 10% used RAP as the backfill material for embankment construction. More details on these embankment projects are shown in Table 2-1. The long-term performance of these embankments has been satisfactory, with no collapse or noticeable distress observed.

Table 2-1 TxDOT experience with RAP backfill [after TxDOT (1999)]

Year Installed	Location	District	TxDOT Specification	Result	Comments
1987	Liberty	Beaumont	N/A	Good	
1987	Jasper	Beaumont	N/A	Excellent	
1993	El Paso	El Paso	TxDOT Material Spec. No.132	Unknown	Used as a stabilizer for shoulder surface
1995	Travis County	Austin	N/A	Unknown	
1996	SH-21 at Brazos River	Bryan	TxDOT Material Spec. No.132	Excellent	Mixed soils with sized RAP

Because RAP has typically been used as a paving material in highway construction, the majority of past research projects on RAP focused on its potential as a paving material. Experimental programs typically focused on the mechanical properties used in pavement design; such as resilient modulus, modulus of elasticity, and fatigue characteristics. However, little attention was given to RAP as a potential backfill material. Experimental data from past research have indicated that RAP offers comparable performance, in terms of a paving material, to virgin aggregates [Kennedy et al. (1977), Maher et al. (1997)]. Also, research has indicated that recycled pavements offer the same durability as pavements constructed with 100% virgin aggregates [TxDOT (1999)].

The most recent TxDOT study on RAP was the TxDOT Project 1348, completed by Saeed et al. in 1995 and 1996. These studies focused on the potential uses of waste and recycled materials in roadbase construction. Eight recycled materials were evaluated in this study including RAP, Reclaimed Portland Cement Concrete Pavement (RPCP), iron blast furnace slag, steel slag, coal ashes, building rubble, glass, and rubber tires. Each recycled material was evaluated separately and four evaluation criteria were used: technical, economic, societal, and environmental. Various methods were used to assign a score for each material and for each criterion. The scores from each criterion were combined in a normalizing equation to indicate the potential use of the material in terms of the "waste recycled material utilization potential" (WRMUP).

The study rated RAP as the most suitable material for roadbase (Table 2-2) mostly due to its high availability in most local TxDOT districts. The report indicates that about 90% (19 out of 21) of the responding districts have stockpiles of old asphaltic concrete and further concludes that only RAP and RPCP are stockpiled in sufficient volume by TxDOT to make their use economically attractive. More detail on how the scores were assigned to each material can be found in TxDOT Report 1348 [Saeed et al. (1995, 1996)].

Table 2-2 Categorization of waste recycled materials as roadbase construction aggregate [after Saeed et al. (1996)]

Material	WRMUP* (%)	Remarks
Reclaimed Asphalt Concrete	68.60	Best Material
Electric Arc Furnace Steel Slag	60.40	Suitable material
Standard crushed limestone roadbase	58.85	For comparison only
Reclaimed Portland cement concrete	50.20	Marginal
Fly ash	45.20	Unsuitable as aggregate in roadbase construction
Bottom ash	45.20	
Pond ash	45.00	

Note: * WRMUP = Waste Recycled Material Utilization Potential

It is known that creep is a concern for all asphaltic materials. Ayoub (1983) studied the long-term behavior of softening agents on RAP produced in a cold process by employing a series of non-destructive creep experiments to evaluate such long-term behavior. At the end of the experimental program, the initial and long-term behavior of the recycled mixtures were reported and compared with the behavior of specimens with virgin aggregates.

According to this study, no significant difference was found between the creep behavior of virgin and recycled mixtures. The test results showed that creep compliance,

which is defined as the creep strain at any given time divided by the applied creep stress, decreased rapidly at early ages because of hardening of emulsified asphalt, then increased slightly due to the effect of the softening agents, but remained essentially unchanged. Temperature is also a major factor when determining creep compliance of the recycled mixture. Higher temperature (140°F) resulted in larger creep compliance, but no significant difference from lower temperature (75°F) was observed in this study.

FHWA (2000) indicates that at least five states (i.e. Connecticut, California, Illinois, Louisiana, and Tennessee) have used RAP directly as a backfill material, while some other states have used RAP as an additive in embankment construction. The performance of RAP in these applications was generally considered as satisfactory to good [FHWA (2000)]. When used as an embankment or fill material, the undersized portion of RAP (smaller than 2 in.) was sometimes blended with soil and/or finely graded aggregates. RAP with larger particles was usually used as an embankment base. The required construction procedures for a RAP embankment (i.e. including material storage, field compaction, quality control, design considerations) are generally the same as for conventional embankments. However, FHWA (2000) has a few specific recommendations regarding construction procedures for RAP embankments as follows:

- Random sampling and testing of the RAP stockpile must be performed because different sources of RAP can have different characteristic properties.

- Additional attention must take place during compaction to ensure that no poorly compacted zones are created in the fill, leading to long-term differential settlement.
- Some jurisdictions may require a minimum separation distance between water sources and fill materials containing RAP to avoid submersion of RAP in water since water leaching from RAP may be a potential environmental concern.

2.4 CURRENT GEOTECHNICAL USES OF CC

The CC has been used successfully in highway construction since the 1940s [Halm (1980)]. Laboratory research on recycled concrete was first carried out in Europe and the USSR shortly after World War II [Halm (1980)], because a considerable amount of CC produced by bombing and shelling during the war was used in rebuilding urban areas. In the U.S., the majority of CC is generated through the demolition of Portland cement concrete elements in roads and buildings, with an estimate of 150 million tons of annual CC production in the year 2000. The primary application of CC in the U.S. is as an aggregate substitute in pavement construction. This practice has become so common that CC aggregate is considered by many agencies as conventional aggregate. Using CC as a backfill material has apparently gained only minor interest compared to other applications. However, it is reportedly one of the first waste materials considered for backfill applications [FHWA (2000)].

Similar to RAP, there are numerous previous studies on CC that evaluated its performance for different engineering applications. Significant attention has focused on the suitability of CC as aggregate substitute for structural concrete in buildings or paving structures. Accordingly, laboratory investigations in most of the previous research have concentrated primarily on the material characteristics of CC for such applications. This previous research has indicated that concrete made with CC aggregate has comparable performance to concrete made with virgin aggregate [Cuttell et al. (1997), Barksdale et al. (1992), ACPA (1993)]. A summary the index properties and engineering properties of CC described in the literature is given in Table 2-3.

FHWA (2000) indicates that CC is generally more angular in shape, has a lower specific gravity, and has higher water absorption than comparatively sized virgin aggregate. The specific gravity of CC ranges from 2.0 to 2.5, while the water absorption varies from 2% to 8%, depending on the size of the CC particles (Table 2-3). This low value of specific gravity is attributed to the presence of mortar from the original concrete structure. As seen in Table 2-3, fine CC particles (passing U.S. sieve No. 4) have a lower specific gravity than coarse CC particles (retained on U.S. sieve No. 4) because more mortar is found in the finer part of the material. This is expected because mortar is more absorbent than natural aggregate [ACPA (1993), Rashwan and AbouRizk (1997), Mohany (1997), Mack and Solberg (1993)].

Table 2-3 Physical properties of crushed concrete material [after ACPA (1993)]

Property	Coarse particles	Fine particles
Specific Gravity	2.2 to 2.5	2.0 to 2.3
Water Absorption (%)	2 to 6	4 to 8

For pavement construction, concrete made with CC aggregate generally exhibits lower compressive and flexural strengths than concrete mixed with natural aggregate [ACPA (1993), Malhotra (1978)]. Malhotra (1978) reports compressive strengths up to 30% lower and flexural strengths up to 20% lower. Additional compressive strength reduction will likely occur when the recycled-aggregate mix also contains recycled fines, because a significant portion of recycled fines is mortar from the concrete. ACPA (1993) further indicates that the majority of strength loss is attributed to the material smaller than 0.08 in.

Other research has focused on the shear strength of CC for geotechnical purposes. O'Mahony and Milligan (1991) indicated that although CC had a lower dry density than crushed limestone, the shear strength of CC was similar (Figure 2-3). O'Mahony and Milligan (1991) further concluded that vertical stress has little influence on the friction angle of the CC over the range of stress applied (Figure 2-4). However, Figure 2-4 seems to show a slight decrease in friction angle with vertical stress, as commonly observed for granular materials.

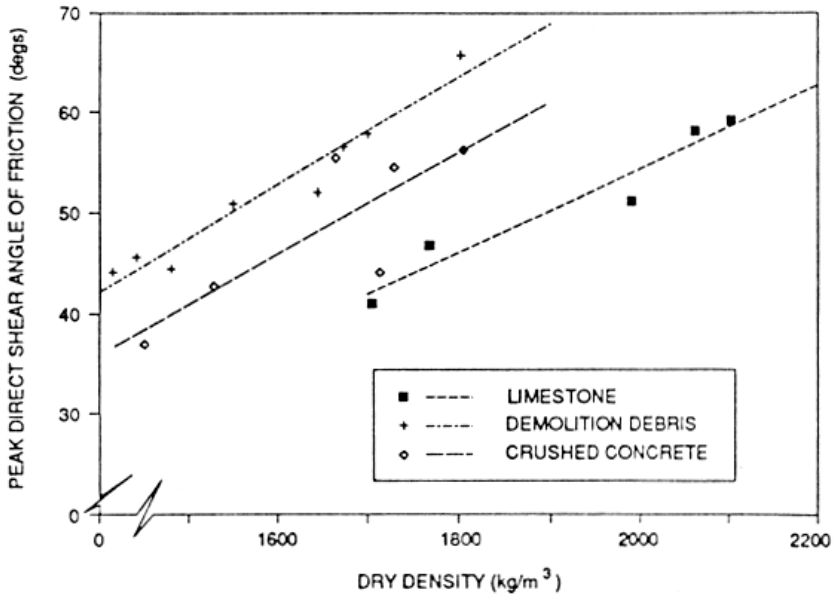

Figure 2-3 Influence of dry density on peak direct shear angle of friction [O'Mahony and Milligan (1991)]

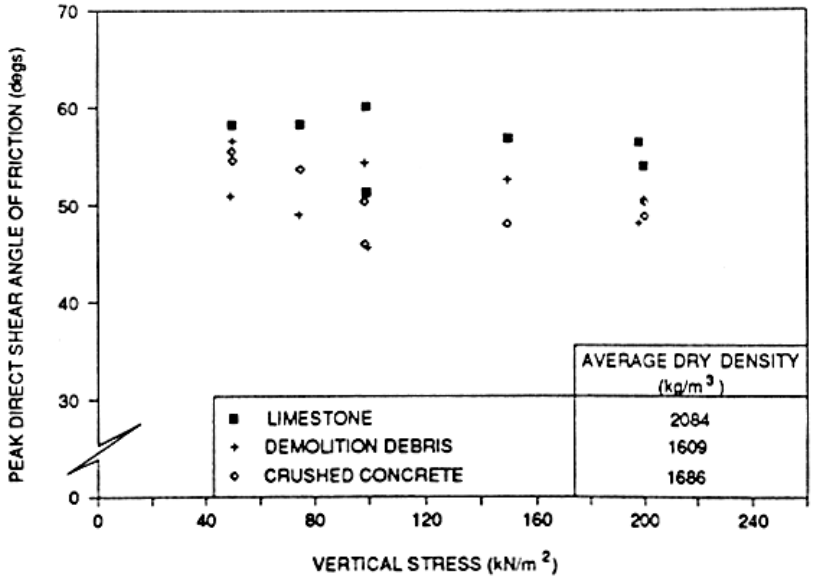

Figure 2-4 Influence of vertical stress on peak direct shear angle of friction [O'Mahony and Milligan (1991)]

The pH of a CC-water mixture often exceeds 11. The high alkalinity of CC can cause corrosion of aluminum or galvanized steel pipes that are in direct contact with CC and in the presence of moisture [FHWA (2000)]. Furthermore, CC may be contaminated with chloride ions, due to the application of deicing salts, or with sulfates, due to immediate contact with sulfate-rich soils. The presence of sulfate is also linked to CC obtained from buildings, which is likely to contain calcium sulfates from plaster or gypsum wallboard [Buck (1973)].

Chloride ions are associated with the corrosion of steel, while sulfate reactions lead to expansive disintegration of cement paste [FHWA (2000)]. However, ACPA (1993) indicates that the quantity of chloride typically found in old concrete pavement is below the critical threshold values of 0.03% to 0.09%. When aluminum is present within the CC, such as conduit pipe surrounded by CC backfill, the high pH environment of the CC can cause accelerated corrosion and formation of expansive products and hydrogen gas [Barksdale et al. (1992)].

TxDOT also has had some previous experience with CC. The first TxDOT project that used CC as aggregate in new pavement was in the Houston district [TxDOT (1999)]. There was no virgin aggregate used in this project, meaning that both coarse and fine aggregates were from recycled concrete, and the performance evaluation on this pavement was reported as good. TxDOT reported three TxDOT projects that used CC as backfill material. Table 2-4 summarizes the key findings from these projected that were reported to TxDOT. It must be noted that the results found from these projects were reported as good and excellent.

Table 2-4 TxDOT's projects using CC as backfill material [after TxDOT (1999)]

TxDOT District	Location	Results	Year Installed	Specification	Comments
Corpus Christi	Various	Excellent	1977	TxDOT Material Spec. No.132	Used for embankment and outfall erosion protection
Lufkin	District wide	Excellent	1982	—	—
Beaumont	SH 82 and SH 87	Good	1994	None	Used for embankment to control erosion on intercoastal waterway

A major concern when using CC as a backfill material in MSE walls is the potential corrosion of metallic reinforcements. This concern is drawn from the hypothesis that the high pH of a CC-water mixture will increase the rate of steel corrosion. Popova et al. (1998) studied the corrosive behavior of crushed concrete for potential use as a backfill material in MSE walls. For a galvanized steel rod embedded in fill material, the authors found that rates of corrosion at the beginning of the test were the same for both CC and typical granular soil fill (approximately 0.02 mm/year). However, the rate of corrosion increased with time for the CC material (0.075 mm/year at 400 days), while it decreased for the case of granular soil fill (0.005 mm/year at 400 days).

Popova et al. (1998) also studied the potential use of cement as a soil stabilization agent and found that the corrosion rates of crushed concrete and concrete stabilized granular soil fill are almost identical when both contain the same cement content. Further, this study indicated that the rate of corrosion of a galvanized steel rod in a cement

stabilized CC mixture was comparable to, and possibly slightly better than, a sample embedded in cement stabilized granular fill. The average values of the rate of corrosion in cement stabilized CC were in the rage of 0.005 mm/year to 0.02 mm/year, which is in the range of the commonly accepted corrosion rate of 0.01 mm/year, given a design life around 100 years [Popova (1998)].

An unresolved issue for a CC backfill is the potential precipitation of tufa (calcium carbonate, $CaCO_3$) contained in the CC leachate. This problem first surfaced when significant CC fines were observed to clog the filter fabric wrapped subsurface drains in CC pavement subbases [Barksdale et al. (1992), Mack et al. (1993)]. A series of possible chemical reactions between portlandite [$Ca(OH)_2$] in CC and other chemical reactants that lead to tufa formation is explained in short as follow:

1. Carbon dioxide (CO_2) from the atmosphere and automobile exhaust reacts with rainwater, forming carbonic acid (H_2CO_3)

$$CO_2 + H_2O \rightarrow H_2CO_3$$

2. Carbonic acid (H_2CO_3) reacts with portlandite [calcium hydroxide, $Ca(OH)_2$] in CC forming calcium bicarbonate [$Ca(HCO_3)_2$].

$$2H_2CO_3 + Ca(OH)_2 \leftrightarrow Ca(HCO_3)_2 + 2H_2O$$

3. At the drainage outlet, water from this enriched solution of calcium bicarbonate [$Ca(HCO_3)_2$] evaporates because of warm temperatures, and carbon dioxide (CO_2) escapes into the atmosphere. This condition leads to the precipitation of calcium carbonate ($CaCO_3$) and the formation of tufa.

$$Ca(HCO_3)_2 \leftrightarrow CaCO_3 (\downarrow) + H_2O (\uparrow) + CO_2 (\uparrow)$$

As can be seen in the last chemical reaction, warm temperatures in the summer months increase the rate of tufa formation, whereas cold temperatures in the winter months cause the carbon dioxide to remain in solution. The preceding chemical reactions indicate that the concentration of water, carbon dioxide, temperature, and humidity are the major contributing factors that control tufa precipitation.

To control the tufa precipitation, washing of CC aggregates is required by some agencies to remove the dust that typically contains free lime [calcium oxide, (CaO)] and portlandite. FHWA recommends using suitable CC that does not contain significant quantities of unhydrated cement or free lime for embankment or fill applications. Also, leachate testing may be required to obtain the tufa precipitation potential of CC for embankment and MSE wall applications.

2.5 MECHANICALLY STABILIZED EARTH WALLS

An MSE wall is defined as a vertical or near vertical earth retaining structure consisting of three major components: a facing panel, earth reinforcement, and reinforced backfill (Figure 2-5). Such walls are similar to reinforced earth systems, but with the addition of facing components for aesthetic purposes. An MSE wall functions through interaction between soil and earth reinforcement. After the vertical stress is introduced to the backfill (e.g. applied surcharge and soil self weight) an inherent horizontal pressure is mobilized simultaneously resulting from the stress transfer between soil particles (Figure 2-6). However, soil itself does not have the tensile strength to resist such lateral pressure, but buried reinforcement can provide efficient soil stabilization.

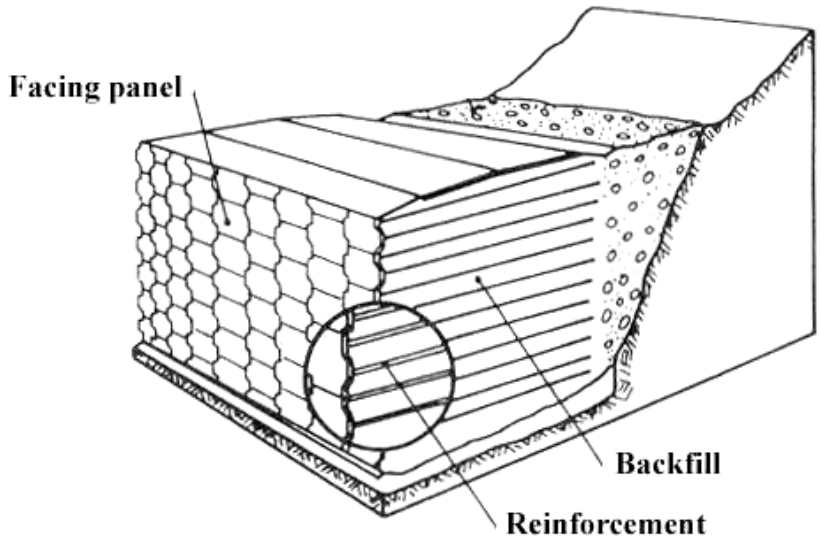

Figure 2-5 Schematic view of a reinforced earth wall [after Schlosser and Delage (1988)]

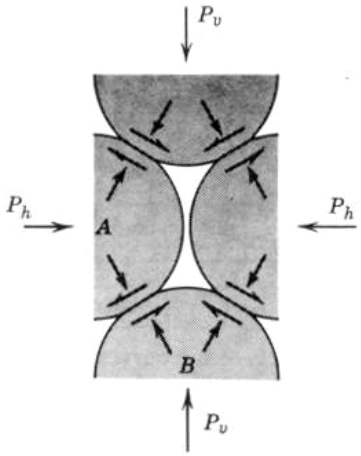

Figure 2-6 Stress transfer mechanism of soil particles when subjected to vertical loading [Lambe and Whitman (1979)]

The concept of soil reinforcement is based on the existence of a strong interaction between soil and reinforcement [Schlosser and Delage (1988)], such that the lateral tensile stress developed in the soil is transferred to the embedded reinforcement. The reinforced soil performs as a composite material that combines the best load carrying features of both components [Morris and Delphia (1999)]. The reinforcement reduces the lateral strain within the backfill through the shear resistance between the backfill soil and the reinforcement. As a result, the reinforced soil behaves as if an additional lateral confinement was applied, leading to an increase in strength in the reinforced zone.

Considering two samples of soil subjected to the same triaxial compression test (Figure 2-7). The first sample is not reinforced while the second sample is reinforced. Assume that a Mohr-Coulomb failure envelope is obtained earlier from a series of triaxial tests on unreinforced samples. With the same stress state (i.e. σ_v and σ_h) applied to both samples, the lateral deformation developed in response to σ_v of the reinforced sample will

be smaller than that of the unreinforced sample because soil particles in the reinforced sample are laterally restrained by soil-reinforcement interface friction. The interlocking of soil particles can be considered an additional lateral compressive stress applied to the soil skeleton ($\Delta\sigma_{h,s}$). This results in the stress state of the soil ($\sigma_{v,s}$ and $\sigma_{h,s}$) for the reinforced soil system being further from the failure envelope (Figure 2-7). A reinforced soil, therefore, can sustain greater stress than an unreinforced soil because of this reason.

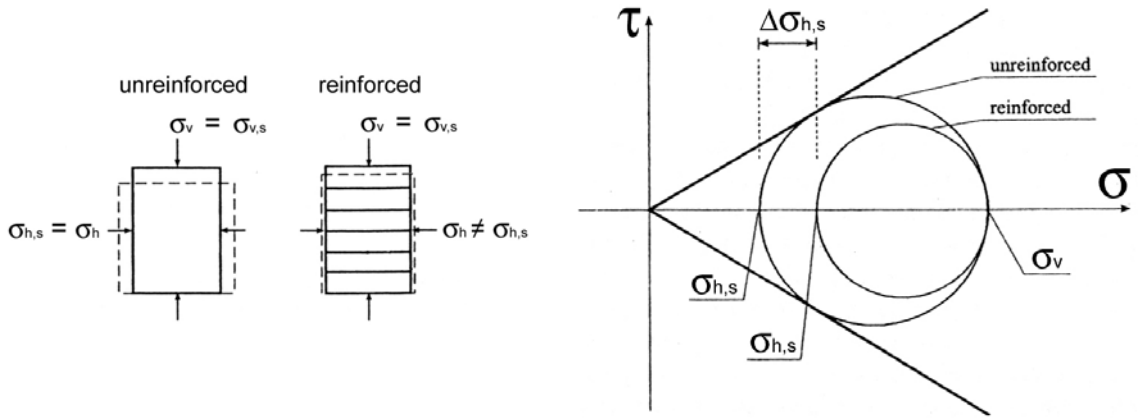

Figure 2-7 Mohr circles of unreinforced and reinforced soil samples under triaxial test

Based on field measurement data, Schlosser (1990) showed that the tensile stress in MSE wall reinforcements drops off in the vicinity of the wall with the maximum value measured at a certain distance from the facing panels. This stress distribution indicates only some of the tensile stress in the reinforcement is transferred to the facing panels (Figure 2-8). This finding suggests that with the strong interaction between the backfill soil and reinforcement, the reinforced soil itself can stand vertically without the facing

system. Therefore, the facing panels are not designed for structural purposes but for an aesthetic appearance and for preventing soil erosion between the reinforcements.

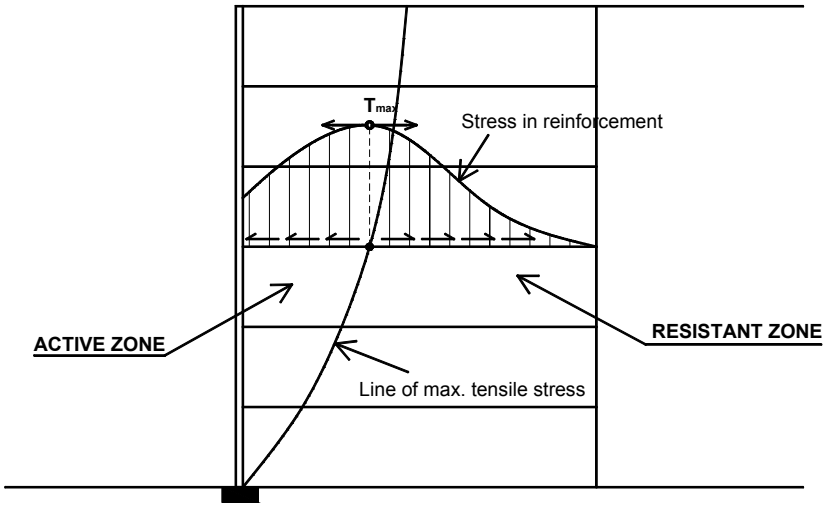

Figure 2-8 Tensile stress in the reinforcement and maximum tensile force line

Segmental pre-cast concrete panels are most often used in MSE walls due to their aesthetic appearance and ease of installation. Each panel is interlocked with adjacent panels to form a continuous and flexible wall facing. Vertically adjacent units are typically connected with shear pins. And as mentioned earlier, facing panels are not designed for structural support purposes. Their primary functions are to prevent backfill erosion and, in some cases, to provide drainage paths through the wall. Geotextile strips are usually placed at the joints to prevent washout of the backfill between the adjacent panels.

The primary function of the reinforcement is to improve the mechanical properties of the backfill. Currently, reinforcement is classified as either metallic

(typically mild steel) or nonmetallic (generally polymer). Also, reinforcements can be categorized based on their extensibility. An inextensible reinforcement is reinforcement with its deformation at failure much less than the deformability of the soil, whereas extensible reinforcement has comparable deformation at failure to soil.

There are two types of stress transfer mechanisms between the reinforcement and soil. First, frictional resistance develops where there is a relative shear displacement and corresponding shear stress between the soil and reinforcement surface [Elias and Christopher (1996)]. Second, passive resistance develops through bearing-type stresses on transverse reinforcement surfaces normal to the direction of relative movement [Elias and Christopher (1996)]. Figure 2-9 illustrates both resistant mechanisms. One of the most commonly used reinforcements in Texas is galvanized ribbed steel strip, which has a combination of the two stress transfer mechanisms.

In general, the cost of the backfill material dominates the total cost of MSE wall construction. Elias and Christopher (1996) indicate that utilizing locally available soil can significantly reduce the total cost of construction on the order of 20% to 60% compared to conventional walls. The major function of the backfill is to provide the weight, compression resistance, and shearing strength to ensure the stability of the retaining wall [Morris and Delphia (1999)]. In terms of physical properties, the select backfill should be well-graded, freely draining, and have high frictional strength. Fine-grained backfills are typically undesirable due to their low strength, creep potential, and poor drainage.

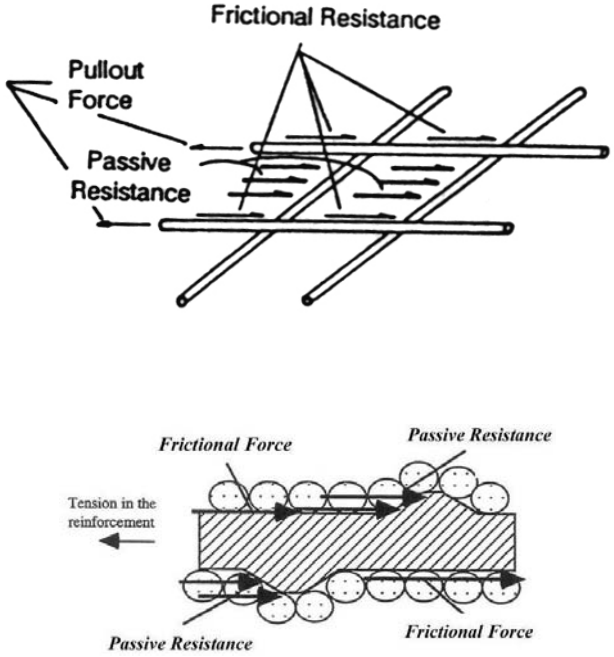

Figure 2-9 Stress transfer mechanisms mobilized on reinforcement
[after Morris and Delphia (1999)]

2.5.1 MSE Wall Design

This section presents in brief the MSE wall design procedures based on FHWA (1996) construction guidelines by Elias et al. The guidelines are for walls with near-vertical faces and identical reinforcement length. The current design procedures consist of determining the geometric and reinforcement requirements to prevent internal and external failure.

2.5.1.1 External Stability

The external stability of an MSE wall involves the geometry of the entire wall system. There are four potential failure mechanisms associated with external stability: (1) sliding, (2) overturning, (3) bearing capacity, and (4) deep seated stability, as shown in

Figure 2-10. After the preliminary dimensions of the entire wall system are chosen, external stability checks are performed.

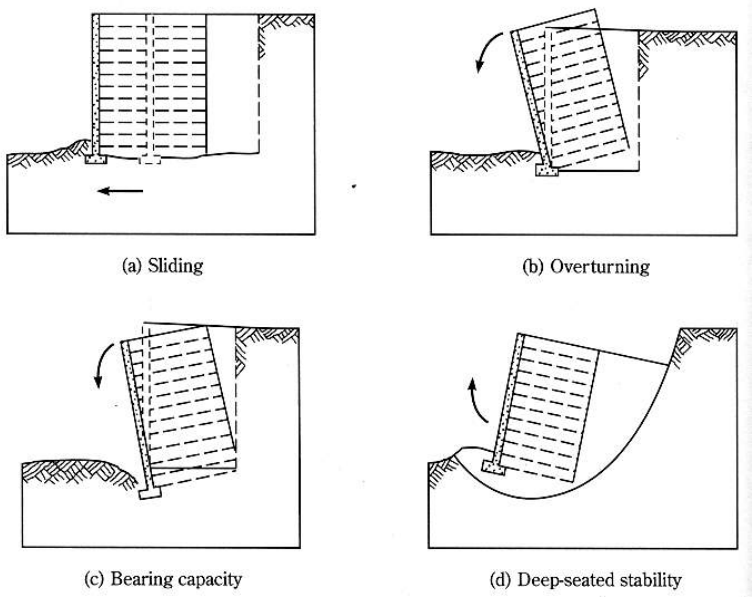

Figure 2-10 External stability mechanisms of failure [Elias and Christopher (1996)]

Sliding Stability - The factor of safety against sliding ($FS_{sliding}$) is the ratio of the total horizontal resisting force divided by the total horizontal driving force acting on the wall. For a general case, the resisting force is the lesser of the shear resistance along the base of the wall or of a weak layer near the base of the wall. The driving force is the horizontal component of the active earth pressure from the retained soil behind the reinforced zone. Backfills with high internal friction angles will contribute to a larger resisting force at the base of the wall. If the calculated $FS_{sliding}$ is less than 1.5, an increase in reinforcement length is required until the new $FS_{sliding}$ is more than 1.5. Such an

increase in the reinforcement length will lead to a higher resisting force due to a larger area of sliding. The requirement for external stability against sliding generally governs the overall dimensions of the wall [Anderson et. al. (1995)].

Overturning Stability - Overturning stability of an MSE wall is determined with respect to the maximum permissible eccentricity of the resulting force. The resulting force (R) is the summation of the vertical forces acting on the reinforced backfill. The eccentricity (e) is computed by summing the moments of the mass of the reinforced soil section about the centerline of the mass and dividing by R. For general practices, the length of reinforcement will be increased if the eccentricity is larger than the recommended value. However, the greater structural flexibility of an MSE wall system as opposed to a more rigid, conventional gravity retaining wall should make its potential for overturning failure highly unlikely [Elias and Christopher (1996)].

Bearing Capacity Failure - Generally, two modes of bearing capacity failure are considered in MSE wall design: general shear failure and local shear failure. A factor of safety against general shear failure is defined by the ratio between the ultimate bearing capacity (q_{ult}), obtained from classical bearing capacity theory, and the vertical stress (σ_v) acting on the effective base area (L-2e) of the wall. FHWA specifies a minimum factor of safety value of 2.5 for bearing capacity failure. Clearly, this mode of failure is controlled by the bearing capacity of the foundation soil and the weight of the backfill material. Backfill material with light compacted unit weight (e.g. RAP) will be a more attractive option when dealing with weak foundation soil.

Deep-seated Stability (Global Stability) - Deep-seated stability can be critical for walls on steep slopes or on soft foundation soils. The overall stability is determined using rotational or wedge limit equilibrium, which can be performed using classical slope stability methods or slope stability software. When computing stability, the entire MSE wall system is considered a rigid body and only failure surfaces completely outside the reinforced soil mass are considered for deep-seated stability analysis. If the preliminary design cannot satisfy deep-seated stability, increasing the reinforcement length beyond the failure surface or ground improvement techniques are generally required.

2.5.1.2 Internal Stability

Evaluation of internal stability involves the interaction between the reinforcing elements and the backfill. The mechanism of the stress transfer depends on the type of reinforcement (i.e. extensible or inextensible). Two internal failure modes are typically taken into account in design: tension failure and pullout failure (Figure 2-11). Required information for an internal stability check include: (1) determination of the maximum developed tensile forces and their locations along a critical slip surface, and (2) evaluation of the tensile resistance and pullout capacity of the reinforcement.

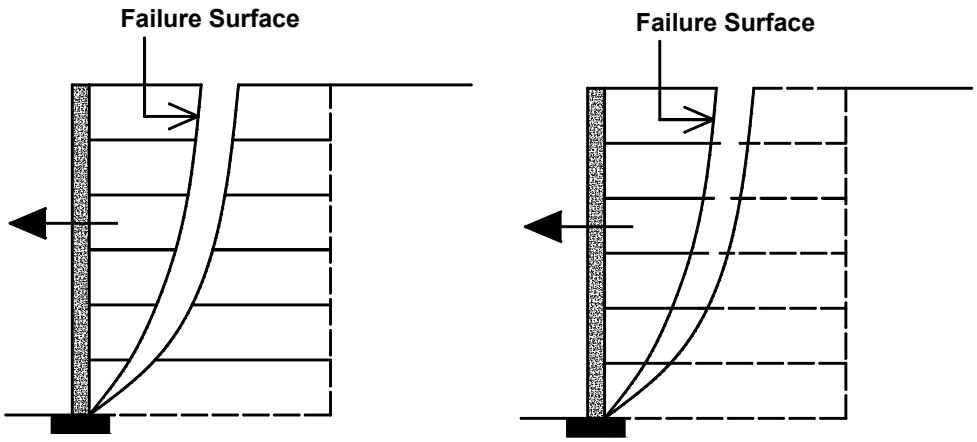

Figure 2-11 Internal failure (a) tension failure (b) pullout failure

Tension failure occurs when the tensile force in the reinforcement becomes so large that the reinforcement elongates excessively or ruptures [Elias and Christopher (1996)]. The analytical check for tension failure involves determining the maximum developed tensile force (T_{max}) and comparing it with the allowable tension (T_a) in the reinforcement. The allowable tension (T_a) is generally provided from the manufacturer's specification or from laboratory testing. The maximum developed tensile force in each layer is obtained by multiplying the lateral earth pressure coefficient, which is a modified value of the active earth pressure coefficient (K_a), by the vertical stress at that depth and the contributing area for each reinforcing element. After the value of T_{max} is calculated, a factor of safety against tension failure is determined by comparing it with T_a. In general, stronger backfill materials exhibit smaller active earth pressures and induce smaller

values of T_{max}. Hence, the use of good backfill material means less expensive reinforcement (i.e. smaller T_a) may be acceptable for the design.

Pullout stability evaluation involves calculating the length of reinforcement in the resisting zone beyond the potential internal failure surface required to resist the maximum tensile force in the reinforcement (T_{max}). A factor of safety of 1.5 is typically used for pullout assessment. Earlier practice assumed that the pullout resistance must be developed behind the Coulomb failure surface. However, field measurements and theoretical analyses have shown that the potential failure surface is coincident with the maximum tensile forces (T_{max}) developed in the reinforcements [Anderson et. al. (1995)]. The locations of the maximum tensile forces are also primarily dependent on the extensibility of the reinforcement. And again, backfill material with high shear strength tends to produce a stronger interactive bond with the embedded reinforcement, resulting in a higher pull-out capacity and shorter required reinforcement.

2.5.2 Critical Backfill Properties

The backfill is a key element in achieving satisfactory performance of an MSE wall. Based on the stability analyses presented earlier, an ideal backfill material should exhibit high drained shear strength parameters (c' and ϕ') and have good drainage properties. To avoid excessive surface deformations, the backfill should also exhibit low compressibility over time. Using high quality material leads to shorter required reinforcement lengths, which understandably lowers the total cost of an MSE wall. Free-draining backfill prevents water from accumulating behind the wall and increasing the lateral pressure on the facing system. These additional pressures may cause excessive

deformation leading to total wall failure. Critical engineering characteristics of a candidate backfill material are discussed below.

Hydraulic conductivity – Backfill materials for all types of retaining walls must be free draining so that water pressures do not build up behind the wall. To ensure a backfill is free draining, specifications typically limit the percentage of fines in the backfill. For MSE walls, backfill materials that are not free draining can also increase the corrosion potential of the metallic reinforcements. Therefore, backfill with high water absorption potential, such as clay or silt, is generally not considered acceptable for MSE wall backfill.

Shear strength – The backfill material should exhibit high shear strength to ensure stability within the backfill and to achieve an adequate interaction with the reinforcement [Morris and Delphia (1999)]. The forces developed in MSE wall reinforcement are related to the horizontal earth pressures acting on the wall at different depths. This horizontal earth pressure is calculated using the shear strength parameters of the backfill. For the general case, when a free draining material is used, effective shear strength parameters (c' and ϕ') are required to calculate the wall stability.

Interface friction – The interface friction angle between the backfill and reinforcement is needed for the design of the reinforcement length. This parameter is generally acquired from pullout tests or through models that relate the characteristics of the backfill and reinforcement to the pullout capacity. A well-graded material with high angularity tends to give higher values of interface friction angle. Also, the moisture

content and fines content of the backfill can affect the pullout resistance of the reinforcement.

Compaction Characteristics – During construction, the backfill must be well compacted to ensure adequate shear strength, adequate interface friction, and minimal compression during and after MSE wall construction. For a given compaction energy, the maximum dry density is affected by the particle shape, grain size distribution, and water content during compaction. Materials with low angularity and a wide range of grain sizes (well-graded) tend to exhibit larger maximum dry density values. Backfill materials compacted at low water contents will have internal capillary stresses that resist the densification of the material, resulting in smaller dry densities [Morris and Delphia (1999)]. Particle breakdown during compaction is another key aspect to backfill drainage properties. The additional fines from this breakdown mechanism may reduce the hydraulic conductivity and change the shear strength properties of the backfill.

Compressibility of compacted material – The presence of excessive fines in the backfill material indicates the potential for long-term settlement. Differential settlement may occur when the backfill is not compacted uniformly throughout the wall area. These settlements can create problems with the performance of overlying pavements on top of the backfill, and may also cause significant damage to the reinforcement and the facing system. When such settlements occur, the reinforcements are forced downward, creating an undesirable vertical stress and deformation on the facing system (Figure 2-12).

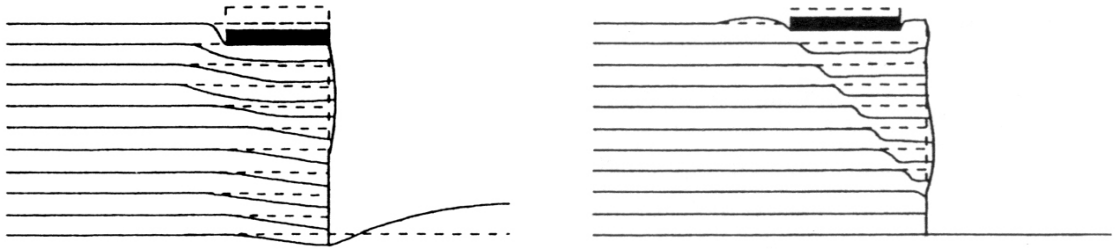

Figure 2-12 MSE wall failures due to poorly compacted backfill settlement

In addition, when a granular backfill is compacted at low dry density and water contents, it can undergo significant settlement upon wetting. This deformation mechanism is called "collapse". A collapsible soil may withstand relatively large applied vertical stress with small settlement while at a low water content, but exhibit considerable settlement after wetting with no additional increase in vertical stress. For typical MSE wall construction, additional water causing undesired wetting to the compacted backfill can come from heavy rainfall during construction or insufficient drainage. Potential problems associated with collapse settlement of an MSE wall backfill may include damage to structures or pavements constructed on the backfill, cracking and failure within the backfill itself, as well as excessive distress to the underground utilities. Also, this collapse settlement of the MSE wall backfill can damage the horizontally aligned reinforcement and break or loosen its resisting hinge connector at the back of the facing panel. Thus, the collapse potential of the candidate backfill must be evaluated to avoid significant damage due to excessive wetting or soaking of the backfill.

Time-dependent (creep) effects – For MSE walls, creep deformations are believed to interfere with the development of forces in the reinforcement and may potentially lead

to a wall failure through excessive deformation or full collapse. Creep behavior is temperature dependent, and is typically enhanced at higher temperature. For long-term stability purposes, a backfill material should not be susceptible to creep. For a given material, a creep testing program can be used to define the relationship between the material creep strength and such factors as time to failure, steady-state or minimum creep rate, strain at failure, and temperature. These relationships assist engineers in selecting the appropriate material properties for use in design for a given loading condition.

Corrosivity – Corrosion is a major concern for MSE walls incorporating metallic reinforcement. Accelerated or unanticipated corrosion of the reinforcements may cause sudden and catastrophic failure of MSE structures, generally along the locations of the maximum tensile stresses in the reinforcements [Elias (1996), see Figure 2-8]. A backfill should not contain highly deleterious materials that could attack the reinforcement or cause some distresses to the material itself. FHWA uses resistivity and pH values as indicators to reflect the corrosion potential of a backfill material.

Resistivity indicates how difficult it is for an electrical current to pass through a material and how effective it is as an electrolyte. A low resistivity value is indicative of high potential for corrosion because it promotes more electrical activity in the medium. Furthermore, highly acidic (low pH) or highly alkaline (high pH) materials are believed to be corrosive because of the presence of ions in the pore water which cause voltage differences between metal surfaces and induces a current. Therefore, current specifications classify an ideal backfill as having high resistivity and exhibiting a pH value in a permissible range.

The resistivity value is also influenced by the presence of soluble salts in the material. High concentrations of soluble salts affect the electrochemical reaction at metal surfaces and decrease the resistivity of the material. The type of ion is also important to the corrosion process. Two major chemical ions that have been identified with high corrosivity potential are chlorides and sulfates [Rabeler (1989)]. In general, standard MSE wall specifications have limited the presence of these two chemicals in the backfill to be less than 100 ppm and 200 ppm for chlorides and sulfates, respectively.

2.6 MSE WALL BACKFILL SPECIFICATIONS

This section presents current specifications for all key geotechnical properties of backfill materials as required in TxDOT (2004) and FHWA (2004) design guidelines. All of the specifications presented were developed for traditional backfill materials. This section also includes other possible concerns regarding the use of RAP or CC as backfill in MSE walls.

2.6.1 Gradation

An important geotechnical aspect commonly used to classify different backfill materials is particle gradation. Gradation is an important factor that affects backfill performance including stability, drainage, and frost susceptibility. Because specifications for recycled materials have not yet been standardized, the gradation requirement for traditional backfill proposed by TxDOT and FHWA can be used as an initial guideline. The backfill should be free from organic and deleterious materials with the material gradation determined through a traditional sieve test. TxDOT and FHWA have relatively

similar requirements on backfill gradation, with the major difference being the allowable maximum particle size.

TxDOT has categorized backfill materials into four types (from Type A to D) based on the material gradation (Table 2-5). Each TxDOT backfill type is designated for a different wall type, unless the plans shown otherwise. Although Type A comparatively has the most stringent gradation requirement for MSE walls on dry land, it is a fairly new requirement and, thus, rarely specified. FHWA has only one backfill specification with a maximum particle size of 4 in. In cases where nonmetallic or epoxy coated metallic reinforcement are used, both FHWA and TxDOT limit the maximum particle size of the backfill to 0.75 in. to ensure minimal abrasion to the reinforcement.

2.6.2 Compaction

It is important to evaluate the compaction characteristics of RAP and CC because these recycled materials may not yield similar moisture-dry density curves with those achieved for the traditional backfill. Also, crushing of the grains during compaction is a concern; thus sieve analysis before and after compaction is essential to evaluate the possible increase in fines content. The following sections describe the compaction tests currently designated by FHWA and TxDOT. Table 2-6 summarizes the compaction test methods used by TxDOT and FHWA.

Table 2-5 Backfill gradation limits by TxDOT (2004) and FHWA (2004)

Classification		**Sieve Size**	**% Passing**	**Recommended for**
TxDOT (2004) Item 423	Type A	3 in.	100	—
		½ in.	0 – 50	
		No. 40	0 – 15	
	Type B	3 in.	100	permanent walls
		No. 40	0 – 60	
		No. 200	0 – 15	
	Type C	3 in.	100	temporary walls
		No. 200	0 – 30	
	Type D	3 in.	100	walls in inundation areas
		$^{3}/_{8}$ in.	0 - 15	
FHWA (2004)		4 in.	100	—
		No. 40	0 – 60	
		No. 200	0 – 15	

Table 2-6 Compaction test methods using by TxDOT and FHWA

Compaction Test Method		Use for Materials	Mold Dimensions		Compaction Hammer			No. of Layers	Blows per layer	Compaction Energy ($ft\text{-}lb/ft^3$)
			Diameter (in)	Height (in)	Weight (lb)	Drop (in)	Face Shape			
Tex-113-E		100% passing 1 ¾" sieve materials with particles > $^7/_8$" base materials treated subgrade/embankment materials	6	8	10	18	sector	4	50	22,900
		"materials difficult to compact" 100% passing 1 ¾" sieve materials with particles > $^7/_8$" base materials treated subgrade/embankment materials	6	8	10	18	twin sector, on neoprene pad	8	100	91,700
Tex-114-E	**I**	≤ 20% retained on ¼" sieve 100% passing $^3/_8$" sieve untreated subgrade/embankment material	4	6	5.5	12	sector	4	25	12,600
	II	> 20% retained on ¼" sieve 100% passing $^7/_8$" sieve untreated subgrade/embankment material	6	8	5.5	12	sector	4	75	12,600
AASHTO T 99-97	**A**	100% passing No. 4 sieve	4	4.584	5.5	12	circular or sector	3	25	12,400
	B	100% passing No. 4 sieve	6						56	12,300
	C	100% passing ¾" sieve	4						25	12,400
	D	100% passing ¾" sieve	6						56	12,300

The TxDOT specifications express the required compaction of backfill materials for retaining structures in terms of percent of maximum dry density determined in accordance with the Tex-114-E compaction method. The specifications require that the backfill be compacted at 95% of maximum dry density determined from Tex-114-E for the top 3 ft. of the backfill, while 90% relative density is required for the underlying layers. However, the Tex-114-E test method limits the maximum particle size to $^{7}/_{8}$ in., which is significantly smaller than the maximum particle size allowed in the backfill and significantly smaller than the maximum particle size typically found in RAP and CC. As a result, Tex-114-E recommends test method Tex-113-E be used for materials containing particles larger than $^{7}/_{8}$ in. The Tex-113-E uses a larger mold, a larger hammer and drop height, resulting in greater compaction energy.

Morris and Delphia (1999) recently studied the backfill specifications for MSE walls. They recommend using a vibrating hammer in reference to British Standard 1377 (1990) as a standard laboratory compaction test because test method Tex-113-E tends to give low values of maximum dry density, especially for coarse materials. However, the subsection on "Materials Difficult to Compact" in Tex-113-E proposes a higher compaction effort with 100 blows per layer to achieve a higher dry density. In a recent study at The University of Texas at Austin [Marx (2001)], it was concluded that this modification to the Tex-113-E method gained the highest dry density among all compaction tests.

FHWA requires that the backfill be compacted to at least 95% of the maximum dry density and within ± 2% of the optimum moisture content determined by AASHTO

T-99 method C or D. This compaction method is similar to the standard Proctor compaction test (5.5-lb hammer compacting 3 equal layers of material with 12-in. drop height). Test methods C and D differ in the diameter of the compaction mold, but the compaction energy is the same. The allowable maximum particle size is ¾ in., which is smaller than the expected maximum particle size for RAP and CC. For such cases, the AASHTO specifications recommend a scalping procedure that maintains the same percentage of coarse particles as in the virgin material. Particles with a size larger than ¾ in. are discarded prior to compaction. Particles passing the 2-in. sieve but retained on the ¾ in. sieve are replaced with an equal weight of material passing the ¾-in. sieve but retained on the No. 4 sieve (4.75-mm).

For field compaction, FHWA (2004) indicates that compaction of RAP and CC can be accomplished with similar methods and equipment as used with conventional backfill materials. It is reported that granular materials containing RAP appear to compact better if incorporated with little or no additional water [Senior et al. (1994)], while compaction of CC usually requires additional water to facilitate particle arrangement. Also, due to the high angularity of CC materials, equipment with higher compaction energy is required to achieve the specified level of relative compaction. Finally, when compacting gravel-size particles (such as RAP and CC), caution is needed to ensure that no large voids are formed within the fill that could subsequently contribute to a future long-term differential settlement.

2.6.3 Hydraulic Conductivity

Backfill materials must be free draining to ensure that pore water pressures do not develop behind retaining structures. Also, the rate of corrosion of metallic reinforcement is primarily dependent on the moisture content in the backfill. Fine-grained particles present in the backfill impede the dissipation of pore water behind the retaining structure, resulting in large forces on the wall and a higher rate of reinforcement corrosion. Therefore, under these primary considerations, fine-grained materials are not recommended for use as backfill. The ideal backfill for an MSE wall is a granular material with little or no plastic fines.

In general, the hydraulic conductivity of an MSE wall backfill is not explicitly measured because the specification on material gradation generally results in a large hydraulic conductivity. FHWA and TxDOT permit up to 15% fines (passing through sieve No. 200) in the backfill, assuming this will result in free draining material. However, it is still unknown how water will interact with RAP and CC backfill. Additionally, crushing of coarse-size particles may occur during compaction of these recycled aggregates, which can potentially lead to a substantial decrease in hydraulic conductivity due to an increase in fines.

CC is expected to have higher water absorption than conventional backfills due to the presence of mortar and debris. Moreover, unhydrated cement in CC may react with seepage water to cause a significant reduction in the hydraulic conductivity of the backfill. Therefore, the hydraulic conductivity may vary with time after compaction is

completed. TxDOT specifies the constant head test in accordance with ASTM D 2434 to measure the hydraulic conductivity of granular materials.

2.6.4 Settlement

Settlement of an MSE wall backfill is normally related to the quality of the backfill material used, the uniformity of the material, and the uniformity of field compaction in the reinforced zone. In general, backfill materials with more fines have a larger tendency for settlement during and after construction. Because significant fines are typically not permitted in MSE wall backfill, field settlement is primarily a function of the compaction method and the uniformity of the backfill. These statements are suitable for a typical, conventional backfill material which normally consists predominately of stiff, granular materials. However, the compressibility characteristics of RAP and CC may not be the same as for conventional backfill.

According to several past studies, the percent fines in produced RAP is typically low (less than 1%), which suggests that RAP may not be susceptible to significant settlement. CC is also expected to have low compressibility, comparable to that of conventional backfill materials. Thus, it is believed that the intrinsic compressibility of RAP and CC will not lead to significant settlement of the backfill after construction.

Additional concern with regards to MSE wall backfill settlement is the collapse potential of the backfill material upon wetting. A granular backfill collapses after subjected to excess water as a result of the backfill material being compacted at low dry density or at a low degree of saturation. Collapsible materials can eventually lead to the differential settlement behind the wall after typical water exposure during or after the

construction. Therefore, experimental measurement of the collapse potential should also be conducted to evaluate the potential for collapse upon wetting.

As for compaction uniformity, settlement of the backfill is primarily expected in the area right behind the facing panels, where only small compaction equipment is allowed. The settlement in this area is generally attributed to the low density of the backfill. Hence, to minimize such settlement problems, TxDOT and FHWA require that the field inspection of backfill materials be periodically performed throughout the construction period.

2.6.5 Shear Strength

The shear strength parameters of the backfill are critical properties in the design phase because they govern the stability of the wall. FHWA and TxDOT specifications on material gradation and compaction should yield a high friction angle backfill. Past laboratory tests on RAP and CC have shown high internal friction angles with little or no cohesion observed. Shear strength of RAP should be comparable to a similarly graded natural aggregate, whereas the shear strength of CC was reportedly similar to that of crushed limestone aggregates [Petrarca and Galdiero (1984)]. Hence, RAP and CC should have an adequate shearing resistance to the backfill system. Because TxDOT and FHWA do not specify the same tests for measuring shear strength, the following subsections describe the shear strength tests specified by each organization.

TxDOT does not specify a minimum internal friction angle for the backfill material. However, the specifications require that shear strength of the candidate backfill material be measured according to test method Tex-117-E, “Triaxial compression tests

for disturbed soils and base materials." This test measures material shear strength using a modified procedure that is broadly analogous to a traditional consolidated-drained triaxial compression test. At the end of the test, shear strength parameters are reported in terms of cohesion and internal friction angle, along with absorption and expansion characteristics of the materials.

Unlike the TxDOT specification, the FHWA design manual specifies that the internal friction of backfill materials, measured by the standard direct shear test (AASHTO T-236), not to be less than 34° for the particles smaller than the No. 10 sieve (2.0 mm). The test specimen is compacted at 95% of AASHTO T-99 (method C or D) and sheared in a consolidated-drained condition at different normal pressures. For a conventional backfill, the design manual specifies that this test is not required if the backfill material contains more than 80% by weight of particles larger than ¾ in. This condition is rarely met for typical RAP and CC gradations.

2.6.6 Creep Characteristics

One common assumption made when designing MSE walls with traditional, granular backfill is that creep is a concern only for the reinforcement, not the soil backfill. However, RAP is susceptible to creep behavior due to the viscosity of the asphalt content in the material. It is possible that excessive creep deformations will occur in RAP backfill or at the RAP-reinforcement interface under sustained loads below failure. Such creep behavior in RAP is likely to be temperature dependent, with higher severity expected at higher temperatures, because the asphalt stiffness is temperature dependent. Because TxDOT and FHWA do not anticipate creep behavior from the

backfill material itself, they do not include any standard creep testing procedure in their specifications or design manuals. However, the creep potential of the backfill can be studied by conducting a classical creep test with a conventional triaxial setup.

One more concern regarding creep characteristics is the creep pullout behavior. This type of creep mechanism is usually associated with creep deformations in polymeric reinforcing elements. Sawicki (1999) has indicated that the creep of an MSE wall tends to take place in the active zone (Figure 2-8), in which the soil is in the plastic state and the reinforcement is in the visco-elastic condition. For a conventional backfill, this plastic flow of the soil in the active zone is controlled by visco-elastic deformations of the reinforcement. However, in a case of reinforced RAP backfill, RAP itself is believed to be a material susceptible to creep. Thus, it is possible that excessive deformation may occur due to the combination of creep from the RAP and the reinforcement.

2.6.7 Summary of Backfill Requirements

Good backfill soil is a key element in the satisfactory performance of an MSE wall. Table 2-7 summarizes the backfill specifications required by TxDOT and FHWA (2004). Both TxDOT and FHWA design manuals recommend the use of granular material due to its high internal friction angle and free draining characteristics. Adequate values of these two material properties are traditionally achieved through the specified particle size distribution. The required compaction methods, method Tex-114-E by TxDOT and method AASHTO T-99 by FHWA, have nearly the same compaction energy (Table 2-6), although the TxDOT specification utilizes additional compaction energy when the backfill has a significant amount of large particles. TxDOT does not have a

requirement for the minimum internal friction angle, while FHWA requires a value greater than 34°. Finally, pH and resistivity are used to indicate the corrosion potential of a candidate backfill, with both specifications having almost the same range of allowable pH and resistivity values.

Table 2-7 MSE wall backfill specifications from TxDOT and FHWA in 2004

Requirement	TxDOT Item 423				FHWA
	Type A	Type B	Type C	Type D	
1. Gradation					
Maximum size	3 in.	3 in.	3 in.	3 in.	4 in.
% passing $^3/_8$ in.	-	-	-	0 -15	-
% passing sieve No. 40	0 -15	0 - 60	-	-	0 - 60
% passing sieve No. 200	-	0 - 15	0 -30	-	0 - 15
2. Plasticity Index (PI)	_				< 6
3. Compaction					
Dry Density	95% (Tex-114-E)				95% (AASHTO T-99)
Moisture content	± 2% of W_{opt}				within 2% dry of W_{opt}
4. Internal Friction Angle	_				> 34°
5. pH	5.5 – 10				5 – 10
6. Resistivity (ohm-cm)	> 3000*				> 3000

Note: * Material with resistivity between 1500 and 3000 ohm-cm may be used if the chloride content is less than 100 ppm and the sulfate content is less than 200 ppm as determined by Tex-620-J.

2.7 SUMMARY

This chapter introduces RAP and CC materials in their general terms, and discusses some engineering findings on the materials reported in the literature. A technical description of RAP and CC and their current geotechnical applications in the U.S. are presented along with past experience with RAP and CC. A general background on MSE walls, the soil-reinforcement interface mechanism, and typical backfill requirements were provided, along with a broad overview of the current design criteria. Critical backfill properties and current MSE wall backfill specifications from TxDOT and FHWA were reviewed as the technical guidelines for material source selection, which will be discussed in Chapter 3.

Chapter 3. Test Materials and Index Properties

3.1 INTRODUCTION

Bulk CC and RAP samples were selected for this study based on their availability in Texas. There are large numbers of CC and RAP producers in Texas, many of whom were very much willing to cooperate in this study. However, it was important to select suppliers that provided materials that were representative of those available in the state. As a result, a state-wide survey with a list of production-related questions was created and distributed to all RAP and CC producers in Texas [Ogalla (2002)]. The survey responses were essential information for the preliminary screening process, in which the most cooperative sources were selected for further evaluation. These sources were asked to send representative samples periodically for an initial characterization, which measured the grain-size distribution, Atterberg limits, pH, and resistivity of each received sample.

The final selection of the CC and RAP material sources was completed using the information from the survey along with the index properties of the candidate materials that were measured during the initial characterization process. A conventional fill material (CFM) was also included in this study for comparison purposes. Twenty tons each of RAP and CC, and ten tons of CFM were delivered and stockpiled at the Pickle

Research Center in Austin, Texas. Index properties of the stockpiled materials were measured.

3.2 STATE-WIDE SURVEY

Because there are many CC and RAP producers in Texas, it was important to study the characteristic variability of RAP and CC between producers before selecting the sources of the test materials for subsequent studies. A state-wide survey was distributed in October 2000 to all possible RAP and CC providers, including both TxDOT districts and private companies that were willing to cooperate in this study. The following subsections describe the survey and the results obtained from this questionnaire study, as presented by Rathje et al. (2001) and Ogolla (2002).

The survey requested information regarding the type of recycled material produced and the annual production. The survey also requested information regarding the existence of stockpiles at their locations. The sources of the raw materials, the typical engineering applications for the product, and its maximum particle size were also requested. The maximum particle size of the recycled material was important because TxDOT has a maximum size limit for MSE wall backfill. Other information requested included: the physical and chemical tests performed and the willingness of the companies and districts to participate in this research project.

The survey was sent to a number of commercial producers and TxDOT districts. All companies and districts that did not respond to the survey were assumed to have no significant interest in the research project. Each source was contacted to ensure that all

surveys reached their intended destination to avoid the error of excluding sources that did not receive the survey. Eleven commercial producers responded by completing and returning the survey sheets, while eighteen survey sheets were returned from the twenty-five TxDOT districts.

Table 3-1 and 3-2 list the survey results from the TxDOT districts and the commercial producers, respectively. The survey results indicate that TxDOT districts typically produce RAP, with a few districts producing both RAP and CC. The maximum annual production of RAP from a single district was observed to be about 118,000 tons in the Corpus Christi district. The average annual RAP production based on TxDOT districts that responded to the survey is about 46,000 tons. The commercial producers that responded to the survey tended to produce both RAP and CC. The quantities produced by these companies were much larger than the TxDOT districts. Based on these survey results, Southern Crushed Concrete and Big City Crushed Concrete are the two largest commercial producers of RAP and CC in Texas, with a combined production of 3 million tons per year. It is observed that the main use of RAP and CC was for pavement construction.

Table 3-1 Survey results from TxDOT districts [after Rathje et al. (2001)]

TxDOT District	Product	Production (tons/year)	Stockpile	Sources of Raw Materials	Applications	Max. Size (in.)	Physical/Chemical Tests	Research Cooperation
Abilene	RAP	33,184	YES	NA	Pvmt, edge repair, hot or cold-mix aggregates	2	NO	
Amarillo	RAP	100,000	YES	Pavement	Pavement	3	Asphalt Content, Gradation	
Atlanta	RAP	25,000	YES		Geotechnical	3	AC, Pen Test, DSR	
Austin	RAP	10,000			Pavement		NO	NO
Childress		35,000	YES	Pavement	Pavement	2	NO	YES
Corpus Christi	RAP	59,000 to 118,000	YES		Pavement	1	NO	YES
Dallas	RAP/CC		YES	Pavement/ Commercial	Pavement/Flexible base	2/1.75	TEX-528C, 502C, 211F, 117E	YES
Fort Worth	RAP/CC	50,000/10,000	YES	Pavement	Pavement	2	Decant, Gradation	YES
Houston			YES	Pavement	Stabilized base, Asphalt mix, Conc.	2/1.75	Atterberg limits, Gradation	YES
Laredo					Pavement	1	NO	YES
Lubbock	RAP	10,000	NO		Pavement	1	NO	YES
Lufkin	RAP	12,000	YES		Pvmt, backfill	2	YES	YES
Odessa	RAP		YES		Pavement, backfill, edge, slopes	2	Phy. Prop. of asphalt in RAP	
Paris	RAP			Pavement	Pavement, backfill, edge, private drives		NO	NO
Tyler	RAP	100,000	YES		Pavement, Geotechnical	1		YES
Waco	RAP	100,000	YES		Pavement, edge, backfill	2	Gradation	YES
Wichita Falls	RAP	20,000	YES		Base material		NO	
Yoakum	RAP	15,000	YES		Pavement, backfill	2.5	NO	

Table 3-2 Survey results from Texas commercial producers [after Rathje, et al. (2001)]

Company	Location	Product	Production (ton/year)	Stockpile	Source of Raw Materials	Applications	Max. Size (in.)	Physical/Chemical Tests	Research Cooperation
Amarillo Road Co.	Amarillo	RAP/CC		NO	95% Pvmt, 5% structures	Pavement	2	Gradation	YES
Archer Western Cont.	Arlington	RAP		NO	Pvmt	Pavement	1.5	NO	YES
Big City Crushed Concrete, Inc.	Dallas	RAP/CC	1 million	YES	Pvmt, structures, bridges	Pavement, Geotechnical	3	pH, resistivity	YES
Cherokee Bridge & Road, Inc.	Junction								YES
Foremost Paving, Inc.	Weslaco	RAP	50,000	YES	Pvmt	Pavement	2	NO	YES
Frontera Materials, Inc.	Weslaco	RAP/CC	20,000	YES	90% Pvmt, 5% structures, 5% pipes	Structures, Pavement	2	Triaxial, Atterberg limits, Gradation	YES
Holms Construction Co., Inc.	Amarillo	RAP/CC	100,000	YES	Pvmt, sidewalks, conc. pvmt.	Pavement	3	NO	YES
J.H. Strain & Sons, Inc.	Tye		250,000	NO		Pavement	2	NO	NO
Jobe Concrete Products	El Paso	RAP/CC	200,000	YES	Pvmt	Pavement	2	Gradation, Atterberg limits	YES
Southern Crushed Concrete	Houston	RAP/CC	2 million	YES	Pvmt, buildings	Pvmt, Strct, Geotechnical	2.5	YES	YES
Valero Refining	Houston	CC	50	NO		Structures, Pavement		YES	NO

3.3 IDENTIFYING SOURCES OF TEST MATERIALS

To avoid variability of the test materials, it was important to select one source of RAP and one source of CC to be used as a representative recycled material for subsequent tests and investigations. Because there were so many producers willing to cooperate in the study, an initial screening program was initiated to further reduce the possible number of sources before final selection. Also, the initial screening would provide insight on the variability of the recycled materials between sources. The initial screening process included a series of measurements of material index properties: gradation, Atterberg limits, specific gravity, pH, and resistivity. These tests were performed by Ogolla (2002).

Big City Crushed Concrete and Southern Crushed Concrete had annual CC and RAP production of 1 million and 2 million tons, respectively. These two companies showed much interest in the research and were willing to provide samples for testing. Therefore, these two companies were selected as sources of recycled material for the characterization tests. The choice of the TxDOT district to be used in the project was heavily influenced by the interest in research on RAP by the Corpus Christi district. Corpus Christi reclaims numerous asphalt pavements each year and their production was expected to increase with time. Given this background, RAP from Corpus Christi was selected for the characterization tests.

Corpus Christi, Big City Crushed Concrete, and Southern Crushed Concrete were asked to periodically sample their products over a period of two months and ship their samples to the research facilities for the initial characterization tests. The purpose of these

screening tests was to determine the variation in properties and characteristics of the materials from different producers and at different times.

The characterization tests were performed by Ogolla in early 2001. Ogolla (2002) reported that all of the recycled materials from the different sources passed TxDOT Type B (for permanent walls) backfill gradation requirement (Figures 3-1 and 3-2) and had very similar characteristics (Table 3-3). Because the test results showed only a small variation between different sources, the final selection of the test materials was based simply on three decisive factors: (1) annual production from the survey results, (2) initial characterization test results, and (3) research cooperation from the districts and commercial producers.

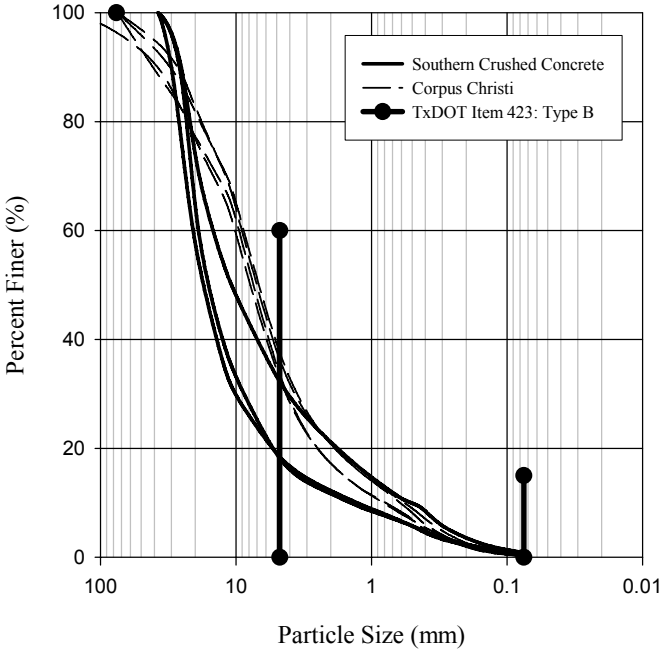

Figure 3-1 RAP gradations from the initial characterization

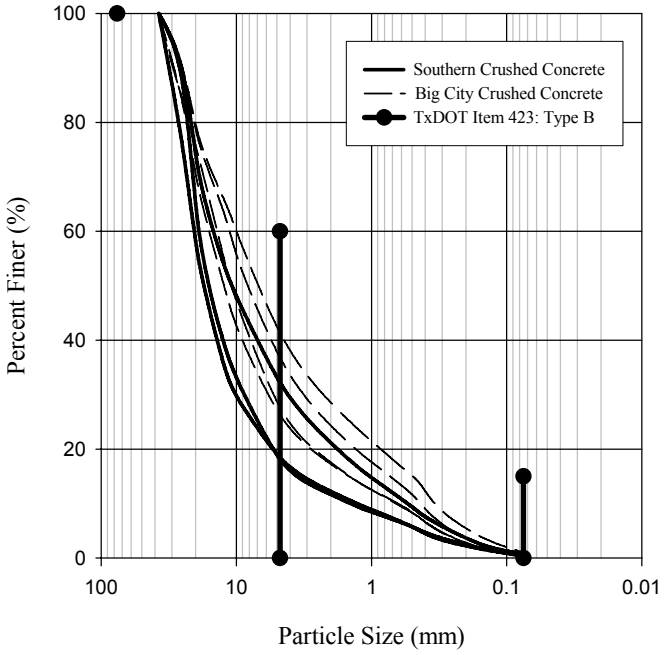

Figure 3-2 CC gradations from the initial characterization

Table 3-3 Summary of test results from the initial characterization [Ogolla (2002)]

Property	RAP		CC		TxDOT Specification (2004)
	Southern Crushed Concrete	Corpus Christi*	Southern Crushed Concrete	Big City Crushed Concrete	
Specific Gravity	2.40	2.25	2.59	2.64	
Liquid Limit	18	23	29	32	
PI	Non-Plastic	Non-Plastic	Non-Plastic	Non-Plastic	
pH	8.41	8.09	12.40	12.34	5.5 – 10
Resistivity (ohm-cm)	3750	4800	760	760	> 3000

Note: * Average value from four RAP stockpiles in Corpus Christi

The Corpus Christi district is one of the leading RAP producers in Texas, with an annual RAP production of about 59,000 to 118,000 tons. The identification of alternative uses of RAP has been an increasingly major concern for this district. For this reason, the Corpus Christi district was selected as the source of RAP for the detailed experimental study. The initial characterization test results indicate that the gradation, plasticity, pH, and resistivity of the RAP samples meet the TxDOT specifications for MSE walls. Moreover, Corpus Christi expressed a great interest in research on the uses of RAP because of the growing number of RAP stockpiles in the district.

Similarly, Big City Crushed Concrete was selected as the source of CC for further investigations. The company showed great willingness and cooperation in providing

information and samples for the research. The surveyed results indicate that Big City is a major producer of both CC and RAP in Texas, with and annual production of 1,000,000 tons/year. The results from the characterization tests show that the gradation and plasticity of CC samples meet the TxDOT specifications for MSE walls, while the measured pH and resistivity values fail the specification requirements. These two parameters are indicative of corrosivity of the material. Further investigations on the corrosive characteristics of CC and RAP were performed by another research team under the supervision of Dr. David Trejo at Texas A&M University.

After the initial characterization of RAP and CC was completed, it was decided that a conventional fill material (CFM) used in MSE walls should be included in the subsequent testing program for comparison purposes. Texas Crushed Stone, a local supplier located in Georgetown, Texas, was chosen as an economical supplier of CFM. This material is a quarried limestone and is similar to materials that have been used as backfill for a number of MSE walls in Texas.

3.4 INDEX PROPERTIES OF THE BULK SAMPLES

This section presents the test results from the index property measurements performed on the bulk samples of RAP, CC, and CFM used in this study. The source of the test materials was systematically selected as discussed in the preceding section. Approximately 20 tons of RAP and CC were delivered in May 2001 and 10 tons of CFM was received in August 2001. The bulk materials were separately stockpiled at the Pickle Research Center in Austin, Texas, with each stockpile placed on a sheet of heavy-duty

geotextile fabric to prevent undesirable conglomeration of test materials with the underlying soils. These three stockpiles were the only sources of the test materials for the subsequent experimental program. The index properties measured in this section include material gradation, pH, Atterberg limits, and specific gravity.

3.4.1 Grain Size Distribution

Grain size distribution was evaluated through a typical dry sieving method in which sieves ranging in size from 3 in. to sieve No. 200 (0.075 mm) were used. Test samples were taken at different locations of the material stockpiles to determine if there was any significant variation in gradation within the stockpile. Each sample weighed about 5000 g and was oven-dried overnight at the appropriate drying temperature (60°C for RAP samples, 110°C for CC and CFM samples). The samples were allowed to cool down at room temperature for two hours before the sieve analysis was performed by a mechanical sieve shaker. The percentage retained on each sieve size was recorded to the nearest 0.1%.

Figure 3-3 shows the grain size distribution of RAP samples taken from four different locations of the RAP stockpile. It can be seen from this figure that the grain size distribution of the RAP is very uniform over the stockpile. Less than 5% of the material is larger than 1.57 in. (40 mm) and no particles larger than 3 in. were observed. Only 2% of the material passes the No. 40 sieve (0.425 mm) and there are no fines passing the No. 200 sieve (0.075 mm). The USCS classification of this material is well-graded gravel (GW). Based on this gradation information, RAP is suitable for both the FHWA and TxDOT Type B backfill gradation requirements for MSE walls.

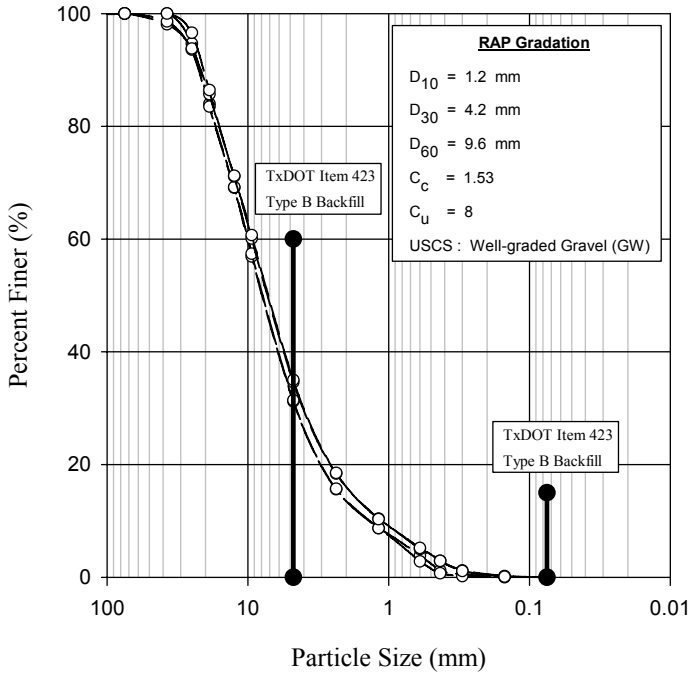

Figure 3-3 Grain size distribution of the RAP stockpile

Figure 3-4 illustrates the grain size distribution of the CC samples taken from four different locations in the stockpile. Again, the grain size distribution of CC is relatively uniform over the stockpile. Less than 5% of the material is larger than 1.57 in. (40 mm), and there are no particles larger than 3 in. Approximately 10% of the material passes the U.S. sieve No. 40 (0.425 mm), but no fines passing the No. 200 sieve (0.075 mm) were present. The USCS classification for this material is poorly-graded gravel (GP). Again, based on these measured gradations, the bulk CC satisfies both the FHWA and TxDOT Type B backfill material gradation requirements for MSE walls.

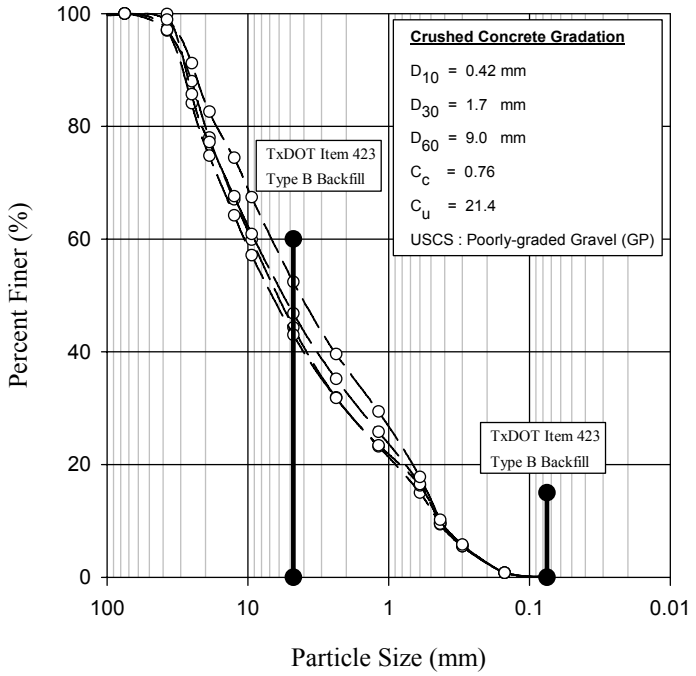

Figure 3-4 Grain size distribution of the CC stockpile

The sieve test results performed on four different CFM samples are shown in Figure 3-5. The results show that the grain size distribution of the CFM is fairly uniform over the stockpile. Less than 5% of the CFM is larger than 1.57 in (40 mm) and no particles are larger than 3 in. However, approximately 28% of the CFM passes the No. 40 sieve (0.425 mm) and about 10% of the CFM passes sieve No. 200 (0.075 mm). Thus, there are significantly more fines in the CFM than in RAP and CC. The USCS classification of this material is poorly-graded gravel (GP). Similarly, based on these measured gradations, the bulk CFM satisfies both the FHWA and TxDOT Type B backfill gradation requirements for MSE walls.

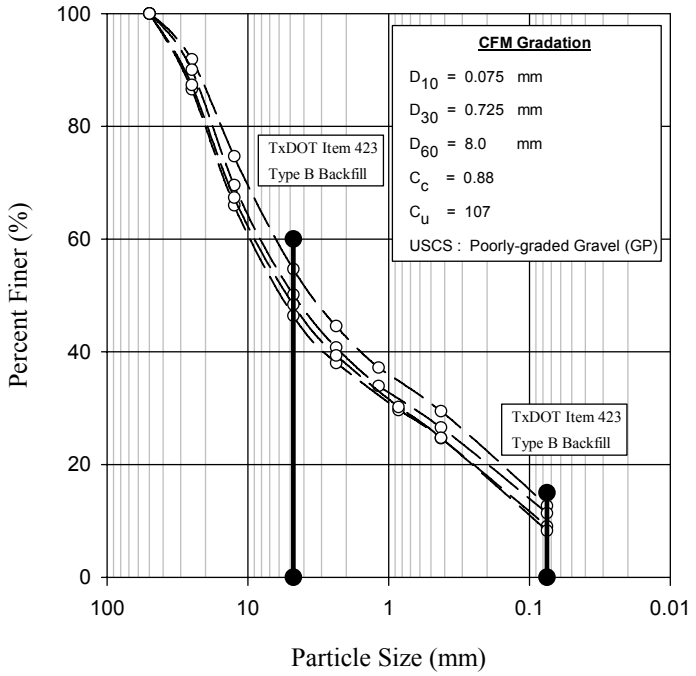

Figure 3-5 Grain size distribution of the CFM stockpile

Because of the different gradations of the stockpiled materials, a single reference gradation was proposed (Figure 3-6). Test specimens for subsequent investigations will be mixed to match this reference gradation. Using a single reference gradation will eliminate the effect of grain size distribution on future test results, thereby allowing tests to concentrate on the effects of the different composition of the materials. Figure 3-6 shows the proposed reference gradation and the average gradations of the material stockpiles. Key grain-size limitations of the reference gradation include limiting the maximum particle size to 2 in (50 mm), limiting the material passing the No. 40 sieve to 7%, and allowing no fines smaller than sieve No. 200. The USCS classification for the reference gradation is well-graded gravel (GW).

Compared with the average gradations of the material stockpiles, the reference gradation is similar to the RAP gradation but slightly different than those for CC and CFM. The CC gradation deviates from the reference gradation in the particle size range of 0.4 to 10 mm. The CFM gradation contains more small particles than the reference gradation with approximately 10% smaller than the U.S. sieve No. 200. As a result, when constructing CFM test specimens, the fines were discarded to conform with the proposed reference gradation.

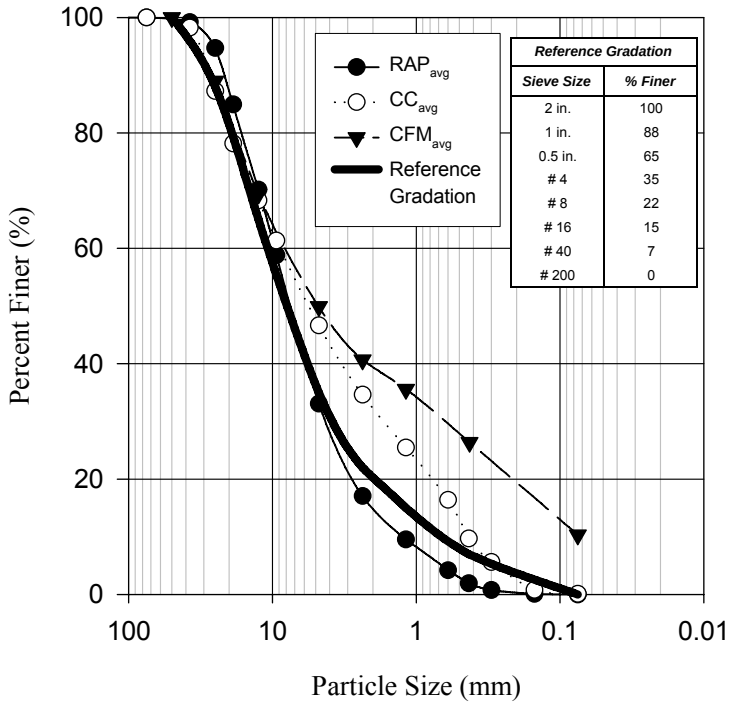

Figure 3-6 Proposed reference gradation for future tests

3.4.2 pH

The pH measurements of RAP-water and CC-water mixtures were performed in accordance with ASTM D 4972. Sample preparation begins by air-drying the test material at room temperature before sieving through a No. 10 sieve (2 mm) to remove the coarser fraction. Then, approximately 10 g of the prepared material is mixed thoroughly with 10 mL of distilled water in a glass beaker and then allowed to stand for one hour. The pH measurement is performed by immersing a pre-calibrated pH electrode into a material slurry solution for at least 30 seconds before a pH reading is taken to the nearest tenth of a whole number. Ten pH samples of RAP and CC were prepared and measured in this study. The test results indicate an average pH of 8.1 for RAP-water mixtures and 12.4 for CC-water mixtures. The pH level of RAP meets both the current TxDOT and FHWA backfill specifications for MSE walls (refer to Table 2-7), while the CC samples exceed the maximum pH requirement. Again, the effect of the material pH on MSE wall reinforcements will be investigated to a greater extent by a research group under the supervision of Dr. David Trejo at Texas A&M University.

3.4.3 Atterberg Limits

The liquid limit (LL) and plastic limit (PL) of RAP and CC were measured using the typical Atterberg Limits test method (ASTM D 4318) These results are used to calculate the plasticity index (PI = LL - PL) of the samples for comparison with the FHWA plasticity requirement (i.e. PI $\leq$ 6). Sample preparation includes sieving an air-dried material through a No. 40 sieve (0.425 mm) and using only the passing material for the tests. The prepared samples are mixed with a small amount of distilled water to form

a soil-water mixture close to the plastic limit state and then allowed to cure for 16 hours in a sealed container before the Atterberg Limits tests are performed.

After a significant number of attempts, RAP and CC samples could not be rolled into a $^{1}/_{8}$-in. (3.2 mm) diameter thread to determine the plastic limit, suggesting that RAP and CC are non-plastic materials (PI≈0) and therefore satisfy the FHWA requirement. For completeness, the liquid limit of the test materials were measured using the multipoint method and the results are plotted in Figure 3-7. Table 3-4 provides a summary of the Atterberg limits of RAP and CC.

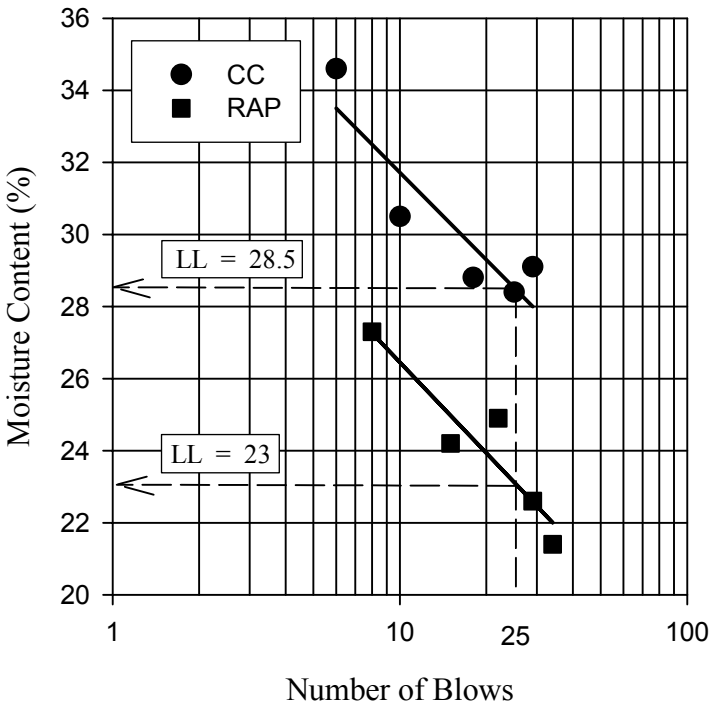

Figure 3-7 Liquid limits of RAP and CC using multipoint method

Table 3-4 Atterberg limits of RAP and CC

Plasticity Property	**RAP**	**CC**
Liquid Limit (LL)	23	28.5
Plastic Limit (PL)	indeterminable	indeterminable
Plasticity Index (PI)	non-plastic	non-plastic

3.4.4 Specific Gravity

Specific gravity (G_s) is defined as the ratio of the mass of a volume of solid particles to the mass of an equal volume of water. The specific gravity of soil solids is often needed for phase relationship calculations. The specific gravity of particles larger than the No. 4 sieve (4.75 mm) was measured using test method ASTM C 127, while the specific gravity of the smaller particles was determined by test method ASTM D 854.

The ASTM C 127 standard involves measuring the weight of a dry sample in the air and measuring the weight of the same material in the fully water-submerged condition. The resulting parameter is called the "apparent specific gravity" because it represents the specific gravity of the impermeable part of solid particles and does not account for any entrapped air voids. The apparent specific gravity is calculated as follows:

$$\text{Apparent Specific Gravity } (G_S) = \frac{A}{(A-C)} = \frac{V\gamma_{dry}}{V\gamma_w} = \frac{VG_s\gamma_w}{V\gamma_w} \qquad (1)$$

where: A = weight of oven-dry test sample in air

C = weight of saturated test sample in water

A – C = $V\gamma_w$ = weight of equal volume of water

For particles smaller than the No. 4 sieve, the ASTM D 854 test method is used. In this method, the specific gravity is still calculated as the ratio of the mass in the air of a given volume of soil to the mass of an equal volume of water. However, the mass of the equal volume of water is measured by considering the mass of a pycnometer flask filled completely with water and the same pycnometer flask filled with soil and water. The specific gravity is calculated with the following equation:

$$G_s = \frac{M_s}{M_s + M_{pw} - M_{pws}} \qquad (2)$$

where: M_s = mass of oven-dried soil

M_{pw} = mass of pycnometer filled with water

M_{pws} = mass of pycnometer filled with water and soil

To attain a proper specific gravity that represents the entire material, a weighted average of the specific gravities measured by ASTM C 127 and ASTM D 854 is

calculated. This weighted average is calculated by weighing each specific gravity by the percent of large and small particles, as shown in Equation 3.

$$(G_s)_{avg} = \frac{1}{\frac{P_1}{100G_1} + \frac{P_2}{100G_2}} \quad (3)$$

where: P_n = percentage by weight of each size fraction

G_n = appropriate specific gravity of each size fraction

Table 3-5 shows the specific gravity of all three materials obtained from this approach. It is observed that for each material, the large and small particles have very similar values of specific gravity. While CC and CFM have very similar values of specific gravity, the specific gravity of RAP is significantly smaller. The lower value of specific gravity for RAP is most likely due to the bitumen coating around the aggregates that creates a larger impermeable volume of solids and, thus, results in a smaller calculated specific gravity.

Table 3-5 Specific gravity of test materials

Specific Gravity	Material		
	RAP	CC	CFM
> No. 4 sieve*	2.36	2.62	2.64
< No. 4 sieve**	2.28	2.62	2.69
$(G_s)_{avg}$	2.33	2.62	2.66

Note: * Apparent specific gravity of coarse materials from ASTM C 127
** Specific gravity of fine materials from ASTM D 854

3.5 SUMMARY

A state-wide survey was used effectively as a first measure to assist in pre-selecting the possible sources of RAP and CC suppliers for this study. The results from the surveys also served as a good database on RAP and CC production in Texas and their current engineering applications. For each material, two candidate suppliers were asked to send their representative samples periodically for index property measurements. These samples showed only a small variation between the two suppliers and little variability over time. As a result, the suppliers of RAP and CC were chosen based upon their willingness to cooperate in the study. For RAP and CC, the chosen suppliers were the Corpus Christi district and Big City Crushed Concrete, respectively.

In 2001, the Corpus Christi district and Big City Crushed Concrete delivered and stockpiled the test materials at the Pickle Research Center in Austin, Texas. The index properties of the actual stockpiled materials were again measured. At this stage, the test results indicated that the RAP samples satisfied FHWA and TxDOT index property

requirements (i.e. gradation, plasticity, and pH). While the CC samples complied with the gradation and plasticity requirements, they exhibited large pH values that did not meet the current TxDOT and FHWA specifications. A single reference gradation curve was created for use in sample preparation for future test specimens. In addition, it was decided to include a conventional fill material (CFM) in this study for comparison purposes.

Chapter 4 Compaction Characteristics

4.1 INTRODUCTION

It is important to evaluate the compaction characteristics of RAP and CC because these materials may not exhibit typical moisture-unit weight compaction curves. In this chapter, conventional laboratory impact compaction was used to evaluate the compaction curves of RAP and CC, and to determine the dry unit weights to be used for sample preparation in the subsequent testing program. Potential particle breakdown of RAP and CC during compaction is also evaluated using the same impact compaction method. Excess fines generated during compaction may yield unsatisfactory shear strength and drainage performances of a backfill.

Field measurement of compacted density and water content is important for quality control and quality assurance during backfill construction. For the last 30 years the nuclear gauge has gained significant popularity among state Departments of Transportation (DOT's) when it comes to field density-moisture content measurements. The applicability of the nuclear gauge for compacted RAP and CC was included in this study because it is anticipated that the different chemical compositions of RAP and CC binder materials may cause unreliable nuclear gauge measurements.

4.2 LABORATORY COMPACTION

Compaction characteristics and moisture-dry unit weight relationships for all three test materials were measured in accordance with the Tex-113-E test method. In this test, soil is compacted in a compaction mold (6 in. diameter by 8 in. height) using a 10 lb hammer with a sector face dropped from a height of 18 in. Compaction is performed in 4 layers, with 50 blows of the hammer applied to each layer. With this compaction procedure, each sample receives a compaction energy of 22,900 ft-lb/ft^3. After the compaction is completed, the sample is weighed, extruded, and dried in the oven for water content determination. By knowing the weight of the moist sample, the volume of the compaction mold, and the compacted water content, the dry unit weight of each compacted sample is determined. The calculated dry unit weight and water content represent a single data point on the dry unit weight-water content relationship. Compacting material at various water contents is continued until a complete compaction curve is obtained.

For each test material, a representative sample taken from the stockpile was oven-dried overnight at an appropriate drying temperature. The oven-dried sample was sieved out to separate different particle sizes and then remixed again to match the reference gradation for the compaction tests. The resulting compaction curves of RAP, CC, and CFM samples are shown in Figure 4-1, 4-2, and 4-3. The zero air voids (ZAV) curve, representing 100% saturation, for the specific gravity of each material is shown on each plot.

The RAP compaction curve (Figure 4-1) indicates a slight peak in dry unit weight at 3% water content, with a slight reduction in dry unit weight at larger water contents. The compaction tests could not be performed at water content greater than 7% because a significant amount of water quickly escaped from the base of the mold before the compaction test could be completed. This observation indicates the large hydraulic conductivity and low water adsorption of RAP because of the bitumen coating. Based on this compaction curve, a water content of 3% and a corresponding dry unit weight of 117 lb/ft^3 were chosen as targets for future testing. In addition, this water content corresponds to about 30% saturation. Although this saturation level is low, it is a practical value because RAP samples could not be constructed at moderate to large water contents, as they would not hold water inside the specimen.

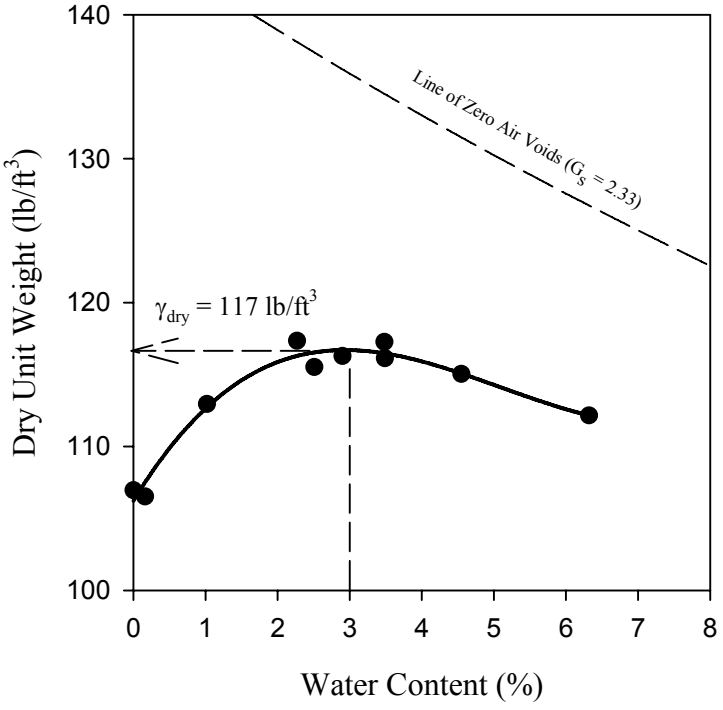

Figure 4-1 Compaction curve for RAP based on the Tex-113-E test method

The compaction curve for CC is shown in Figure 4-2. This plot indicates that the dry unit weight increases as water content increases from 0 to 12%. The dry unit weight remains relatively constant when the water content was greater than 10%; at this point the specimens were close to complete saturation. CC specimens could not be constructed at water contents greater than about 14% because excess water drained out of the compaction mold. The CC compaction curve does not exhibit a distinct peak, which is typical for gravelly soils because their density is not significantly sensitive to water content [Lambe and Whitman (1979)]. Therefore, a water content of 10% and the corresponding dry unit weight of 119 lb/ft^3 were chosen as targets for future testing. A water content of 10% corresponds to approximately 70% saturation. This value of water content represents a value that is practical to handle in the laboratory, while still yielding a moderate dry unit weight.

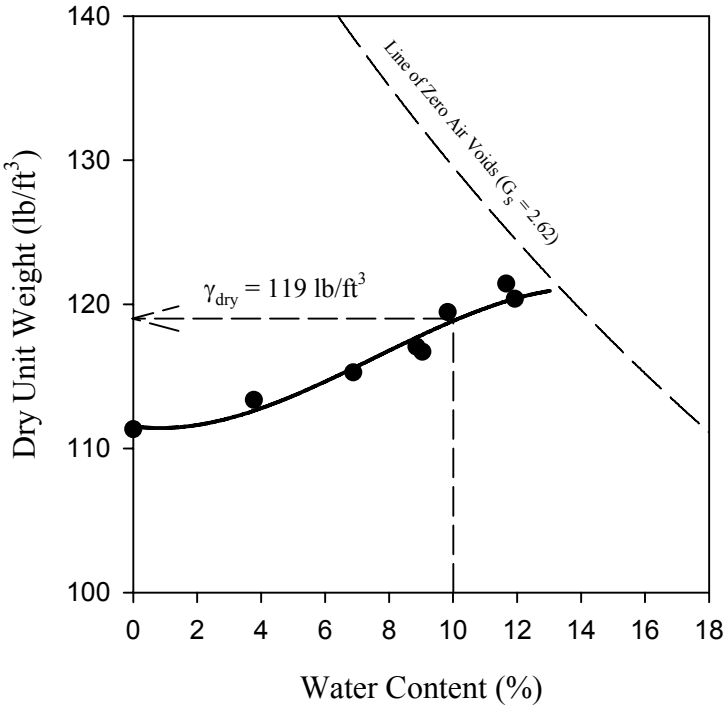

Figure 4-2 Compaction curve for CC based on the Tex-113-E test method

The compaction curve for CFM (Figure 4-3) is similar to the compaction curve for CC. The dry unit weight increases with increasing water content until a water content of about 11% is reached. All of the compaction tests at 11% water content resulted in dry unit weights that fell close to the zero air voids curve which is indicative of near complete saturation. Based on this compaction curve, a water content of 10% and a corresponding dry unit weight of 125 lb/ft^3 were chosen as targets for future testing. This water content corresponds to about 80% saturation. Finally, Table 4-1 summarizes the recommended water contents and expected dry unit weights for the test specimens of the future testing. Figure 4-4 shows a comparison of the compaction curves determined for all three test materials.

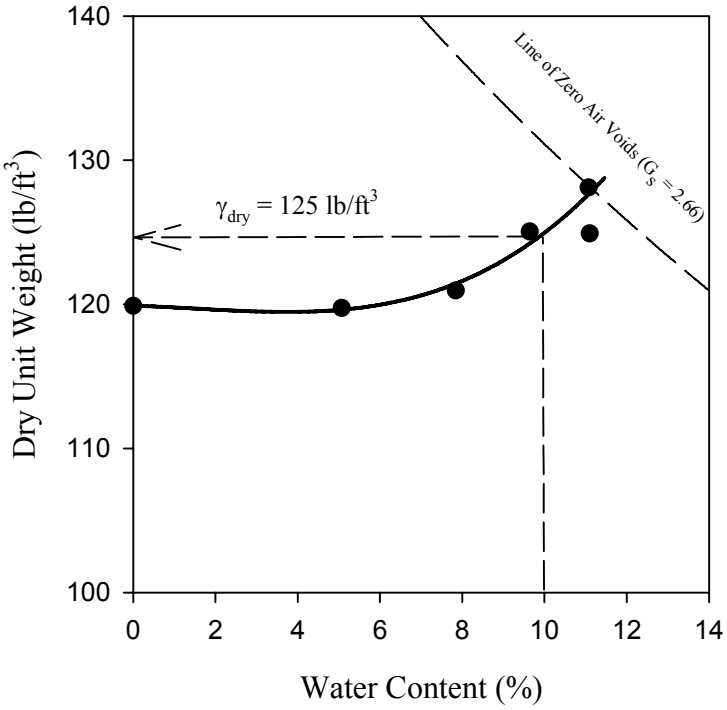

Figure 4-3 Compaction curve for CFM based on the Tex-113-E test method

Table 4-1 Recommended specimen water contents and dry unit weights

Material	**Recommended water content (%)**	**Expected dry unit weight (lb/ft^3)**	**Compacted void ratio (e_i)**	**Compacted degree of saturation (%)**
RAP	3	117	0.243	29
CC	10	119	0.374	70
CFM	10	125	0.328	81

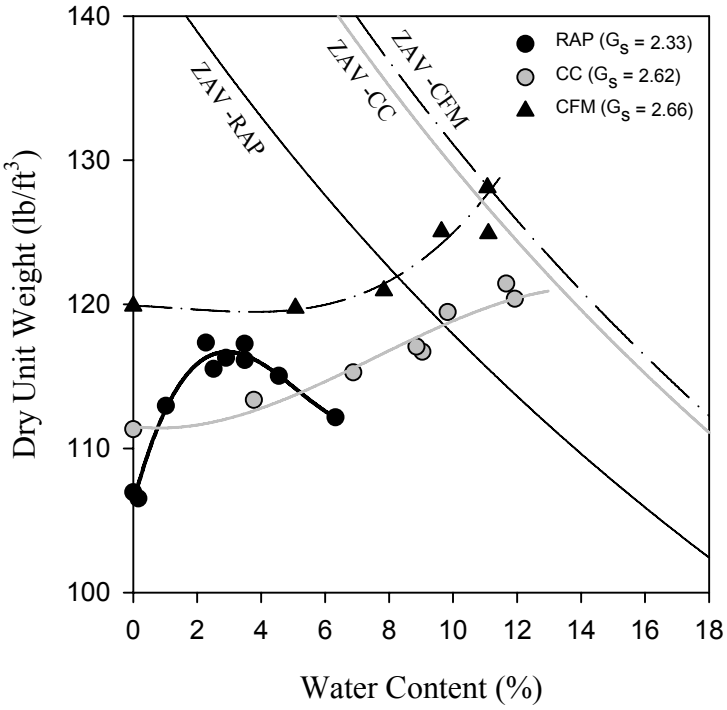

Figure 4-4 Comparison of compaction curves between test materials

Fines content (particles passing sieve No. 200) is a major factor in assessing the quality of backfill material. With crushed and recycled materials, additional fines may be created during compaction when larger particles in the material are crushed. The potential degradation of RAP, CC, and CFM was evaluated by simple impact compaction. Though impact compaction may not completely mimic the true compaction mechanism that happens in the field, the simple laboratory compaction would provide insight into the relative potential for material breakdown. Five samples of each test material were mixed to match the reference gradation and the recommended water content. The material was then subject to impact compaction following the Tex-113-E test method. The grain size distribution curves of the test materials before and after compaction are shown in Figure

4-5. Each curve represents the average grain size distribution of multiple test specimens. Based on the results shown, RAP and CC appear to exhibit lower particle breakdown potential compared with the CFM. The increase in fines content for RAP (0.6%) and CC (1.6%) is less than half of that for CFM (3.6%). This finding suggests that RAP and CC are not likely to produce a significant amount of fines during field compaction.

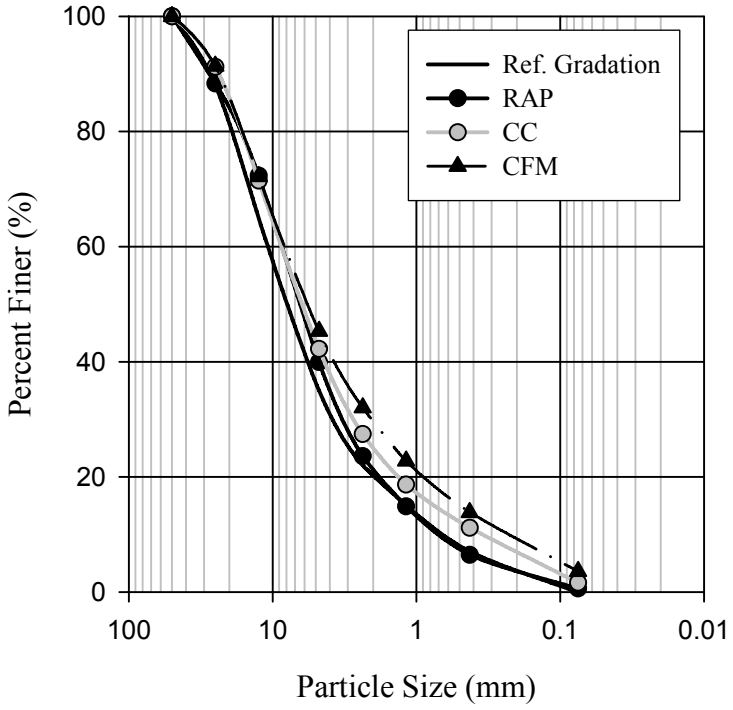

Figure 4-5 Grain size distribution of materials after compaction

4.3 FIELD COMPACTION CONTROL

Control of backfill compaction during construction of an MSE wall is critical for proper wall performance. The water content during compaction and the compacted density affect the permeability, compressibility, and shear strength of the material, as well as the pullout capacity of the reinforcing elements in the fill. For granular materials, a greater compacted dry unit weight yields a stronger, less compressible material. For backfill materials with significant fines, relatively small variations in compaction water content can adversely affect backfill drainage, compressibility, shear strength, and reinforcement capacity. Moreover, backfills that are too wet during MSE wall construction can make it difficult to maintain acceptable facing alignment, whereas materials that are compacted too dry may experience excessive settlement upon subsequent wetting [Elias and Christopher (1996)].

Because the compacted dry unit weight and moisture content are critical to the performance of an MSE wall, field density measurements should be performed on a regular basis during backfill construction. For the construction of highway fills, the nuclear gauge is widely used to measure in-place density and moisture content. The nuclear gauge is popular primarily because the test results can be obtained rapidly. Figure 4-6 shows the equipment needed for a typical nuclear gauge test performed in the field. This section describes an experimental investigation conducted to study the accuracy of the nuclear test method in measuring the in-place density and water content of CC, RAP, and CFM. The following sections describe the test methods for measuring field density and water content, the experimental program utilized in this study, and the test results.

Figure 4-6 Nuclear gauge testing for field compaction control

4.3.1 Field Density Measurement Methods

Sand cone and rubber balloon (volumeter) methods have long been used to measure the in-place density of compacted material. These conventional methods require manual excavation of a small test hole and are somewhat time consuming. Water contents are obtained by drying the excavated material in an oven, a step that normally takes 12 to 24 hours and significantly delays the final test results. The nuclear gauge, introduced in the 1950's, provides a more rapid means of measuring in-place density and water content. Much research has been conducted to study the correlation between densities and water contents measured by the nuclear gauge and those measured by conventional methods [e.g. Burati and Elzoghbi (1987), Mamlouk (1988), Kennedy et al. (1989), Sanders et al. (1994), Nagi and Whiting (1999)]. The following sections describe testing procedures for

the sand cone, rubber balloon, test pit, and nuclear gauge tests. The advantages and disadvantages of each method are also discussed.

4.3.1.1 Sand Cone Method (ASTM D 1556)

The sand cone test method is generally accepted as an accurate means of measuring in-place soil density [Mamlouk (1988)]. The test is performed by first excavating a hole in the test material. The excavated material is weighed and stored in a container for later moisture content determination. A dry, uniform reference sand with a known density is then poured into the hole. The weight of the sand placed in the hole is measured and, knowing the density of the reference sand, the hole volume can be determined. The moist density is calculated from the weight of excavated material and the hole volume, while the dry density is computed from the measured moist density and water content.

The sand cone method takes a substantial amount of time (approximately 10 minutes per test), and the water content must be determined by oven drying. Further, the sand cone method is limited to soils that are stiff enough for an excavated hole to remain open without significant deformation or volume change during the test. In addition, this test works best in unsaturated soils where water will not seep into the excavated hole. One further drawback is the inevitable mixing of the reference sand with the test material after the test is completed.

4.3.1.2 Rubber Balloon Method (ASTM D 2167)

The rubber balloon method is similar to the sand cone method. However, instead of pouring a reference sand into the excavated hole, the hole volume is measured with a water-filled balloon under a calibrated operating pressure. The volume of the water required to fill the hole, and thus the hole volume, is determined from a graduated cylinder. With the volume of the hole and weight of excavated material known, the in-place density of the test material can be calculated.

One of the potential problems associated with the rubber balloon method is the deformation of the excavated hole during the application of the operating pressure. Expansion of the hole is more pronounced when testing materials that are relatively soft or deformable. Inaccurate results can also be attributed to the presence of rocks or coarse particles that make the sides of the hole irregular, as rough sides make it difficult for the balloon to fill the entire hole. Moreover, the test can be difficult to perform in materials containing sharp particles that may puncture the rubber balloon. The rubber balloon method is also time consuming, taking up to about 10 minutes to perform one test. Again, water contents must be determined by oven drying.

4.3.1.3 Test Pit Method (ASTM D 5030)

The test pit method is based on the same principle as the rubber balloon test, but the excavated size is significantly larger. In general, the test pit method involves excavating the test location and replacing the existing soil with a known amount of water. This step determines the volume of the excavation. And hence by knowing the volume

and the weight of the soil excavated, the in-place moist density can be calculated. This method typically is used for materials that contain particles larger than 3 in. The test pit method is reasonably simple and straightforward, but it is more time consuming (approximately 30 minutes per test) than the other two methods because of the larger excavation required.

4.3.1.4 Nuclear Gauge Method (ASTM D 2922 and ASTM D 2950)

Over the last 50 years, the nuclear gauge has become a popular tool for measuring soil compaction, and it has also been used to evaluate asphalt and concrete density. The test method is rapid (less than 5 minutes per measurement) and allows repetitive measurements to be made at a single test location. A nuclear gauge obtains concurrent, independent measurements of the moist density and water content of the compacted material. For density measurements, the device employs a small gamma radiation source and one or more gamma photon detectors. The moisture content determination involves a fast neutron source and a thermal neutron detector. There are two methods of operation for the nuclear gauge, routinely referred to as the "direct transmission" method and "backscatter" method.

For direct transmission, a rod containing a cesium-137 source is lowered to a predetermined depth (Figure 4-7a). Gamma photons emitted by the source travel through the material to the detector, which is located at the base of the nuclear gauge. The density measured by this mode is representative of the material density in the path between the source and the detector [Regimand and Gilbert (1999)].

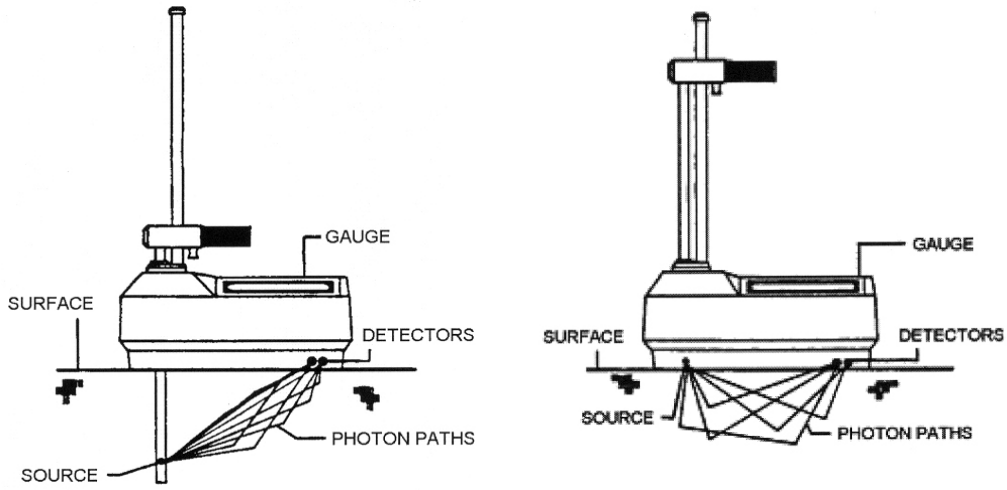

(a) (b)

Figure 4-7 Nuclear gauge setup: (a) direct transmission method and (b) backscatter method [from Troxler (2001)]

For the backscatter mode, the cesium-137 source is placed on the surface of the test material (Figure 4-7b). The gamma photons are introduced into the material and must be reflected to reach the detector [Troxler (2001)]. Because the measured photons are reflected, the average energy of the photons detected by this method is usually lower than the average energy of the photons detected by the direct transmission method. The density measured in the backscatter method is representative of the average density of the material near the surface.

The nuclear gauge measures density indirectly by counting the emitted gamma photons that reach the detector. While traveling through the soil from the source to the detectors, the gamma photons collide with electrons present in the material. These collisions reduce the number of the photons that reach the detectors. Consequently, the

number of gamma photons reaching the detectors is inversely proportional to the material density. The number of detected gamma photons is usually referred to as the “count ratio”. A calibration chart that relates count ratio to material density is used to determine the material density during testing.

The chemical composition of the material being tested may affect the measured densities, because elements with high atomic numbers will absorb more photons [Nagi and Whiting (1999)]. Therefore, a calibration developed from one type of material may not yield an accurate result if it is used to measure density in a different type of material. For that reason, some researchers have recommended that a calibration curve be developed for the particular material to be tested [Kennedy et al. (1989), Nagi and Whiting (1999)].

To measure water content, the nuclear gauge emits neutrons, usually from an americium-241 source, into the test material. These neutrons are uncharged and collide with the nuclei of other atoms, which reduces their velocity to a minimum. Neutrons traveling at this minimum velocity are called "thermalized" neutrons. Hydrogen nuclei are most efficient in thermalizing neutrons, so the number of thermalized neutrons is proportional to the mass of hydrogen in the material [Nagi and Whiting (1999), Troxler (2001)]. Thus, by counting the thermalized neutrons that reach the detector, one obtains a measure of the number of hydrogen atoms in the material. It is important to note that this procedure yields a measure of the number hydrogen atoms present, not the number of water molecules [Nagi and Whiting (1999)]. This procedure will cause errors when

measuring the water content of materials that contain significant sources of hydrogen other than water.

4.3.2 Field Testing Program

In this study, field tests were performed to evaluate the suitability of the nuclear gauge for routine density and moisture content measurements of CC and RAP during MSE wall construction. More specifically, the study was performed to determine if the elemental composition of CC and RAP affects the accuracy of the nuclear gauge. Tests in a CFM stockpile were also conducted for comparison purposes.

The experimental program was performed on the three material stockpiles located at the Pickle Research Center at the University of Texas at Austin. These stockpiles (Figure 4-8) are the sources for samples to be tested in other phases of this study. A front-end loader was used to level off the top of each stockpile, while maintaining a minimum height of about 2 ft within the stockpile (Figure 4-9). The same front-end loader was driven back and forth on the stockpiles to introduce some degree of compaction in the material. The surfaces of the stockpiles at each test location were leveled using a straight edge. The test locations on the CFM, CC, and RAP stockpiles are shown in Figures 4-10, 4-11, and 4-12, respectively. Before testing, water was introduced to vary the water content at each test location.

Figure 4-8 Test material stockpiles at Pickle Research Center, Austin, TX

Figure 4-9 Light compaction of the test site using a front-end loader

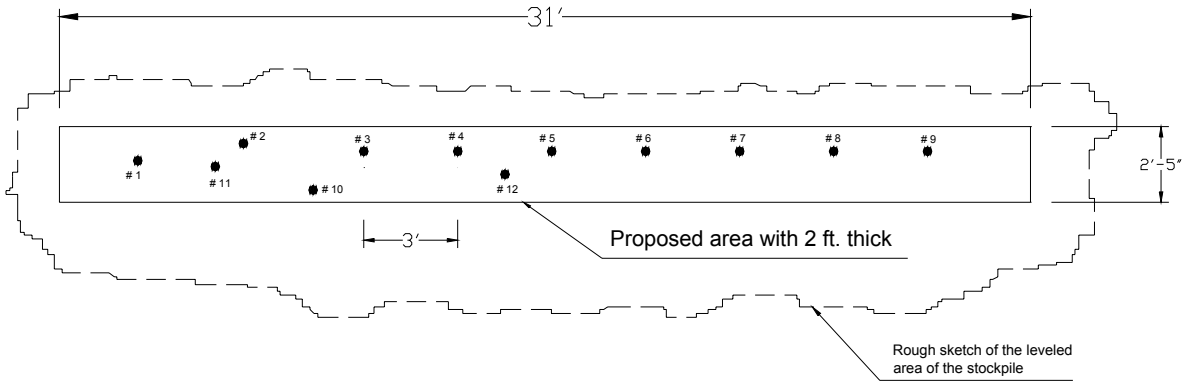

Figure 4-10 RAP stockpile and test locations

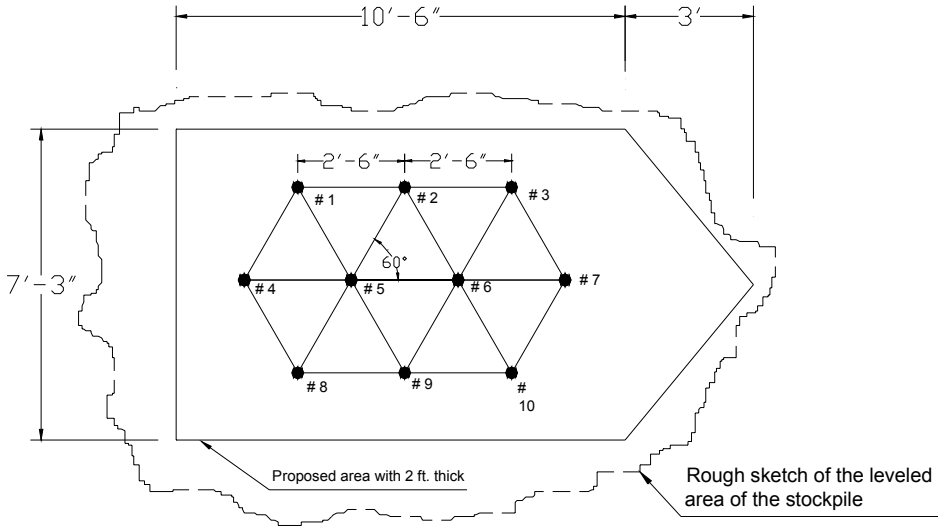

Figure 4-11 CC stockpile and test locations

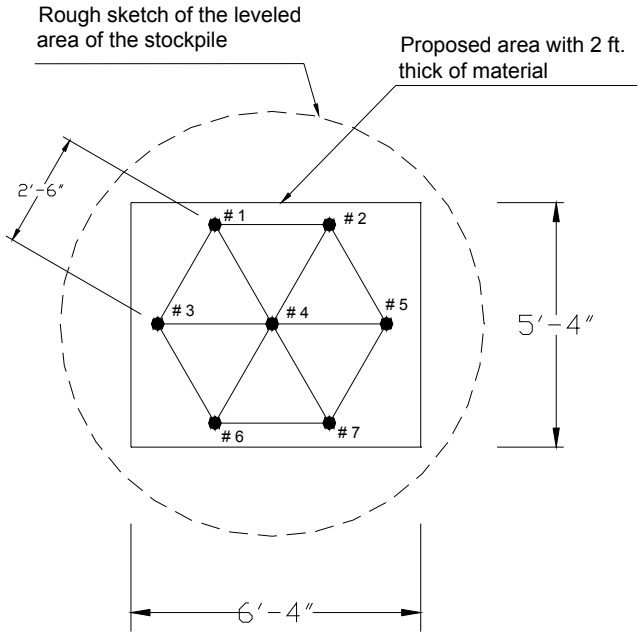

Figure 4-12 CFM stockpile and test locations

The experimental program was designed to compare moist densities measured by the nuclear gauge with moist densities obtained from the conventional rubber balloon method. For these tests, the rubber balloon method was selected over the sand cone method to avoid mixing sand into the stockpiled material, which will be used in other tests later in this study. Moisture contents obtained with the nuclear gauge were compared to water contents measured by drying the excavated material overnight in an oven (about 105°C for CC and CFM, 60°C for RAP). Nuclear gauge testing (Figure 4-13) was performed on October 9, 2001, by Trinity Engineering Testing Corporation of Austin, Texas.

Figure 4-13 Nuclear gauge testing on material stockpile

The moist density and water content were measured at each test location with the nuclear gauge. For this experiment, the direct transmission mode was used because it yields more accurate results [Troxler (2001)]. Before performing each test, a scraper plate and guide rod were used to prepare the test location and drive a hole for the instrument rod. The radioactive source on the instrument was then advanced in the hole to a depth of 6 in.

Immediately after the nuclear gauge was removed from the test location, a rubber balloon test was performed. As shown in Figure 4-14, a 4 in. diameter hole was excavated to a depth of about 5 in., with the center of the 4-in diameter hole lying directly

between the previous locations of the radioactive source detector. The excavated materials were weighed and stored in containers for moisture content determination through oven drying. The volume of the excavated hole was then measured using a rubber balloon apparatus, with a pre-calibrated operating pressure of 4 psi, as seen in Figure 4-15.

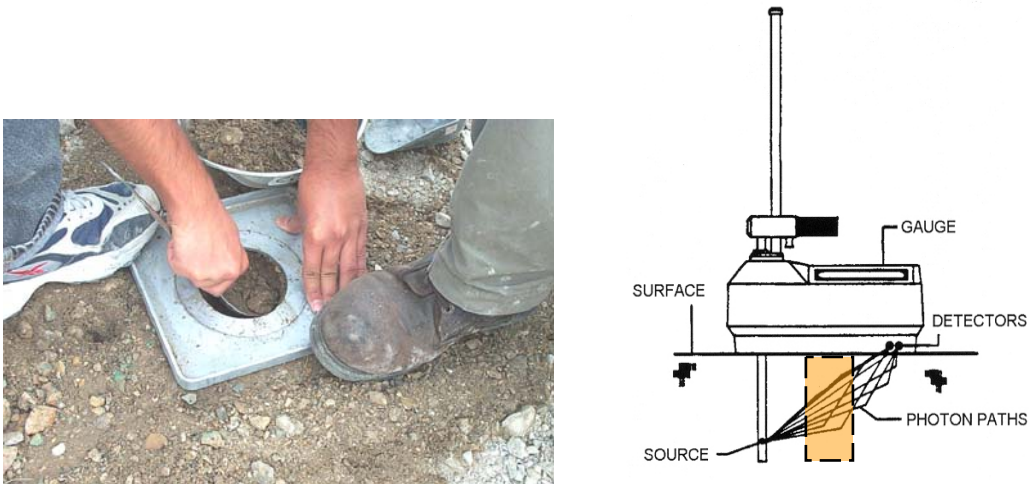

Figure 4-14 Hole excavation for rubber balloon test and its location

Figure 4-15 Rubber balloon test performed on material stockpile

4.3.3 Test Results and Discussions

The nuclear gauge and rubber balloon methods were used to measure moist densities and water contents at seven to ten locations within each stockpile. The measurements are compared below.

4.4.3.1 Moist Density Test Results

The moist densities for the CFM, CC, and RAP as measured by the nuclear gauge and rubber balloon method are compared in Figure 4-16. It can be seen that the moist density measured by the nuclear gauge was consistently larger than the moist density measured by the rubber balloon method for all of the test materials. For each material, the

nuclear gauge shows a relatively small variation in the measured densities with all values within ±5% of each other, suggesting that all three stockpiles had a fairly uniform density, while the moist densities measured by the rubber balloon method scatter significantly. Furthermore, the moist densities measured from the rubber balloon method were much smaller than those from the nuclear gauge. This observation is consistent across all of the materials.

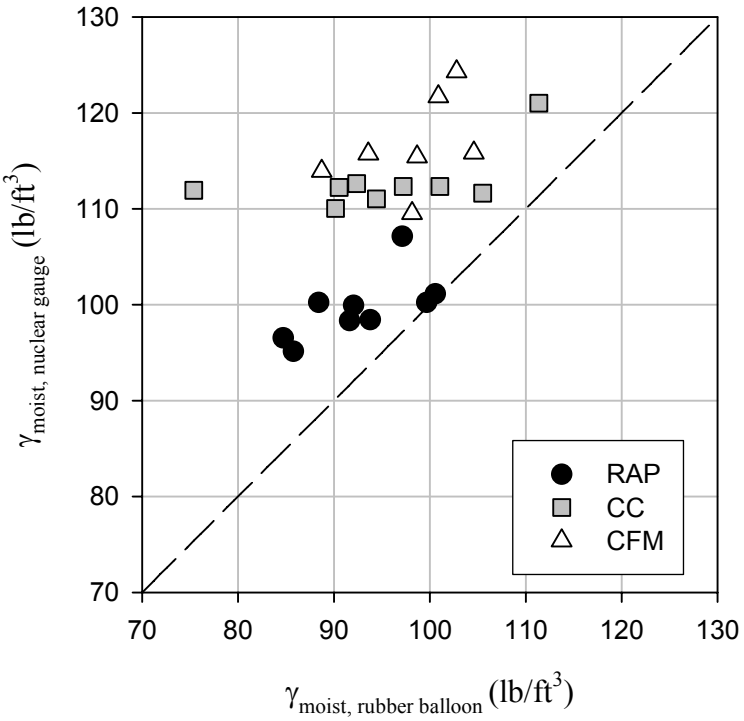

Figure 4-16 Comparison of moist densities measured by rubber balloon and nuclear gauge methods in all three material stockpiles

A comparison of these data can be made in terms of the ratios between the values measured from the nuclear gauge ($\gamma_{m,NG}$) and the values obtained from the rubber balloon method ($\gamma_{m,BAL}$). Table 4-2 shows the average ratio and standard deviation of the ratios of

each material tested, as well as the minimum and maximum ratios. On average, the nuclear gauge reports moist densities nearly 20% higher than the rubber balloon method for CFM and CC. For RAP, the nuclear gauge is about 10% higher. The scatter in the data is most significant for the CC. These differences are larger than reported in other studies that found the nuclear gauge only slightly overpredicted density [Kennedy et al. (1989), Sanders et al. (1994)].

Table 4-2 Ratio of moist densities measured by nuclear gauge ($\gamma_{m,NG}$) and rubber balloon method ($\gamma_{m,BAL}$)

Ratio		**RAP**	**CC**	**CFM**
$\frac{\gamma_{m,NG}}{\gamma_{m,BAL}}$	Average	1.08	1.19	1.19
	Std. Dev.	0.05	0.13	0.06
	Min. to Max.	1.01 to 1.14	1.06 to 1.48	1.11 to 1.28

The discrepancies in the test data could be attributed to several factors. It is possible that the soil used to calibrate the nuclear gauge was significantly different from the materials used in this study, making the calibration less accurate. As mentioned previously, calibration of the nuclear gauge with one material may not be appropriate for other materials. For this reason, a calibration curve should be developed for the particular materials on site to ensure accurate results. This is most critical when the test material contains high atomic number elements that can affect the gauge count [Nagi and Whiting

(1999)]. CC and CFM are most susceptible to this type of error, because calcium ions (Ca^{2+}) are one of their key chemical compositions.

Other factors may have contributed to the differences in the measured densities. The excavated hole may have expanded under the applied operating pressure during the rubber balloon test. Deformation of the hole would lead to a larger measured excavation volume and result in an artificially lower soil density. The measured densities from the rubber balloon method are all lower than those from the nuclear gauge, indicating this error is consistent with the measured densities. However, the field material was stiff and most likely did not deform significantly under the balloon pressure.

The presence of large-sized particles is also another factor that may have contributed to the observed differences. When the test material contains large particles or large voids, irregularities may occur in the source-detector path and cause higher or lower measured densities, respectively. To minimize this problem, per ASTM D 2922, multiple nuclear gauge tests should be run at adjacent locations to get an average. However, considering the manner in which the stockpiles were compacted, the nuclear gauge data in Figure 4-16 exhibit relatively limited scatter, especially for the RAP and CC.

Large particles may also affect the rubber balloon test results if the excavated hole is too small to adequately sample all particle sizes. ASTM D 2167 specifies larger excavation volumes for materials containing larger particle sizes. For the maximum particle size of the test materials in this study (2 in.), ASTM D 2167 recommends a minimum excavation volume of 2840 cm^3. Unfortunately, the rubber balloon apparatus used in this study could accommodate volumes only up to 1420 cm^3, not large enough for

the particle size distribution of the test materials. These issues may have adversely affected the densities measured with the rubber balloon method.

The possible effect of large particle sizes on the rubber balloon densities was studied further by comparing the moist densities measured using the test pit method with moist densities measured by a rubber balloon device. Nine test locations were chosen on newly re-compacted stockpiles of RAP and CC for this comparison study. At each test location, a rubber balloon measurement was first performed, followed promptly by a test pit measurement at the same location (Figure 4-17). Moist densities measured from both methods are compared in Figure 4-18. The comparison plot shows that seven out of nine rubber balloon test results are lower than the densities measured by the test pit method. On average, the rubber balloon densities are 10% lower. This result suggests that the undersized holes excavated for the rubber balloon test did not adequately sample all of the particle sizes. Also, the results suggest that the type of test material did not affect the discrepancies.

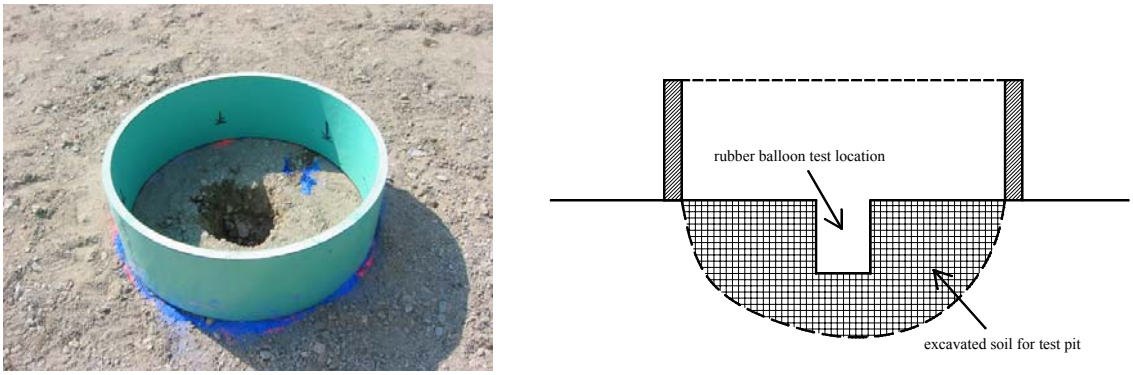

Figure 4-17 Test pit performed over a previously rubber balloon-tested location

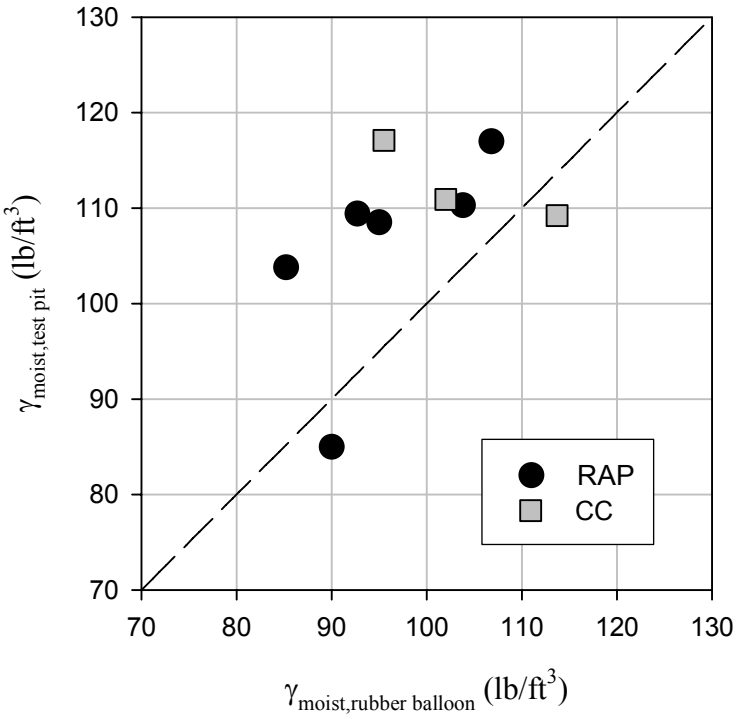

Figure 4-18 Comparison of moist densities measured by rubber balloon and test pit methods

Finally, a direct comparison between nuclear gauge and test pit measurements was performed to identify the suitability of the nuclear gauge device for RAP and CC density measurements. Additional measurements were performed on the CC and RAP stockpiles using the test pit and nuclear gauge methods. At each test location, a nuclear gauge measurement was immediately followed by a test pit measurement. Moist densities measured from these two techniques are compared in Figure 4-19. The nuclear gauge still reported larger moist densities (approximately 2% larger for CC and 6% larger for RAP, on average), but the difference was less than indicated by the rubber balloon and nuclear gauge comparisons (Figure 4-16). Hence, it is most likely that the inadequate size of the rubber balloon excavation was the contributing factor for the differences found earlier.

Assuming that all the test pit measurements were accurate, this last set of test results suggest that the nuclear gauge, when well calibrated, can be an adequate density measuring device for RAP and CC backfill.

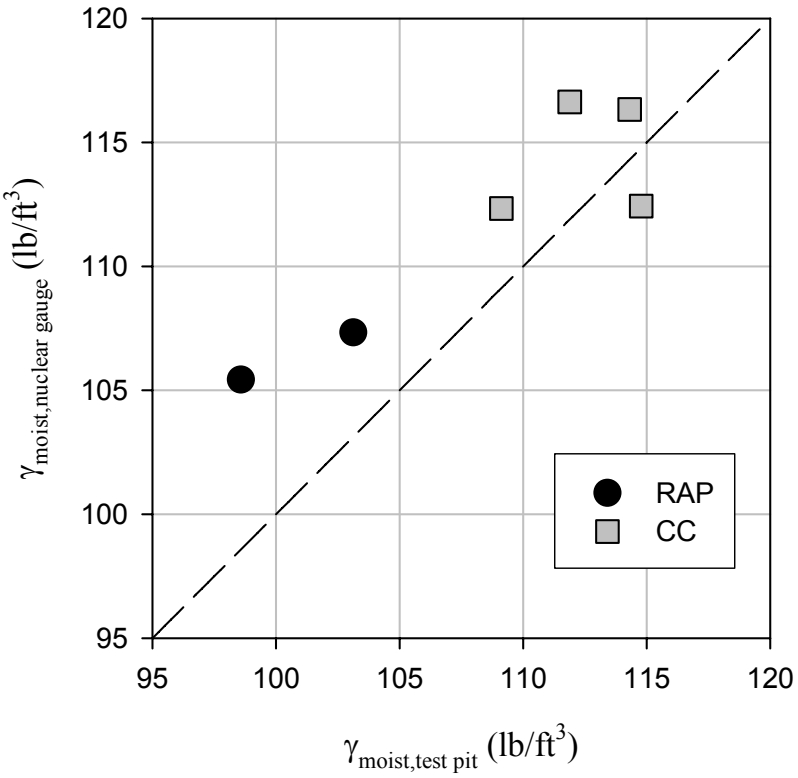

Figure 4-19 Comparison of moist densities measured by test pit and nuclear gauge

4.4.3.2 Moisture Content Test Results

Moisture contents measured by the nuclear gauge and oven drying for RAP, CC, and CFM are compared in Figure 4-20. The ratios of water contents measured by the two methods for each material are given in Table 4-3. The nuclear gauge gives acceptable

water contents for the CFM as compared to the oven-dried values, with an average ratio of 0.99. Moisture contents measured by the nuclear gauge for CC are somewhat higher (about 20% higher, on average) than the values measured by oven drying. For RAP, the nuclear gauge moisture contents are considerably higher. On average, the nuclear gauge reports water contents in the RAP that are three times as large as obtained from oven drying.

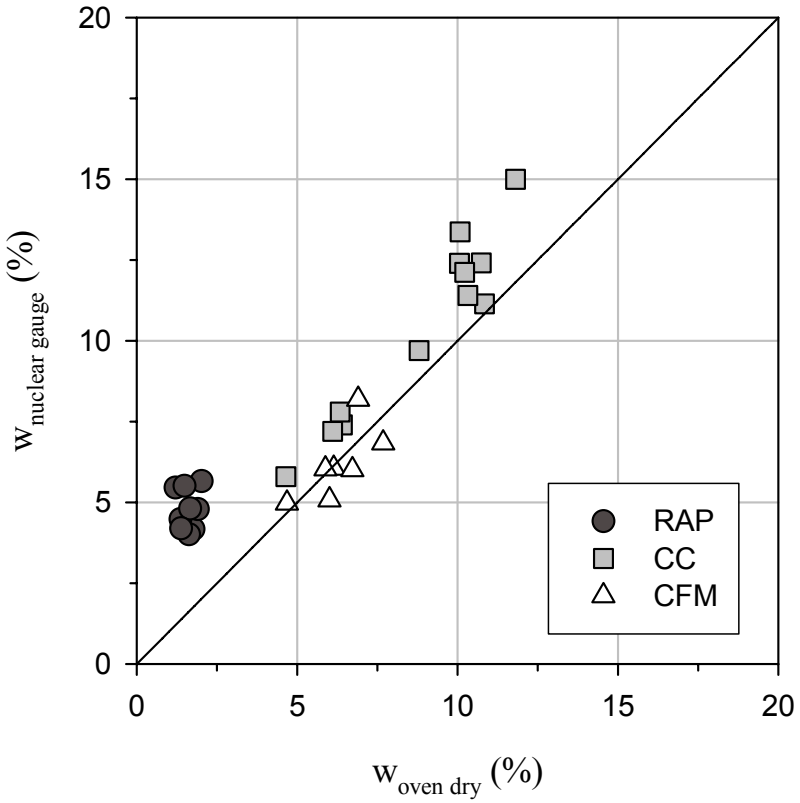

Figure 4-20 Comparison of the moisture contents measured with the nuclear gauge and oven drying

Table 4-3 Ratio of moisture contents measured by nuclear gauge (w_{NG}) and oven drying (w_{oven})

Ratio		**RAP**	**CC**	**CFM**
$\frac{w_{NG}}{w_{oven}}$	Average	3.07	1.19	0.99
	Std. Dev.	0.69	0.10	0.12
	Min. to Max.	2.36 to 4.51	1.03 to 1.33	0.84 to 1.19

The overestimation of the moisture content in the CC and RAP is a result of the nuclear gauge measuring the amount of hydrogen atoms in the material, and not the amount of water. The slightly higher measured water contents in CC may be the result of additional hydrogen atoms in the admixtures, modifiers, and cement paste [Nagi and Whiting (1999)]. For RAP, there are two potential sources of hydrogen other than free water in the mix. Excess hydrogen atoms can be found in the asphalt cement binder and within the minerals of the aggregates [Black (1995)]. The asphalt cement binder, a petroleum product comprised of a mixture of hydrocarbon molecules, is the main source of excess hydrogen atoms in RAP. Therefore, these excess hydrogen atoms from the asphalt cement binder lead to the overestimation of water content as measured by the nuclear gauge.

Because the elemental composition of the fill material affects the moisture contents determined by the nuclear gauge, separate calibrations for RAP and CC are needed to obtain accurate measurements of the compaction water content. Because the

measurements for RAP appear to be very sensitive to the hydrogen content of the asphalt, it may not be feasible to develop a generic calibration for measuring the compaction water content of RAP with the nuclear gauge method. Rather, field calibrations at each project site may be necessary to obtain reliable water contents in RAP from the nuclear gauge device.

4.4.4 Conclusions from Field Compaction Control Tests

The suitability of the nuclear gauge to measure the moist density and water content of CC, RAP, and a crushed limestone CFM was evaluated in a series of field tests on all three material stockpiles. The nuclear gauge consistently measured larger densities than the rubber balloon method, most likely because the excavated holes used in the rubber balloon tests were not large enough given the maximum particle size of the test materials. Given the uncertainty associated with the rubber balloon measurements, it is difficult to conclusively determine the accuracy of the nuclear gauge data in these evaluation tests. However, the nuclear gauge appears to provide adequate density values.

Elemental composition of the material can have a major influence on the moisture content measured by the nuclear gauge. Because the nuclear gauge actually measures hydrogen atoms rather than free water molecules, the water contents measured by the nuclear gauge were larger than the oven-dried values for CC and RAP. This effect was particularly pronounced in the RAP, where large amounts of hydrogen are contained within the residual asphalt binder.

Overall, the test results indicate that the nuclear gauge measurements are material dependent. Because there are many factors affecting nuclear gauge measurements,

frequent field verification of nuclear gauge results are recommended. Separate calibrations should for developed for RAP and CC, especially for determinations of water content from the nuclear gauge method.

4.5 SUMMARY

Compaction curves for all three test materials were developed using the Tex-113-E test method. The compaction curves were used to recommend water contents and corresponding dry unit weights for each material for future sample preparation. Potential degradation of RAP and CC after compaction was evaluated using the Tex-113-E test method and the results showed that RAP and CC are less degradable than the CFM. A field test study was performed on lightly-compacted material stockpiles to evaluate the effectiveness of the nuclear gauge to measure moist densities and water contents of RAP and CC. The results showed that a nuclear gauge can measure moist density with an acceptable accuracy. However, when dealing with moisture content determination, excess hydrogen atoms other than those from the water molecules caused the nuclear gauge to overestimate the moisture content of the compacted material. Therefore, it is recommended that pre-calibration of the nuclear gauge with the target material prior to performing the measurement is critical for these materials.

Chapter 5. Shear Strength, Hydraulic Conductivity, and Collapse Potential of RAP and CC

5.1 INTRODUCTION

Shear strength, hydraulic conductivity, and collapse potential are key properties of a backfill material that relate to its suitability for MSE wall applications. This chapter discusses the test equipment and experimental program that were used for the assessment of these important properties. Three laboratory testing programs were designed to evaluate the shear strength, hydraulic conductivity, and collapse potential of the test materials. The shear strength of the three test materials (RAP, CC, and CFM) was characterized in terms of the drained shear strength parameters (i.e. ϕ' and c'), as determined by triaxial and direct-shear tests. Hydraulic conductivity measurements were performed on all three test materials using the falling head-rising tail method in a flexible wall triaxial setup. Also, some constant head, fixed wall hydraulic conductivity tests were conducted and compared with the flexible wall results. The collapse potential upon wetting of the three test materials were evaluated through large-scale, one-dimensionally constrained compression tests. A collapse index (I_c) was defined for each material and compared.

5.2 TEST EQUIPMENT

This section describes the triaxial test system and the large-scale direct shear apparatus that were used in this study to evaluate the shear strength, hydraulic conductivity, and collapsible potential of RAP, CC, and CFM. The general system setup and configuration are described herein along with the instrumentation.

5.2.1 Triaxial System

An electro-hydraulic triaxial test system (Figure 5-1) built by GCTS of Tempe, Arizona, was used for three different types of experiments: consolidated-drained triaxial tests, flexible-wall hydraulic conductivity tests, and creep tests (discussed in Chapter 6). The GCTS system is a closed-loop, digitally-controlled servo-hydraulic system with a computer interface that connects the system analog signals to the computer board for data acquisition. The load frame consists of two vertical stainless steel columns with a crosshead to support a double-acting diaphragm hydraulic cylinder of 7000-lb capacity. A 5000-lb external load cell with 0.04% accuracy is mounted at the bottom of the piston rod for measurement of the piston load during triaxial tests. The triaxial cell is constructed of three stainless steel columns with an acrylic cell that can sustain up to 145 psi cell pressure. The triaxial system can accommodate cylindrical specimens of up to 4-in in diameter and 8-in high with pressure lines for top and bottom specimen drainage. Figures 5-1 and 5-2 illustrate the triaxial cell and the loading components described above.

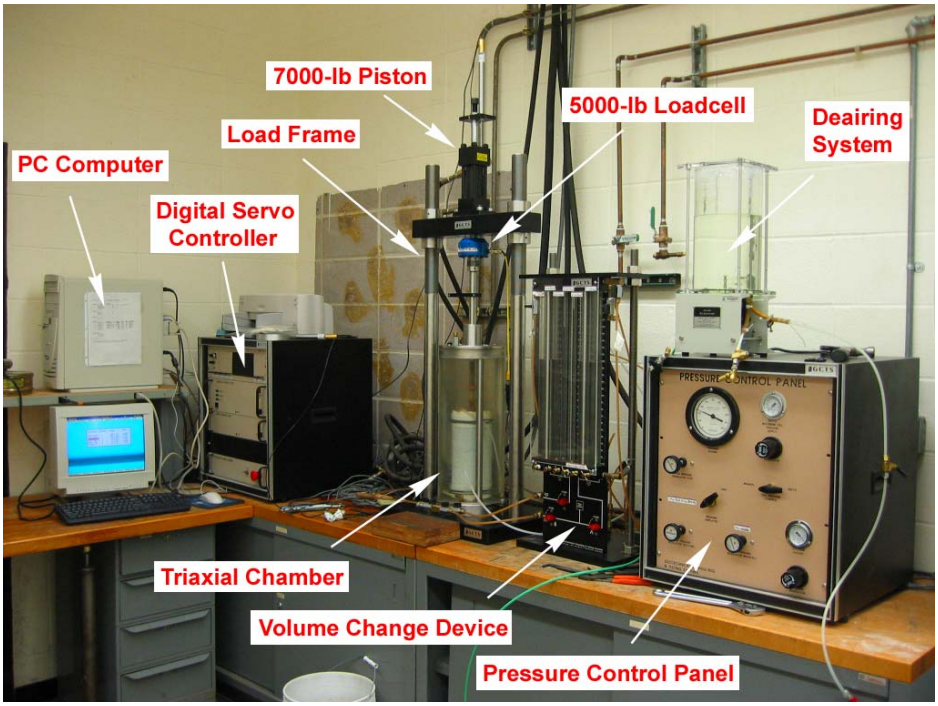

Figure 5-1 GCTS triaxial test system

The pressure control panel is equipped with pressure regulators, pressure gages (0.7 psi resolution), and sensors, allowing full manual control of the cell pressure and pore water pressures at the top and bottom of the test specimen. Behind the volume change device are three low-compliance pressure transducers for the measurement of cell pressure, effective stress, and volume change during testing. The effective stress is determined using a differential pressure transducer which measures the difference between the cell pressure and the pore water pressure at the bottom of the specimen. Similarly, the volume change transducer measures the difference in the pressure at the top and bottom of the water column with a sensitivity that can detect the specimen volume change of less than 0.05 cc.

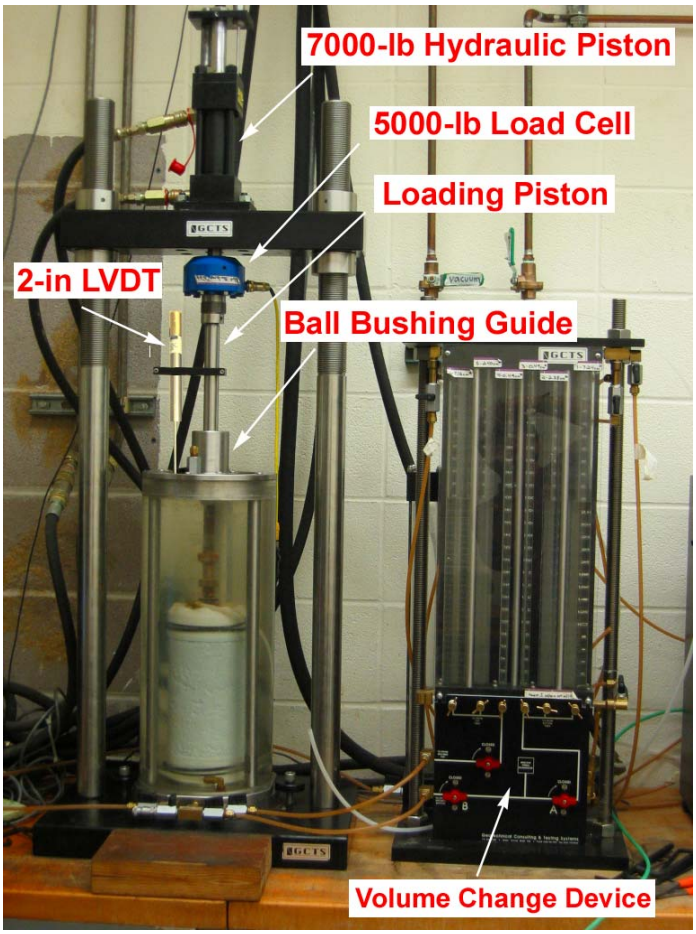

Figure 5-2 Triaxial cell and loading components

Axial displacement during testing is measured using an external linear variable differential transducer (LVDT) mounted in a bracket that is attached to the loading piston (Figure 5-2). The LVDT has the total travel range of 2 in. with a resolution of 0.0004 in. (0.01 mm). The test system came equipped with the GCTS Triaxial test software module that automatically performs triaxial shear tests.

All electronic instrumentation (i.e. load cell, LVDT's, and pressure transducers) were calibrated against reference standards prior to the testing program. The calibration

was performed in three cycles, in which each cycle covered the full range of the transducer. The slope of the calibration curve is assigned to the Triaxial software module as a conversion factor converting the transducer voltage readings to corresponding values in engineering units. Details of the sample preparation and test procedures are discussed in later sections.

5.2.2 Large-Scale Direct Shear Machine

A large-scale direct shear device (Figure 5-3) was designed as part of this study with the specific purpose to test large specimens containing particles up to 2 in. in size at applied normal stresses as high as 30 psi. This normal pressure represents roughly 40 ft. of in situ overburden pressure. The general criterion for a direct shear specimen is that the width of the specimen must be at least ten times larger than the maximum particle size diameter (ASTM D 3080), and the width to thickness ratio of the box should be 2:1. Given that test materials in this study contain particles up to 2 in., a square shear box with an inside width of 20 in. was selected. The machine was designed to accommodate a maximum anticipated horizontal shear force of approximately 17,000 lb, which was estimated from the expected shear resistance of the test materials subjected to 30 psi normal stress.

The structure of the reaction frame was designed such that any relative structural deformation would be minimized during testing. Also, the frame was designed in a way that the reactive force generated during the shearing process was transferred entirely into the reaction frame. As a result, the complete test setup is self-contained and readily movable because it does not need to be positioned against a rigid wall or bolted down to a

concrete floor. Figure 5-3 is a photograph of a complete setup of the large-scale direct shear machine during testing, and Figure 5-4 shows a cross-section of the setup.

The shear box is situated inside a water tank which is filled with water during the test to eliminate any capillary stresses developed in the test specimens that may affect the measured shear strength. The water tank is rigidly attached to the lower half of the shear box, and both move laterally during shearing. The upper half of the shear box is held stationary in the horizontal direction by plates that react against four low-friction rollers, but these rollers also allow the top of the box to move freely in the vertical direction (Figure 5-4). These rollers allow for dilation and contraction of the specimen, and also minimize rocking. During shearing, the lower half of the shear box and the surrounding water-filled tank are pulled horizontally by a pneumatic actuator (12 in. diameter, 5 in. stroke) and ride on two linear bearings. Normal stresses are applied to the top of the test specimen using an air-pressurized rubber bladder, which receives a constant air pressure supply from the house pressure line. The horizontal pneumatic actuator is operated with pressures up to 250 psi delivered from high-pressurized bottled air, and can deliver over 27,000 lb of horizontal shear force.

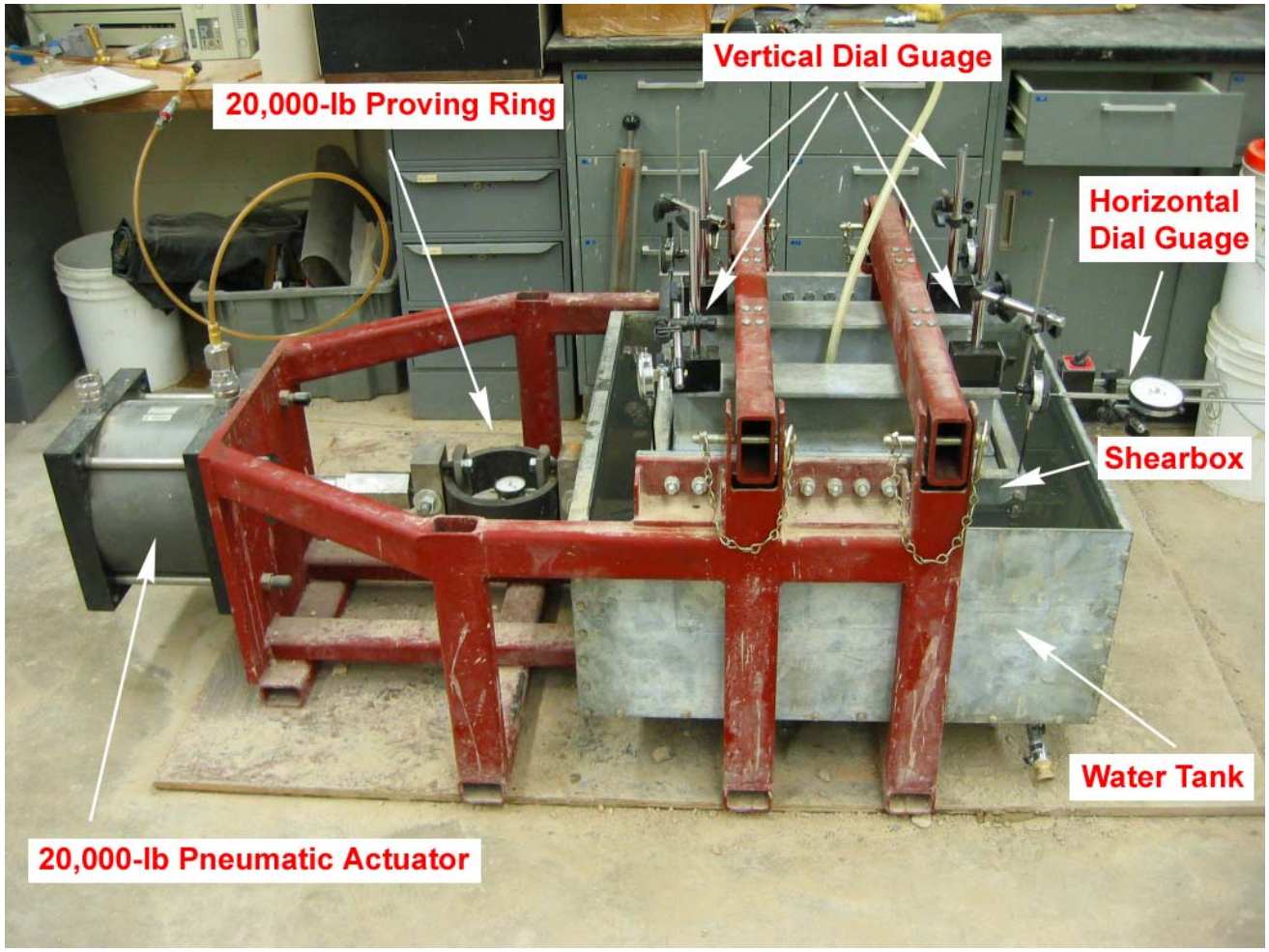

Figure 5-3 Large-scale (20 in x 20 in) direct shear machine during testing

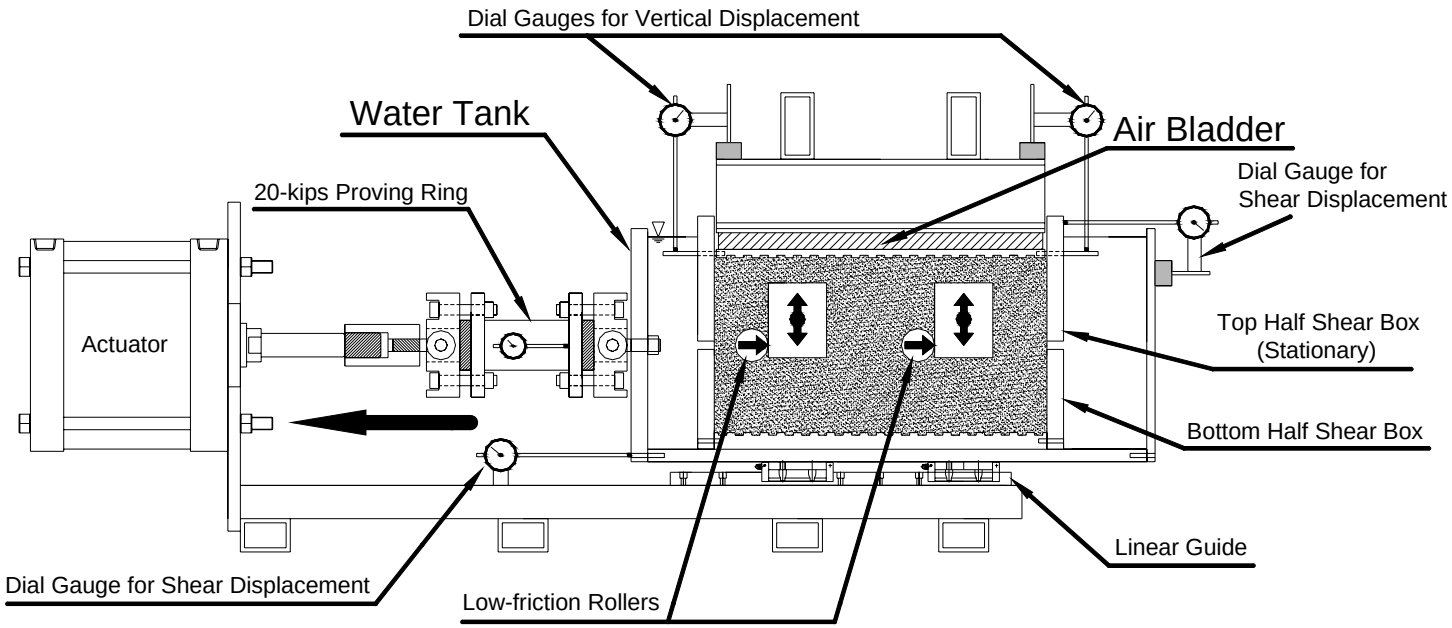

Figure 5-4 Cross section of the large-scale direct shear machine

The direct shear machine is used to conduct force-controlled direct shear tests, where the shear force is applied in increments by progressively increasing air pressure to the actuator. The shear force is increased when no additional shear displacement due to the preceding load is observed. Operation of the direct shear machine with pneumatic pressure regulators allows for simple, accurate control for tests of this type. The vertical and horizontal displacements of the specimen are monitored by a system of six dial gauges, two for horizontal displacement (one measuring relative displacement between the top and bottom boxes and the other measuring absolute displacement of the bottom box), and four for vertical displacement (at each corner of the test specimen). The dial gauges are capable of resolving displacements as small as 0.0001 in. All instrumentation was calibrated against the reference standards at the beginning of the testing program. All data from the tests were recorded manually using a high resolution pressure gauge for the normal stress, a 20-kip proving ring for the applied shear force, and the set of dial gauges for the shear and vertical displacements.

In addition to the measurement of drained shear strength, the direct shear machine was also used to assess the potential for post-construction settlement of these test materials upon wetting (i.e. collapse potential). Vertical compression of the specimens was measured during application of the normal stress and then during subsequent submergence in water. The large scale of these test specimens provided a unique opportunity to assess this behavior in the laboratory using a representative sample gradation containing all particle sizes.

5.3 SHEAR STRENGTH CHARACTERISTICS

The shear strength parameters of MSE wall backfill are critical properties in the design phase because they govern the stability of the wall. Generally, MSE wall backfill should have high frictional strength to ensure stability within the backfill itself and to achieve the required interaction with the reinforcements. High shear strength materials usually come from well-graded, angular soils that contain a minimal amount of fines. Based on visual inspection and their measured gradations, RAP and CC should exhibit high shear strength parameters due to their significant angularity and the absence of fines.

The ASTM standard for triaxial testing (ASTM D 4767) states that triaxial specimens should have a diameter at least six times larger than the largest particles contained in the test specimen. Given a maximum sample diameter of 4 in. for the triaxial setup, any particles larger than about 0.67 in. must be removed before forming the test specimens. However, removal of larger particles may yield unrealistically high strength because these larger particles may be fractured, and therefore weaker, than the smaller grains. Thus, the shear strength measured in the triaxial tests may not be representative of the bulk material. Due to this reason, additional large-scale direct shear tests on specimens measuring 20 in by 20 in. in plan section, accommodating all particle sizes in the reference gradation, were included in the strength testing program.

5.3.1 Consolidated-Drained Triaxial Tests

A series of fourteen consolidated-drained, strain-controlled triaxial compression tests were completed on compacted specimens of RAP, CC, and CFM. Four tests at four different effective confining pressures (i.e. 20, 30, 40, and 50 psi) were performed on CC

and CFM specimens. RAP specimens were tested at the same effective confining pressures, as well as two additional tests performed at 5 and 10 psi effective confining pressures to investigate the potential curvature of the RAP failure envelope at low confining pressures.

5.3.1.1 Sample Preparation and Testing Program

A consistent reference gradation was selected in Chapter 3 for the preparation of all test specimens. However, as noted previously, the 4-in specimen diameter for the UT triaxial apparatus requires that all particles larger than 0.67 in. be removed. This scalping was accomplished by using only material that passes a 0.63 in. sieve, the closest available sieve size to 0.67 in. It must be noted that an attempt was made to create a modified gradation that is parallel to the original gradation but with a maximum particle size of 0.63 in. This can be done by shifting the original gradation to the right in parallel to the original location. However, this parallel gradation would require up to 5% of materials passing sieve No. 200. But as discussed earlier in Chapter 3, RAP and CC used in this study did not contain any particles passing sieve No. 200. Because of the limited material resource, it was decided to adopt a gradation illustrated in Figure 5-5 for all triaxial test specimens. It was well understood that using gradation that does not mimic the same curvature with the original gradation may lend additional variable to this study. This speculation may possibly be explored later after comparing the triaxial results with the ones from large-scale direct shear tests.

As previously mentioned in Chapter 3, all test materials were separately stockpiled at the Pickle Research Center in Austin, Texas, outside the research facility

building without a protective cover. As a result, all test materials were fully exposed to the ambient environment and often times were in damp condition due to seasonal rains. Therefore, the test materials were required an oven-drying at an appropriate temperature (60° C for RAP, and 110° C for CC and CFM) before they were separated into different particle sizes using a dry sieving process. After the dried materials were sieved, each particle size was stored and labeled in separate 5-gallon buckets before they were brought back to the laboratory for further testing.

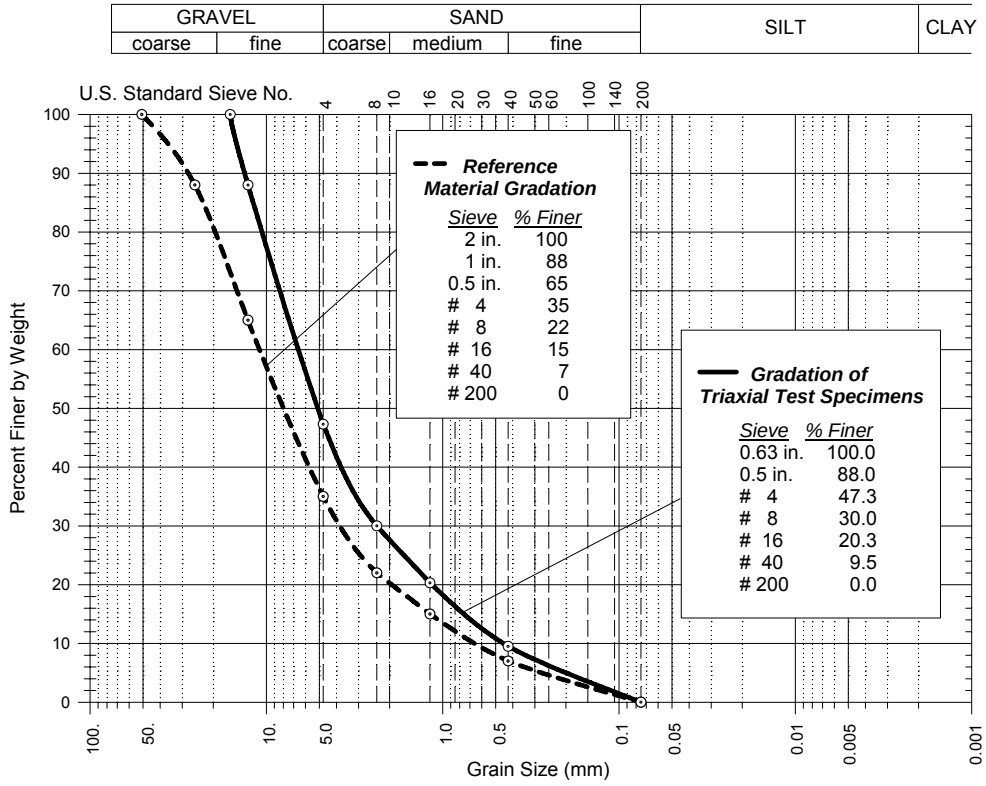

Figure 5-5 Grain size distribution of reference gradation and triaxial test specimens

At the laboratory, sample preparation involved scalping out particles larger than 0.63 in. and then mixing the test materials to match the predetermined triaxial gradation shown in Figure 5-5. After mixing, an appropriate amount of water was added and thoroughly mixed with the sample to achieve the optimum moisture content (refer to Chapter 4). The soil-water mixture was allowed to sit for 16 hours in a sealed container after which it was compacted in a split mold of 4-in diameter and 8-in high using a compaction energy per unit volume equivalent to the Tex-113-E method. After removing the compacted specimen from the mold, the specimen was placed on top of the base pedestal with a saturated porous stone and saturated filter paper. A saturated porous stone and saturated filter paper were placed on top of the specimen before the top cap was situated. It was observed that all compacted specimens were reasonably stiff such that no vacuum back pressure was needed to hold the test specimens in place during the sample preparation process.

A rubber membrane with a thickness of 0.025 in. (less than 1% of the specimen diameter, as recommended by ASTM D 4767) was rolled onto the specimen from top to bottom, after which the specimen was secured to the top cap and the bottom platen using two rubber O-rings at each end. All the appropriate drainage lines and pressure transducers were flushed with deaired water to ensure minimal presence of entrapped air bubbles. The top drainage line was then attached to the top cap. The alignment of the specimen and the top cap was again checked, and readjusted if needed, to assure no eccentricity. Finally, the triaxial cell was assembled and was consequently filled with

deaired water. A schematic drawing of a complete triaxial specimen setup is shown in Figure 5-6.

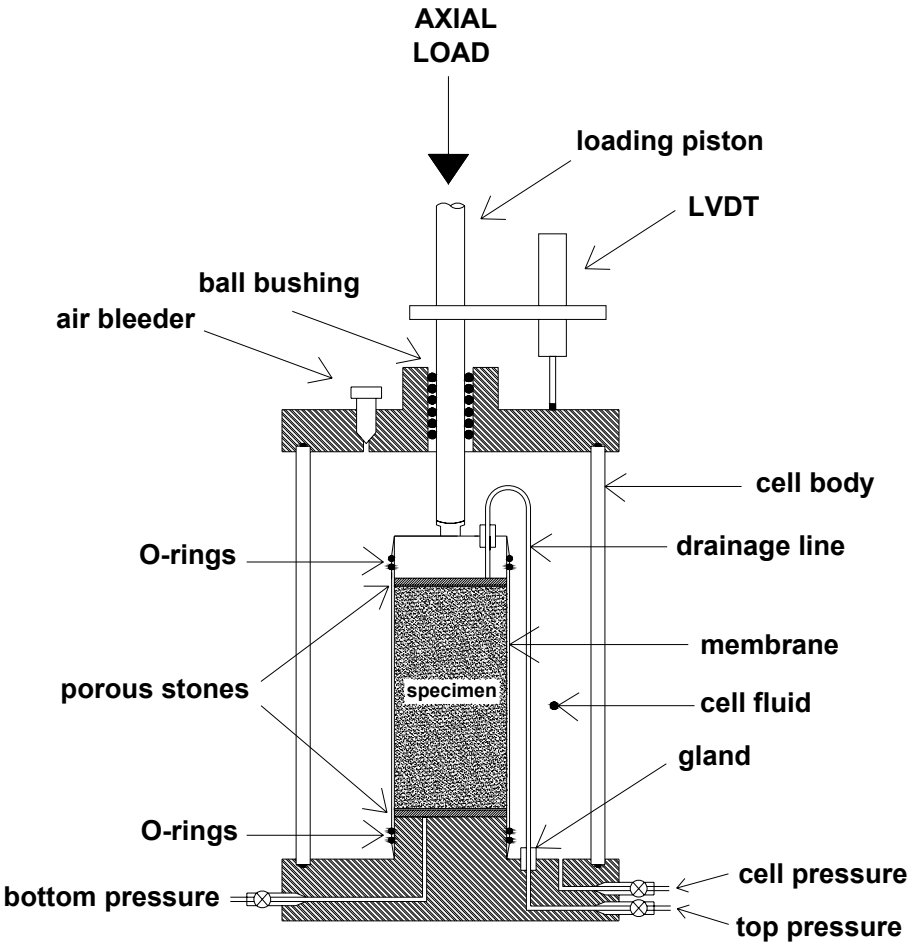

Figure 5-6 Details of the complete triaxial test specimen setup

Deaired water was introduced at the bottom of the specimen by gravitational force with the aid of a small vacuum pressure (~ 2 psi) applied to the top of the specimen. This process filled the voids and displaced as much pore air as possible, and was continued until no air bubbles were visually detected leaving the drain line connected to the top of

the specimen. Then, the specimen was back pressure-saturated by simultaneously increasing the cell pressure and the back pressure in small increments. Back pressure saturation and B value (i.e. pore pressure parameter, $\Delta u/\Delta\sigma_3$) measurements were carefully performed such that the difference between cell pressure and the back pressure never exceeded 2 psi to avoid overstressing the test specimen above the target effective consolidation stress.

Back pressure saturation was continued until the measured B value was at least 0.92 or higher. Various procedures were attempted to increase the B value of the specimens above this value, including leaving the specimens under high back pressures (up to 80 psi in some cases) for 96 hours. However, these practices did not lead to significant gain in the B value. Black and Lee (1973) derived an analytical expression for the B values based directly on the Boyles Law ($P_1V_1 = P_2V_2$ = constant; P and V are the pressure and volume of a confined, ideal gas held at a constant temperature). Using typical values of void ratio (e) and compressibility of four different classes of soil, Black and Lee (1973) back-calculated the theoretical B values, with the equation shown below, at complete and nearly complete saturation, as shown in Table 5-1.

$$Saturation\ Level\ \ (S_i) = \frac{1 - Z(1-B)}{1 - ZBn_i \dfrac{C_w}{C_d}}$$

where:
$$Z = \frac{C_d \dfrac{\Delta\sigma_3}{n_i}}{1 - \dfrac{P_i}{P_i + B\Delta\sigma_3}}$$

B = Pore pressure parameter

C_d = compressibility of the soil skeleton

C_w = compressibility of water (i.e. 0.33×10^{-5} psi^{-1})

n_i = initial porosity of the soil ($n = e / [1 + e]$)

P_i = initial back pressure

$\Delta\sigma_3$ = change in cell pressure

Table 5-1 Theoretical B values for typical soils at and near full saturation [after Black and Lee (1973)]

Soil Category	**Description**	**Degree of Saturation**		
		100%	**99.5%**	**99%**
Soft	normally consolidated clays ($e \approx 2$, $C_d \approx 1 \times 10^{-2}$ 1/psi)	0.9998	0.992	0.986
Medium	compacted silts and clays, lightly overconsolidated clays ($e \approx 0.6$, $C_d \approx 1 \times 10^{-3}$ 1/psi)	0.9988	0.963	0.930
Stiff	overconsolidated clays, average sands ($e \approx 0.6$, $C_d \approx 1 \times 10^{-4}$ 1/psi)	0.9877	0.69	0.51
Very Stiff	very dense sands, very stiff clays ($e \approx 0.4$, $C_d \approx 1 \times 10^{-5}$ 1/psi)	0.913	0.20	0.10

Note: e = void ratio and C_d = soil compressibility

Table 5-1 indicates that B values close to 1.0 can easily be achieved for softer soils. However, very stiff soils that have compressibilities that start to approach the compressibility of water ($C_w \sim 0.33 \times 10^{-5}$ psi^{-1}) cannot achieve B values close to 1.0, even at full saturation. The RAP, CC, and CFM specimens are quite stiff and have void ratios less than 0.4. Thus, the B value criterion of 0.92 used for RAP, CC, and CFM specimens

most likely indicates a degree of saturation larger than 99.5%, which is generally acceptable. RAP specimens generally reached the desired B value after leaving them under the highest possible back pressure for 24 hours, while it usually took at least 48 hours for CC and CFM specimens to reach the same B value.

After the desired B value was reached, the specimen was consolidated isotropically to the target effective confining pressure (σ'_3). The consolidation stage was terminated when there was no water coming out of the specimen, which was confirmed by no change in the volume change transducer. Because of the large hydraulic conductivity of the test materials, the end of primary consolidation was achieved fairly quickly (t_{100} less than 30 seconds in most cases). With $t_{100} \approx 0.5$ min and an estimated axial strain at failure (ε_f) of 5%, the theoretical maximum rate of strain to be used for the shearing stage is equal to 1% per minute (ASTM D 4767). However, it was decided to set the strain rate at 0.5% per minute for all tests to ensure no excess pore water pressure would develop during shearing.

The shearing continued with both top and bottom specimen drainage valves open until 15% axial strain was reached. In a few cases, membrane puncture was detected at intermediate strains when tests were performed at high effective confining pressures. All data were recorded electronically and were interpreted later using a spreadsheet program.

5.3.1.2 Test Results and Discussion

Results from the consolidated-drained triaxial compression tests performed on CFM, CC, and RAP specimens are plotted in terms of principal stress difference ($\sigma_d = \sigma_1 - \sigma_3$) versus axial strain ($\varepsilon_a$) and volumetric strain (ε_v) versus axial strain (ε_a) in Figures 5-

7, 5-8, and 5-9, respectively. The principal stress difference was computed by dividing the applied piston load by the corresponding cross-sectional area of the specimen, assuming a right circular cylinder area correction. Failure was defined as the maximum principal stress difference (i.e. $[\sigma_1 - \sigma_3]_{max}$). The values of major and minor principal stresses at failure (i.e. σ'_{1f} and σ'_{3f}) were used for plotting the Mohr circles of stress at failure under drained conditions, after which a best-fit Mohr-Coulomb strength envelope was drawn for each test material.

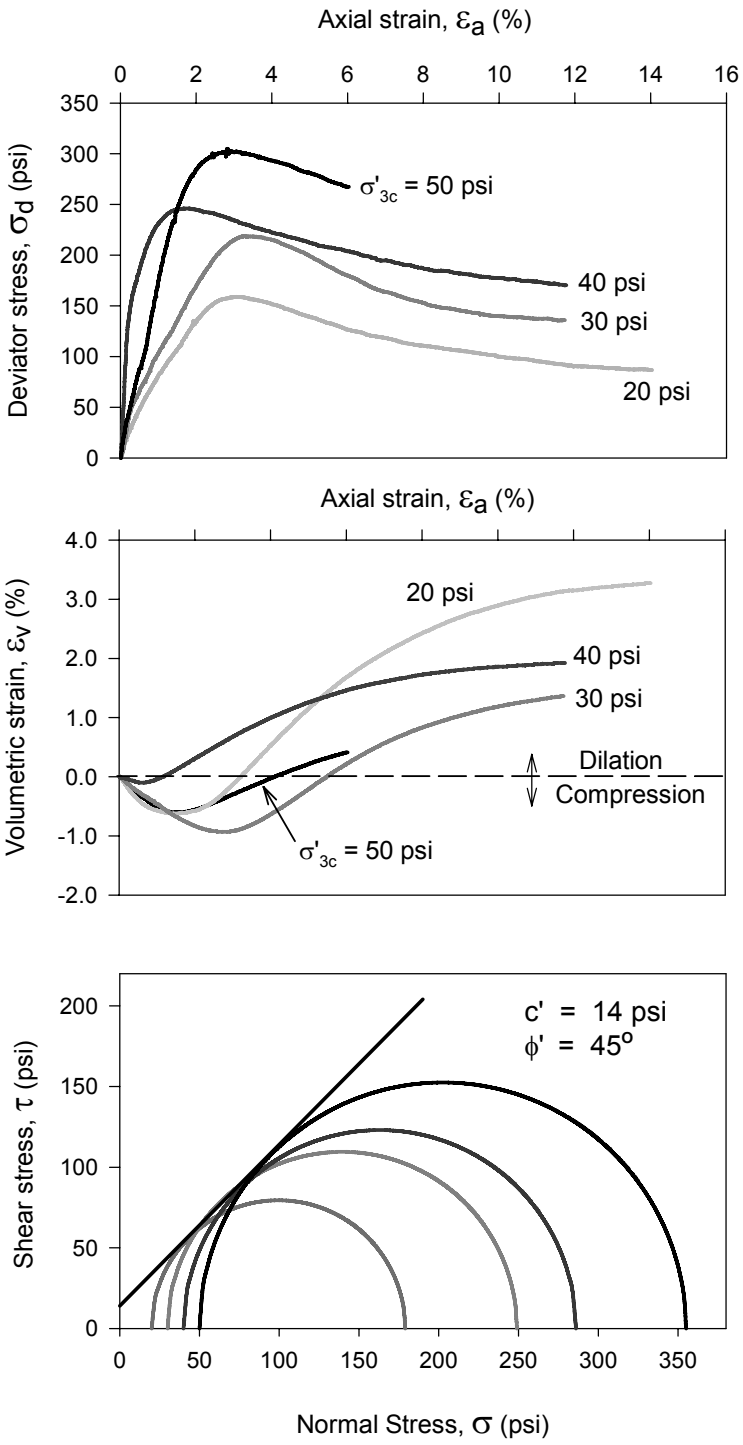

Figure 5-7 Drained shear triaxial test results from four CFM specimens

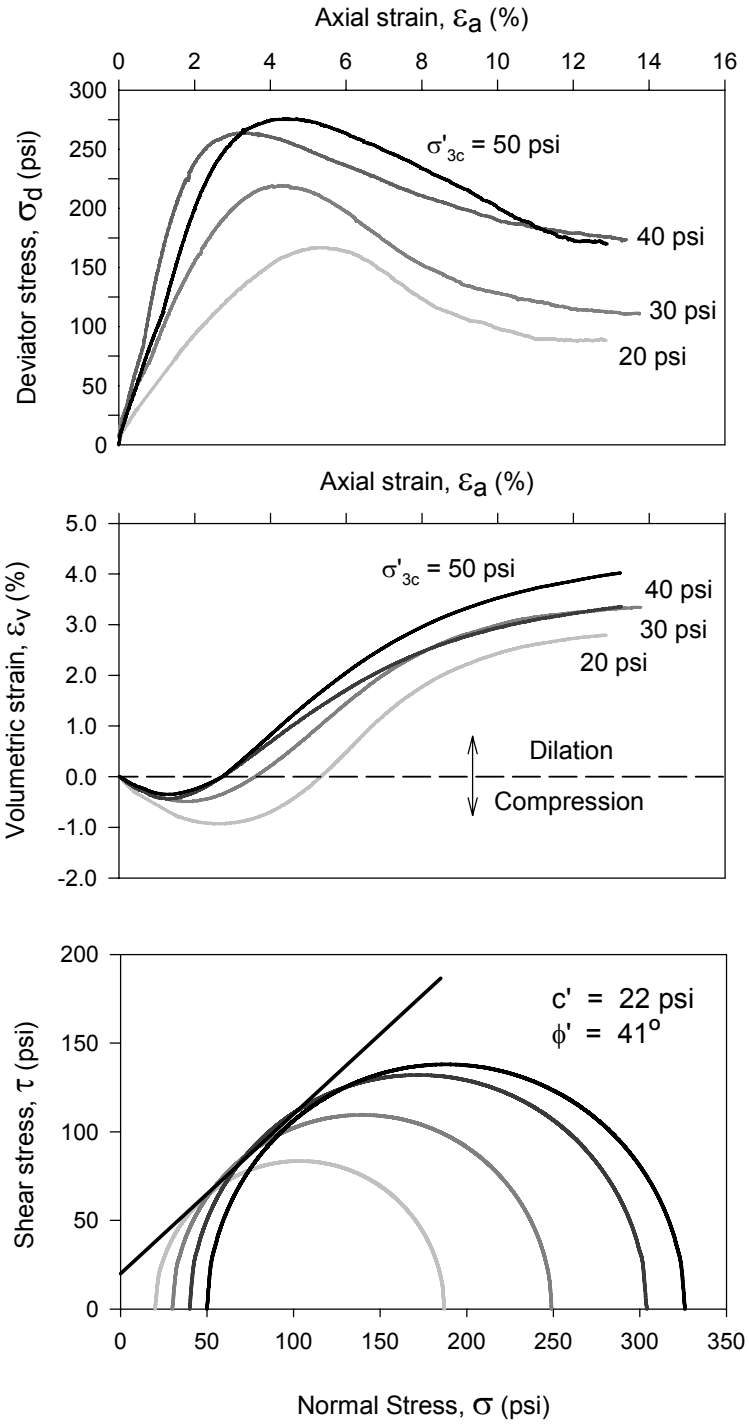

Figure 5-8 Drained shear triaxial test results from four CC specimens

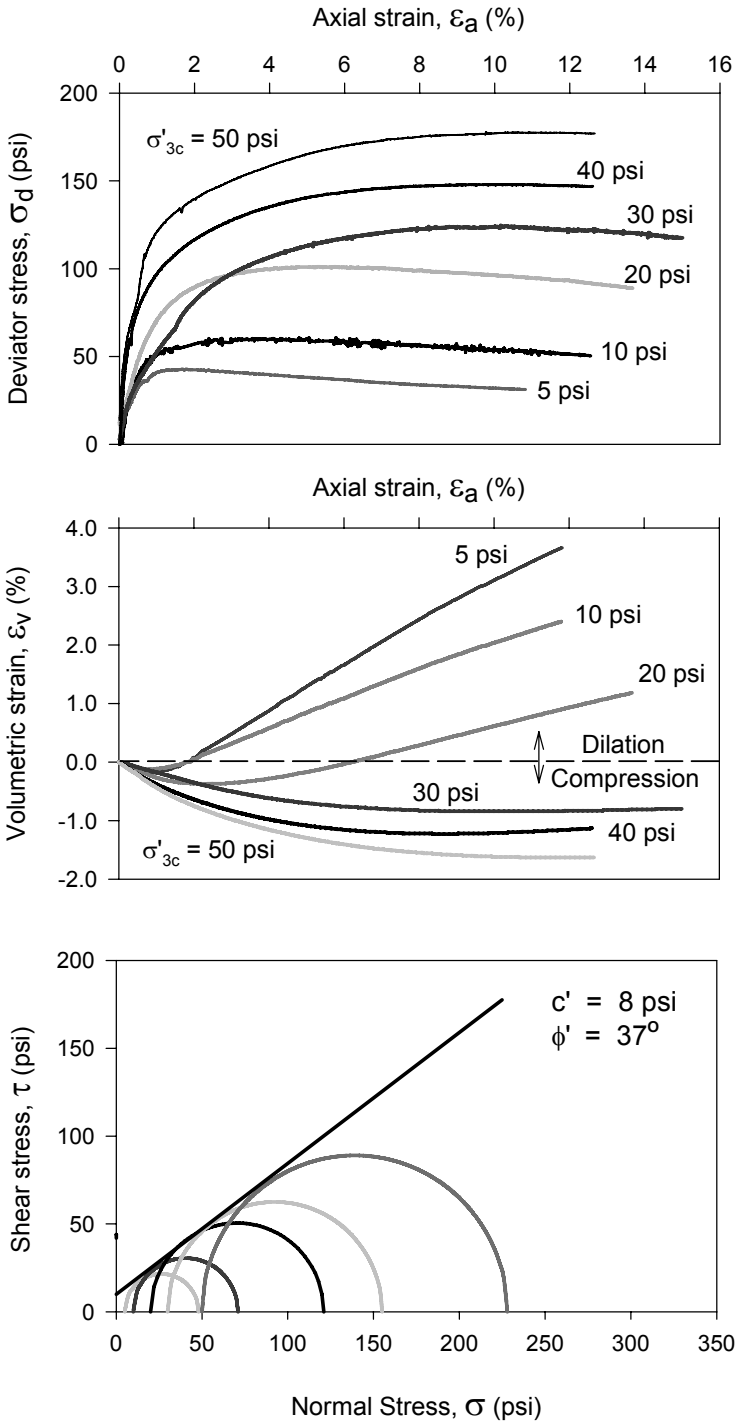

Figure 5-9 Drained shear triaxial test results from five RAP specimens

Figure 5-7 shows that all of the CFM specimens exhibited strain-softening behavior, reaching a maximum principal stress difference at less than 4% axial strain and then declining to a residual value. It should be noted that the CFM specimen sheared at 50 psi effective confining pressure was stopped prematurely due to excessive membrane puncture at large strains. Several additional tests with various corrective measures were performed at this same confining pressure, but all resulted in similar puncture due to the high angularity of the material. Each specimen that reached full failure experienced between 1% and 3% shear-induced volumetric dilation at the end of testing. Additionally, all of the CFM specimens displayed a distinct failure plane through the specimen. The strain softening behavior and the distinct failure plane after sheared are typical responses of a dense material during drained shear. The effective cohesion (c') and effective friction angle (ϕ') based on the maximum principal stress differences measured from these four tests are 14 psi and 45°, respectively (Figure 5-7). It is not common for uncemented, coarse grained material to exhibit cohesion during drained shear. The cohesion intercept found for CFM is speculated as a result of either re-cementation of the limestone material or the linear extrapolation of the failure envelope from larger confining pressures. The direct shear test program includes a number of drained shear tests performed at lower confining pressures, which can further identify whether the CFM strength envelope is curved or is a straight line with cohesion.

Tests on CC also exhibited strain-softening behavior as shown in Figure 5-8, reaching a maximum principal stress difference at less than 6% axial strain and then declining to a residual value. The CC specimens experienced between 3% and 4%

dilation at the end of testing. As with CFM, all CC specimens displayed a distinct failure plane through the specimen. The effective cohesion and effective friction angle based on these four tests are 22 psi and 41°, respectively (Figure 5-8).

During the preparation of one CC test specimen, some visual evidence was observed that suggests unhydrated cement paste may be present in the crushed concrete. Subsequently, several samples of uncompacted, wet CC were dried overnight in an oven. Upon removal from the oven, the material had a distinct, hardened crust. The individual aggregate grains were noticeably conglomerated, forming larger chunks of cemented material that were visibly different from the original material. It is possible that bonding occurred due to rehydration of cement paste in the CC. If true, then the strength of compacted CC may increase to some extent with time following compaction. Only freshly compacted material was evaluated in this study, so this effect is minimal in the test data presented. However, the cohesion intercept found for the CC strength envelope may be attributed to cementation due to rehydration of the cement paste in CC. Again, the direct shear tests were performed at lower confining pressures and provide more data to accurately evaluate the strength envelope in this stress range.

It is evident that CC has similar shear strength characteristics as CFM. Both the CFM and CC are highly angular materials with relatively large drained shear strength at confining pressures up to 50 psi, although lower friction angles can be expected at larger confining pressures. Also, because the tests reported here were conducted on specimens in which all particles larger than 0.63 in. had been removed, the strength of the composite

material may be somewhat lower, as the largest particles of this crushed material may be more fractured.

Tests on RAP were performed at effective confining pressures ranging from 5 to 50 psi (Figure 5-9). All tests exhibited strain-hardening behavior, with the deviator stress continuing to rise or remaining essentially steady throughout the duration of the test. Final volumetric strains ranged from dilative for tests run at low confining pressures to contractive for tests performed at higher confining pressures. The contractive response is in contrast to the purely dilative response observed in the tests on CFM and CC. In addition, no RAP specimens displayed a distinct failure plane during shear. Rather, the specimens compressed vertically and exhibited a slight radial bulge near the center as the axial load was applied. These responses are typical for a loose material in drained shear, although it is somewhat unexpected that compacted specimens would exhibit contractive behavior at these confining pressures.

The effective stress friction angle for RAP based on these five tests is 37°, with an effective cohesion intercept of 8 psi (Figure 5-9). The observed cohesion (c' = 8 psi) likely results from the residual bitumen bonding the particles together. Although the measured shear strength of RAP was lower than that for the CFM and CC, RAP appears to exhibit marginal to adequate strength properties for use as MSE wall backfill material. The lower friction angle for RAP, compared with that of CC and CFM, may result from more rounded aggregate particles or from reduced interparticle friction due to the residual bitumen in the RAP. Additional investigations were performed in this study to assess the

stability of this material, particularly to determine whether RAP is susceptible to creep failure at large to moderate shear stress levels.

Figure 5-10 graphically shows the best-fit, straight line Mohr failure envelopes for the test materials, while Table 5-2 summarizes the drained strength parameters for all three test materials based on the triaxial test results. It is clear that CC has comparatively similar strength characteristics to CFM, particularly at the confining pressures representing the heights of typical MSE walls. RAP has smaller shear strength characteristics than CC and CFM, but still maintains adequate strength for typical MSE backfill applications.

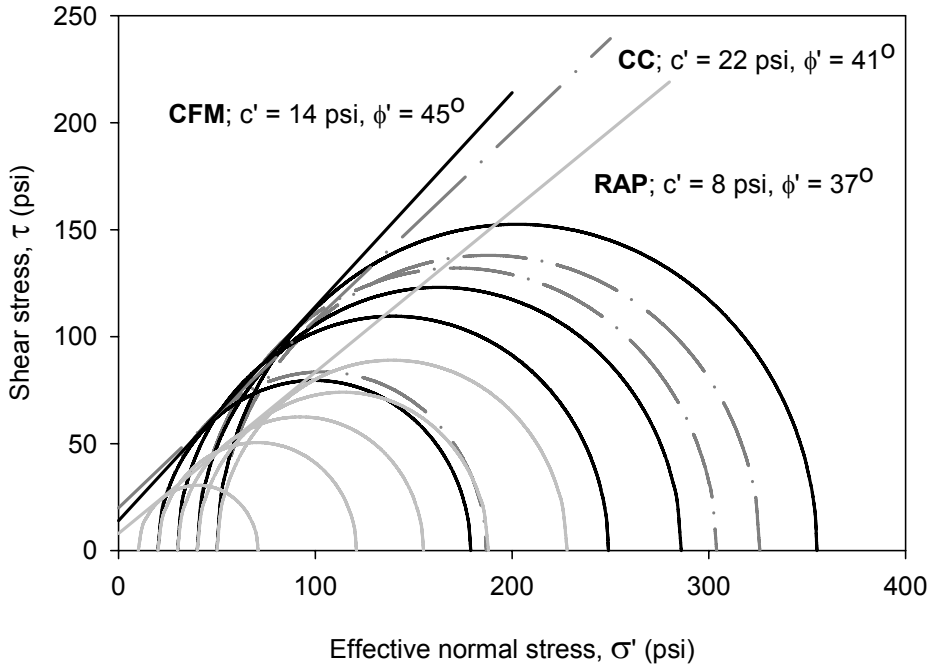

Figure 5-10 Mohr failure envelopes based on the triaxial test results

Table 5-2 Drained shear strength parameters of the tested materials based on the triaxial test results

Drained Strength Parameter	RAP	CC	CFM
Cohesion (c'), psi	8	22	14
Internal friction angle (ϕ'), degree	37°	41°	45°

5.3.2 Large-Scale Drained Direct Shear Tests

A series of eleven drained, force-controlled direct shear tests were performed on compacted specimens of CFM, CC, and RAP with an initial applied normal stress ranging from 5 psi to 28 psi. At the beginning of the test program, three trial tests were performed on washed mortar sand, a material with known shear strength parameters, to assess the accuracy of this newly designed and constructed direct shear system.

5.3.2.1 Sample Preparation and Test Program

Sample preparation for large-scale direct shear testing began by remixing the previously dried, sieved material back to the reference gradation as shown in Figure 5-5. A sufficient amount of water was mixed with the dried material to achieve the desired water content and then allowed to stand for 3 hours prior to compaction. The two halves of the shear box were aligned and connected together by clamping screws before specimen compaction. The 10-in high specimen was compacted in five, 2-in lifts, making sure that the third lift was not coincident with the shear plane defined by the shear box. All five consecutive compacted layers were prepared using a modified compaction

hammer with the compaction energy per unit volume equivalent to what is recommended by the Tex-113-E compaction method. Unit weights of all compacted specimens were determined after the compaction and were found to be within ± 3 lb/ft^3 of the target unit weights.

After the last layer was compacted, a top grid plate was placed on top of the sample, followed by an air bladder and a top bearing plate. Four vertical dial gauges were positioned on the reaction frame with their tips seated on four bolts extending rigidly from the top bearing plate (Figure 5-4). These bolts move vertically during shear, and correspond to the vertical movement of the top of the sample. Relative horizontal displacement between the boxes during shear was measured by a dial gauge mounted on the water tank, which is rigidly connected to the lower shear box, with its tip seated on the upper shear box (Figure 5-4). After complete assembly, the specimen was consolidated to the appropriate normal stress and saturated with water to measure its collapse potential. Complete details of the collapse potential measurements are discussed in Section 5.5. After the collapse upon wetting was measured, the aligning screws connecting the two halves of the box were removed and a 0.5-in vertical gap between the two boxes was created using four gap screws.

The large-scale direct shear apparatus was designed to perform force-controlled tests rather than deformation-controlled tests. The force-controlled test is achieved by progressively and slowly increasing the air pressure in the actuator in small increments, which ensures minimal generation of excess pore water pressure in the shearing zone. Relative horizontal displacement between the two halves of the specimen, vertical

movements at the top of the specimen, and the applied shear force are all recorded simultaneously during the shearing process. Each set of readings is taken after a new increment of shear force is applied and the shear movement has come to a complete stop.

Because the large-scale direct shear apparatus was newly designed and built for this study, a validation study was initiated to compare test results obtained from this large-scale device to those measured previously. Dry, uniformly-graded washed mortar sand was selected for this preliminary study. Direct shear tests using a typical (3 in. by 3 in.) device were performed and reported by Najjar and Rauch (2003). The large-scale test specimens were prepared using the same dry pluviation technique as the small-scale specimens. Despite the same technique used for sample preparation, the initial void ratios of the large-scale specimens were found to be greater than the void ratios of the small samples (i.e. 0.51 to 0.56 compared to 0.45 to 0.49). Figure 5-11 shows large-scale direct shear results obtained for this material performed at three different normal stresses.

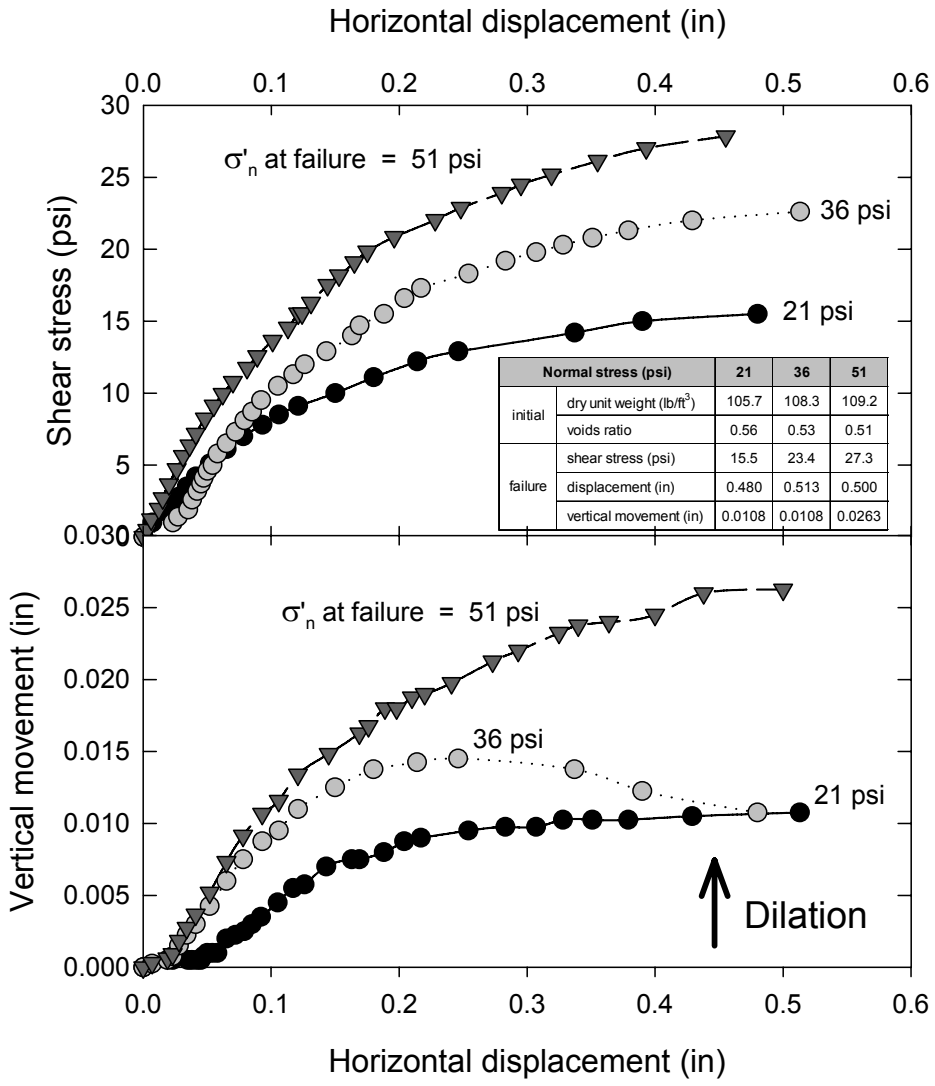

Normal stress (psi)		21	36	51
initial	dry unit weight (lb/ft^3)	105.7	108.3	109.2
	voids ratio	0.56	0.53	0.51
failure	shear stress (psi)	15.5	23.4	27.3
	displacement (in)	0.480	0.513	0.500
	vertical movement (in)	0.0108	0.0108	0.0263

Figure 5-11 Results from large-scale drained direct shear tests on washed mortar sand

The shear stress at failure (τ_f) and its corresponding normal stress (σ_n) for all three large-scale specimens are plotted in Figure 5-12 along with the results obtained from the small-scale specimens. It can be seen that two out of three large-scale direct shear data points fit reasonably well with the small-scale direct shear results, with one outlier point that deviates slightly from the regression line. It is not clear why the large-scale specimen

at 50 psi produced such a low value of strength. Nonetheless, the reasonably good agreement of these two groups of data suggests that the large-scale direct shear test apparatus is capable of measuring drained shear strength with acceptable accuracy.

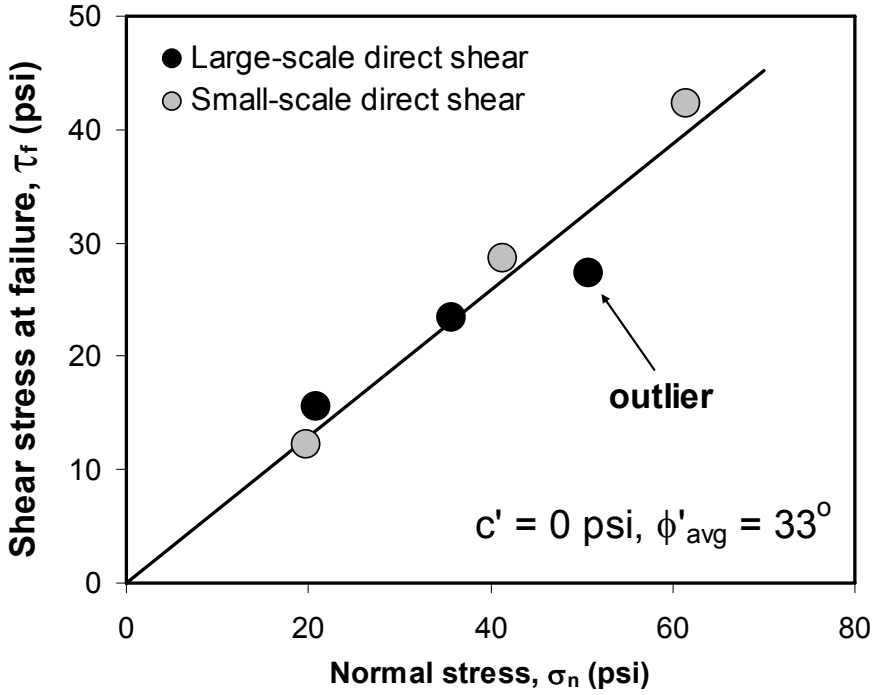

Figure 5-12 Comparison of small-scale vs. large-scale direct shear tests on washed mortar sand

5.3.2.2 Test Results and Discussion

Five drained large-scale direct shear tests were performed on CFM and CC specimens with initial applied normal stresses (σ_n) ranging from 5 to 28 psi. Two tests were performed on RAP at σ_n equal to 10 and 20 psi, but creep problems were encountered. The results from the three tests series are discussed below.

The direct shear test results for RAP are shown in Figure 5-13. The test at 10 psi initial normal stress was completed with minor creep observed during shearing, although the test took nearly six hours to reach the failure point because of the time it took for deformations to stop at each force level. The test indicated a shear stress at failure of approximately 12 psi, at an area-corrected normal stress of 10.5 psi. Based on this normal stress and the previously measured values of c' = 10 psi and ϕ'=36° from the triaxial tests, the predicted shear stress at failure should have been at about 17.6 psi. This value is much larger than the measured value, indicating that the specimen may have experienced creep rupture rather than shear failure.

The test at 20 psi normal stress began to creep noticeably at very small force/deformation levels, after about 0.085 in. of horizontal shear displacement. At this point, the next two readings had to be recorded while creep was still taking place and no definite termination of creep was observed in any of these last few load increments. The last obtainable data was taken at about 0.21 in. of horizontal shear displacement after about four hours from the beginning of the test. The next load increment was applied and at this point the shearing seemed to be taken over completely by creep deformation that accelerated and eventually led the specimen to complete failure. At no point in time during this last load increment was the proving ring reading steady enough for accurate data acquisition. The last data point for the 20 psi test indicated a shear stress at failure of about 12 psi, while the previously measured Mohr-Coulomb shear strength parameters would predict a value of 24.9 psi. This comparison supports the conclusion that the specimen experienced creep rupture rather than shear failure.

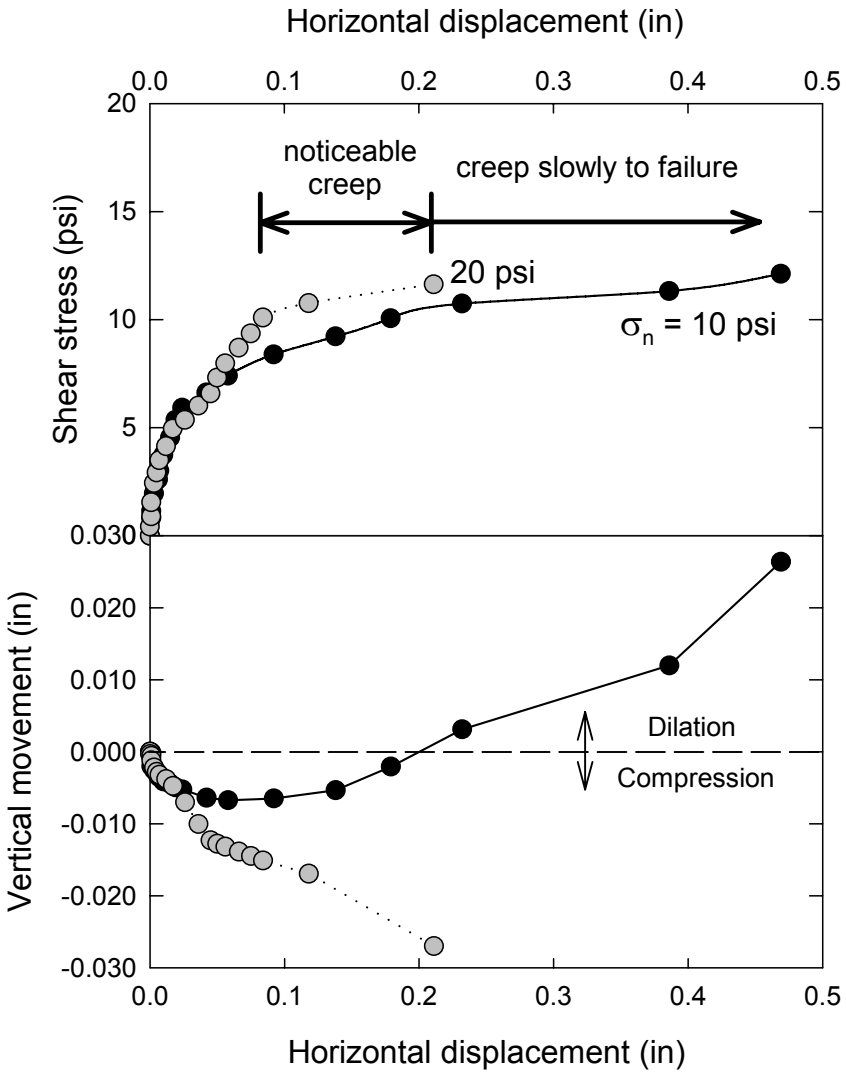

Figure 5-13 Large-scale, load-controlled direct shear tests on RAP specimens

As a result of this excessive creep behavior of RAP during shear, it was decided to terminate the direct shear test program on RAP and to study its creep behavior more thoroughly using triaxial creep tests (Chapter 6). The experiments on RAP led to the conclusion that force-controlled direct shear measurements are unsuitable for materials

with high creep potential, such as RAP, because test specimens may fail prematurely in creep rupture at shear stresses well below the actual strength of the material.

In contrast to the tests on RAP, tests on CFM and CC were accomplished with no difficulty. After each load increment application, shearing progressed to a complete termination of deformation and data were obtained. Figure 5-14 and Figure 5-15 show plots of shear stress versus relative horizontal displacement, and vertical displacement versus relative horizontal displacement for CFM and CC specimens. An area correction that utilizes the actual specimen shearing surface to calculate the shear and normal stresses was applied. Also, calculation of the final effective normal stress at failure included the summation of the extra loads from the top half of the compacted specimen, air bladder, top bearing plate, and grid plate, minus the estimated water pressure in the shear zone based on the water level in the water tank.

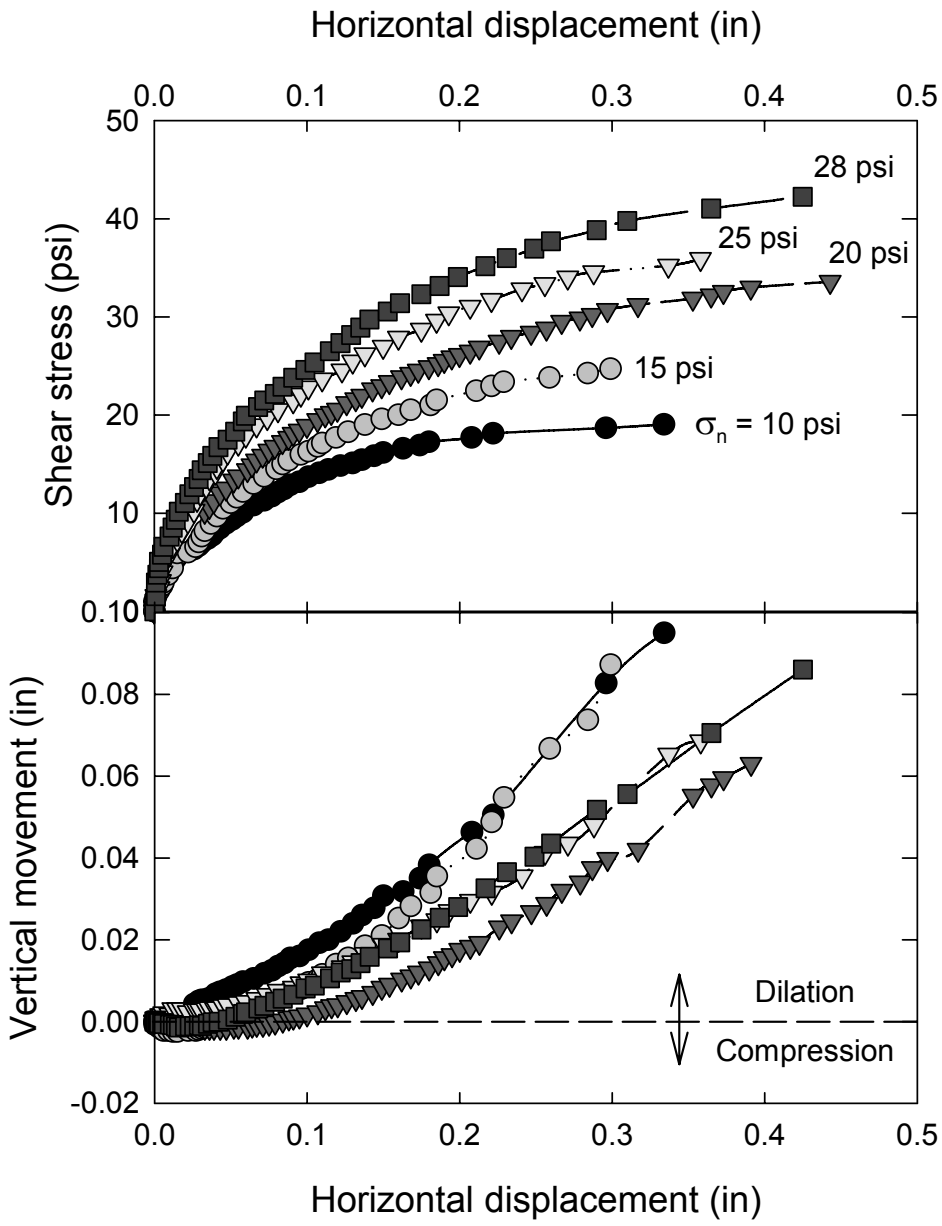

Figure 5-14 Results from large-scale direct shear tests on CFM

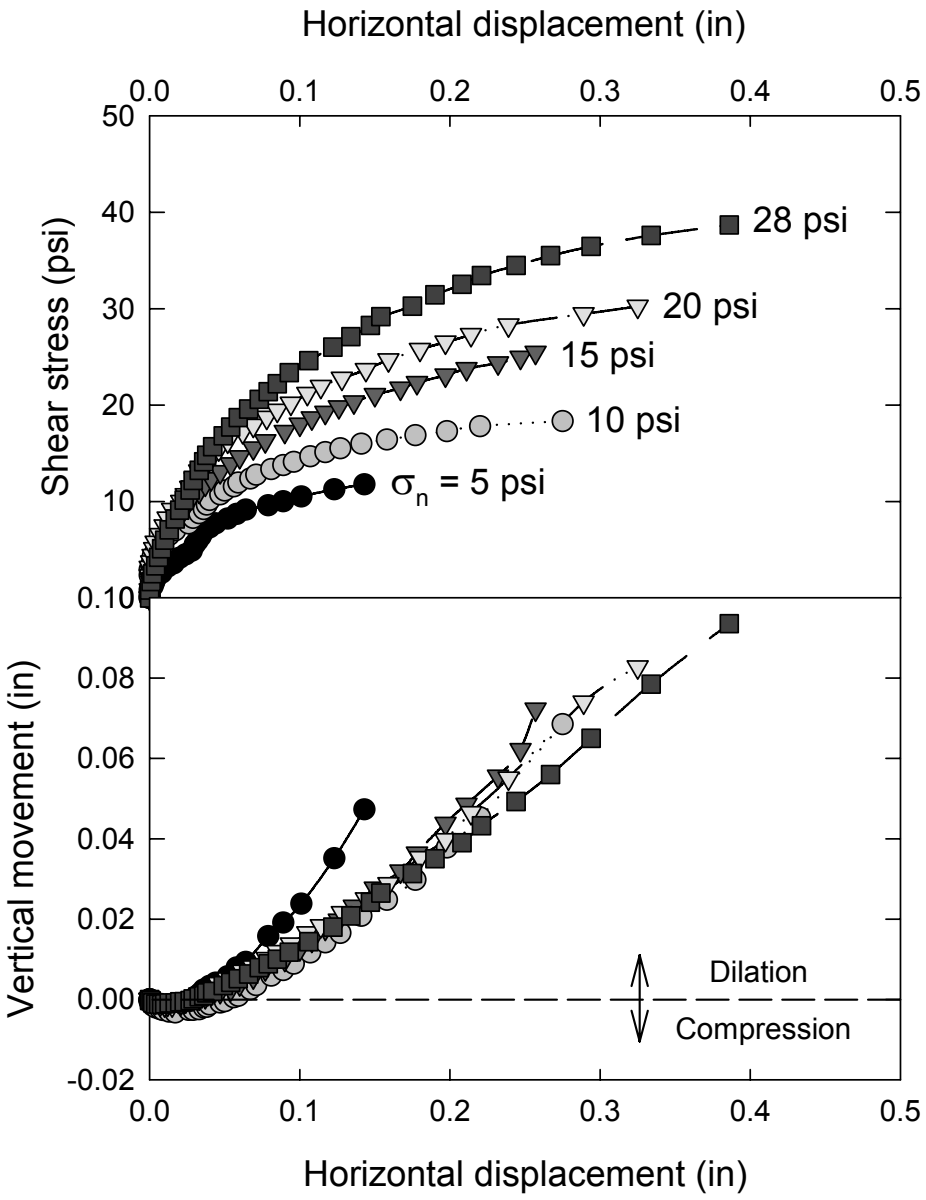

Figure 5-15 Results from large-scale direct shear tests on CC

Results from the drained, large-scale direct shear tests on CFM and CC specimens show that both materials have very similar responses when sheared. The CFM and CC specimens all exhibited a dilative response, which is typical for dense materials. The degree of expansion depends heavily on the applied normal stress, with less dilatancy occurring at large normal stresses, in general.

The shear stresses and the corresponding corrected normal stresses at failure for the large-scale direct shear test specimens are plotted in Figure 5-16 to determine the best-fit Mohr-Coulomb shear strength parameters for CFM and CC. The data resulted in remarkably similar values of c' and ϕ' for the two materials (c' = 6 psi and $\phi' = 51°$ for CFM, c' = 6 psi and $\phi' = 49°$ for CC). The non-zero values of cohesion for both materials in the direct shear tests were also observed in the triaxial test results and may be caused by the re-cementation of the material after compaction or a nonlinear failure envelope.

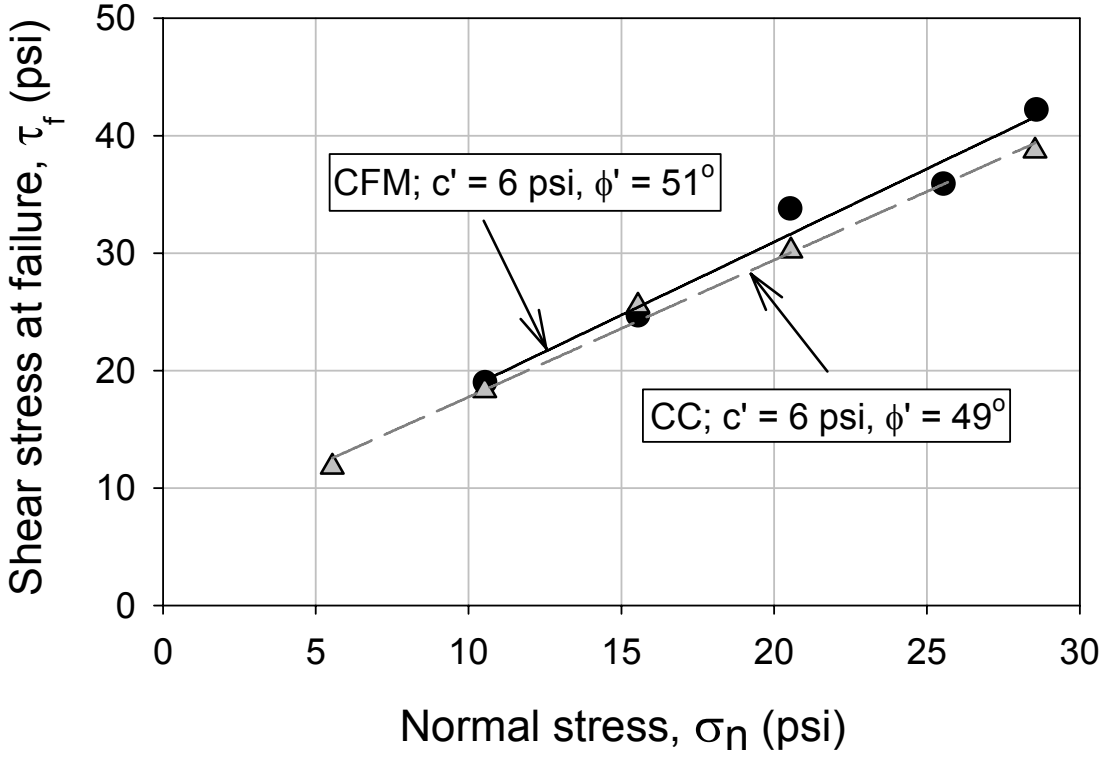

Figure 5-16 Best-fit Coulomb envelopes for large-scale drained direct shear tests on CFM and CC specimens

5.3.3 Integration of Shear Strength Results

Results from the drained triaxial tests and large-scale direct shear tests were combined to develop a better understanding of the strength of each of the two materials. The direct shear tests included the entire material gradation and were performed at lower normal stresses than the triaxial tests. Mohr-Coulomb failure envelopes were obtained by performing regression analysis on the combined (triaxial and direct shear) data for CFM and CC separately. Because no accurate direct shear data were collected for RAP due to its excessive creep behavior, only the triaxial data are considered for RAP.

Results from the direct shear tests are plotted directly on the shear stress-normal stress coordinate system because this test measures directly the stresses on the shear failure plane at failure. The triaxial test measures the major and minor principal stresses at failure (i.e. σ'_{1f} and σ'_{3f}), which allows one to draw a complete Mohr's circle, but these stresses do not represent the stresses on the failure plane of the test specimen at failure. Therefore, to combine these two datasets appropriately for further analysis, it is necessary to identify a single point for each complete Mohr's circle that represents the shear and normal stresses on the failure plane at failure. Ideally, this point can be identified mathematically using basic algebra, if each Mohr's circle is tangent to the failure envelope. That was not the case here, so the failure stresses were identified as the point on each individual Mohr's circle that was closest to the average shear strength envelope. This procedure was performed visually and is illustrated graphically in Figure 5-17, where coordinates (x_1, y_1) and (x_2, y_2) are the closest points to the average failure envelope for two separate tests.

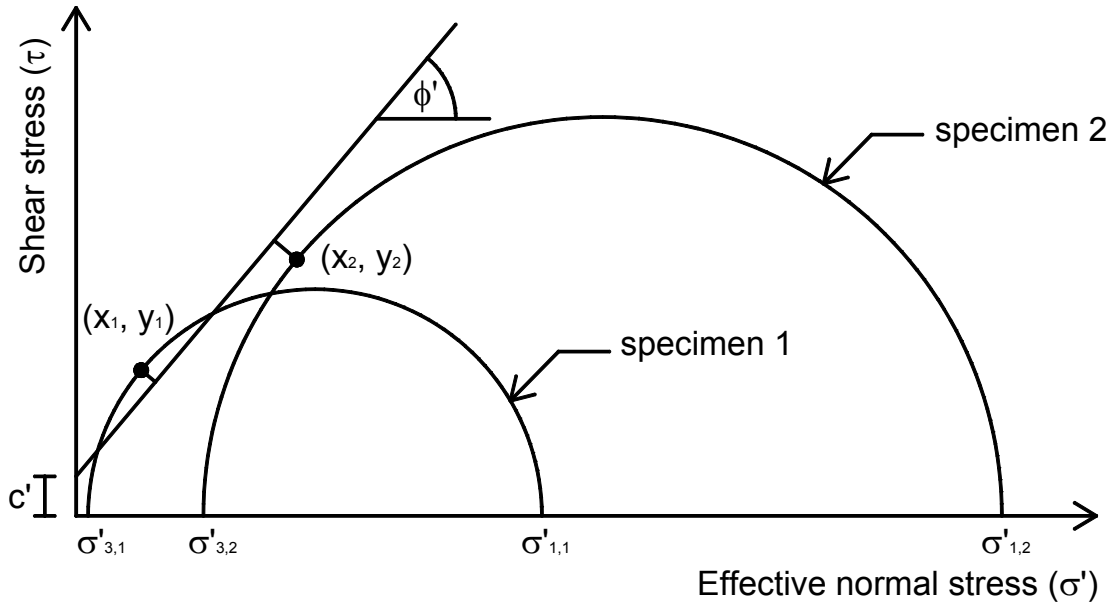

Figure 5-17 Diagram showing Mohr circles' closest coordinates to the strength envelope

Subsequently, Figures 5-18 and 5-19 illustrate the combined triaxial and direct shear data for CFM and CC along with their best-fit Mohr-Coulomb failure envelope. It was observed after combining these two sets of data that the failure envelopes may be curved because the data points representing the direct shear test results seem to be gradually moving towards the origin, especially in the case of CC. To further evaluate if the failure envelopes are curved, a plot between secant friction angle (ϕ'_{sec}) and the logarithm of the normalized confining pressure ($\log(\sigma'_3/P_a)$ or $\log(\sigma'_n/P_a)$, where P_a is atmospheric pressure) is plotted in Figure 5-20 for each test material based on all the available data (i.e. triaxial and direct shear results). It is observed in Figure 5-20 that a straight line can be drawn through each group of data with reasonable R^2 values (> 0.95 for CC and RAP, > 0.8 for CFM). The lower R^2 for CFM is caused by the differences in

friction angle between triaxial and direct shear testing in the confining pressure range of 1.0 to 2.0 atm. The straight line relationships observed in this plot further suggest that the secant friction angle of the test materials tends to decrease with increasing confining pressure. It was also observed in Figure 5-18, 5-19, and 5-20, that scalping of particles larger than 0.63 in. for the triaxial tests did not significantly alter the strength characteristics of the materials as the data from the two tests lined up well against each other.

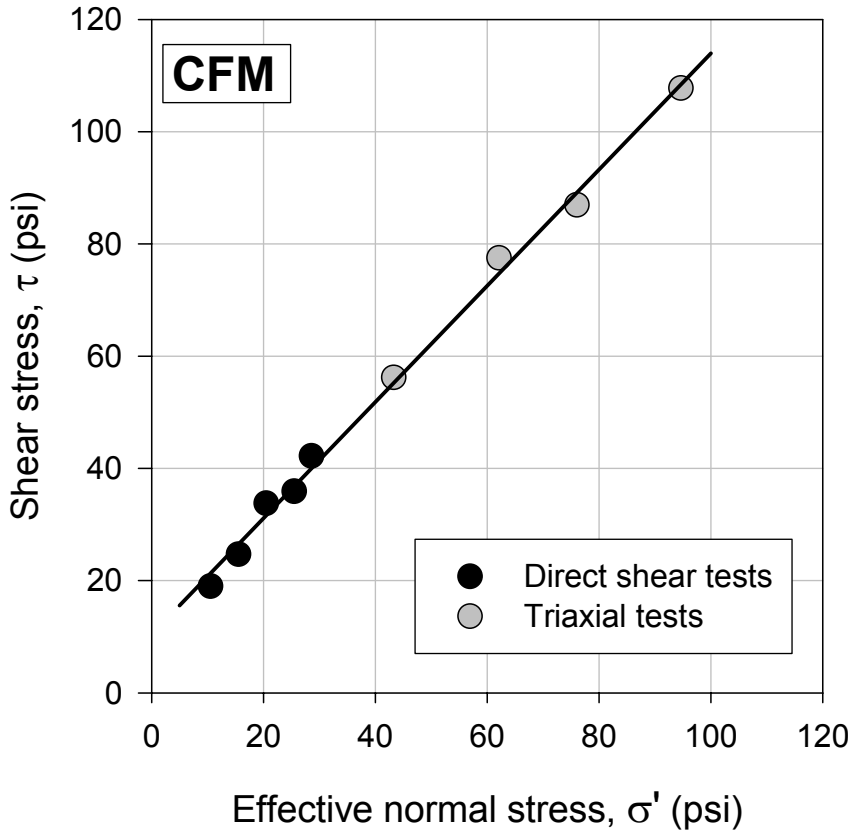

Figure 5-18 Combined direct shear and triaxial shear strength data for CFM

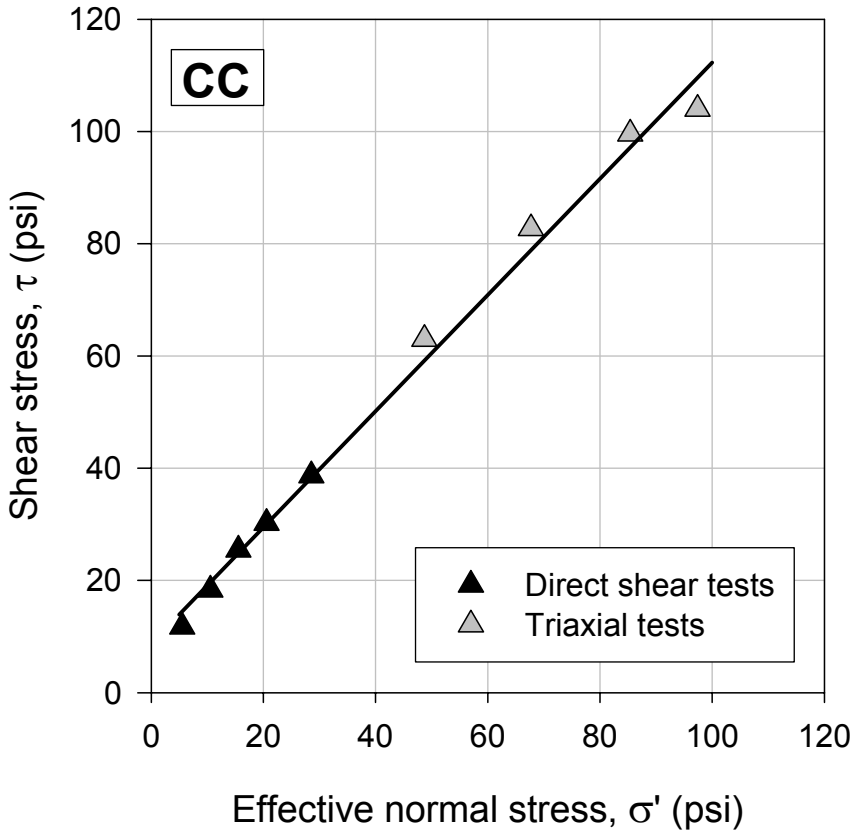

Figure 5-19 Combined direct shear and triaxial shear strength data for CC

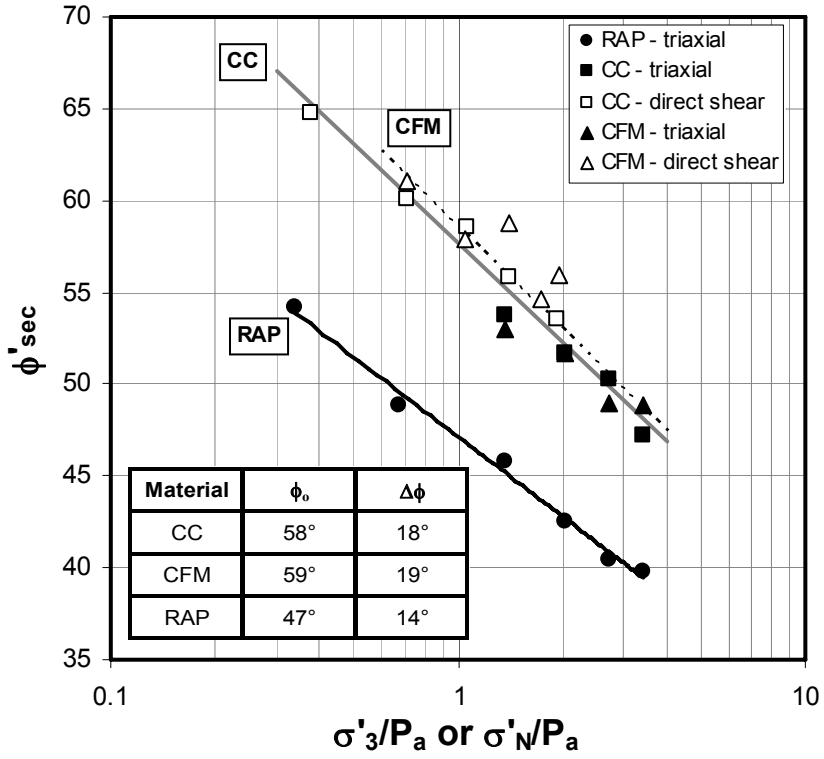

Figure 5-20 Secant friction angles vs. log (σ'_3/P_a) [or (σ'_n/P_a)]

The values of friction parameters for each test material, ϕ_o = secant friction angle at one atmosphere and $\Delta\phi$ = reduction in friction angle per log cycle of σ'_3/P_a or σ'_n/P_a, were determined from the straight line relationships and are also included in Figure 5-20. It is observed that the $\Delta\phi$ values for RAP, CC, and CFM are all very high, and because $\Delta\phi > 10°$ is normally considered significant and indicative of a curved failure envelope, it is therefore decided that the failure envelopes for RAP, CC, and CFM are curved. The identification of the curved failure envelopes reveals that these test materials do not have a true cohesion component during shearing (i.e., c' = 0).

Based on the data in Figure 5-20, the secant friction angle (coupled with c' = 0) varies significantly with confining pressure. These data can be used to model the shear strength of RAP and CC with confining-pressure dependent secant friction angles or used to select for design a lower bound friction angle based on the maximum pressure expected in the field. If one assumes that the maximum confining pressure within the backfill of an MSE wall is 3 atm, the secant friction angles of RAP, CC, and CFM can be taken, conservatively, as 40°, 48°, and 50°, respectively. Each of these friction angles represents adequate shear strength for use as backfill in MSE walls.

Although the FHWA MSE wall specifications do not explicitly specify a minimum friction angle for an MSE wall candidate backfill, Elias and Christopher (1996) reported that a lower bound frictional angle of 34° is consistent with materials that have been successfully used in MSE walls. In addition, Palossy et al. (1993) indicated that several European countries including France, Great Britain, Germany, and Hungary have designated a minimum angle of internal friction (ϕ_{min}) of 25° for MSE wall backfills. Palossy et al. (1993) also reported that two Hungarian retaining walls were structurally safe using backfill material containing significant amounts of silt and fine sand that marginally satisfied the ϕ_{min}. RAP and CC both meet these minimum friction angle requirements. The significant volumetric dilation of CC and CFM during drained shear also encourages the use of these materials as backfill materials in MSE walls because the dilatancy effect increases the soil-reinforcement interface friction [Guilloux et al. (1979)]. RAP, on the other hand, displays significant creep behavior that potentially makes it less attractive as MSE wall backfill, even though it displays an adequate friction angle.

5.4 HYDRAULIC CONDUCTIVITY MEASUREMENTS

Free draining materials are typically used as MSE wall backfill and only limited experience is reported on MSE walls constructed with poorly draining backfill. Because MSE wall facing panels are not structurally designed to withstand large horizontal forces, it is important that free draining materials be used to minimize the potential development of water pressures behind the wall facing. Also, the buildup of pore water pressures may reduce the backfill soil strength and its developed interface friction with the reinforcement. Finally, using less permeable materials increases the potential for corrosion of metallic reinforcements behind the wall, which reduces the wall service life.

Hydraulic conductivity (k) is the soil property that expresses how well water flows through a particular soil of interest. However, current standards for backfill materials do not specify minimum values of hydraulic conductivity, but rather rely on the specified grain-size distribution to produce acceptable values of hydraulic conductivity. The current grain-size specifications require a significant amount of coarse-grained particles to ensure adequate drainage. Nevertheless, this section is intended to compare the hydraulic conductivities of RAP and CC with CFM using conventional laboratory setups.

5.4.1 Sample Preparation and Testing Program

A total of fifteen laboratory hydraulic conductivity tests were conducted on the test materials using the falling head-rising tail flexible wall method in accordance with ASTM D 5084. Each material was tested at five different effective confining pressures ranging from 5 to 50 psi. All tests were performed on specimens that were subsequently

used for the drained triaxial test measurements. Thus, the sample preparation techniques described in section 5.3.1.1 were used. Figure 5-21 depicts a schematic drawing of the complete test setup showing the main components that were required for the falling head-rising tail method used in this study.

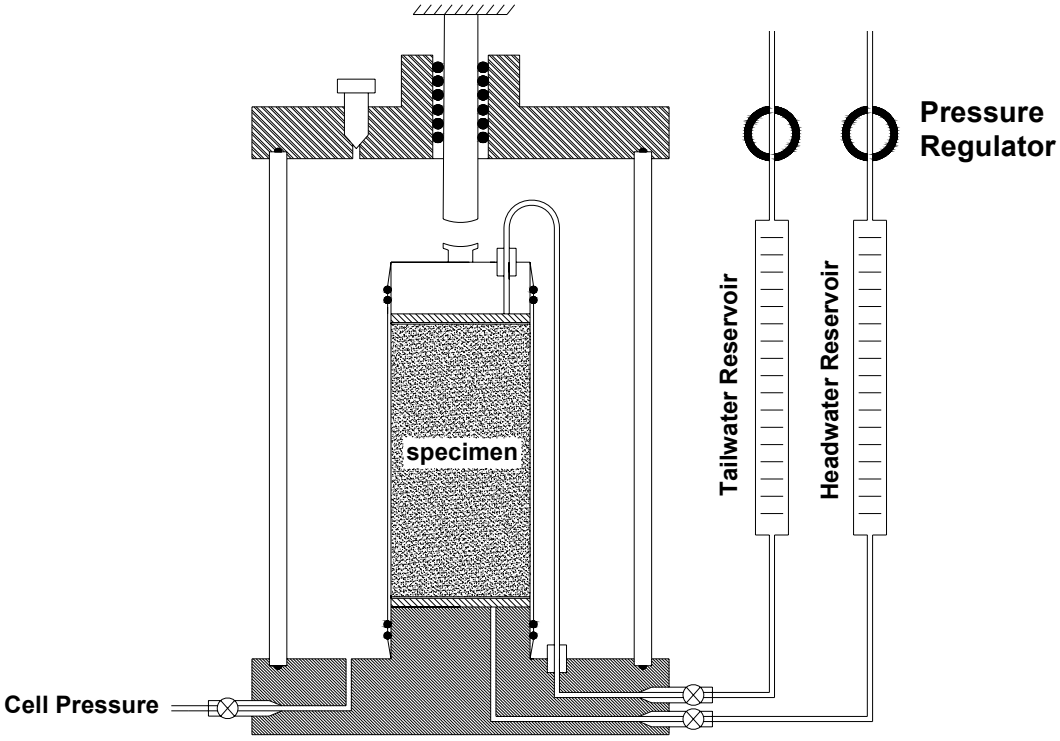

Figure 5-21 Schematic drawing of the test setup for hydraulic conductivity measurement [after ASTM D 5084]

Hydraulic conductivity test was performed after backpressure saturation to the desired B value and after primary consolidation to the target effective confining pressure. During hydraulic conductivity testing, the backpressure applied to the top of the

specimen (effluent, tailwater line) and base of the specimen (influent, headwater line) was equal, and the test water flowed due only to the difference in elevation head between the falling headwater and the rising tailwater. This small head difference (< 40 cm.) was intended to ensure that the hydraulic gradient (*i*) did not exceed a value of two, which is the recommended value for particle sizes of this range (ASTM D 5084). Five measurements of hydraulic conductivity were made on each specimen at each effective confining pressure.

5.4.2 Test Results and Discussion

The ratio of the outflow volume to the inflow volume ranged between 0.95 and 1.05 throughout this study, indicating near complete saturation of the test specimens and no significant specimen volume change during the test. The hydraulic conductivity was calculated from the test data using the following equation from ASTM D 5084:

$$k = \frac{a_{in} \cdot a_{out} \cdot L}{(a_{in} + a_{out}) \cdot A \cdot \Delta t} \ln\left[\frac{h_1}{h_2}\right]$$

where: k = hydraulic conductivity, cm/sec

a_{in} = cross-sectional area of influent reservoir, cm^2

a_{out} = cross-sectional area of effluent reservoir, cm^2

L = length of specimen, cm

A = cross-sectional area of specimen, cm^2

Δt = elapsed time between determination of h_1 and h_2, second

h_1 = difference in hydraulic head across the specimen at time t_1, cm

h_2 = difference in hydraulic head across the specimen at time t_2, cm

Because the test specimens have a relatively large value of *k*, a correction for the head loss from the porous stones and filter paper was considered. This correction, however, resulted in only a small change in the second significant digit of the measured *k* values, and this difference is not considered meaningful for this type of test. Table 5-3 lists the corrected *k* values of the test materials averaged from five measurements at each effective confining pressure. In this table, *k* values are reported in units of 10^{-4} cm/s.

In general, RAP has comparable *k* values with CFM (Table 5-3). The *k* values of the CC specimens, however, are at least one order of magnitude smaller than those for RAP and CFM measured at the same σ'_c. Because the grain-size distributions of all of the test specimens are identical, it is believed that re-cementation of the CC particles may have impeded the water flow and resulted in the smaller *k* values. The large *k* values for RAP may be the result of the bitumen coating in RAP that does not attract or absorb water. A hydraulic conductivity of 10^{-4} cm/s has been proposed as an approximate boundary between free draining and poorly draining materials under low gradients [Casagrande and Fadum (1940)]. Based on this criterion, CC would be classified marginally as poorly draining, while RAP and CFM would be designated as free draining.

Table 5-3 Summary of hydraulic conductivity of the test materials

Effective Confining Pressure, σ'_c (psi)	**Hydraulic Conductivity, k (x 10^{-4} cm/s)**		
	RAP	**CC**	**CFM**
5	38.4	1.6	13.8
20	25.7	0.84	21.8
30	27.7	0.18	6.4
40	12.7	0.12	4.5
50	5.5	0.11	6.0
Hsieh (2003)*	54.3	2.3	18.3
Hsieh (2003)**	51.7	0.66	9.7

Note: * specimens prepared at reference gradation
** specimens prepared at reference gradation scalped at 0.75 in.

The *k* values from Table 5-4 for each material are plotted in Figure 5-22 as a function of effective confining pressure. These data indicate that the *k* values for each test material generally decrease with increasing effective confining pressure. The *k* of CC and CFM starts to decrease appreciably after σ'_c exceeds 20 psi, while the *k* of RAP does not start to decrease until after 30 psi. The RAP and CC display almost one order of magnitude decrease in *k* over the applied stress range, while the reduction for CFM is slightly less.

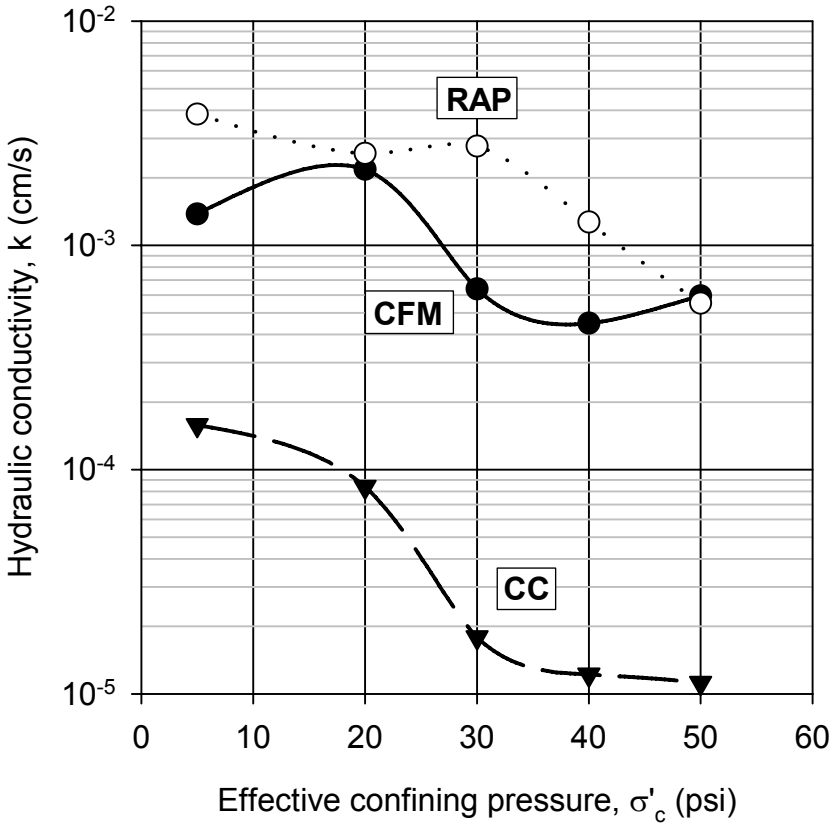

Figure 5-22 Hydraulic conductivity of test materials at different confining pressures

Recall that the triaxial specimens were scalped at 0.63 in., and field materials would include larger particles. The particle scalping may affect the measured *k* values, although typically the smallest particle sizes affect *k* the most. Hsieh (2003) performed constant head, fixed-wall hydraulic conductivity tests on the test specimens mixed to the reference gradation and specimens scalped at 0.75 in. sieve. During these tests, no surcharge load in excess of the weight of the top porous stone was applied to the top of the specimens. The load from the top porous stone translates into approximately 0.15 psi normal stress. The average *k* values reported by Hseih (2003) are included in Table 5-3.

Compared with the *k* values measured at low effective confining pressure (i.e. 5 psi) in the falling head-rising tail tests, the constant head tests produce similar values. These results are in agreement with the theory that *k* is affected most by the percentage of fine particles, not the distribution of large particles. Therefore, it is concluded that scalping large particles (> 0.63 in.) for the 4-in diameter test specimens did not significantly alter the *k* values of the bulk materials.

5.5 COLLAPSE POTENTIAL

When a granular backfill is compacted at low dry density and water content, it can undergo significant settlement upon wetting. This deformation mechanism upon wetting is called collapse. ASTM D 5333, titled "Standard Test Method for Measurement of Collapse Potential of Soils", defines a collapsible soil as a soil that can withstand relatively large applied vertical stress with small settlement while at a low water content, but exhibits considerable settlement after wetting with no additional increase in vertical stress. Therefore, a large applied vertical stress alone is not solely responsible for collapse.

The study of collapsible soils has been reported in the literature [such as Lutenegger and Saber (1988), Lawton et al. (1992), Houston et al. (1993)]. Many of these studies concluded that the most critical factors controlling the collapse potential of a given compacted soil are the as-compacted degree of saturation, the as-compacted dry density, and the total overburden pressure, with the collapse potential decreasing with increasing dry density and as-compacted water content. Two additional important

observations reported by Lawton et al. (1992) are that there is a critical value of vertical stress and a critical value of degree of saturation, above which negligible collapse occurs.

5.5.1 Sample Preparation and Testing Program

The experimental study on collapse potential was conducted in accordance with ASTM D 5333. Because this test simply involves a one-dimensional deformation measurement of a laterally confined material upon wetting, it was decided to perform this test on the direct shear test specimens prior to performing the direct shear tests.

After each specimen was compacted to its full height inside the direct shear box and all the vertical dial gauges were in place, a seating pressure of 1.5 psi was applied to the top of the specimen. Normal stress increments were applied to the specimen until the target normal stress was reached. Each stress increment was maintained on the specimen until no additional vertical movement was observed. After the target normal stress was reached, water was slowly introduced into the water tank from the bottom to avoid trapping of air bubbles inside the specimen, and water was added until the specimen was fully inundated. Vertical movement of the specimen was recorded throughout this entire process. Readings were taken until no significant additional change in vertical movement was observed.

5.5.2 Test Results and Discussion

Collapse measurements were conducted on five specimens of CFM and CC, at applied normal stresses ranging from 1.5 to 28 psi. Because direct shear tests on RAP were only performed at 10 and 20 psi due to creep issues, only two collapse measurements were obtained for RAP. Figure 5-23 illustrates the measured vertical

deformation versus applied normal stress for the CC and RAP specimens obtained from this study. The initial deformation was offset to zero at the 1.5 psi seating pressure to remove any compression from specimen surface irregularity and machine compliance. It can be seen from this figure that more vertical deformation was experienced at smaller normal stresses than at larger normal stresses. However, upon soaking the RAP experienced significant settlement, while the CC experienced very little deformation.

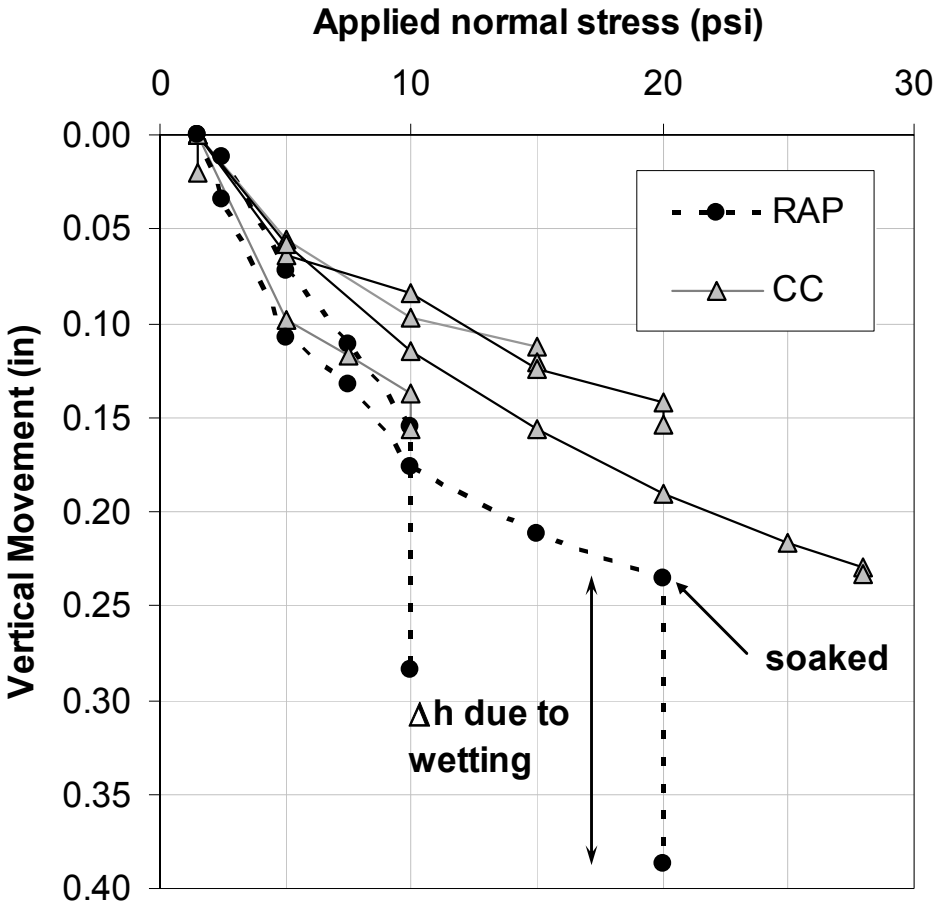

Figure 5-23 Compression curves from collapse potential tests

ASTM D 5333 defines a parameter called the collapse index (I_c) to quantitatively characterize the collapse potential of any particular soil for the specific vertical stress of interest. This index property is simply the vertical strain, in percent, due to wetting and, thus, can be directly used to estimate field settlement upon wetting of the same soil under the same vertical stress. The collapse index is defined as follows:

$$I_c(\%) = \frac{\Delta h}{h_o} \cdot 100$$

where:

Δh = change in specimen height due to wetting (in)

h_o = initial specimen height prior to wetting (in)

The compression due to wetting for each test specimen was used to calculate the collapse index. Figure 5-24 displays the resulting collapse indexes of the test materials at different applied normal stresses. For CC and CFM, I_c is very small (0.05 to 0.2%) and there is no observable trend with normal stress. The ASTM classification for soil collapse potential based on the laboratory-measured I_c value is shown in Table 5-4. Based on this classification, CC and CFM both fall on the low end of the "slight" collapse potential range. RAP showed significantly higher values of I_c than CC and CFM (~1.5% vs. ~0.2%), but still classifies as "slight" collapse potential, although at the upper end of the range.

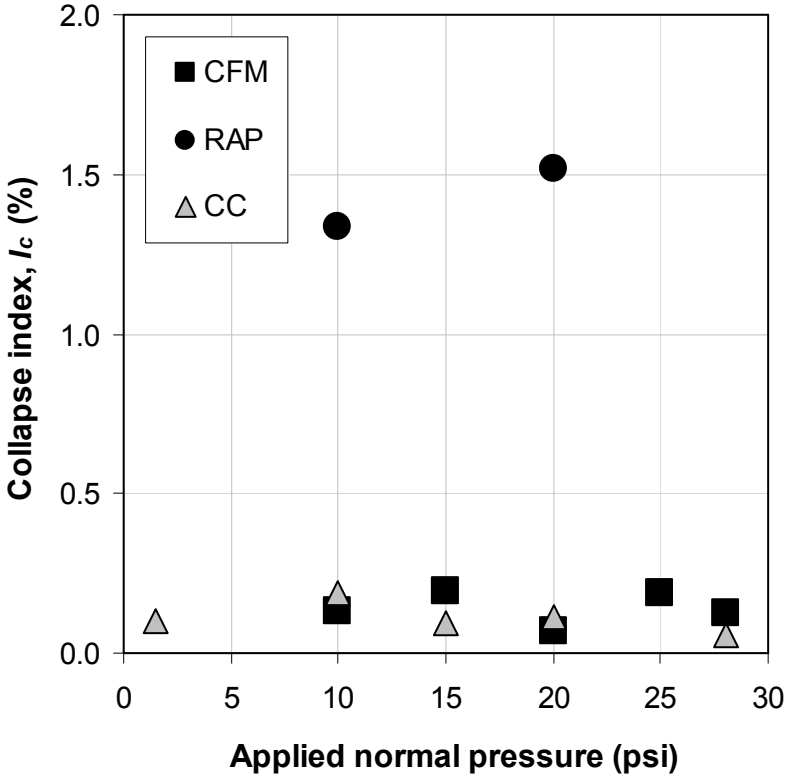

Figure 5-24 Collapse indexes of test materials at different normal stresses

Table 5-4 ASTM classification of collapse index

Degree of Collapse	**Collapse Index, I_c (%)**
None	0
Slight	0.1 to 2.0
Moderate	2.1 to 6.0
Moderately severe	6.1 to 10.0
Severe	> 10

The more severe collapse of RAP is most likely due to its initial low degree of saturation (approximately 30%) as compared to those of CC and CFM (approximately 70% and 80%, respectively). The RAP specimens were not constructed at larger water contents/saturation values because they could not hold additional water due to the bitumen coating (see compaction results in Chapter 4). RAP particles also are less angular than CC and CFM, and thus may collapse more easily. Finally, the collapse potential for CC and CFM may be so small because of the perceived re-cementation of the particles. Cementation of the particles would inhibit deformation of the particles, and minimize its collapse potential.

5.6 SUMMARY

Shear strength characteristics of RAP, CC, and CFM were evaluated through triaxial and large-scale direct shear tests. The combined sets of data from the two types of tests concluded that CC and CFM have comparable values of effective friction angle (ϕ'), and these values are more than adequate ($\phi' \geq 40°$) for typical MSE wall backfill applications. RAP displayed a smaller value ($\phi' = 37°$), which is marginal when compared with the lower bound value of 34° specified by the FHWA MSE wall design manual. The excessive creep behavior of RAP observed during the direct shear tests indicates that this viscous effect in RAP may be a weakness of this material when considering it for MSE wall backfill. Further study on this creep effect in RAP will be discussed in Chapter 6.

Results from hydraulic conductivity tests show that RAP and CFM can be classified as free draining materials, while CC is a marginally poorly draining material. The re-cementation of CC particles appeared to be primarily responsible for the low k values observed. On the other hand, the bitumen coating in RAP allowed water to flow through the voids more easily because the bitumen in general does not attract or absorb water.

The collapse potential of the test materials were evaluated and compared through a one-dimensional constrained compression test and the index property called the collapse index (I_c). The resulting I_c values for all three materials classified them as materials with only a slight degree of collapse potential upon wetting, although RAP exhibited notably greater collapse than CC and CFM. The larger degree of collapse potential for RAP was believed to be the result of its smaller initial degree of saturation and lower angularity. Nonetheless, RAP and CC should not exhibit significant collapse settlement upon wetting in the field, at least in the pressure range used in this study.

Chapter 6. Creep Potential of RAP

6.1 INTRODUCTION

In the United States, materials with any indication of creep potential have traditionally been avoided as backfill in MSE walls primarily due to the difficulties involved in understanding the interaction between the creeping backfill material and the reinforcement. Over the last few decades, many European countries have been exploring the possibility of using backfill with creep potential, in areas where local granular soil is not available. Jones (1984) reported that the UK design memoranda allows using backfill for reinforced earth structures that has 100% passing the 0.063 mm sieve and classifies as a low plasticity clay (CL) in the Unified Soil Classification System. Furthermore, Palossy et al. (1993) noted that many reinforced earth structures in Europe have used similar material and yet no post-construction problems have been reported.

Creep is a concern for RAP because of the viscoelastic behavior of the bitumen coating that surrounds the aggregate particles. The tendency for RAP to fail due to creep rupture rather than typical shear failure was observed during the large-scale direct shear tests performed on RAP (Chapter 5). Consequently, this chapter describes an experimental investigation initiated to study the creep behavior of RAP.

6.2 THEORETICAL BACKGROUND

Figure 6-1 is a typical plot of axial creep strain versus time under a constant deviator stress for a creeping soil. The curve displays three distinct regions of creep behavior (primary creep, secondary creep, and tertiary creep) followed by creep rupture. Primary creep occurs immediately after application of the shear stress in which the strain rate decreases with time. During secondary creep, the strain rate reaches a minimum value ($\dot{\varepsilon}_{\min}$) and remains essentially constant over an extended period of time before the strain rate starts to accelerate. This point of accelerating deformation represents the initiation of tertiary creep, and leads finally to complete creep rupture at the end of the tertiary creep.

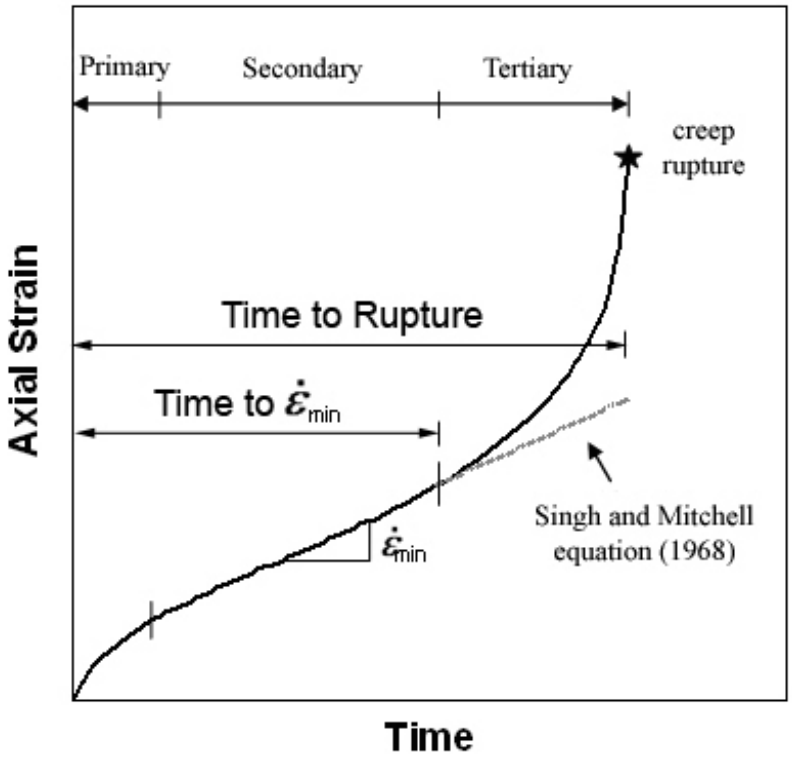

Figure 6-1 Time-dependent creep deformation under a constant stress level

A significant number of studies on soil creep have been reported in the literature, many of which focus on implementing constitutive model to fully capture the time dependency of the stress-strain properties of soils. The majority of the existing constitutive models proposed in the literature can be divided into two main categories: rheological models and empirical models. The rheological models are composed of complex combinations of linear or nonlinear springs with linear or nonlinear dashpots and slider elements. Often times it is difficult to accurately evaluate the coefficients for these models, and they generally give little indication of the basic mechanisms responsible for the observed behavior [Febres-Cordero and Mesri (1974)]. On the other hand, many engineering empirical models have been developed that adequately describe the observed macroscopic creep behavior with simple mathematical expressions. Although Augustesen et al. (2004) pointed out that none of the models developed to date is sufficiently general to account for the range of observed time effects in soils, empirical models have been used extensively to predict the creep behavior of soil [such as Murayama and Shibata (1961), Mitchell et al. (1968), Mesri et al. (1981), Adachi and Takase (1981), and Nicholson et al. (1996)]. Thus, a simple 3-parameter empirical model, developed by Singh and Mitchell (1968), is used here to describe the creep behavior of RAP.

The Singh and Mitchell creep model (1968) is a widely accepted empirical model for soil creep that uses a simple three-parameter empirical phenomenological equation. This model is used as the primary constitutive model to fit the observed creep data obtained in this study. The Singh and Mitchell (1968) creep model was developed based on the

premise of the rate process theory, which was first introduced by Eyring (1936). Studies on the use of rate process theory to predict the creep behavior of soils were performed extensively during the early to mid 1960's [such as Murayama and Shibata (1958, 1961, 1964), Mitchell (1964), and Christensen and Wu (1964)], after which Singh and Mitchell (1968) introduced a practical, yet simple, three-parameter creep model.

The basic relationship developed by Singh and Mitchell (1968) to predict the time dependent strain rate for a given shear load is:

$$\dot{\varepsilon} = Ae^{\alpha D}\left(\frac{t_1}{t}\right)^m \quad \text{or} \quad \dot{\varepsilon} = Ae^{\bar{\alpha}\bar{D}}\left(\frac{t_1}{t}\right)^m \tag{6.1}$$

where: $\dot{\varepsilon}$ = strain rate

t_1 = reference time

D = deviator stress, $(\sigma'_1 - \sigma'_3)$

$\bar{D}$ = deviator stress level, $[(\sigma'_1 - \sigma'_3)/(\sigma'_1 - \sigma'_3)_{ult}]$

A = strain rate at time t_1 and D (or $\bar{D}$) = 0

m = absolute value of slope of a log(strain rate) vs. log(time)

α, $\bar{\alpha}$ = slope of linear portion of plot between log(strain rate) vs. deviator stress (D) and log(strain rate) vs. stress level ($\bar{D}$), respectively, at a given time after load application

This form of this relationship is independent of whether the soil is undisturbed or remolded, wet or dry, normally consolidated or overconsolidated, or tested drained or undrained [Singh and Mitchell (1969)]. However, it is truly suitable only for soils that are subjected to deviator stress levels ($\bar{D}$) within the range of 0.30 to 0.90 (i.e., 30% to 90% of the soil's deviator stress at failure as determined by monotonic strength tests), a range considered to fall within engineering interest. Also, Equation 6.1 only calculates the time-dependent creep deformation of a given soil up to the end of the secondary creep, and does not model deformations during the tertiary creep (Figure 6-1).

Experimental results have been used to verify the functional form of the Singh and Mitchell (1968) creep equation and to derive the parameters for the model. For example, Murayama and Shibata (1958) plotted the logarithm of strain rate versus the logarithm of time from undrained creep tests on Osaka clay (Figure 6-2). These data show that for most of the applied stresses (i.e., those that represent stress levels less than about 0.9) the logarithm of the strain rate decreases linearly with the logarithm of time, and that the slopes of the lines are independent of stress level. This relationship can be expressed mathematically by

$$\ln \dot{\varepsilon}(t, D) = \ln \dot{\varepsilon}(t_1, D) - m \ln\left(\frac{t}{t_1}\right) \tag{6.2}$$

where the term $\dot{\varepsilon}(t_1, D)$ is the axial strain rate at the reference time (t_1) as a function of stress level (D), and m is the absolute value of the slope of the curves shown in Figure 6-

2. Because *m* represents a linear relationship, Equation (6.2) can only predict the creep strain rate up to the end of secondary creep, where the strain rate reaches a minimum (Figure 6-2).

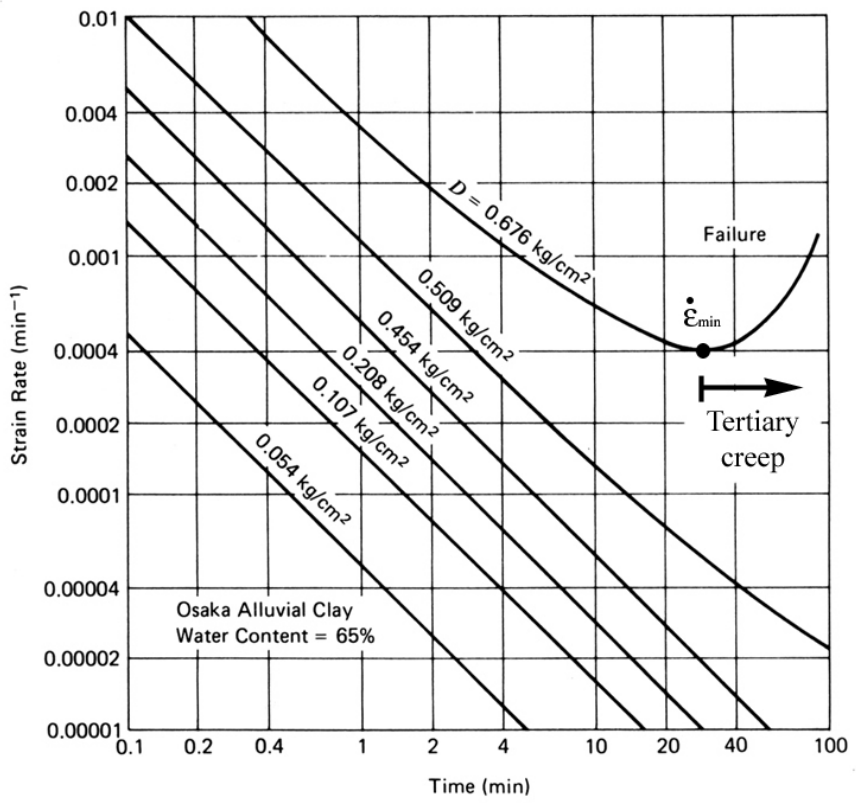

Figure 6-2 Strain rate vs. time relationships during undrained creep of Osaka alluvial clay [after Murayama and Shibata (1958)]

Figure 6-3 graphically displays the relationship between the logarithm of strain rate and the deviator stress level at different elapsed times after stress application (e.g. t_1, t_2, and t_3). It may be observed from this figure that for stress levels between 0.3 and 0.9 (the range of engineering interest), a linear relationship is found between the logarithm of

strain rate and stress level. For any given time, t_1, this relationship can be expressed mathematically as:

$$\ln \dot{\varepsilon}(t_1, D) = \ln \dot{\varepsilon}(t_1, D = 0) + \alpha D \tag{6.3}$$

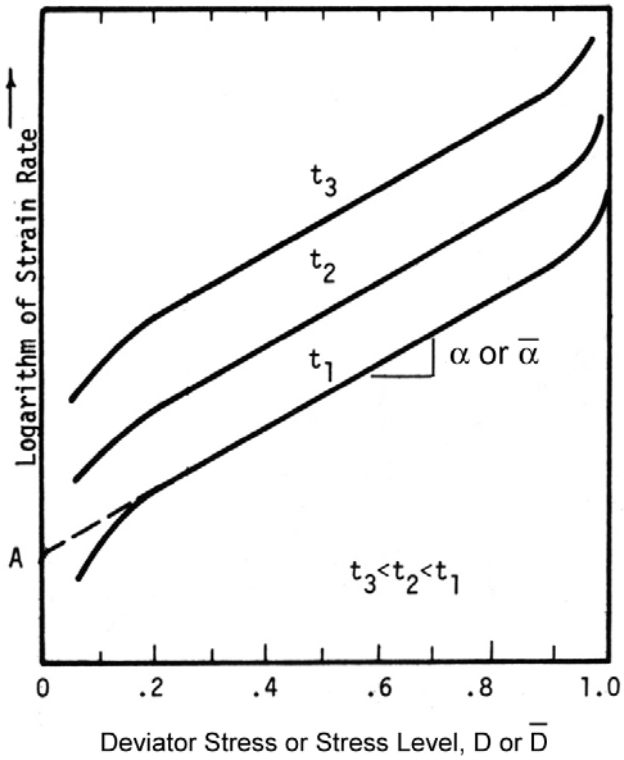

Figure 6-3 Typical plot between strain rate and stress level at any given time after stress application [after Febres-Cordero and Mesri (1974)]

The term $\ln \dot{\varepsilon}(t_1, D = 0)$ in Equation (6.3) represents the intercept of the linear curve when extrapolated to D = 0 (point A in Figure 6-3). The term α represents the slope of the linear portion of the logarithm strain rate versus stress level curve. By inserting Equation (6.2) into Equation (6.3) and setting $\dot{\varepsilon}(t_1, D = 0) = A$, one obtains:

$$\ln \dot{\varepsilon}(t, D) = \ln A + \alpha D - m \ln\left(\frac{t}{t_1}\right) \tag{6.4}$$

$$\dot{\varepsilon}(t, D) = A e^{\alpha D}\left(\frac{t_1}{t}\right)^m \tag{6.5}$$

A minimum of two creep tests is required to obtain the values of A, α (or $\bar{\alpha}$), and m for any given soil. The parameter A is a parameter that reflects composition, structure, and stress history. The parameter $\bar{\alpha}$ indicates the effect of deviator stress level ($\bar{D}$) on the creep strain rate. The parameter m controls the rate at which the strain rate decreases with time. By integration of equation (6.5), a general relationship between time and axial strain can be obtained. The integration provides two solutions depending on the value of m, as shown below.

$$\varepsilon(t, D) = A e^{\alpha D}(t_1)^m\left(\frac{1}{1-m}\right)t^{1-m} + C \qquad (\text{for } m \neq 1) \tag{6.6}$$

$$\varepsilon(t, D) = A e^{\alpha D} t_1 \ln t + C \qquad (\text{for } m = 1) \tag{6.7}$$

The constants of integration (C in equations 6.6 and 6.7) in the above equations can be obtained from a known value of strain at some known value of time. It can be seen from equation (6.6) and (6.7) that creep axial strain is described by a power function, in which a linear relationship is found between axial strain and the logarithm of time for m = 1, and a non-linear relationship results for $m \neq 1$, as shown in Figure 6-4. Also in this

figure an important physical significance of the *m* parameter is observed. A soil with an *m* value greater than 1.0 eventually reaches an asymptotic axial strain value, while a soil with *m* less than 1.0 does not reach an asymptotic strain value and eventually experiences creep rupture.

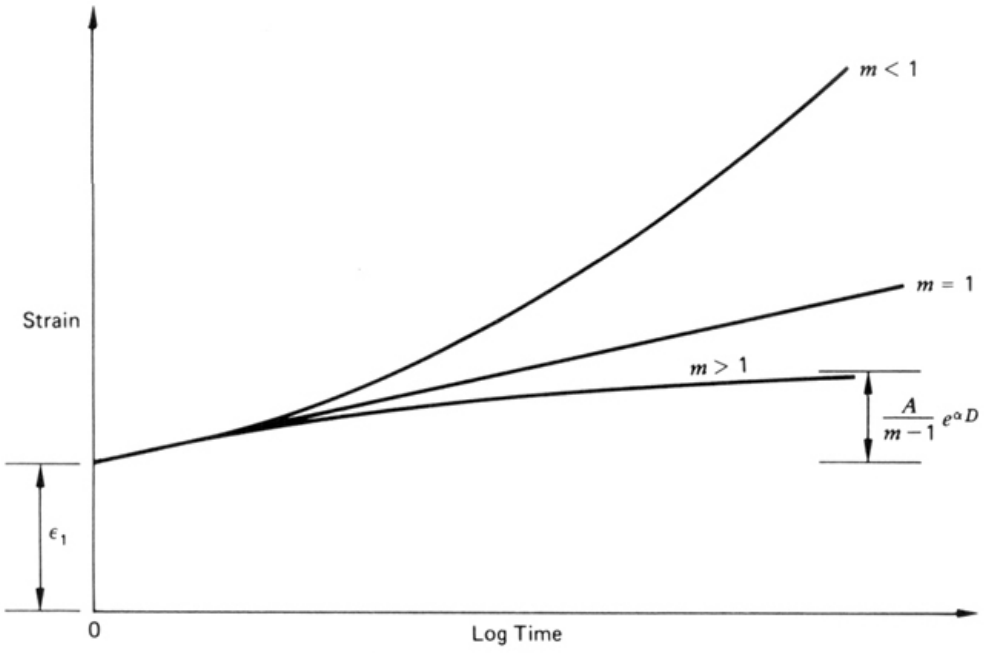

Figure 6-4 Effect of *m* values on predicted creep strains [after Mitchell (1993)]

Because of its significance, the parameter *m* is considered the most meaningful parameter in the Singh and Mitchell (1968) creep equation as it directly indicates the creep potential of a given soil. It is noteworthy that the typical values of *m* that have been reported in the literature range from 0.7 to 1.3 [Mitchell (1993)].

6.3 EXPERIMENTAL PROGRAM

A series of constant-stress, drained triaxial creep tests was performed on a number of RAP specimens using the triaxial test equipment discussed earlier in Chapter 5. Drained tests were performed rather than undrained tests because RAP is expected to respond in a drained condition in the field due to its large hydraulic conductivity. Also, Mitchell et al. (1968) presented evidence that a soil's resistance to shearing deformation occurs at interparticle contacts, which are effectively solid-to-solid in nature. This observation explains past studies that showed that the presence of water in a soil did not significantly alter the creep response, as wet and dry clays, and wet and dry sands, exhibited qualitatively similar creep behavior [Mitchell (1993)]. This is because the interparticle bond strength of soils, as can be directly related by their activation energy, is much greater than that for the viscous flow of water [Mitchell (1993)].

Table 6-1 lists values of activation energy for creep of various materials, including asphalt, soil, and water. Theoretically, for creep of soils, the activation energy represents the amount of energy required to displace the flow units (soil particles in this case) that are initially at equilibrium and constrained by an energy barrier to new positions [Mitchell (1968)]. Thus, the activation energy is the amount of energy needed to overcome the energy barrier that is created by a state of equilibrium, and larger values of activation energy indicate more resistance to creep. Table 6-1 shows that the activation energy of asphalt and soil is from five to ten times larger than that for the viscous flow of water, suggesting that for soil and RAP interparticle slippage through water films at the interparticle contact points is not likely [Mitchell et al. (1968)]. Furthermore, Mitchell et

al. (1968) discovered that the activation energy measured from dried illite was essentially the same as the activation energy of the same material tested in a saturated condition. These observations suggest that the presence of water does not impact creep behavior of typical earthen materials.

Table 6-1 Activation energies of typical materials

Material	**Activation Energy, in 1000 calories per mole**	**Reference**
Water	4 – 5	Glasstone, Laider, and Eyring (1941)
Asphalt	14 – 20	Herrin and Jones (1963)
Soils	25 – 45*	Ripple and Day (1966), Mitchell et al. (1968)
Concrete	54	Polivka and Best (1960)
Metals	>50	Finnie and Heller (1959)

Note: * from tests on both sand and clay materials

Most importantly, the drained condition used for this study should not affect the modeling implementation because the Singh and Mitchell (1968) creep model can be applied to deviatoric creep tests irrespective of the drainage condition during testing.

The same specimen preparation techniques used for the shear strength tests discussed in Chapter 5 were used for the triaxial creep tests. After saturation and isotropic consolidation, but prior to application of the creep stress, the height of each test specimen was re-determined. Each creep specimen was gradually loaded to its deviatoric stress level following the same loading path and rate of loading obtained earlier from the strain-controlled, monotonic triaxial strength measurements. After the target stress level was

reached, generally within 2 minutes after of the initiation of the stress application, the deviator stress was maintained constant at that stress level throughout the test duration (Figure 6-5). To maintain a constant deviator stress on the test specimen, the deviator load was periodically adjusted as necessary based on the change in specimen cross-sectional area due to the volumetric expansion and contraction during the drained shearing process.

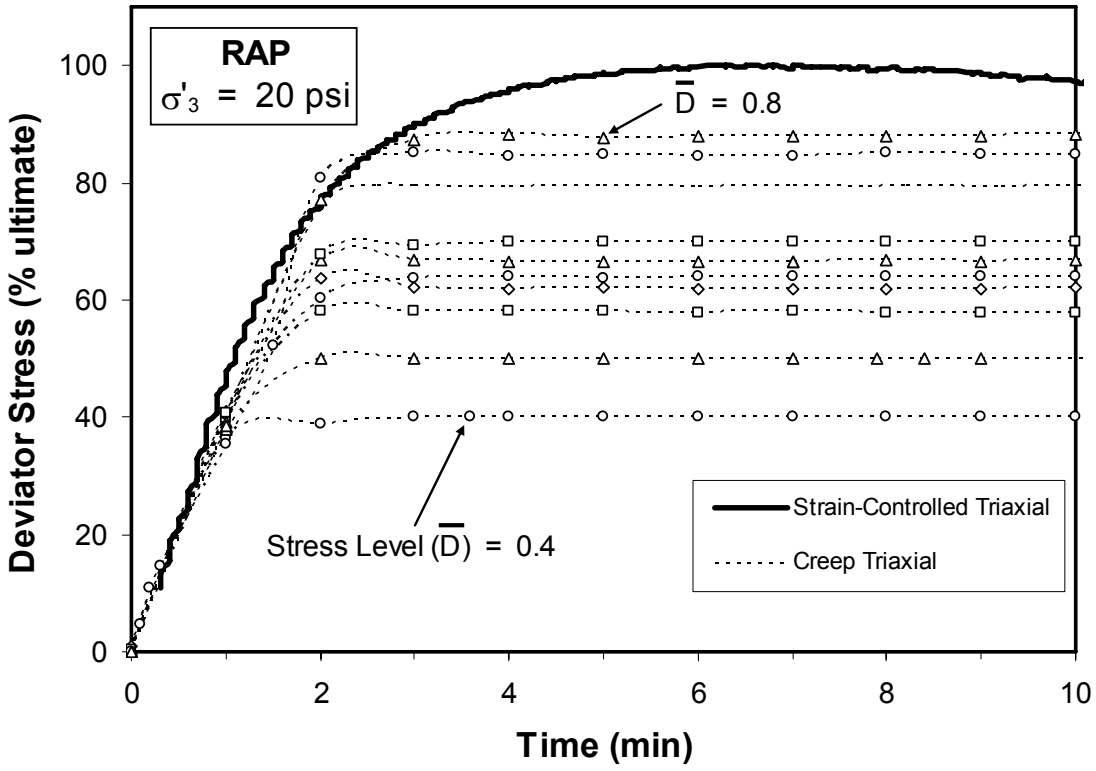

Figure 6-5 Stress paths applied to creep test specimens at σ'_3 = 20 psi

Although asphalt behavior is temperature dependent, it is believed that the temperature variation in an enclosed backfill material behind a typical MSE wall will be relatively small. This assumption is supported by the field study performed by Cosentino and Kalajian (2001) to monitor the change in field temperature during the summer months of a compacted RAP section at different depths from the surface. The authors concluded based on their findings that the RAP becomes insulated below 18 inches and that air temperature have only little effect at depths greater than this depth. Therefore, all creep tests were performed at a constant room temperature of about 72°F. During testing, the axial deformation and deviator stress were recorded with time by an external LVDT and an external load cell (Chapter 5). Each creep test was continued until the specimen experienced complete creep rupture, or until 10,000 minutes (~ 7 days) elapsed.

6.4 TEST RESULTS AND DISCUSSIONS

A total of twenty-four constant-stress, drained triaxial creep tests were performed on compacted RAP specimens. The entire testing program is subdivided into three sections: creep tests at an effective confining stress (σ'_3) of 20 psi, creep tests at σ'_3 = 40 psi, and creep tests at a constant $\bar{D}$ of 0.8 (i.e., 80% of the ultimate strength) performed at different effective confining pressures. The following sections describe experimental results and the derived Singh and Mitchell's creep parameters (i.e. *A*, *m*, and $\bar{\alpha}$). The RAP creep parameters were compared to the values reported for typical soils. In addition to deriving creep parameters from the test results described above, the data were used to

investigate the time to creep rupture and to compare the creep rupture of RAP with that of other soils reported in the literature.

6.4.1 Creep Tests at σ'_3 = 20 psi

Ten drained creep tests were performed at σ'_3 = 20 psi with stress levels ($\bar{D}$) ranging from 0.40 to 0.88. Figure 6-6 shows plots between axial creep strains (ε) versus log(time). Tests with $\bar{D} \geq 0.64$ reached the tertiary creep stage within one week (~10,000 minutes) after stress application. At any given time the magnitude of the axial creep strains are generally in accord with the stress levels, with larger axial strains observed for larger stress levels. It appears that the creep tests performed at $\bar{D} < 0.64$ may have eventually reached complete creep rupture had the applied stress been maintained longer. However, it was very likely that these samples would take more than a month to reach complete creep rupture at the rate of axial strain observed.

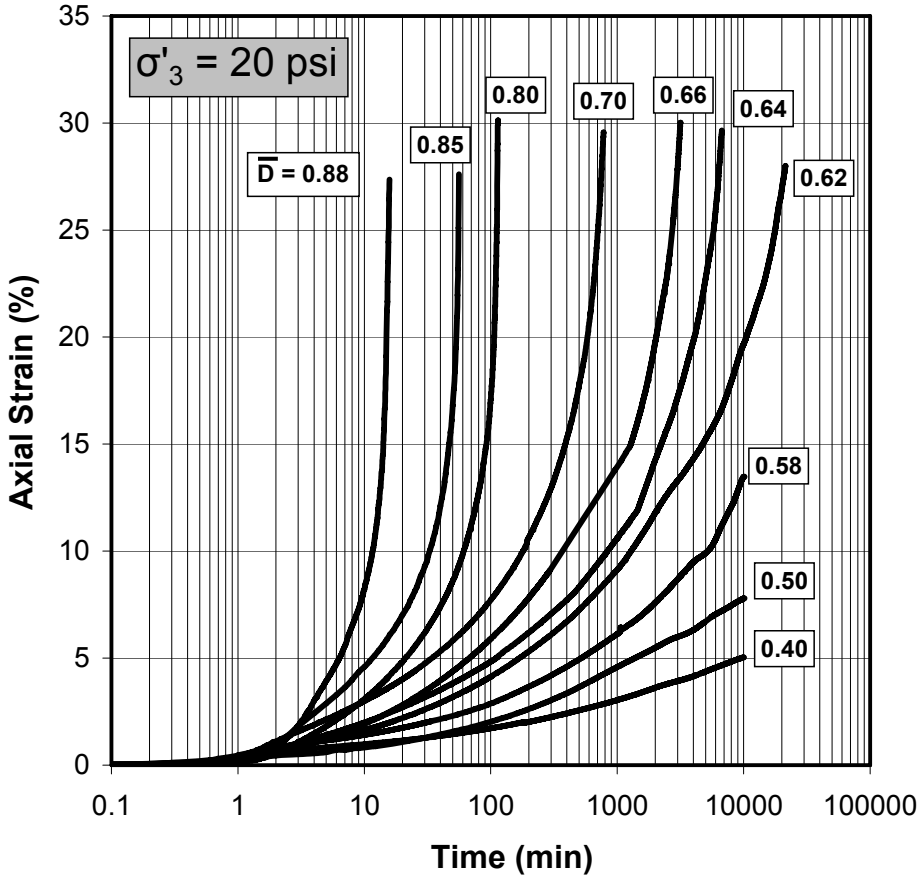

Figure 6-6 Axial strain vs. time for RAP specimens tested at σ'_3 = 20 psi

By differentiating the data in Figure 6-6 with respect to time, the axial strain rate ($\dot{\varepsilon}$) can be determined and plotted against time as shown in Figure 6-7. The data reveal larger strain rates for larger $\bar{D}$ at any given time. Large values of initial strain rate (0.1 to 1 %/minute) are also observed. The linear relationship between log($\dot{\varepsilon}$) and log(time) is clearly noticeable, especially for $\bar{D} \leq 0.70$. At large stress levels, $\bar{D} \geq 0.64$ for this case, this linear behavior is followed by an increase in strain rate as creep rupture is approached. Figure 6-7 is an essential plot to evaluate the *m* parameter for the Singh and Mitchell (1968) creep model.

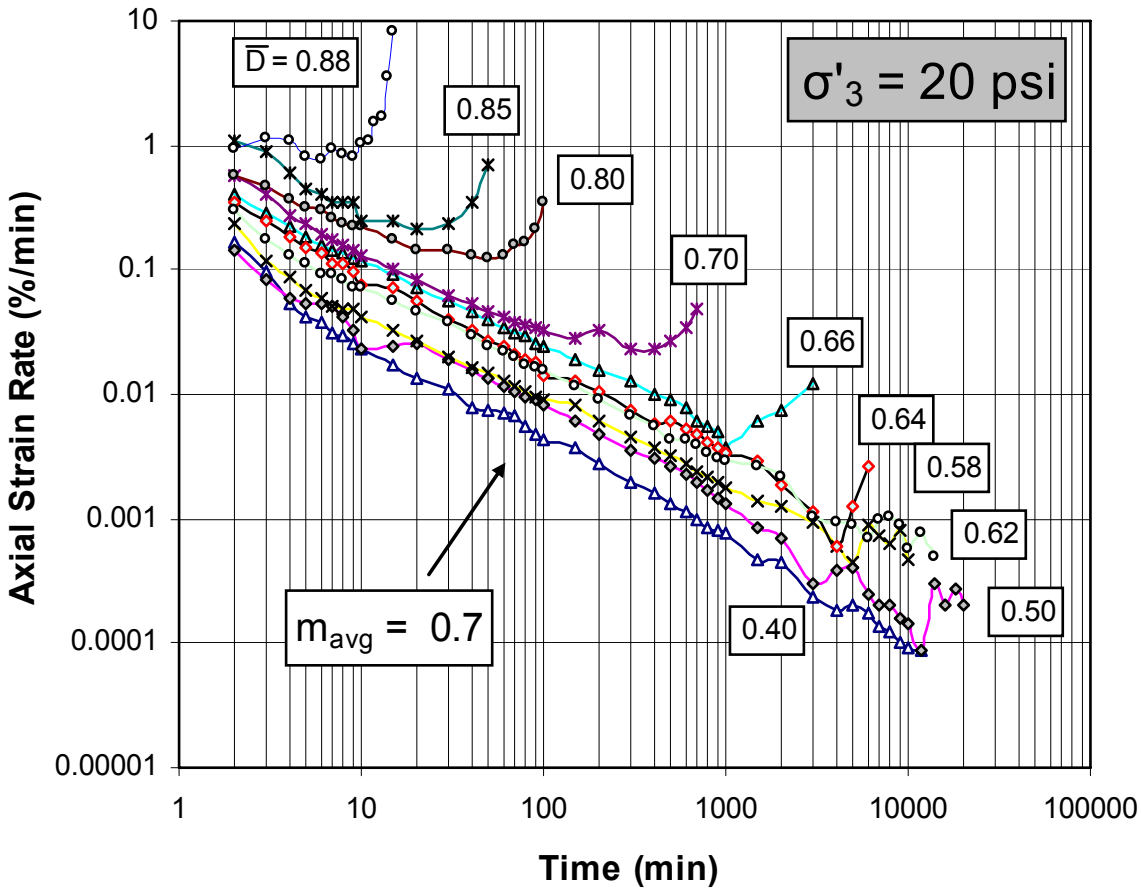

Figure 6-7 Axial strain rate vs. time for RAP specimens tested at σ'_3 = 20 psi

The best-fit *m* value was determined separately for each stress level by fitting a line through a range of data that is appeared to be most linear and choosing the *m*-value that produces the highest R^2 value. Sample plots showing this fitting process for several stress levels are shown in Figure 6-8. An average *m*-value that is perceivably appropriate for all stress levels was also determined (Figure 6-9). Figure 6-9 summarizes the best-fit *m*-values for each individual stress level. In general, the *m*-values are in good agreement with each other and vary between 0.67 and 0.79. The exceptions are the *m*-values for

stress levels of 0.80 (m = 0.60), 0.85 (m = 0.75), and 0.88 (m = 0.30). These stress levels are very close to the upper limit of 0.90 designated by Singh and Mitchell (1968), and in these cases creep proceeds rapidly into the secondary and tertiary stages. Thus, the data do not follow a linear trend for a significant amount of time and it is difficult to define an accurate m value. Nevertheless, it is determined that the average m-value for tests with $\bar{D} \leq 0.70$ was 0.70, which represents a value equal to the lowest m-value for typical soils reported by Mitchell (1993).

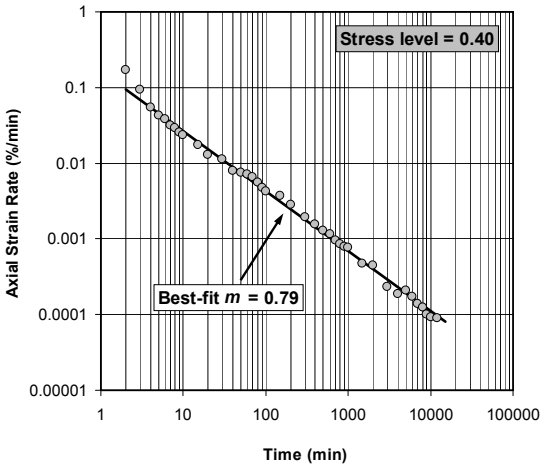

(a)

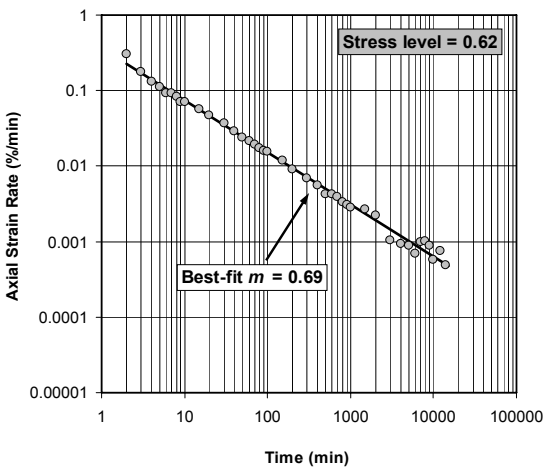

(b)

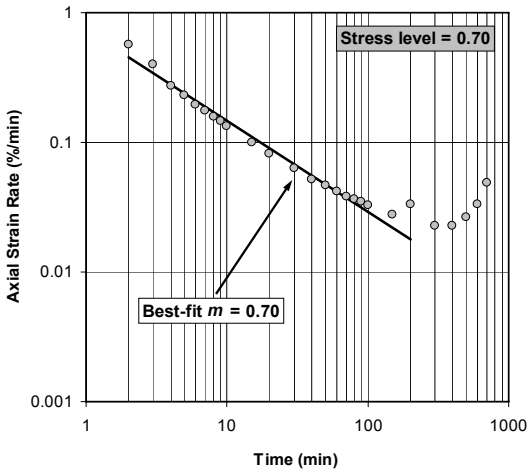

(c)

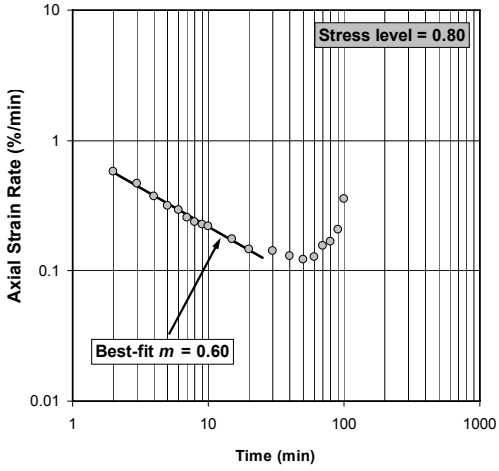

(d)

Figure 6-8 Sample plots used to develop best-fit *m*-values for creep tests at σ'_3 = 20 psi
(a) $\bar{D}$ = 0.40; (b) $\bar{D}$ = 0.62; (c) $\bar{D}$ = 0.70; (d) $\bar{D}$ = 0.80

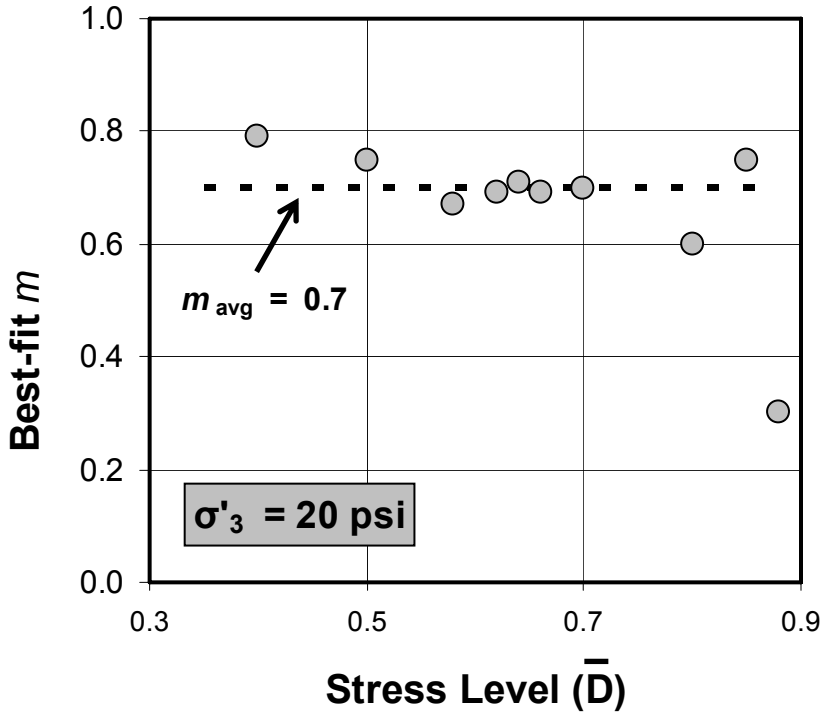

Figure 6-9 Best-fit *m* values vs. stress levels for creep tests at σ'_3 = 20 psi

To determine the *A* and $\bar{\alpha}$ parameters, one must plot the relationship between log(axial strain rate) and stress level for different times after stress application (Figure 6-10). Four possible reference times (t_1) were considered: two, five, ten, and twenty minutes. Straight lines were fit to the data for each value of t_1, and the R^2 values of the best-fit regression lines are all 0.9 or greater. A reference time value of t_1 = 5 minute was considered appropriate for this study with the resulting *A* and $\bar{\alpha}$ values equal to 2.8 x 10^{-3} %/min and 6.12, respectively.

Kuhn and Mitchell (1993) reported that typical soils with t_1 = 1 minute have *A* and $\bar{\alpha}$ values ranging from 2 x 10^{-8} to 4 x 10^{-3} %/min, and 1.0 to 7.0, respectively. The $\bar{\alpha}$ parameter, which represents the effect of $\bar{D}$ on the strain rate, is theoretically

independent to the value of t_1 selected (Figure 6-3). Thus, by direct comparison, RAP displays an $\bar{\alpha}$ value close to the high end reported for typical soils. The *A* value, on the other hand, is dependent on the value of t_1 selected because it is the intercept of the log(axial strain rate)-stress level curve. Smaller values of t_1 result in larger *A* values (Figure 6-3). The *A* value for RAP determined in this study for t_1 = 5 minute is 2.8 x 10^{-3} %/min, which is close to the larger values reported by Kuhn and Mitchell (1993). The *A* value for RAP at t_1 = 1 minute would be even larger and probably well above the largest value reported by Kuhn and Mitchell (1993). Thus, the large *A* value for RAP again indicates a significant creep potential. In summary, the low value of *m* and large values of *A* and $\bar{\alpha}$ for RAP suggest that RAP exhibits creep behavior similar to that of clay with high creep susceptibility.

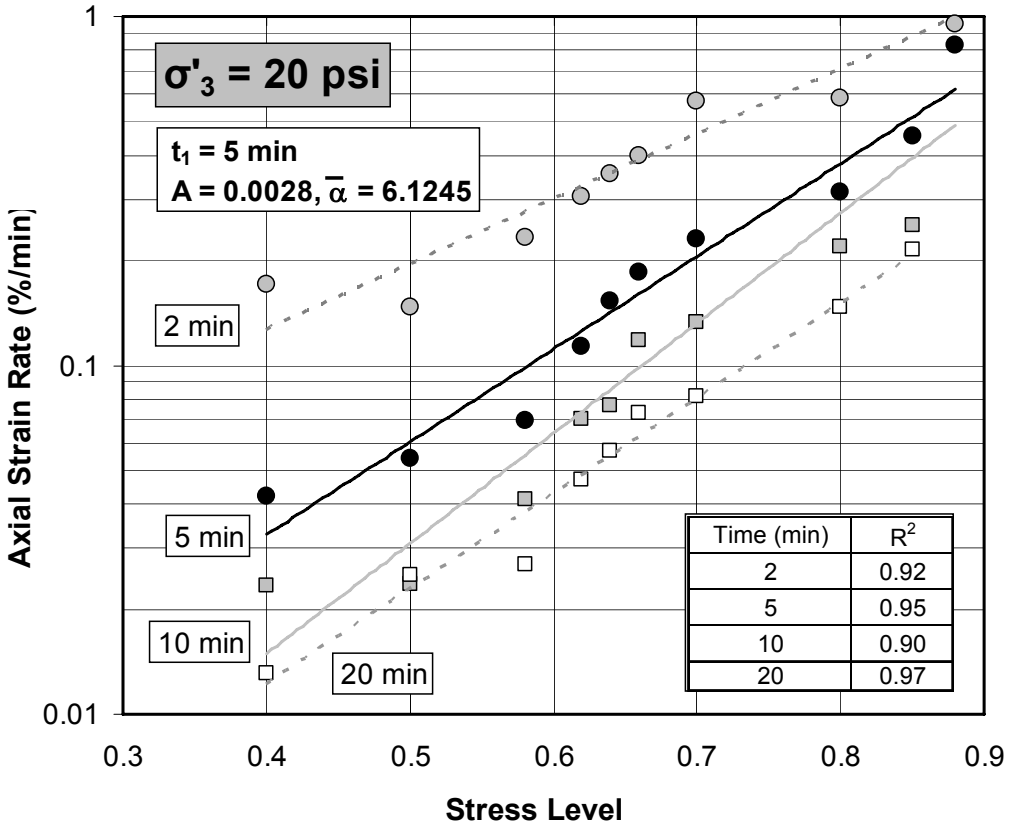

Figure 6-10 Axial strain rates vs. stress levels at select times for tests at σ'_3 = 20 psi

6.4.2 Creep Tests at σ'_3 = 40 psi

A total of ten creep tests were performed at σ'_3 = 40 psi to investigate the influence of effective consolidation pressure on the creep behavior of RAP. The tests were conducted at stress levels ranging from 0.50 to 0.90. The sample preparation and testing procedures were essentially the same as for the tests performed at σ'_3 = 20 psi, except that these test specimens were consolidated to σ'_3 = 40 psi before application of the creep stress and that the stress levels were applied based on the deviator stress at failure at σ'_3 = 40 psi. Figure 6-11 graphically displays the observed axial creep strain

versus log(time). In comparison with the data from σ'_3 = 20 psi (Figure 6-6), it is evident that the specimens tested at σ'_3 = 40 psi required more time to reach the same deformation level, even at the same stress level ($\bar{D}$). Another noticeable observation is that stress levels greater than approximately 0.80 were required to reach creep rupture within 10,000 minutes for σ'_3 = 40 psi, whereas stress levels above approximately 0.64 were required for specimens tested at σ'_3 = 20 psi. Thus, it appears at this point that creep behavior of RAP is confining pressure dependent.

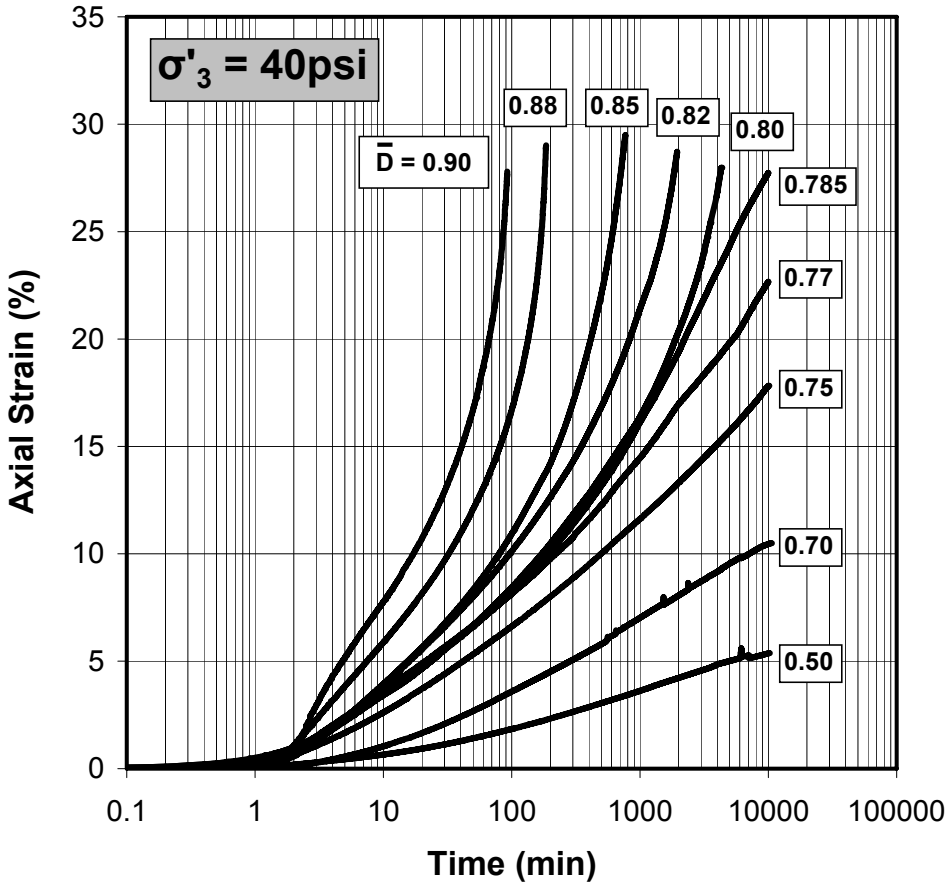

Figure 6-11 Axial strain vs. time for RAP specimens tested at σ'_3 = 40 psi

The test data shown in Figure 6-11 were differentiated with respect to time to obtain axial strain rates for subsequent Singh and Mitchell (1968) model interpretation. Figure 6-12 shows the log(strain rate) versus log(time) data for the σ'_3 = 40 psi tests. Several observations can be made by comparing the data in Figure 6-12 for σ'_3 = 40 psi with the results in Figure 6-7 for σ'_3 = 20 psi. First, the initial strain rates (at $t \sim 2$ minutes) are similar for the two sets of tests (i.e. 0.1 to 1 %/min). Second, the primary creep stage, during which the log(strain rate) decreases with log(time), is longer for the tests performed at σ'_3 = 40 psi. And finally, the slopes of the curves in Figure 6-12 for σ'_3 = 40 psi are larger than the slopes of the curves in Figure 6-7 for σ'_3 = 20 psi. Sample plots showing the best-fit *m*-values for several different stress levels are illustrated in Figure 6-13. An average *m*-value of 0.87 was obtained for the σ'_3 = 40 psi data (Figure 6-14), and less scatter was observed among the individual best-fit *m*-values for the σ'_3 = 40 psi tests (m = 0.79 to 0.88 for all tests with $\bar{D} < 0.90$). The larger average *m*-value indicates that the strain rate decreases more quickly at σ'_3 = 40 psi than at σ'_3 = 20 psi, resulting in less creep strain at any given time.

Again, A and $\bar{\alpha}$ values were determined from the relationship between log(strain rate) and stress level (Figure 6-15). For t_1 = 5 minute, the corresponding A and $\bar{\alpha}$ values are 2.1 x 10^{-3} %/min and 6.46, respectively. These values differ only slightly from the A and $\bar{\alpha}$ values determined earlier for the tests at σ'_3 = 20 psi (i.e., 2.8 x 10^{-3} %/min and 6.12). The similarity of the $\bar{\alpha}$ values observed in this study for tests at different σ'_3 is supported by the previous findings reported by Singh and Mitchell (1968). Singh and Mitchell (1968) concluded based on the test results shown in Figure 6-16 that the $\bar{\alpha}$

value (i.e., slope of each plot) did not vary greatly with consolidation pressure or overconsolidation ratio. However, they did find that the *A* value was affected by these parameters.

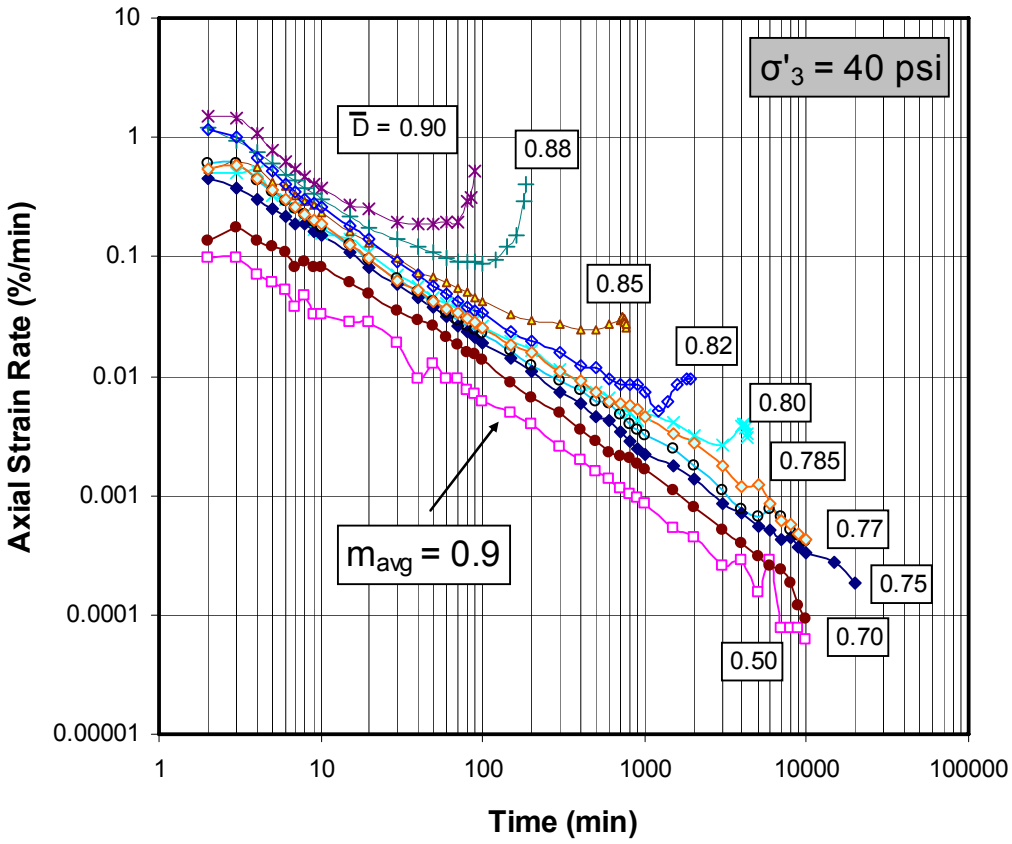

Figure 6-12 Axial strain rate vs. time for RAP specimens tested at σ'_3 = 40 psi

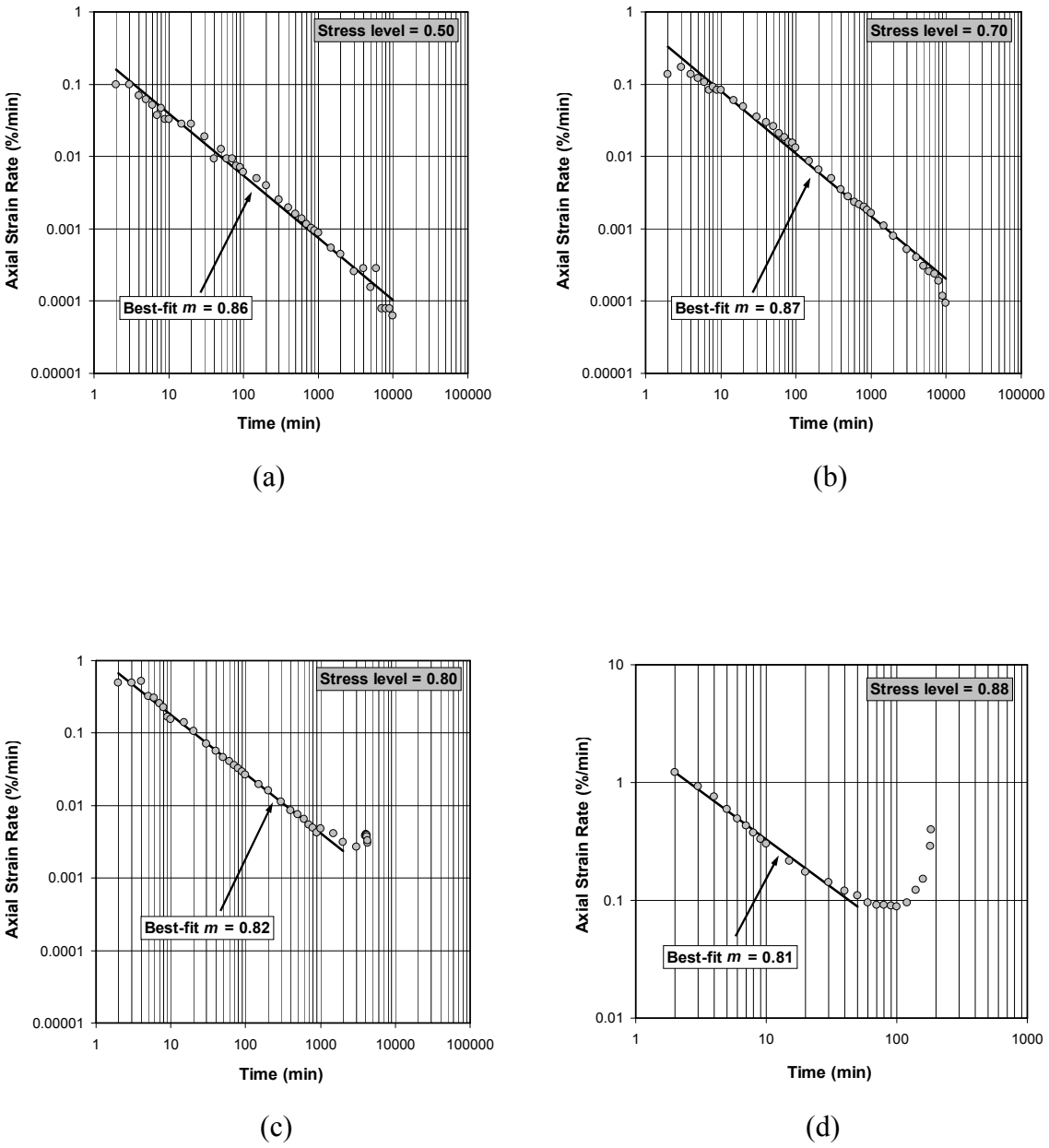

Figure 6-13 Sample best-fitting plots of appropriate *m* values for creep tests at $\sigma'_3 = 40$ psi: (a) $\bar{D} = 0.50$; (b) $\bar{D} = 0.70$; (c) $\bar{D} = 0.80$; (d) $\bar{D} = 0.88$

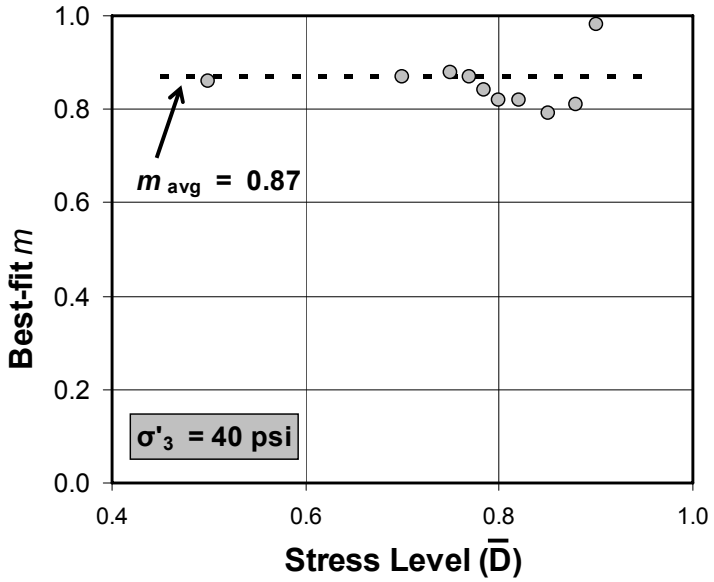

Figure 6-14 Best-fit *m* values vs. stress levels for creep tests at $\sigma'_3 = 40$ psi

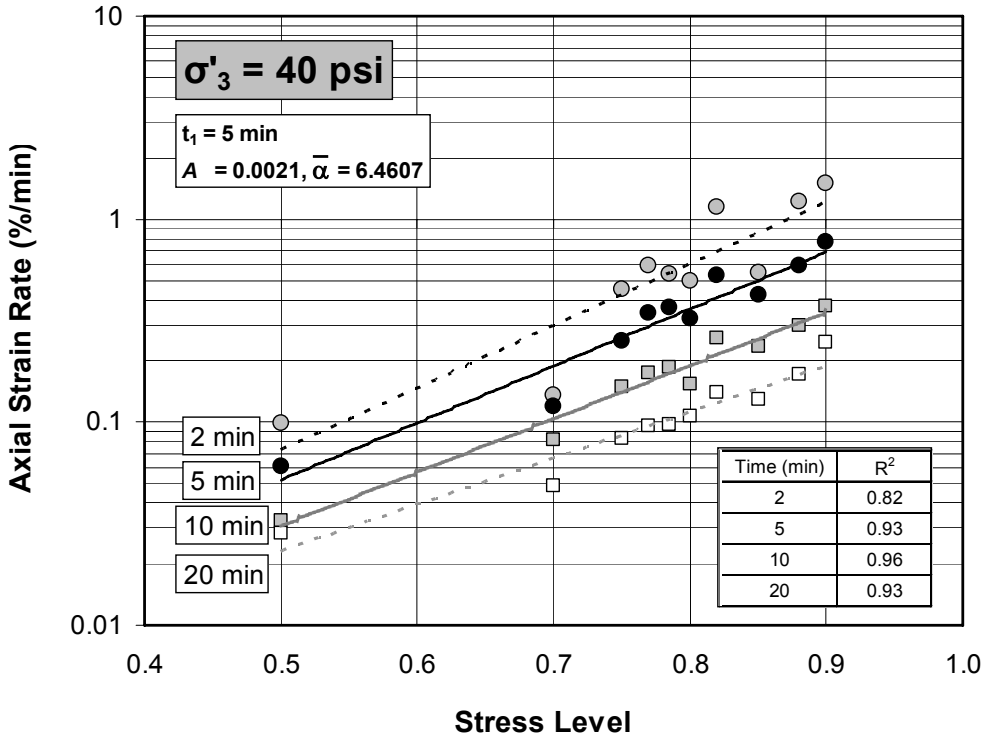

Figure 6-15 Axial strain rates vs. stress levels at select times for tests at $\sigma'_3 = 40$ psi

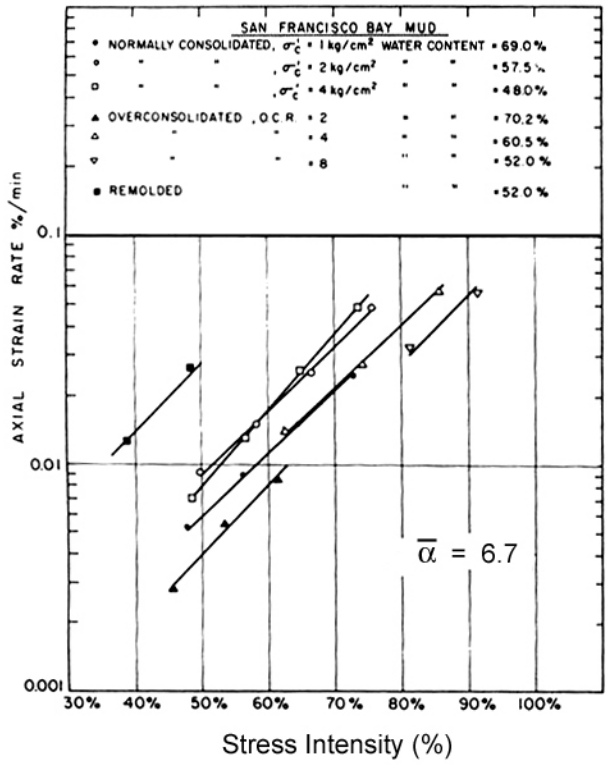

Figure 6-16 Effect of consolidation pressure and overconsolidation ratio on A and $\bar{\alpha}$ for an undisturbed San Francisco Bay mud [after Singh and Mitchell (1968)]

The effect of consolidation pressure on RAP can be evaluated further by plotting together the observed strain rate vs. stress level at t_1 = 5 minute for the two sets of tests at σ'_3 = 20 and 40 psi (Figure 6-17). The data points are in excellent agreement, with the best-fit line displaying an R^2 value of 0.95. The deviation of the data points from the best-fit line does not suggest any discernable trend with consolidation stress. Therefore, it is concluded that consolidation stress has little influence on either *A* or $\bar{\alpha}$ for RAP at confining stresses greater than 20 psi. Thus, the strain rate after initial application of the deviator stress, which is controlled by the *A* and $\bar{\alpha}$ parameters, is similar at the two

confining pressures, and the differences in creep behavior observed at the two confining pressures are a result of the different values of *m*.

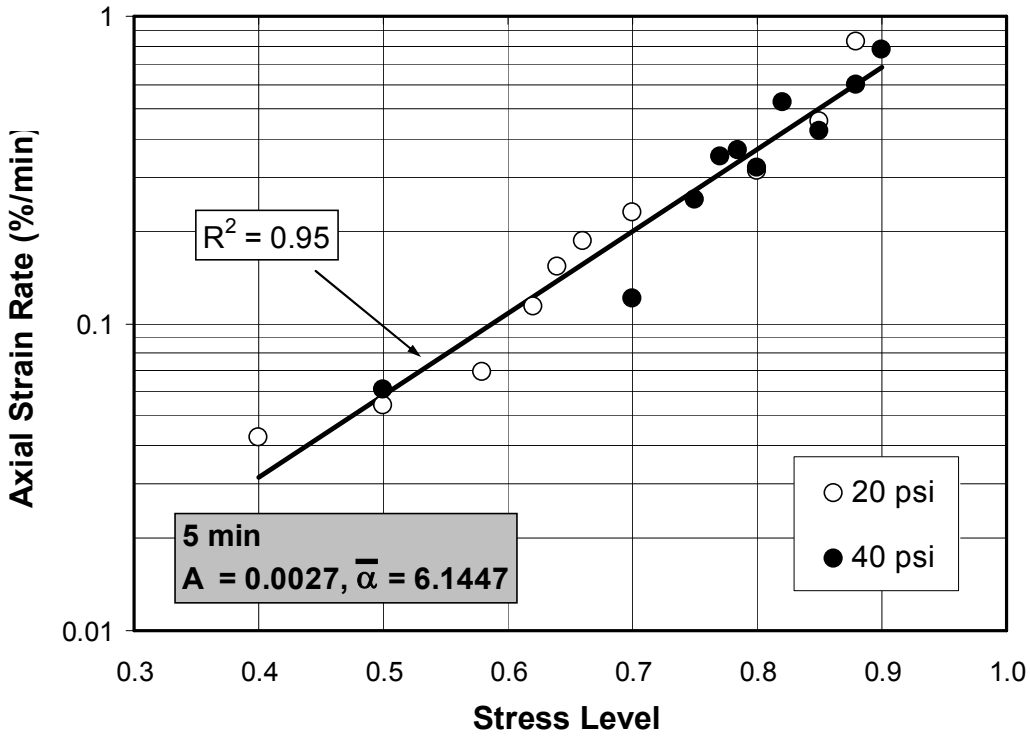

Figure 6-17 Combined plot from two set of tests at σ'_3 = 20 and 40 psi after 5 minute of stress application

6.4.3 Effect of Confining Pressure on RAP Creep Behavior

The influence of consolidation pressure on the creep equation parameters (i.e. *m*, *A*, and $\bar{\alpha}$) was investigated in the previous section, with the conclusion that confining pressure has a greater effect on the *m* parameter than on *A* and $\bar{\alpha}$. This finding is very important because the *m* parameter indicates the creep potential and potential for creep

rupture of a soil (Figure 6-4). Therefore, it was decided at this point to expand the experimental program to investigate the effect of consolidation pressure on the RAP creep behavior more thoroughly.

Six creep tests were performed at confining pressures of 5, 10, 20, 30, 40 and 50 psi and at a constant stress level ($\bar{D}$) of 0.8. A large value of $\bar{D}$ was chosen to ensure that most of the specimens experienced creep rupture within one week testing period. The observed axial strain data are plotted versus log(time) in Figures 6-18. These results indicate that the confining pressure significantly affects the strain generated at any one time, as well as the time to creep rupture. Further, the effect of confining pressure is not systematic. The creep strain increases as confining pressure increases from 5 to 20 psi, but then decreases as the confining pressure increases from 20 to 50 psi. Additionally, the shapes of the curves are inconsistent. The tests at 5 and 10 psi initially experienced very small strains but then quickly accelerated to creep rupture, while the tests at larger confining pressures initially experienced larger strains but took longer to reach creep rupture.

A distinct shape of the plotted curve was observed for 50 psi. This specimen experienced the largest strains over the first 20 minutes, but thereafter the curve flattened out and did not reach creep rupture within the one week test. An additional specimen was tested at this same confining pressure to validate the data in Figure 6-18. However, the results from this additional test were similar to those shown in Figure 6-18.

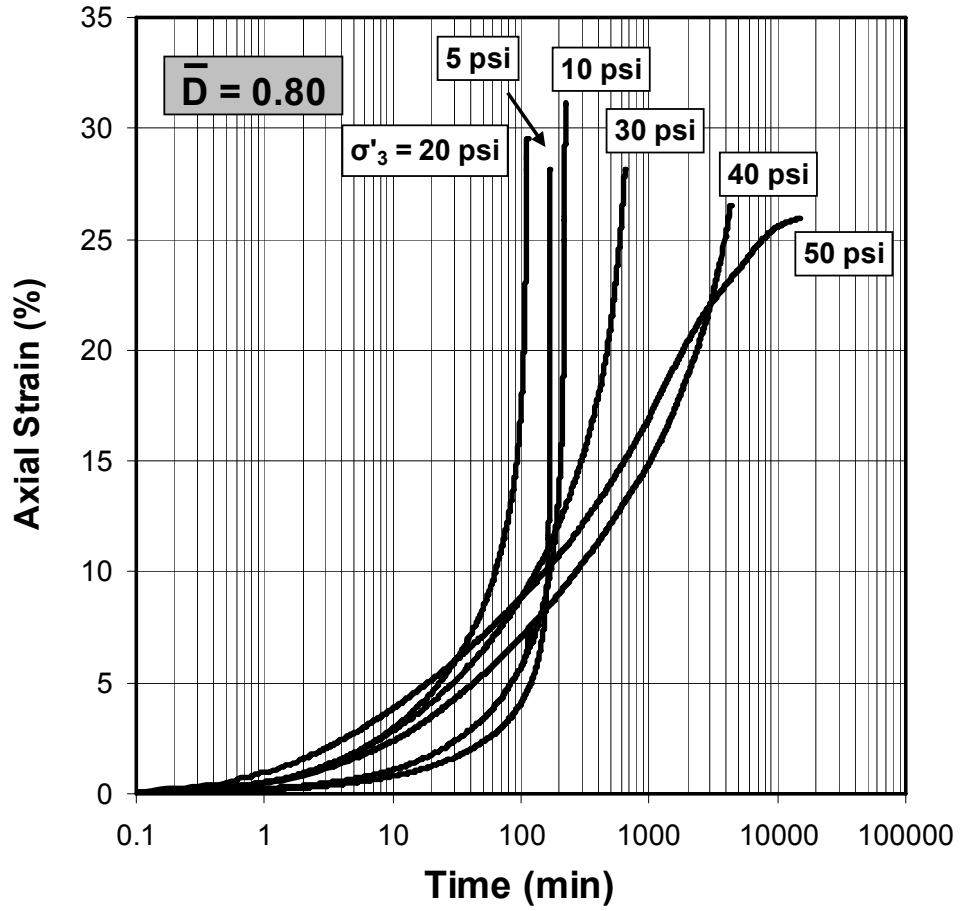

Figure 6-18 Axial creep strain vs. time performed at different σ'_3

The data in Figure 6-18 were used to compute strain rate and the resulting data are plotted versus log(time) in Figure 6-19. Recall that the test series performed at 20 and 40 psi indicated that the A and $\bar{\alpha}$ creep model parameters were not stress dependent. Thus, for tests performed at the same stress level ($\bar{D}$), equation (6.1) predicts the same axial strain rate at t_1 for all confining pressure levels. Using the A and $\bar{\alpha}$ parameters derived previously in Figure 6-17 for the data from 20 and 40 psi (A = 0.0027 %/min, $\bar{\alpha}$ = 6.15), equation 6.1 predicts an axial strain rate of 0.37 %/min at t = 5 minutes for $\bar{D}$ = 0.8.

Considering the results in Figure 6-19, the data at $\sigma'_3 \geq 20$ psi all reveal strain rates between 0.2 and 0.3 %/min at t = 5 min, which are generally consistent with the value predicted by equation (6.1), but the data at σ'_3 = 5 and 10 psi display much smaller values (0.07 to 0.09 %/min). These smaller values of initial strain rate for the lower confining pressures further indicate creep behavior that is distinct from the larger confining pressures.

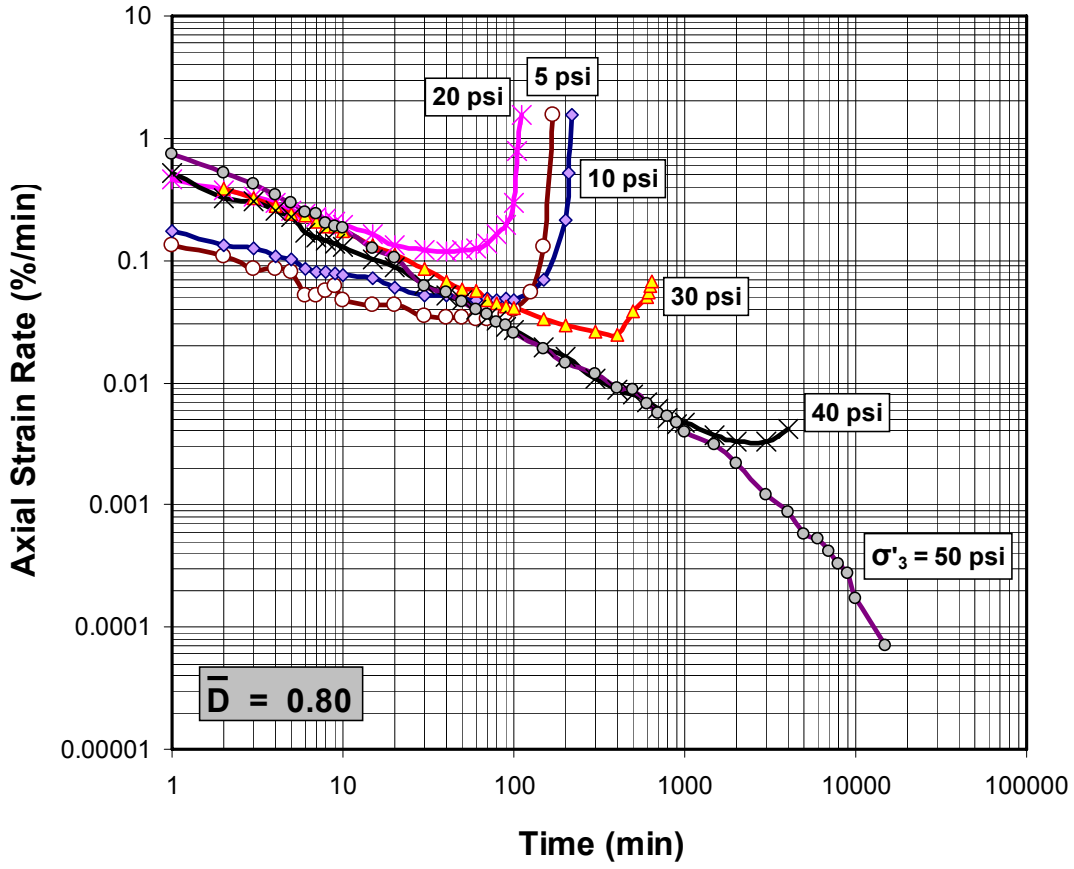

Figure 6-19 Axial strain rate vs. time performed with same $\bar{D}$ = 0.8 at various σ'_3

The data in Figure 6-19 also exhibit that the 50 psi test series experienced some unique behavior, with the strain rate decreasing with time more quickly than the other confining pressures. Also, the slope of the log(strain rate) – log(time) curve increased with time from an *m* value of about 0.8 for $t < 1{,}000$ min, to an *m* value of about 1.4 for $t = 1{,}500$ min to 10,000 min, and a terminal *m* value of about 2.6 for *t* between 10,000 and 15,000 min. This observed behavior is in contradiction with the other tests performed in this study, and is in contradiction with various creep models. The results from testing at 50 psi indicate that it is possible that at larger confining pressures creep deformation in RAP eventually ceases with time, even if the material initially displays an *m* value less than 1.0.

It is difficult to explain the test results at 50 psi. It is possible that the initial, rapid deformation may be attributed to some particle crushing because of the large axial stress applied in this test (~142 psi). On the other hand, the accelerating decrease in strain rate over time (i.e., increase in the *m* parameter) may indicate that at larger confining pressures the bitumen coating becomes compressed enough that the creep deformation starts to take place at the grain-to-grain contacts of the aggregate particles, and these particle contacts are less susceptible to creep.

The data in Figures 6-18 and 6-19 indicate that the effect of confining pressure on the creep behavior of RAP appears to be different at smaller and larger confining pressures. One possible explanation for this observation is the difference in volumetric response of RAP during sheared. As shown in Chapter 5 (Figure 5-9), triaxial tests on RAP specimens performed at $\sigma'_3 \geq 20$ psi exhibited a contractive volumetric response,

while at $\sigma'_3 \leq 20$ psi the specimens initially exhibited small compressive volumetric strains (smaller than the $\sigma'_3 \geq 20$ psi specimens) followed by a significant dilative response. The dilative response is most pronounced for specimens tested at $\sigma'_3 = 5$ and 10 psi where the dilation initiates within the first 1 to 2% of axial strain. In light of this finding, RAP samples that were consolidated to $\sigma'_3 = 20$, 30, 40, and 50 psi can be considered contractive specimens, whereas the two samples that were consolidated to $\sigma'_3 = 5$ and 10 psi can be considered dilative specimens. This progression from a dilative to contractive state may explain the observed differences in creep behavior.

Creep of the two dilative specimens (5 and 10 psi) began at noticeably lower initial strain rates than those of the contractive specimens (Figure 6-19). Figure 6-20 shows the strain rate data from Figure 6-17 along with the strain rate data acquired from this additional set of experiments at variable confining pressure. The strain rate data from 30 and 50 psi generally agree with the data from the 20 and 40 psi tests, but the strain rates from the 5 and 10 psi tests are noticeably smaller. This new figure reemphasizes the effect of volumetric response on the initial strain rate. It also suggests that dilative behavior may also alter the A and $\bar{\alpha}$ values for RAP. To assess the effect of material dilation on A and $\bar{\alpha}$, more test data on dilative specimens at varying stress levels would be needed. Nevertheless, the low values of strain rate during the first 100 minutes of loading for the dilative specimens explains why their creep strains are smaller than those of the contractive specimens during the same time period (Figure 6-18). Additionally, the strain rate decreased at a slower rate (i.e. smaller m-values) for the dilative specimens than for the contractive specimens (Figure 6-19).

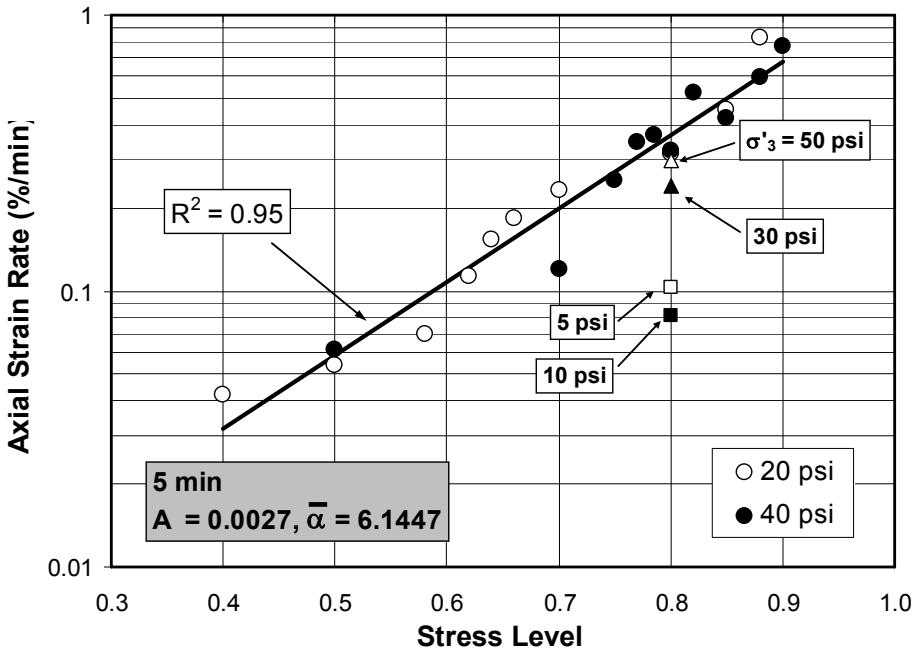

Figure 6-20 Axial strain rates vs. stress levels after 5 minute of stress application

Another noticeable observation is that the two dilative specimens exhibited very similar creep behavior in terms of their measured strain and strain rate curves (Figures 6-18 and 6-19), and these curves are visibly different from those of the contractive specimens. This result suggests that dilative RAP specimens may exhibit similar creep behavior, irrespective of the confining pressure applied. However, more creep tests at varying small confining pressures, where dilation is most pronounced, are required to confirm this hypothesis.

Finally, Figure 6-21 was generated based on the observed, best-fit *m* values determined from the test results shown in Figure 6-19. It must be noted that these best-fit *m* values represent the linear part of the plotted data at time less than 1,000 min. This

summary plot indicates that the observed *m* parameter increases with confining pressure. The observed *m*-values generally increase from 0.32 for the tests at σ'_3 = 5 and 10 psi to 0.8 for the tests at σ'_3 = 40 and 50 psi. The data shown in Figure 6-21 clearly indicate that the *m*-value for RAP is confining pressure dependent.

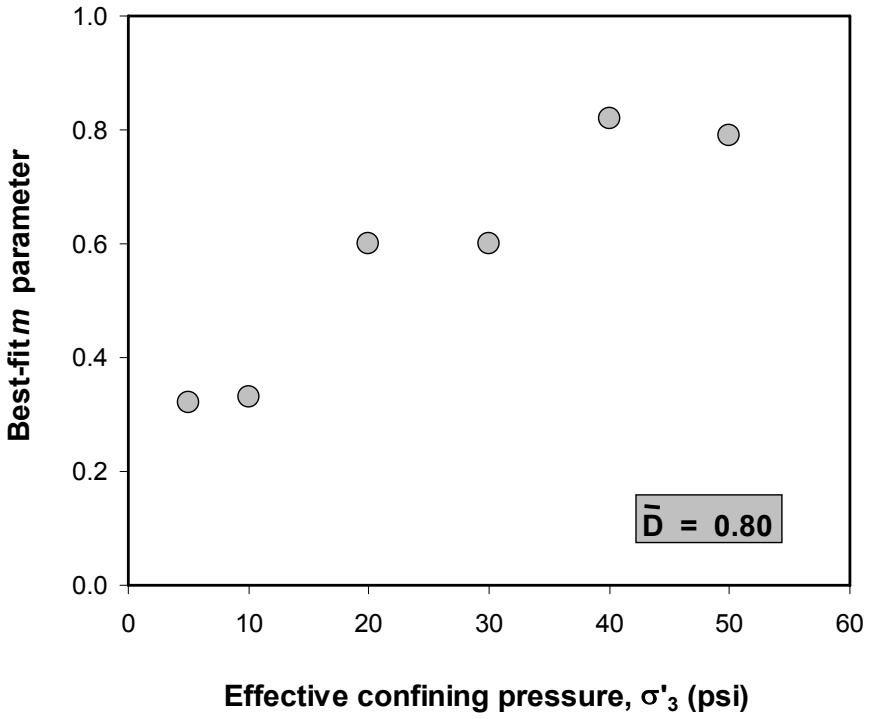

Figure 6-21 Effect of the confining pressure on *m* parameter

6.4.4 RAP Creep Rupture

Creep rupture is traditionally defined as the rupture of soil at the end of tertiary creep where the axial strain approaches an asymptotic point in the axial strain versus log (time) plots (e.g. Figure 6-1). Hence, time to rupture (t_r) is the total elapsed time from the

initiation of creep until final rupture. For the creep test data acquired in this study, the Singh and Mitchell (1968) creep model provided acceptable agreement with the measured axial strains for the primary and secondary stages of creep (Figure 6-22). The model, however, does not include tertiary creep nor does it contain any mathematical prediction regarding when creep failure may initiate or when complete creep rupture will be reached. As mentioned earlier, this is because the model was developed based strictly on the linear portion of the relationship between log(strain rate) and log(time).

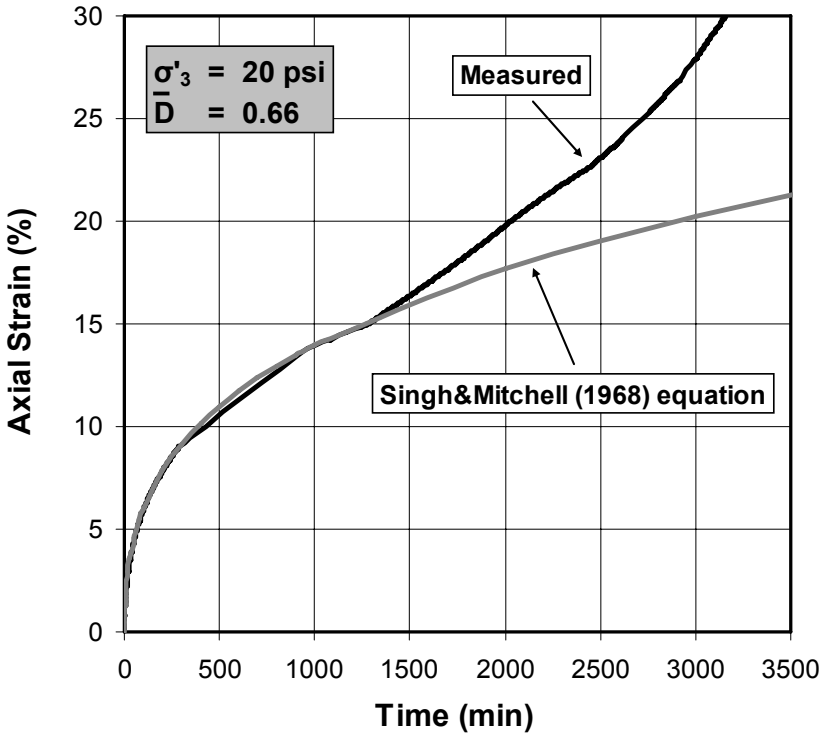

Figure 6-22 Typical comparison between predicted and measured creep strains

Traditionally, creep rupture has been treated separately from the Singh and Mitchell (1968) creep equation. Saito and Uezawa (1961) demonstrated that an experimentally-derived relationship between log(time to rupture, t_r) and log(minimum strain rate, or $\dot{\varepsilon}_{min}$) can be used effectively to predict the time to failure in creeping soils. The relationship was established based on various experimental results (Figure 6-23) and the developed relationship, including a range that bounds 95% of the observed data, was [Saito and Uezawa (1961)]:

$$\log(t_r \text{ in minute}) = 2.33 - 0.916 \cdot \log(\dot{\varepsilon}_{min} \text{ in } x10^{-4}/\text{minute}) \pm 0.59$$

or

$$\log(t_r \text{ in minute}) = -1.334 - 0.916 \cdot \log(\dot{\varepsilon}_{min} \text{ in minute}^{-1}) \pm 0.59 \qquad (6.8)$$

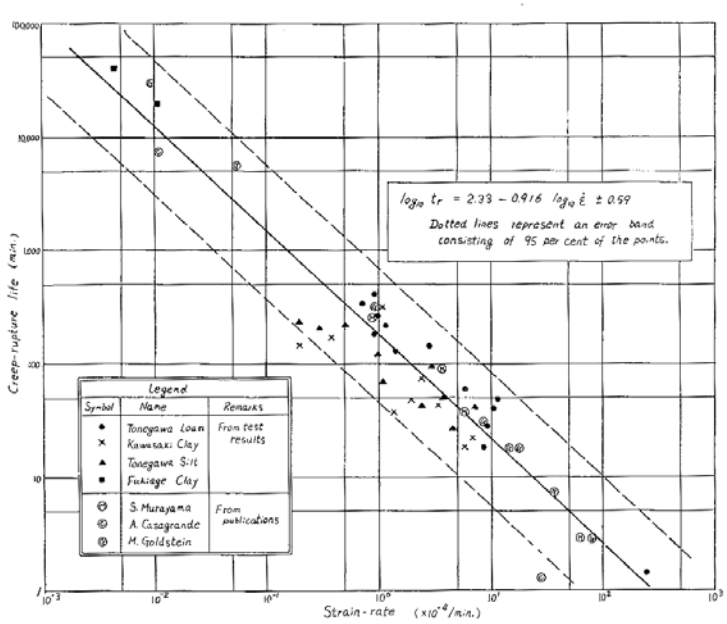

Figure 6-23 Plot of creep rupture life vs. minimum strain rate [Saito and Uezawa (1961)]

The authors suggest that this relationship is valid for a given soil irrespective of the confining pressure. A general observation based on this relationship is that the time to rupture (t_r) is inversely proportional to minimum strain rate ($\dot{\varepsilon}_{min}$). This relationship between log(t_r) and log($\dot{\varepsilon}_{min}$) has also been reported in the creep rupture of metals [Monkman and Grant (1956)] and plastics [Pao and Marin (1952)], suggesting that this relationship may be applicable to a wide range of materials that are subject to creep. Equation 6.8 can be rewritten in a general form as:

$$\log(t_r) = \log(b) - a\log(\dot{\varepsilon}_{min}) \qquad \text{or} \qquad \dot{\varepsilon}_{min}^{a} t_r = b \tag{6.9}$$

where *a* and *b* are constants that reflect the slope and intercept, respectively, of the linear relationship between log (t_r) and log ($\dot{\varepsilon}_{min}$).

Campanella and Vaid (1974) suggested that the *b* parameter is related to the soil fabric and soil composition, based on different *b* values they measured for different soils tested at different stress conditions. Table 6-2 shows *a* and *b* values reported in the literature. Based on these data, it is observed that values of *a* are generally close to 1.0, but that the *b* values vary significantly.

Test results from the two main groups of creep tests performed on RAP at σ'_c = 20 and 40 psi, as well as those single tests discussed in Section 6.4.3 that experienced creep rupture (5, 10, and 30 psi), were used to develop a relationship between log (t_r) and log ($\dot{\varepsilon}_{min}$). Only the fifteen tests that experienced creep rupture were used to develop this relationship, and these data are shown in Figure 6-24. Generally, all RAP creep data fall

on the same straight line, except for the 5 psi test, thus a single line was fit to the data. The resulting values of *a* and *b* were 0.93 and 0.208. The *a* value is similar to those previously reported, but the *b* value is significantly larger than those reported for clays (Table 6-2).

Table 6-2 Typical *a* and *b* values for materials subject to creep stress

Material	***a****	***b****	**Source**
loam, silt, clay – triaxial and unconfined compression	0.92	0.046	Saito and Uezawa (1961)
Haney clay - isotropic triaxial	1.11	0.017	Campanella and Vaid (1974)
- k_o triaxial	1.09	0.004	
- k_o plane strain	1.07	0.005	
Ohya stone – isotropic triaxial	1.05	0.001	Adachi and Takase (1981)
Strahov claystone	0.96	0.083	Feda (1992)

Note: * *a* and *b* derived from $\dot{\varepsilon}_{min}$ in min^{-1} and t_r in min

Figure 6-24 also displays the relationships represented by the *a* and *b* values reported in Table 6-2. It can be seen by visual comparison that all of the relationships, including RAP, are nearly parallel to each other due to the similar *a* values. The best-fit regression line for RAP is situated well above other relationships (indicative of a larger *b* value), suggesting that for a given minimum strain rate it takes longer for RAP to reach creep rupture as compared to the other soils.

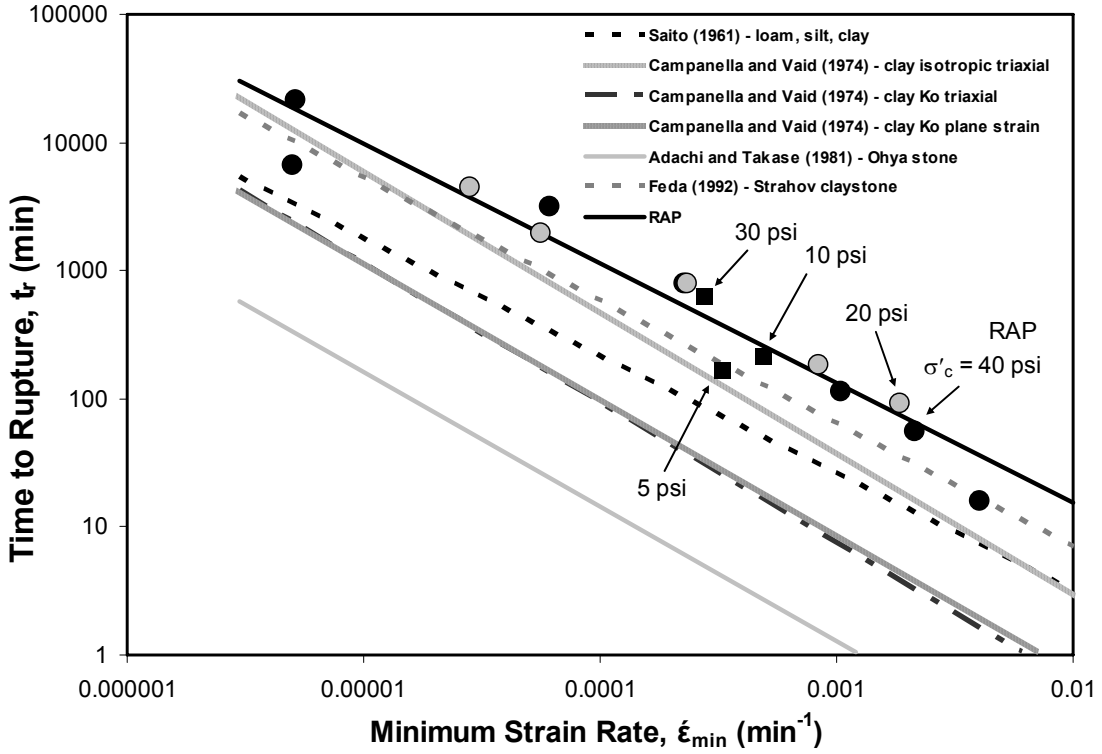

Figure 6-24 Plots between time to creep rupture (t_r) and minimum strain rate ($\dot{\varepsilon}_{\min}$)

To use the relationships shown in Figure 6-24 to predict t_r of an actual earth structure, an in situ estimate of $\dot{\varepsilon}_{\min}$ is required. This measurement is unfeasible for most practical applications. Additionally, the data in Figure 6-24 is somewhat misleading because it does not consider how long it will take the material to reach the given values of $\dot{\varepsilon}_{\min}$. A more useful expression would relate the time to rupture, t_r, to the stress level, $\overline{D}$, because the stress level can be more easily estimated.

Relationships between t_r and the stress level, and between $\dot{\varepsilon}_{\min}$ and the stress level have been reported in the literature by a number of researchers [such as

Campanella and Vaid (1974), Adachi and Takase (1981)]. Data from these studies are shown in Figure 6-25. The observed relationships indicate that t_r decreases with increasing applied creep stress level, and that $\dot{\varepsilon}_{min}$ increases with increasing applied creep stress level.

Figure 6-26 shows plots of log(t_r) vs. $\overline{D}$ for the RAP creep tests performed at σ'_3 = 20 and 40 psi, along with data from a series of undrained creep tests on Haney clay reported by Vaid and Campanella (1977). The Vaid and Campanella (1977) data in Figure 6-26 were not reported directly in their paper, but rather the data were derived from the reported stress levels and the undrained shear strength reported from isotropically consolidated triaxial tests performed at a strain rate of 1% per minute. Straight lines were fit through each set of data, although it is clear that the Vaid and Campanella (1977) data point at the smallest $\overline{D}$ deviates from a linear trend. The effect of confining pressure on the time to rupture for RAP is clearly observed, with significantly larger values of t_r occurring at σ'_c = 40 psi than at σ'_c = 20 psi. This difference is larger than one order of magnitude at some levels of $\overline{D}$, although the difference between confining pressures is not as large at larger values of $\overline{D}$. Compared with Haney clay, RAP consolidated to 20 psi ruptures more quickly, but RAP consolidated to 40 psi ruptures at longer values of t_r. Thus, the creep rupture behavior of RAP can be less severe or more severe than that of typical clays, depending on the confining pressure.

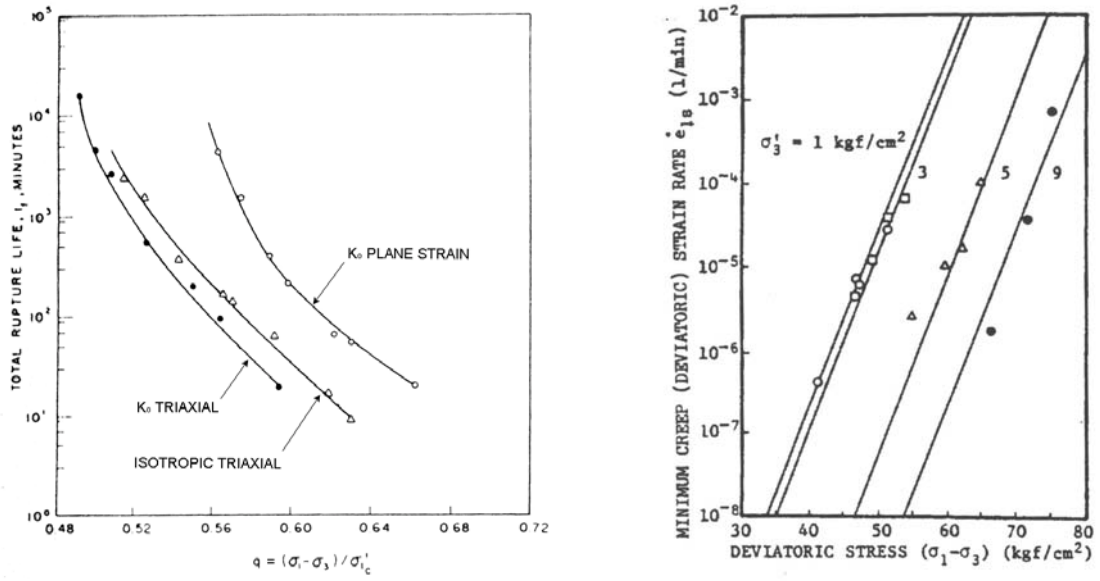

(a) (b)

Figure 6-25 (a) log (t_r) vs. σ'_c-normalized creep stress level for Haney clay [Campanella and Vaid (1974)], (b) log ($\dot{\varepsilon}_{min}$) vs. creep shear stress for Ohya stone [Adachi and Takase (1981)]

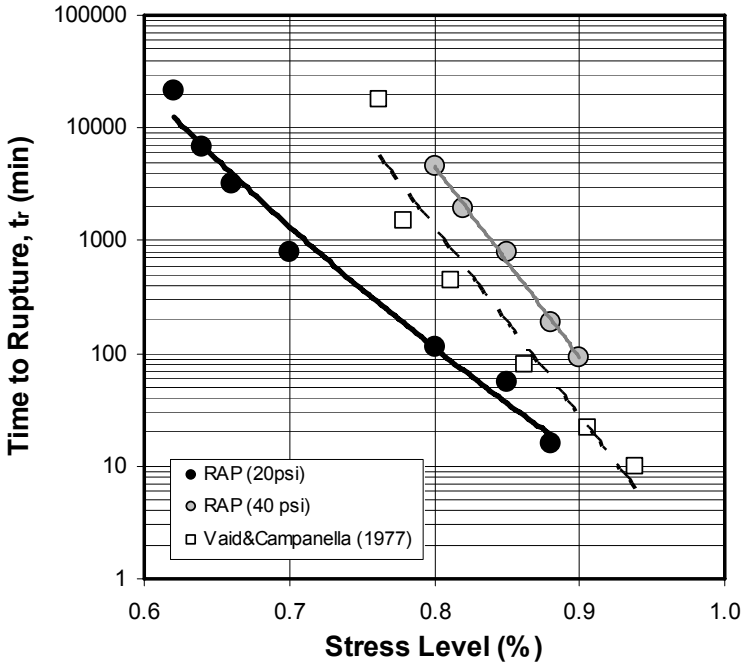

Figure 6-26 Time to rupture vs. stress level

Figure 6-27 compares log ($\dot{\varepsilon}_{min}$) vs. $\overline{D}$ data for RAP, Haney clay [Vaid and Campanella (1977)], and undisturbed undrained San Francisco Bay Mud [Singh and Mitchell (1968)]. Figure 6-27 reemphasizes the direct impact of $\overline{D}$ on $\dot{\varepsilon}_{min}$, with larger values of $\overline{D}$ experiencing larger values of $\dot{\varepsilon}_{min}$. Additionally, the impact of confining pressure on the RAP creep behavior is apparent, with RAP specimens consolidated at 20 psi experiencing larger values of $\dot{\varepsilon}_{min}$. Interestingly, the RAP behavior at 40 psi is very similar to what was observed for tests on Haney clay. However, the minimum strain rates for San Francisco Bay Mud appear to be much larger than for the other materials.

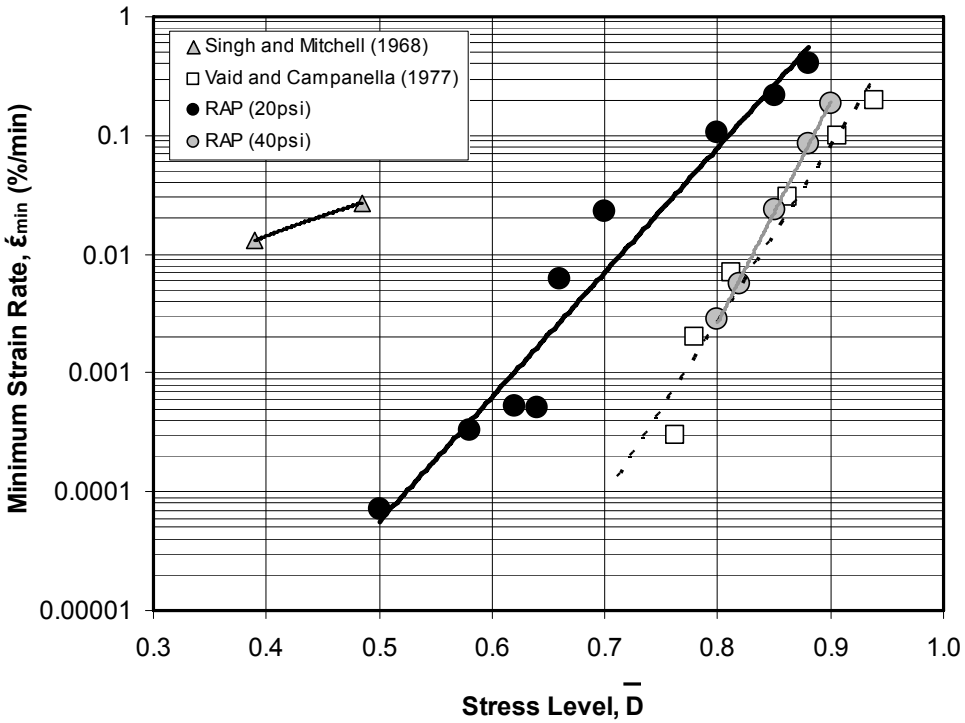

Figure 6-27 Minimum strain rate vs. stress level

The data in Figure 6-26 and Figure 6-27 indicate that the creep characteristics of RAP are similar to those for other soils with significant creep potential (i.e., clays). However, another issue to consider is the possible existence of an upper yield strength. The upper yield strength is defined as the limiting stress below which creep rupture will not occur, even after significant time. The term upper yield strength was first introduced by Murayama and Shibata (1961) and then re-emphasized by Campanella and Vaid (1977).

While values of *m* less than 1.0 are indicative of a high potential for creep deformations, some researchers have shown that these soils may also exhibit an upper yield strength. Vaid and Campanella (1977) reported that Haney clay, with an *m* value close to 0.7, displayed an upper yield strength, which they based on the asymptotic shape of a stress-rupture life relationship (Figure 6-28). This asymptotic behavior for Haney clay can be observed in Figure 6-26 in the Campanella and Vaid (1977) data point that deviates from the linear relationship. Campanella and Vaid (1977) concluded that Haney clay has an upper yield strength, in terms of normalized creep stress [$q = (\sigma_1 - \sigma_3)/ \sigma'_{1c}$], equal to 0.5. This stress level corresponds to stress level of about 0.74 based on the ultimate shear strength of the material provided by the authors. The concept of an upper yield strength is utmost important because theoretically if the shear stress can be maintained below the upper yield strength then creep rupture will not occur. However, significant creep deformation may still be possible.

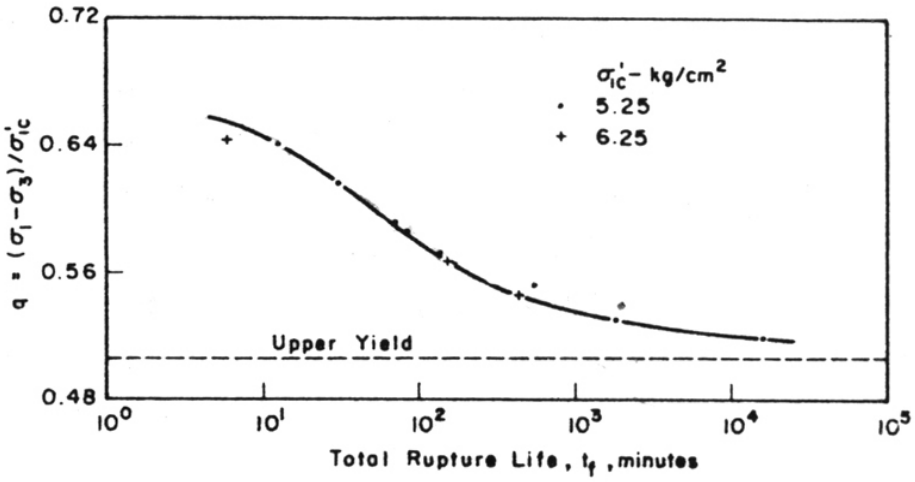

Figure 6-28 Upper yield stress for Haney clay tested with constant stress creep under isotropic triaxial test condition [Vaid and Campanella (1977)]

Figure 6-29 illustrates the normalized creep stress (q) vs. log (t_r) for RAP tested at two confining pressures and for Haney clay (reproduced from Figure 6-28). Note that the q values for RAP are much larger than for Haney clay, because the drained strength of RAP is much larger than the undrained strength of Haney clay. The RAP data indicate the possible existence of the upper yield strength for RAP, as the lines appear to approach an asymptotic value at smaller normalized creep stresses. Unfortunately, no additional test data on RAP at normalized creep stresses smaller than about 3.0 are available to identify the upper yield strength from Figure 6-29 more accurately. Another interesting observation from Figure 6-29 is that the Haney clay data did not display an effect of confining pressure on the normalized creep stress vs. log(t_r) curves (note the two consolidation stresses in Figure 6-29), while the RAP data again displayed a confining pressure dependence. Because of the significant difference in the q values for Haney clay

and RAP, the data were regenerated in Figure 6-30 as a plot of stress level ($\overline{D}$) vs. log(t_r). This plot allows the shapes of the RAP and Haney clay curves to be more easily compared. It can be seen from this figure that the line representing Haney clay is situated between the data for RAP at 20 psi and at 40 psi. Thus, at the same $\overline{D}$, Haney clay would reach complete creep rupture quicker than RAP at σ'_3 = 40 psi, but would reach creep failure after RAP at σ'_3 = 20 psi. Finally, the RAP rupture data at 20 psi appear more clearly to display an asymptotic relationship than the RAP data at 40 psi, although the curve is not as flat as the Haney clay data. However, tests at additional $\overline{D}$ values and for longer times should be able to confirm the values of upper yield strength for RAP.

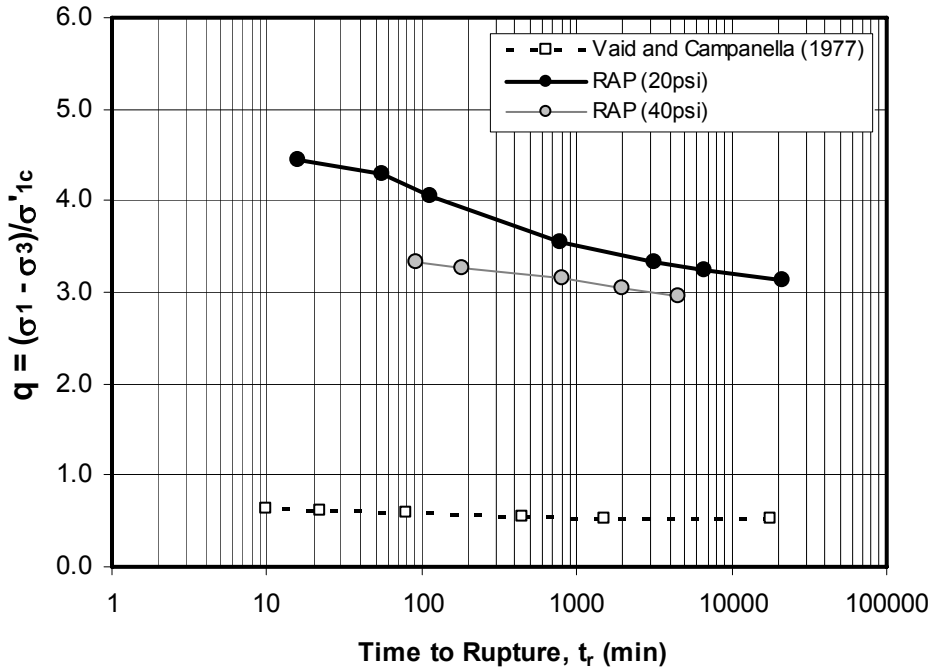

Figure 6-29 Creep stress normalized with σ'_{1c} versus log (time to rupture)

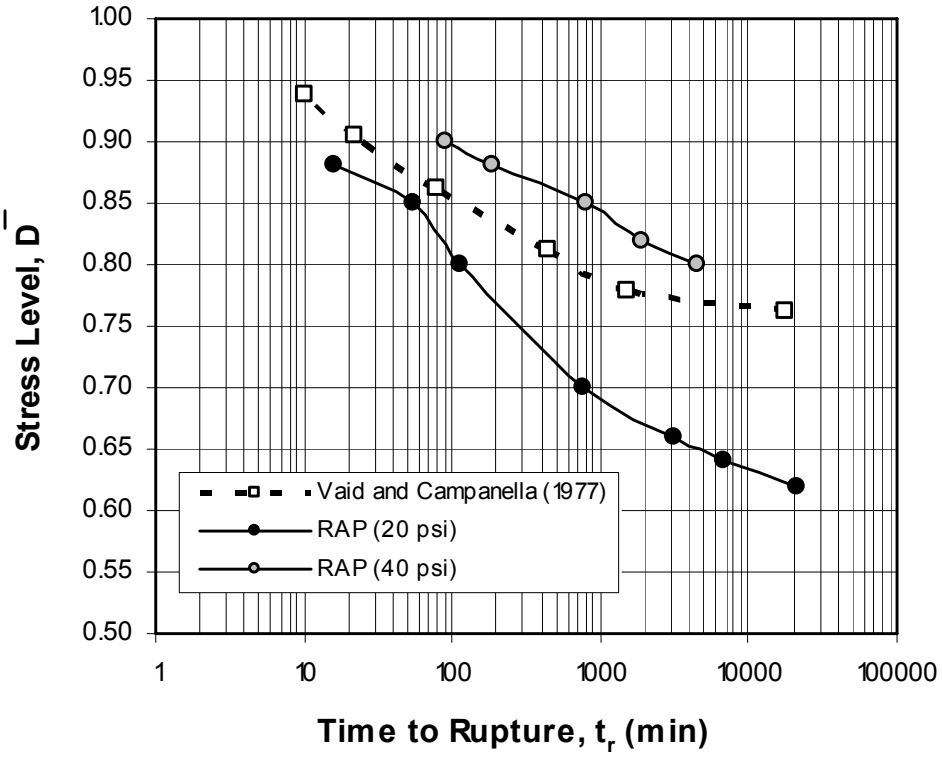

Figure 6-30 Stress level versus log(time to rupture)

An additional technique was considered to identify the upper yield strength of RAP without performing additional tests. Snead (1970) suggested that the upper yield strength is the y-intercept of the relationship between the creep stress and the cube root of the minimum strain rate ($\sqrt[3]{\dot{\varepsilon}_{\min}}$). Plots of these relationships for the RAP and Haney clay creep test data are given in Figure 6-33. Using this procedure, the Haney clay data shows a y-intercept at $\overline{D}$ of about 0.74, which is similar to the upper yield strength determined from the Vaid and Campanella (1977) data shown in Figure 6-30. This favorable comparison provides some confidence in the Snead (1970) method to define an upper

yield strength. Values of upper yield strength for RAP as determined from the Snead (1970) method (Figure 6-31) were $\overline{D}$ equal to 0.59 and 0.78 for RAP tested at σ'_c = 20 psi and 40 psi, respectively. These upper yield strength values appear to be reasonable considering the observed data shown in Figures 6-7 and 6-12 where no initiation of tertiary creep was detected within one week for creep tests with $\overline{D}$ less than 0.64 and 0.8 at 20 psi and 40 psi, respectively. The discovery of an upper yield strength for RAP is an important finding, because it acknowledges that creep rupture will not occur in RAP if the shear stresses are small enough to maintain the stress level below the upper yield strength.

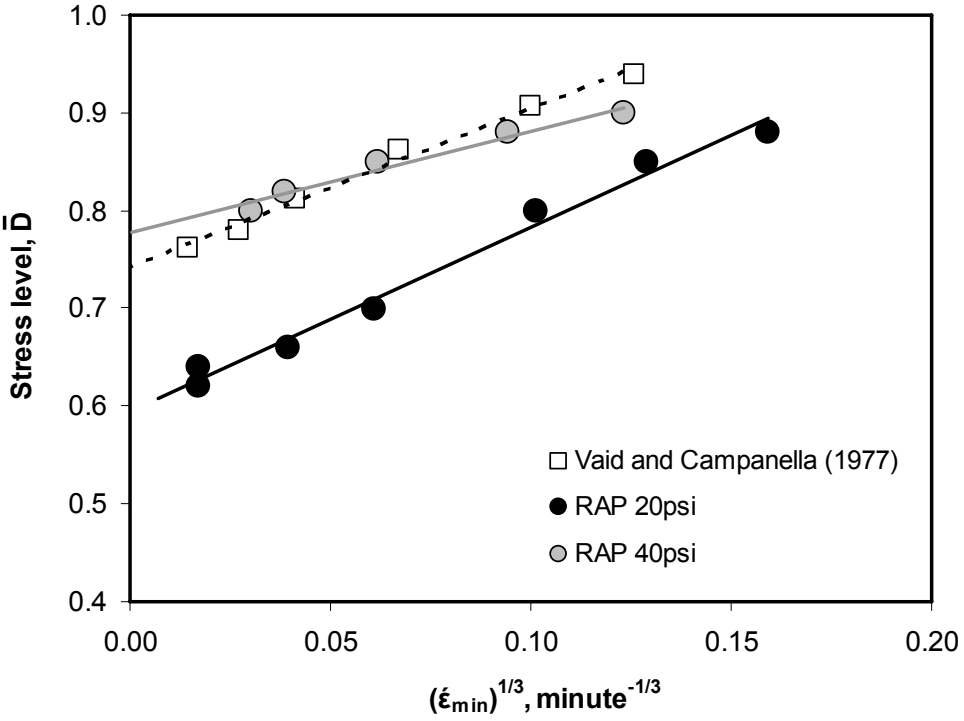

Figure 6-31 Determination of upper yield strength

6.5 CONCLUSION

A series of constant stress, drained triaxial creep tests was performed on compacted RAP specimens to evaluate its creep potential in comparison with a number of soils that have been reported in the literature. Tests were performed at a range of confining pressures and stress levels to investigate the effect of theses parameters on the creep characteristics of RAP. In general, classical creep behavior was observed in the test specimens, with strain rates decreasing linearly with the logarithm of time until creep rupture occurred. The Singh and Mitchell (1968) creep model appeared to be valid for predicting the creep deformation of RAP during the primary and secondary stages of creep. The creep parameter *m* for RAP was found to be smaller than 1.0, indicating that RAP has a significant potential for creep and creep rupture. The *m*-values observed for RAP were generally between 0.7 and 0.9, which are similar to the values reported in the literature for soils with significant creep potential (i.e., clays). Furthermore, this study found a noticeable trend of increasing *m*-value with confining pressure. In contrary to the *m*-parameter, the *A* and $\bar{\alpha}$ creep parameters of RAP were unaffected by changes in confining pressure, as long as the specimens were tested at larger confining pressures where their volumetric response was purely compressive. The *A* and $\bar{\alpha}$ parameters observed for RAP fall towards the upper range observed for clays, which is an additional indication of high creep potential. Tests performed on compacted RAP specimens at small confining pressures (5 and 10 psi) displayed smaller initial strain rates, most likely because of the dilative volumetric response of RAP at these smaller confining pressures.

Creep tests performed at large stress levels experienced creep rupture. The time to rupture decreased as the stress level increased. The time to rupture for RAP was also related to the minimum strain rate found at the end of secondary creep. This log-linear relationship was situated above similar relationships found for other soils. The upper yield strength, defined as the stress level below which creep rupture does not occur, for contractive RAP was estimated as 0.59 for RAP tested at 20 psi, and as 0.78 for tests performed at 40 psi. The creep potential of RAP appears to be at least as high, if not higher, than that of clay.

Chapter 7. Tufa Precipitation Potential of Crushed Concrete

7.1 INTRODUCTION

Although crushed concrete appears to exhibit adequate shear strength and drainage characteristics for use as a backfill material, a number of recent studies have raised some concerns for its potential to generate a byproduct in the form of calcium carbonate precipitate (Calcite; $CaCO_3$), also known as "tufa". Field investigations conducted in the mid of 1980s found evidence of tufa precipitation in drainage outlets for pavement subbases constructed of crushed concrete. This chapter describes an experimental investigation regarding the potential for tufa precipitation from different particle sizes of CC and the material characteristics that indicate tufa potential.

7.2 BACKGROUND ON TUFA PRECIPITATION

7.2.1 Previous Studies

One of the first complete reports on tufa precipitation causing highway problems was by Feldmann (1981). Feldmann (1981) reported that tufa from calcareous subbase materials (i.e. slag in this study) clogged subdrains along newly constructed highways in Northeastern Ohio. Because these tufa deposits were blocking the discharge outlets for the road surface and subbase, several problems were observed, such as the breaking down of flexible pavement and the surface pumping of fines from beneath rigid pavement slabs.

Feldman (1981) surveyed 124 field locations and found that some of the drain outlets were heavily clogged by tufa, while a number of drains were partially filled. Sample pictures of the observed tufa deposits are shown in Figures 7-1 and 7-2. As part of the chemical testing program, draining water was collected from various locations and it was discovered that the dominant anions found in the samples were of the carbonate species (CO_3). The author concluded that the use of slag as subbase was the cause of the tufa formation observed.

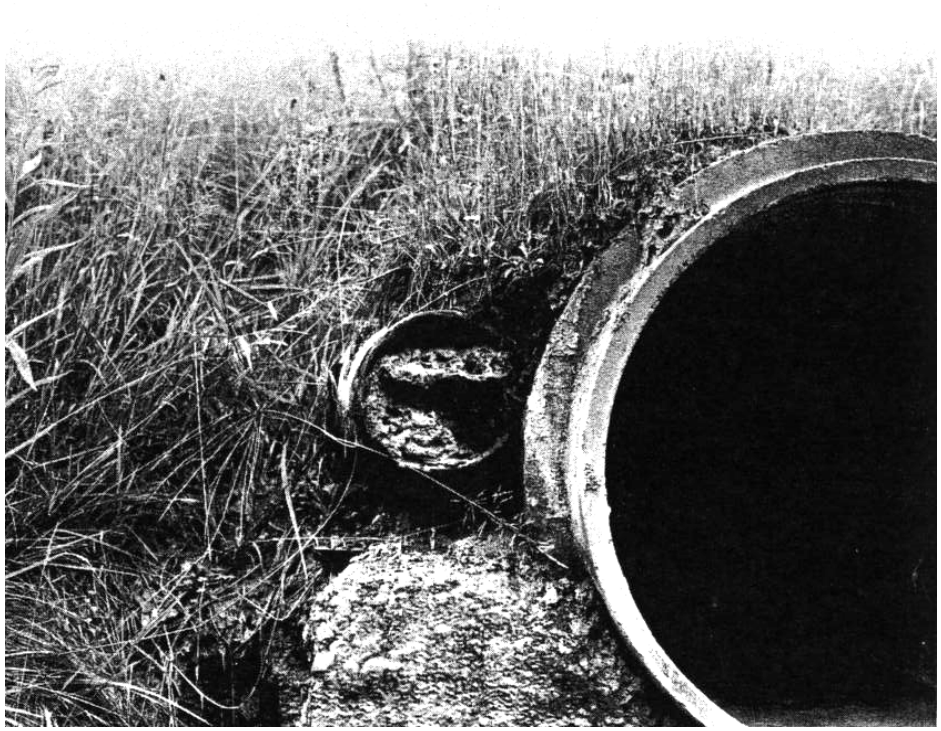

Figure 7-1 Tufa totally blocking an 8-in diameter drain [Feldmann (1981)]

Figure 7-2 Tufa forming at the mouth of a 6-in diameter drain [Feldmann (1981)]

Feldmann's work was subsequently followed by a number of field and laboratory studies [e.g. Ford (1987), Muethel (1989), Bruinsma and Snyder (1995), and Snyder (1995)] that further investigated the occurrence of tufa deposits caused by a wider range of road construction materials, including crushed concrete. The majority of the field studies generally included: measuring the reduction in permittivity of filter fabric wrapped around drainage pipes where tufa deposits were evident, chemical composition testing on precipitates sampled from pavement subdrainage systems, and measuring pH levels of the drainage water. The laboratory investigations on tufa typically involved: experimental evaluations attempting to correlate pH measurements with tufa precipitation potential, leachate and precipitate testing on laboratory-prepared samples in a controlled

environment, and calcium concentration measurements of the crushed concrete leaching effluent. Many significant findings were established from these field and laboratory studies, and key observations that are related to the scope of this study are summarized below:

- Precipitate deposits were composed primarily of tufa, although significant amount of insoluble residue (i.e. noncarbonate materials and organic matters) were also found. [Tamirisa (1993, Snyder and Bruinsma (1996)]
- Free lime (CaO), portlandite [$Ca(OH)_2$], and possibly other significant calcium-based compounds in crushed concrete are responsible for the formation of tufa, with portlandite being the major reactive component. [Muethel (1989), Tamirisa (1993), and Bruinsma et al. (1997)]
- Calcium-based compounds are present in most crushed concrete aggregates in quantities sufficient to be leached and precipitated in the presence of carbon dioxide. [Snyder and Bruinsma (1996)]
- The precipitate production of crushed concrete increases with decreasing particle size. This is because crushed concrete fines possess higher surface area and, thus, greater amount of freshly exposed cement paste surface. [Muethel (1989) and Tamirisa (1993)]
- Selective grading or blending with natural aggregates can reduce, but not eliminate, precipitate problems. [Ford (1987), Snyder (1995)]

- Tufa precipitation is enhanced by a greater degree of exposure to atmospheric carbon dioxide. Contact time between carbonated water and crushed concrete also plays a major role in the pH level, and possibly the amount of material precipitate produced. [Bruinsma et al. (1997)]
- Precipitate deposits were found to significantly reduce permittivity (up to 53% permittivity loss after 8 years of service) of the filter fabrics surrounding drain pipes. [Snyder and Bruinsma (1996)]

7.2.2. Indicators used for predicting Tufa Potential

Based on a number of previous publications on the possible chemical reactions required for tufa formation in various fill materials [e.g., Gupta et al. (1994), Bruinsma et al. (1997), and Hurd (1988)], it can be concluded that tufa precipitation in crushed concrete is initiated by the dissolution of portlandite and unhydrated free lime when exposed to infiltrating water that carries carbonic acid. Because portlandite constitutes up to 20% to 30% of Portland cement paste, while only 1% or less of cement paste is unhydrated free lime, portlandite is clearly the main calcium ion donor for tufa precipitation. The water exposure of portlandite and unhydrated free lime releases calcium ions (Ca^{2+}) and hydroxide ions (OH^-) into solution. This particular chemical reaction can be expressed by two simple chemical equations as follows:

$$\text{CaO (unhydrated free lime)} + H_2O \leftrightarrow Ca^{2+} + 2(OH)^- \quad (7.1)$$

$$Ca(OH)_2 \text{ [portlandite]} \leftrightarrow Ca^{2+} + 2(OH)^- \quad (7.2)$$

The hydroxide ions in the above equations confirm why water leaching through crushed concrete displays initial pH values between 10 and 12.

Beyond calcium, carbonate ions [$(CO_3)^{2-}$] are required for tufa precipitation. Carbonate ions are generated from a chemical reaction between carbon dioxide (CO_2), from the atmosphere and automobile exhaust, and water, which forms carbonic acid (H_2CO_3):

$$CO_2 + H_2O \leftrightarrow H_2CO_3 \qquad (7.3)$$

Carbonic acid disassociates into hydrogen (H^+) and bicarbonate ions [$(HCO_3)^-$]. This reaction (equation 7.4) is favored by high pH environments, such as the one found in water leaching through crushed concrete:

$$H_2CO_3 \leftrightarrow H^+ + (HCO_3)^- \qquad (7.4)$$

Depending on the pH level and other thermodynamic factors, some of the bicarbonate ions can disassociate further into hydrogen and carbonate ions [$(CO_3)^{2-}$]. Likewise, this reaction (equation 7.5) is favored in a high pH environment.

$$H(CO_3)^- \leftrightarrow H^+ + (CO_3)^{2-} \qquad (7.5)$$

It is the releasing of hydrogen ions during the reactions indicated in equations 7.4 and 7.5 that leads to a drop in the pH of a crushed concrete-water solution over time.

Finally, all associated ions combine together into calcium bicarbonate [$Ca(HCO_3)_2$], which is more soluble in water than calcium carbonate ($CaCO_3$) [Gupta et al. (1994)]:

$$2H^+ + 2H(CO_3)^- + Ca^{2+} + 2(OH)^- \leftrightarrow Ca(HCO_3)_2 + 2H_2O \qquad (7.6)$$

$$4H^+ + 2(CO_3)^{2-} + Ca^{2+} + 2(OH)^- \leftrightarrow Ca(HCO_3)_2 + 2H_2O \qquad (7.7)$$

At any air-interfacing zone, such as a drainage outlet or the inside of a fabric-wrapped pipe, the enriched solution of calcium bicarbonate evaporates during the warm weather, the carbon dioxide (CO_2) escapes into the atmosphere, and calcium carbonate precipates out. It is this condition that leads to the formation of tufa [Gupta et al. (1994)]:

$$Ca(HCO_3)_2 \leftrightarrow CaCO_3 (\downarrow) + H_2O (\uparrow) + CO_2 (\uparrow) \qquad (7.8)$$

Again, warm temperatures in the summer months increase the rate of tufa formation, while cold temperatures in the winter months cause the carbon dioxide to remain in solution. The preceding chemical reactions clearly demonstrate that calcium ions, water, carbon dioxide, temperature, and humidity are the primary factors controlling tufa formation. However, calcium ions and carbon dioxide are the two principle chemical ingredients required for any tufa formation. With unlimited sources of carbon dioxide

from the atmosphere and from automobile exhaust, the number of available calcium ions in the solution becomes the main parameter controlling the amount of tufa that can form.

At this point, the next question is what is the appropriate indicator to identify the tufa precipitation potential of crushed concrete. Clearly, the releasing of OH^- ions shown in Equations 7.1 and 7.2 will result in elevated pH values of water leaching through crushed concrete, and the amount of released OH^- ions should be proportional to the amount of dissociated Ca^{2+} ions in the same solution. Thus, as pH measurements are simple to perform, it is a straightforward, yet indirect, method that can be used to predict the amount of Ca^{2+} ions that may have dissociated into solution. However, pH values reflect the H^+ and OH^- ion concentration in the test solution. Hence, if there is any fluctuation in the H^+ or OH^- concentrations due to an outside source, the pH measurement on crushed concrete will no longer reflect the quantitative amount of dissociated Ca^{2+} ions.

Referring to Equations 7.3 through 7.5 shown above, the introduction of atmospheric CO_2 results in the subsequent release of free H^+ ions into the test solution. This process is picked up by a decrease in pH value with time even though the number of Ca^{2+} ions in the solution remains unchanged. Thus, pH measurements are only a good initial assessment regarding tufa precipitation potential, when the measurements are done before any disturbance to the system from outside sources can take place. Finally, the pH value can be significantly affected by changes in ambient conditions such as temperature. Based on these issues, a direct measurement of the calcium ion concentration is a more

appropriate indicator for tufa precipitation potential than pH, because it reflects the actual quantitative amount of the Ca^{2+} ions present in the solution.

7.3 EXPERIMENTAL PROGRAM

An experimental program was initiated in this study assuming that the degree of tufa precipitation should depend primarily on the number of available calcium ions released from crushed concrete. It is anticipated that the amount of calcium ions released from the crushed concrete will vary with the exposed surface area, which in turn is a function of particle size. As a result, a series of calcium ion concentration measurements were taken on different particle size ranges of crushed concrete. The experimental results should produce a relationship between grain size and the amount of calcium ions released into the crushed concrete-water solution, and possibly will identify a threshold particle size below which the number of released calcium ions is most significant. This information can be very useful during the design phase of the backfill for which a design engineer can, to some extent, specify the allowable percentage of crushed concrete particles having particle sizes smaller than the threshold value.

The testing program involved mixing a known weight of oven-dried crushed concrete of various particle size ranges with approximately 1000 grams of deionized water (Figure 7-3). Each sample was carefully stirred in an attempt to ensure full exposure of CC particles with the water. All samples were allowed to settle for two days before the first measurement was taken. Table 7-1 summarizes the amount of dried material and deionized water prepared for each test sample. The amount of dried material

varied from approximately 50 grams for samples with particles smaller than U.S. sieve No. 4, to as much as 267 grams for particles larger than 1 in.. More material was required for larger particles to ensure that an adequate number of disassociated calcium ions were released into the solution.

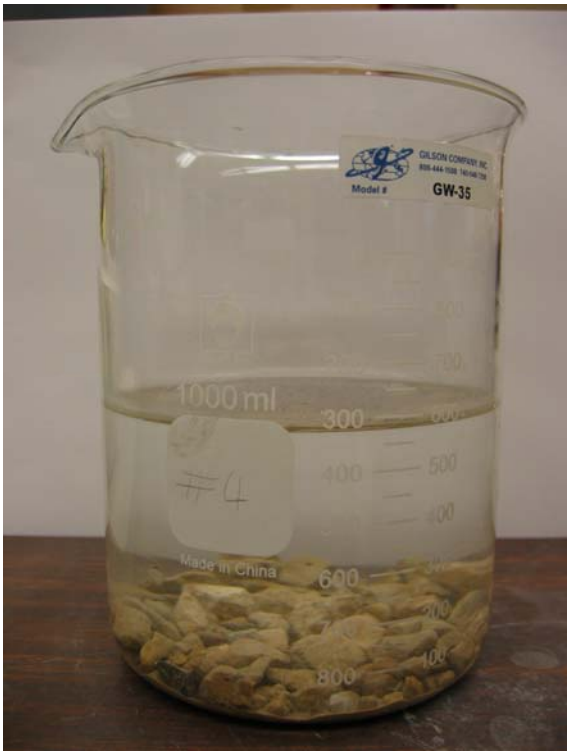

Figure 7-3 Picture of a CC-water mixture sample for the Ca^{2+} ion measurement

Table 7-1 Dry material-water mixing proportions of the test samples

Sample Label	Range of Particle Size (S)	Dried Material (g)	Deionized Water (g)	Material to Water Ratio
1 in.	larger than 1.0″	267.1	1002.4	0.27
0.5 in.	0.5″ < S < 1.0″	151.6	1027.3	0.15
#4	Sieve #4 < S < 0.5″	102.3	1007.1	0.05
#8	Sieve #8 < S < Sieve #4	50.0	1008.7	0.05
#16	Sieve #16 < S < Sieve #8	50.2	1003.5	0.05
#40	Sieve #40 < S < Sieve #16	54.0	1001.7	0.05
#200	Sieve #200 < S < Sieve #40	50.1	1000.6	0.05
Fines	Smaller than Sieve #200	50.0	1004.8	0.05

It should be noted that a pilot test was conducted to estimate the amount of calcium ions that can possibly dissociate from the crushed concrete. This pilot study was performed by mixing dry material and deionized water at various proportions to assure that the mixing proportion for the actual measurement would produce calcium ion concentrations that are within the maximum limit (i.e. less than 200 mg/L) for the type of Ca^{2+} measurement technique used in this study. It is understood that these Ca^{2+} concentrations may be adequate to precipitate $CaCO_3$ if sufficient CO_3^{2-} ions are present in the solution. Snoeyink and Jenkins (1980) estimated that the solubility of $CaCO_3$ is about 14 mg/L and 8 mg/L at pH levels of 10 and 12, respectively, at an atmospheric CO_2 pressure of $10^{-3.5}$ atm. Assuming sufficient CO_3^{2-} ions are present in the test solution, Ca^{2+} ion concentration of over 5.6 mg/L and 3.2 mg/L, theoretically, would be adequate to precipitate out $CaCO_3$. However, it is believed that only a small amount of

precipitation would take place given the fact that ambient CO_2 pressure (source of CO_3^{2-} ions) in a typical closed-room laboratory should be lower than the atmospheric CO_2 pressure, and that the mixing water should only have negligible amount of CO_3^{2-} ions to begin with initially. Nonetheless, if the precipitation would actually occur, it should only take place limitedly at the top surface water where ion exchange process is more active, not the entire sample in the beaker.

The number of calcium ions dissolved in the solution was determined using the ethylenediaminetetraacetic acid (EDTA) titrimetric method in accordance to the Test No. 3500-Ca B. outlined in the "*Standard Methods for the Examination of Water and Wastewater*" by Clescerl et al. (1999). This method follows the same principles as all standard laboratory titration methods, in which a titration agent is added that reacts chemically with the substance under consideration. The titrant solution is added until it reacts with all of the available test substance (i.e. the end point), and the amount of the titrant added is related to the amount of the test substance. In this study, a standard EDTA reagent is the titrant and free calcium ions in the test solution are the reactants/test substances. The titration occurs by constantly and slowly adding EDTA into the test solution until the end point is reached, which is signaled by a change in color of the indicator, murexide in this case, which was added to the solution at the beginning of the titration.

For this study, a measurement begins by taking approximately 50 mL of CC-water solution from the surface water of the mixing sample. Approximately 2.0 mL of sodium hydroxide (NaOH) is subsequently added to the solution to produce a pH of 12 to

13. The added NaOH becomes a source of dissolved OH^- ions that attract any free magnesium ions (Mg^{2+}) that are in the solution and precipitates them into insoluble magnesium hydroxide (MgOH). Because Mg^{2+} ions react with EDTA in the same way as Ca^{2+} ions, it is important to eliminate any free Mg^{2+} ions. After addition of the NaOH, two drops of indicator is added before the titration takes place.

The titration process is performed by adding slowly a standard EDTA titrant from a microburet with continuous hand stirring until the proper end point is reached. With the type of indicator used in this study, the end point is recognized by a change in color from pink to purple. The duration of the titration was limited to 5 minutes to minimize the tendency towards $CaCO_3$ precipitation. Finally, by knowing the EDTA/Ca^{2+} equivalence, the amount of Ca^{2+} ions (mg) present in each 50 mL representative sample and its concentration (mg/L) can be calculated. It is assumed that the concentration of calcium ions (in mg/L) determined from the 50 mL sample is representative of the concentration of the entire testing solution at the time of the measurement. The measurement was performed every two days and was terminated after two weeks of testing, which was when no noticeable amount of calcium ions was further released into solution. To promote optimum exposure of all CC particles in the solution and the free water, a mild hand stir was conducted daily on all the test samples.

7.4 TEST RESULTS AND DISCUSSIONS

Measurement of the calcium concentration of 50-mL specimens was conducted on all test samples for a duration of two weeks. The amount of calcium ions (in milligrams) and its concentration (in mg/L) for each of the 50-mL specimens was determined as discussed in the previous section. The measured calcium concentrations versus time for each CC particle size range are shown in Figure 7-4. The measured concentrations vary from about 25 mg/L to 60 mg/L, and the data demonstrate that the calcium concentrations generally increase with time. The exception is samples with CC particles larger than sieve No. 4 (samples #4, 0.5 in, and 1 in), which displayed concentrations that leveled off after four days. The data also indicate that the calcium concentration is generally inversely proportional with the size of the CC particles, with larger concentrations measured for smaller particle sizes. The plot also illustrates that the largest calcium concentrations are observed for CC particles smaller than about sieve No. 8 (2.38 mm).

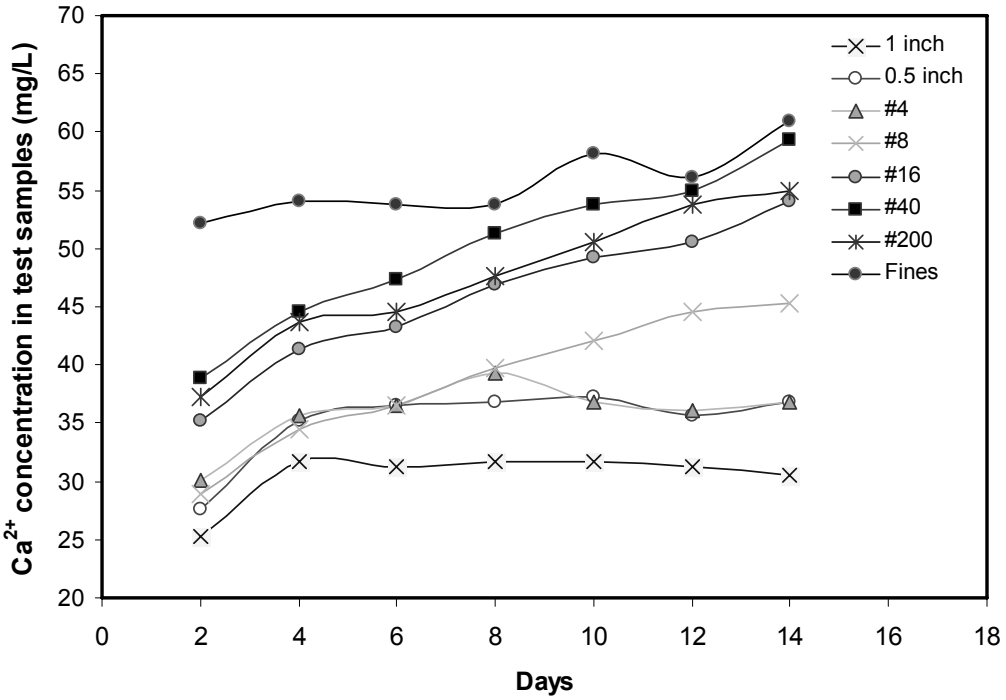

Figure 7-4 Calcium ion concentrations in the test samples vs. time

The data in Figure 7.4 can be somewhat misleading because the amount of dry material used in the mixtures varied from sample to sample (Table 7-1). Thus, the measured calcium concentrations in Figure 7-4 were normalized with respect to the weight of the dry CC used in each sample, and are plotted in Figure 7-5. This figure illustrates that calcium concentration in the test solutions varies from about 0.1 mg/L to 1.2 mg/L per gram of dry material, and that measured concentrations increased with decreasing particle size of the CC. More importantly, this figure shows a more distinctive separation, in terms of weight normalized calcium concentration, between samples with particles smaller than sieve No. 4 and the samples with larger particle sizes. This graphical observation suggests the possible existence of a threshold particle size.

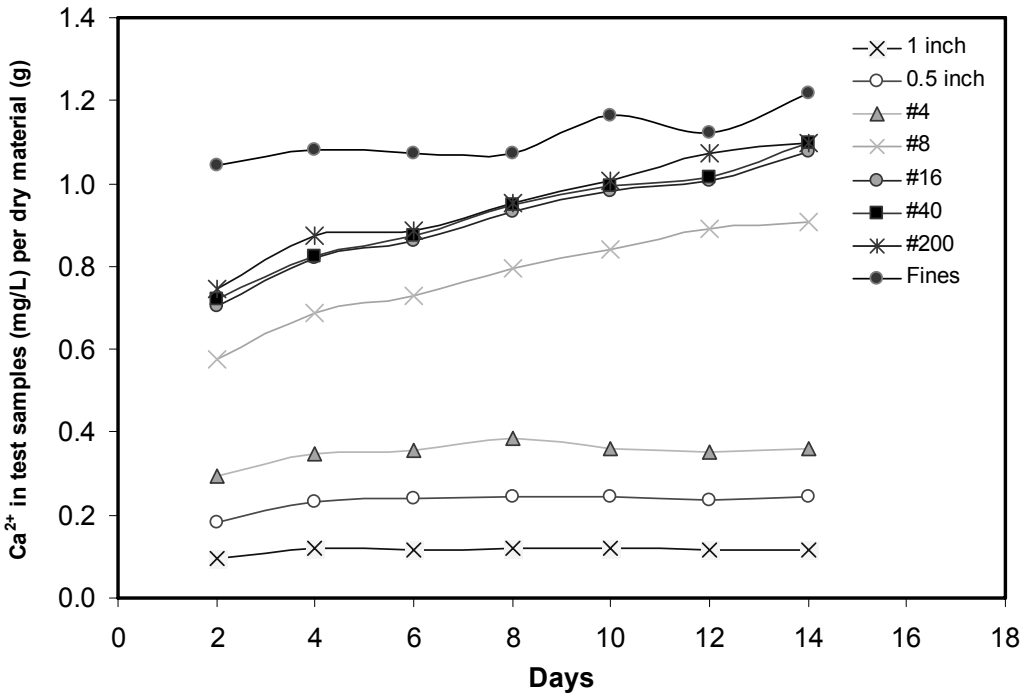

Figure 7-5 Calcium ion concentration per weight of dry material vs. time

It must be noted, however, that the increase in Ca^{2+} ion concentration with time shown in Figures 7-4 and 7-5 is influenced by the removal of free water for concentration testing and by the approximately 20 mL of water that was lost due to evaporation each day. For these reasons, Figure 7-6 was created to illustrate plots of the total calcium ions (in mg) released per weight of dry material (in g) over time. Each data point was calculated from the total weight of calcium ions in solution on the day of testing (i.e., Ca^{2+} concentration times the volume of water in beaker at the time of sampling) plus the weight of calcium ions that had been removed during prior measurements, divided by the initial weight of the dry material used.

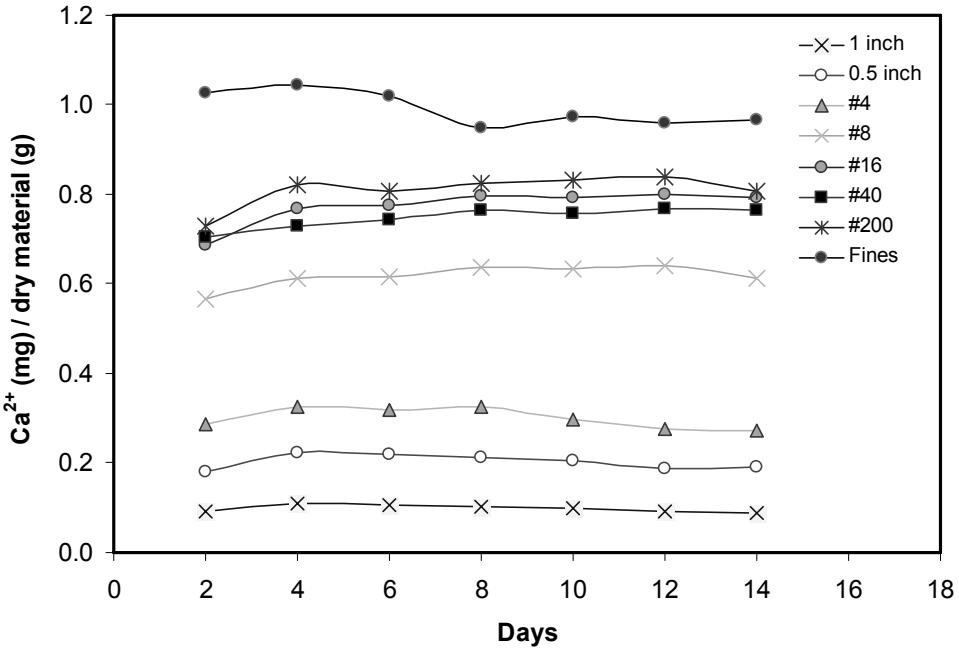

Figure 7-6 Weight of dissolved calcium ions per weight of dry material vs. time

It can be seen in Figure 7-6 that there was an apparent increase in the total amount of calcium ions between Day 2 and Day 4 for most of the test samples. After Day 4, little dissociation of calcium ions was observed for samples #8, #16, #40, and #200, whereas a declining number of ions were observed for the other test samples. It should be noted that some precipitation of calcium carbonate was observed at the top of the test solution and along the side of the beaker in some of the samples. This precipitation was most pronounced for the CC fines sample. This precipitation is what would lead to the reduction in calcium ions over time, as calculated from the measured calcium concentrations. Though such precipitations may have contributed some uncertainty to the accuracy of this investigation, they appeared to be of small magnitude and should not significantly alter the observations from this study.

The data in Figure 7-6 are unique in that they reflect the total amount of calcium ions that can possibly discharge from CC materials within different particle size ranges. Such information can be very beneficial to the engineers to predict the maximum amount of $CaCO_3$ that can precipitate from a given gradation of CC. For instance, with the reference gradation shown in Figure 3-6 and an assumed compacted dry density of 120 lb/ft^3, the total tufa precipitation per cu. ft. of compacted CC backfill can be estimated as shown systematically from left to right in Table 7-2. This calculation involves computing the weight of each particle size range within one ft^3 of compacted material, using the data from Figure 7-6 to compute the weight of Ca^{2+} discharged from each particle size range, and computing the weight of $CaCO_3$ precipitate based on the discharged Ca^{2+} weight. It must be noted that precipitated tufa has a molecular weight roughly 2.5 times higher than calcium atomic (100 g/mol for $CaCO_3$ vs. 40 g/mol for Ca^{2+} ion), and this information was taken into account when calculating the expected amount of tufa precipitation in the last column of Table 7-2.

Table 7-2 Sample calculation for the expected total calcium ions release from CC backfill

Particle Size (S)	Percent by Weight (%)	Weight portion per cu. ft. of compacted dry material (lb)*	Expected Ca^{2+} ions discharged ($x10^{-3}$ lb per lb of dry material)**	Ca^{2+} discharged from 1 ft^3 of compacted material (lb)	Expected $CaCO_3$ precipitation from 1 ft^3 of compacted material (lb)
larger than 1.0″	12	14.4	0.099	0.0014	0.004
0.5″ < S < 1.0″	23	27.6	0.203	0.0056	0.014
Sieve #4 < S < 0.5″	30	36.0	0.301	0.0108	0.027
Sieve #8 < S < Sieve #4	13	15.6	0.617	0.0096	0.024
Sieve #16 < S < Sieve #8	7	8.4	0.773	0.0065	0.016
Sieve #40 < S < Sieve #16	8	9.6	0.747	0.0072	0.018
Sieve #200 < S < Sieve #40	7	8.4	0.809	0.0068	0.017
fines	0	0.0	0.991	0.0000	0.000
			Total	**0.0479**	**0.120**

Note: * Assumed dry unit weight of 120 pcf ** Average values determined from Figure 7-5

According to Table 7-2, the total tufa precipitation from the reference gradation is estimated as 0.12 lb per cu. ft. of compacted CC backfill. Based on the specific gravity of 2.7 for normal tufa precipitate [Snoeyink and Jenkins (1980)], the total volume of tufa precipitate would be 0.0007 ft^3 (1.23 in^3) per ft^3 of compacted CC backfill. Conceptually, by knowing the total volume of CC material in an entire CC fill, one can estimate the total volume of tufa precipitate that can potentially form. This information would allow a design engineer to design an appropriate drainage system to minimize clogging. This system would include filter fabrics around drainage pipes with sufficiently high initial permittivity and large diameter drain pipes with substantial openings. It should be noted, however, that this assessment of precipitation volume may be a conservative estimate of the actual amount of tufa that can possibly form under real field conditions because the CC particles were fully exposed to free water in the experiments, which is not likely to

happen in the field. However, in the field, fresh water will percolate through the CC over time, which may allow more Ca^{2+} to leach into the water, and precipitate into $CaCO_3$, over time.

The data in Figure 7-6 also allows for the identification of a threshold particle size. By definition, the threshold particle size is the grain size below which the number of released calcium ions is most significant. As seen in Figure 7-6, a significant increase in measured calcium ions is observed between sample #4 and sample #8. This observation can be observed more effectively in Figure 7-7, which shows the amount of dissolved calcium ions versus particle size. In Figure 7-7, a significant increase in the dissolved calcium is observed from sample #4 to sample #8. Therefore, it is concluded that the U.S. sieve No. 4 (4.75 mm) is the threshold particle size for the CC used in this study, which coincides with the threshold size for gravel-sized particles. This finding is similar to recommendations developed by Muethel (1989) and Snyder and Bruinsma (1996), who suggested minimizing the inclusion of CC particles that are smaller than sieve No. 4. However, neither of these studies explicitly identified a threshold particle size or discussed how they derived at such a conclusion.

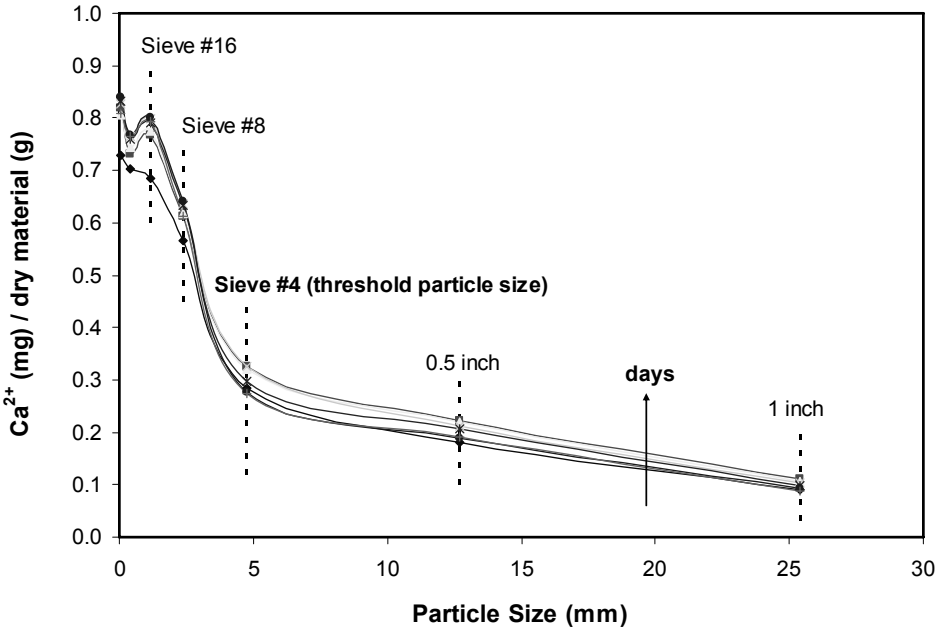

Figure 7-7 Calcium ions per dry material vs. particle sizes

It is conclusive at this point that inclusion of CC particles smaller than sieve No. 4 can significantly increase the tufa precipitation potential. The pie chart in Figure 7-8 demonstrates the relative contributions of each particle size range to the production of calcium ions. It can again be seen from this figure that particle sizes larger than #4 contribute most significantly to the amount of calcium ions. In fact, more than 85% of the calcium ions come from particles smaller than the #4 sieve (sand-sized particles and fines), while about 22% of the calcium ions come from the fines smaller than the #200 sieve.

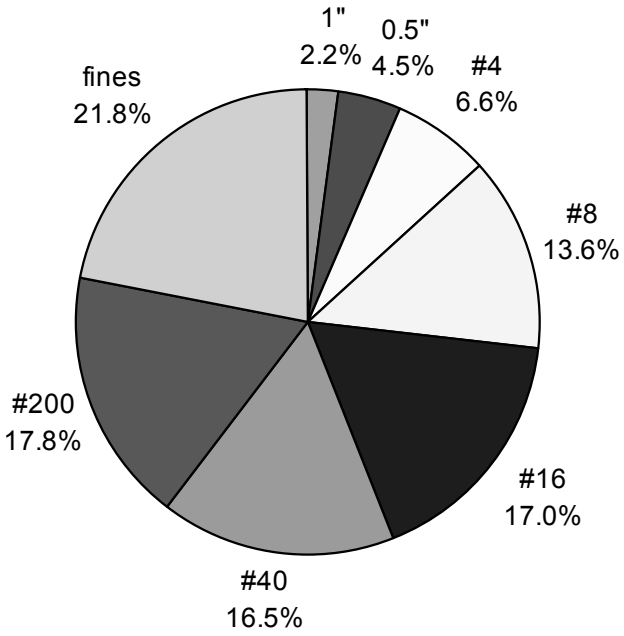

Figure 7-8 Percent contribution of calcium ions from different CC particle sizes

An additional experiment was performed to investigate the effectiveness of material washing in reducing the tufa precipitation potential. A new bulk sample of CC material was used for this study. One half of the bulk material was subjected to conventional dry sieving, while the other half was subjected to wet sieving. The test material separated by wet sieving was oven-dried over night. Only two material sizes (i.e. #40 and #200) were involved in this study. It was observed that approximately 14% and 5% by weight of the original material was washed away during the wet sieving process for material sizes #40 and #200, respectively. The CC-water mixture samples were prepared and the experimental program was conducted using the same procedures as described earlier.

The results, in terms of Ca^{2+} weight per weight of dry material, are shown in Figure 7-9. It is apparent from these data that the washing process did not significantly reduce the amount of calcium ions released from the CC aggregates. On average, the washing process produced only a 0.4% and 14.8% reduction in Ca^{2+} for material sizes #40 and #200, respectively. Such a small reduction for material size #4 is surprising especially when considering 14% of the original material, which potentially was fines adhered to the grain aggregates, was removed by wet sieving. Therefore, it is concluded that the washing process does not significantly reduce the tufa precipitation potential of CC.

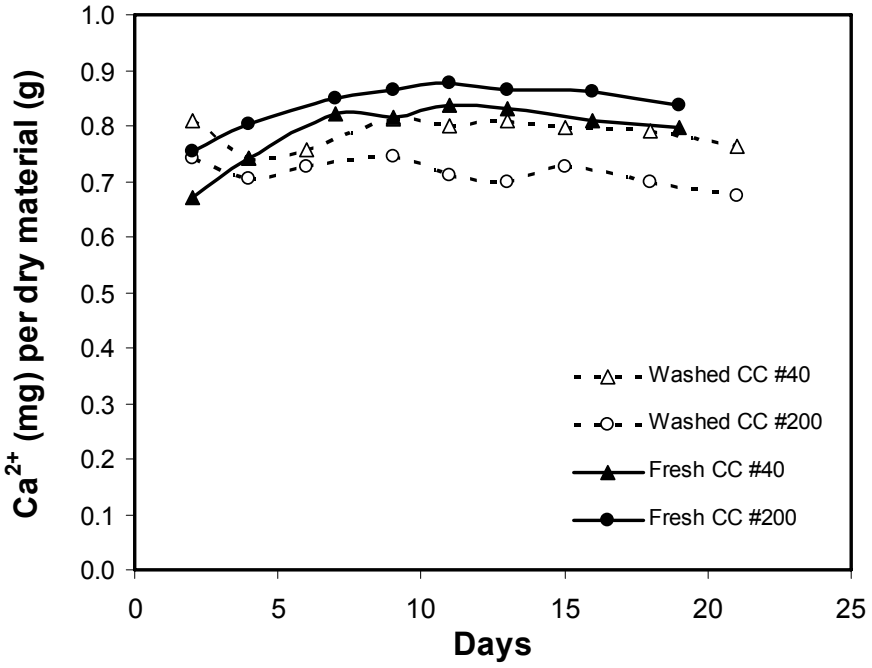

Figure 7-9 Calcium ion dissolution vs. time for washed and unwashed CC particles

7.5 CONCLUSIONS

Tufa precipitation has been one of the unresolved issues regarding the use of CC as backfill because only a limited number of studies have been reported on this subject. The basic chemical reactions required to form tufa were discussed in this chapter along with several thermodynamic parameters that control the rate or the quantity of tufa formation. Even though the amount of tufa formation is dependent on several factors, including the ambient pH of the solution and the presence of atmospheric carbon dioxide, the key ingredient that allows the precipitation to occur is the available free calcium ions released from CC. As a result, a series of calcium ion measurements were carried out on a number of test samples, each of which was a mixture of deionized water and CC within a select range of grain sizes.

The test results indicated that most of the calcium disassociates from the CC within a few days and remains constant after that time. The test results also suggested that U.S. sieve No. 4 is the threshold particle size, which indicates that particles smaller than the #4 sieve generate the most calcium ions. Some simple calculations showed that the different particle sizes of CC can release between 0.1×10^{-3} and 1.0×10^{-3} lb of free calcium ions per one pound of original dry material, with the released amount generally inversely proportional with the size of the particles. Additional tests also revealed that the washing process did not significantly reduce the amount of free calcium ions released from the CC, and therefore, it is not effective as a preventive measure to this problem.

Chapter 8. Summary and Conclusions

8.1 SUMMARY

This research aimed to experimentally investigate the potential use of recycled asphalt pavement (RAP) and crushed concrete (CC) as backfill material for MSE walls. One of the main incentives for this study is the growing need for alternative materials to replace conventional select backfills, which are increasingly scarce in some areas of the U.S. Other motivations that make RAP and CC attractive backfill materials are increasing landfill disposal fees for waste materials and the tendency for more stringent environmental regulations and land use policies from state environmental agencies.

This dissertation presented the experimental results from the geotechnical component of a larger investigation sponsored by the Texas Department of Transportation (TxDOT). Thus, the studies conducted for this research and presented in this dissertation are focused primarily on the intrinsic geotechnical properties of RAP and CC. Separate experimental investigations to evaluate the material-reinforcement interaction, material durability, and material corrositivity were conducted by other members of the research team [i.e. Ogalla (2002), Jain (2004), and Esfeller (2006)]. The geotechnical investigative efforts conducted can be divided into three main parts: (1) an assessment of index properties and compaction characteristics of the test materials; (2) an assessment of shear strength, hydraulic conductivity, and collapse potential of the test materials; and (3) an assessment of potential problematic properties of RAP and CC.

8.1.1 Assessment of index properties and compaction characteristics

The assessment of index properties and compaction characteristics of RAP and CC was conducted in comparison with a conventional fill material (CFM). The index properties evaluated include gradation, pH measurement, Atterberg limits, and specific gravity. The test results from RAP and CC were compared with those of CFM as an initial evaluation in terms of their basic properties. Conventional laboratory impact compaction was employed to determine and establish the compaction curves of RAP, CC, and CFM. In addition, a supplemental assessment that determined the potential for particle breakdown of the test materials was included at the end of the laboratory compaction testing.

The applicability of typical field compaction control techniques, such as the nuclear gauge device, rubber balloon method, and test pit method, for RAP and CC was evaluated in the field using compacted stockpiles. The in situ total unit weights and moisture contents measured from the nuclear gauge device were compared with those obtained from using the other two techniques conducted at approximately the same locations. The potential problems associating with using the nuclear gauge to measure the in situ unit weight and moisture content of RAP and CC were addressed.

8.1.2 Assessment of shear strength, hydraulic conductivity, and collapse potential

Three laboratory testing programs were designed to evaluate the shear strength, hydraulic conductivity, and collapse potential of RAP and CC. The results from these tests were compared with tests performed on the CFM. The shear strength of the test materials was characterized in terms of the drained shear strength parameters (i.e. c', ϕ'),

as determined by triaxial tests performed on 4-in diameter specimens and large-scale direct-shear tests performed on 20-in by 20-in square specimens. Hydraulic conductivity measurements were performed on all three test materials using the falling head-rising tail method in a flexible wall triaxial setup, and these results were compared with results from the constant head-fixed wall hydraulic conductivity method. The collapse potential upon wetting was evaluated through large-scale, one-dimensional, constrained compression tests. The collapse potential of the three test materials was compared in terms of their collapse index (I_c), a parameter suggested by the ASTM standard (ASTM D 5333).

8.1.3 Assessment of potential problematic properties

For each material (RAP and CC), one potential problem was identified related to the intrinsic material composition. For RAP, creep was identified as a significant concern, while for CC the precipitation of calcium carbonate was identified as a potential problem.

Creep is a concern for RAP because of its viscoelastic behavior due to the bitumen coating that surrounds the aggregate particles. The tendency for RAP to fail due to creep rupture, rather than in typical shear, was observed during the load-controlled, large-scale direct shear tests. In light of that discovery, a series of constant-stress, drained triaxial creep tests were performed on a number of compacted RAP specimens to evaluate its creep potential. The study of RAP creep behavior was conducted through three different test series: (1) creep tests at variable shear loads at 20 psi confining pressure, (2) creep tests at variable shear loads at 40 psi confining pressure, and (3) creep

tests at variable confining pressures and an applied shear stress equal to 80% of the ultimate shear strength. A simple three-parameter empirical model developed by Singh and Mitchell (1968) was fit to the experimental data and used to describe the creep behavior of RAP. Expressions to predict creep rupture were investigated. The laboratory data were also used to identify values of upper yield strength, defined as the shear stress level below which creep rupture does not occur.

The main concern associated with using CC as a backfill material is its potential to generate a byproduct in the form of calcium carbonate precipitate (Calcite; $CaCO_3$), also known as "tufa". This byproduct is derived from the dissociated calcium ions found in cement paste. For that reason, a series of calcium ion concentration measurements was performed on different particle size ranges of crushed concrete. The experimental results produced a relationship between grain size and the amount of calcium ions released into the crushed concrete-water solution, and also identified a threshold particle size below which the number of released calcium ions is most significant.

8.2 CONCLUSIONS

The conclusions of this research program are presented in four parts: index properties and compaction characteristics; shear strength, hydraulic conductivity, and collapse potential; creep potential of RAP; and tufa precipitation of CC.

8.2.1 Index Properties and Compaction Characteristics

RAP has an average pH level of 8.1 which meets both the current TxDOT and FHWA backfill specifications for MSE walls. The average pH level of CC was 12.4, which exceeds the maximum pH requirement of 10. Tests for the Atterberg limits showed that RAP and CC are both non-plastic materials. CC has a specific gravity similar to the CFM ($G_s \sim 2.62$), while RAP has a significantly smaller specific gravity ($G_s \sim 2.33$) due to the bitumen coating around the aggregates.

RAP displayed a compaction curve with a distinct peak at around 3% water content. The compaction curves for CC and CFM did not exhibit distinct peaks, which is typical for gravelly soils. RAP and CC appeared to exhibit less particle breakdown during compaction as compared with the CFM. The increases in fines content after laboratory compaction for RAP (0.6%) and CC (1.6%) were less than half of that for CFM (3.6%). This finding suggests that RAP and CC are not likely to produce a significant amount of fines during field compaction.

Field compaction control tests revealed that the nuclear gauge, when well calibrated, can adequately measure the in situ total unit weight of RAP and CC backfill. However, moisture contents measured by the nuclear gauge for RAP and CC were overestimated (3 times higher for RAP and 20% higher for CC) as compared with values

measured by oven drying. The overestimation of water content by the nuclear gauge was caused by the fact that the nuclear device measures hydrogen atoms as an indicator of water, and RAP and CC contain hydrogen atoms that are in excess of those found in the free water in the material. As a result, separate moisture content calibrations for RAP and CC are recommended to obtain accurate measurements of the compaction water content.

8.2.2 Shear Strength, Hydraulic Conductivity, and Collapse Potential

The combined sets of data from the triaxial and large-scale direct shear tests concluded that RAP, CC, and CFM have zero values of effective cohesion (c' = 0). The effective friction angle (ϕ') of CC and CFM were at least 46°, which is more than adequate for typical MSE wall backfill applications. RAP, on the other hand, displayed a smaller ϕ' (i.e. 40°), which is only slightly larger than the lower bound value of 34° specified by the FHWA MSE wall design manual. The favorable comparison between the measured shear strength parameters obtained from the triaxial tests, which required particle scalping, and the large-scale direct shear tests, which did not, suggested that the presence of large particles (> 0.63 in.) did not significantly change the shear strength of the compacted soil.

Results from hydraulic conductivity tests showed that RAP and CFM can be classified as free draining materials with $k > 10^{-4}$ cm/s, while CC is marginally a poorly draining material ($k \sim 10^{-4}$ to 10^{-5} cm/s). The re-cementation of CC particles may be responsible for the low k values observed. For RAP, the bitumen coating on the particles allowed water to flow through the voids more easily because in general it does not attract or absorb water.

The measured collapse index (I_c) values for all three materials classified them as materials with only a slight degree of collapse potential upon wetting, although RAP exhibited notably greater collapse than CC and CFM. The larger degree of collapse potential for RAP was believed to be the result of its lower initial degree of saturation. Nonetheless, RAP and CC should not exhibit significant collapse settlement upon wetting in the field, at least in the pressure range used in this study and at the saturation levels tested.

8.2.3 RAP Creep Behavior

In general, classical three-stage creep behavior was observed in all of the RAP specimens, with strain rates decreasing log-linearly with time until creep rupture occurred. The Singh and Mitchell (1968) creep model appeared to be valid for predicting the creep deformation of RAP during the primary and secondary stages of creep.

Values of the creep parameter *m* observed for RAP were generally between 0.7 and 0.9, which indicate that RAP displays significant creep behavior. The *m* values found in RAP are similar to the values reported in the literature for clays with significant creep potential. The *A* and $\bar{\alpha}$ parameters observed for RAP fall towards the upper range for clays, which is an additional indication of the high creep potential of RAP.

There is a noticeable trend of increasing *m* value with confining pressure irrespective of the volumetric response of the RAP during sheared. Based on this relationship found herein, an *m* value larger than 1.0 would be observed at a confining pressure approximately at least 70 psi. An *m* value greater than 1.0 indicates limited creep potential. Test results at a confining pressure of 50 psi showed that the *m* value eventually

became higher than 1.0, even though the material initially displayed an *m* value less than 1.0. Thus, it appears that RAP is less susceptible to creep at large confining pressures. It is postulated that at larger confining pressures the bitumen coating becomes compressed enough such that there is little bitumen at the grain-to-grain contacts of the aggregate particles. Because these direct particle contacts are less susceptible to creep, less creep is observed at higher confining pressures.

The variation in confining pressure did not appear to affect the *A* and $\bar{\alpha}$ creep parameters at confining pressures above 20 psi, but appear to alter the value of *A* and $\bar{\alpha}$ at lower confining pressures where the compacted RAP specimens tended to dilate during sheared. This dilative response of RAP during sheared appeared to also reduce the initial strain rates and prolonged the time to reach creep rupture for RAP.

The time to reach creep rupture for RAP was inversely proportional to applied stress level and to confining pressure for specimens at confining pressures greater than 20 psi. The time to rupture for RAP decreased log-linearly with the minimum strain rate observed at the end of secondary creep. Compared with data reported for clays, the log-linear relationship for RAP has a comparable slope but was situated well above the other relationships. This result suggests that for a given minimum strain rate, it takes longer for RAP to reach creep rupture as compared to the other soils.

The upper yield strength, defined as the shear stress level below which creep rupture does not occur, was identified from the test series performed at 20 psi and 40 psi. The upper yield strength was estimated as 0.59 for RAP tested at 20 psi and as 0.78 for tests performed at 40 psi confining pressure. These values again indicate that RAP is less

susceptible to creep at larger confining stresses. The identification of an upper yield strength is important because it illustrates that creep rupture can be avoided in RAP if the design stress is kept below the upper yield strength value.

8.2.4 Tufa Precipitation of CC

Test results indicated that most of the calcium disassociates from the CC within a few days and remains essentially constant after that time. Different particle sizes of CC can release between $0.1x10^{-3}$ and $1.0x10^{-3}$ lb of free calcium ions per one pound of original dry material, with the released amount inversely proportional with particle size.

It was observed that U.S. sieve No. 4 is the threshold particle size, which suggests that CC particles smaller than the No. 4 sieve generate the most calcium ions. If tufa precipitation will affect the performance of an earth structure, the inclusion of these particles should be limited during the design of the backfill gradation.

Additional tests also revealed that the washing process did not significantly reduce the amount of free calcium ions released from CC, and therefore, it is not effective as a preventive measure for tufa precipitation. Due to the tufa precipitation issue, it is concluded that MSE walls with CC backfill should include adequate drains and high permittivity filter fabrics behind the wall to avoid long-term drainage problems.

8.3 RECOMMENDATIONS FOR FUTURE RESEARCH

While this research study provided a thorough characterization of RAP and CC in terms of their use as MSE backfill materials, many aspects in this study can be modified or expanded to broaden the current understanding of the two materials. The following are recommendations fur future research on this topic:

1) It is well understood that asphalt properties are temperature dependent because of the bitumen coating. Therefore, the shear strength and creep behavior of RAP is expected to be influenced similarly by temperature. A laboratory study that investigates the influence of temperature on the shear strength and creep properties of RAP should be performed. Such a study can be made possible by a simple modification to the existing triaxial setup that involves the addition of a heat exchanger that circulates a constant temperature water (or air) into and out of the triaxial chamber during the test. It is anticipated that the duration of the creep tests will be much shorter when using elevated temperatures, such that the entire testing program can be performed more quickly.
2) It is understandable that the pavement sources of RAP can vary greatly, which means that the geotechnical properties of RAP may vary considerably depending on the type of aggregate and the percent asphalt content used in the original pavement material. An investigation should be established to study the effect of the aggregate type and the percent asphalt content on RAP strength and creep behavior.

3) One possible remedy to mitigate the creep potential of RAP is to mix it with a non-creeping material. A similar creep test program can be performed on compacted specimens with varying percentages of RAP in order to determine appropriate mixtures for which creep is not be a major concern.
4) Understanding of the RAP creep behavior was established in this study by using the Singh and Mitchell (1968) three-parameter creep model. The next step would be to perform a numerical analysis of an MSE wall that integrates the time-dependent creep model for RAP derived in this study with numerical models that properly describe the interface friction between the reinforcing elements and RAP. An integrated numerical model will allow geotechnical engineer to fully understand the effect of time dependent creep on the performance of MSE walls. Some commercial finite element programs (e.g., ABAQUS) already include the Singh and Mitchell (1968) creep model and thus may be used to study this issue.
5) A full-scale field study should be conducted in which an MSE wall is constructed with RAP backfill and monitored over time. The reinforcement spacing can be selected based on the reduced shear strength of RAP that reflects the upper yield strengths obtained in this study, and the field monitoring program should be used to observe whether creep deformations are significant.

References

Adachi, T. and Takase, A. (1981), "Prediction of Long Term Strength of Soft Sedimentary Rock," *Proc. Int. Symposium on Weak Rock - Soft, Fractured and Weathered Rock,* Theme 1: Engineering Property on the Weak Rock, Tokyo, pp. 93-98.

Ahmad, I. and Lovell, C. W. (1992), "Use of recycled materials in highway construction: State of the practice and evaluation of selected waste products," *Transportation Research Record*, Vol. 1345, Transportation Research Board, National Research Council, Washington, D.C.

Ahmad, I. (1991), "Use of recycled materials in highway construction," *Research Report FHWA/IN/JHRP-91/3*, School of Civil Engineering, Purdue University, West Lafayette, Indiana.

American Concrete Pavement Association (ACPA) (1993), "Concrete paving technology: Recycling concrete pavement," *Report No. TB-014P*, Arlington Heights, Illinois, 20 pp.

Anderson, L. R., Nelson, K. J., and Sampaco, C. L. (1995), "Mechanically stabilized earth walls," *Transportation Research Circular*, Vol. 444, 17 pp.

ASTM C 127 (2001), "Standard Test Method for Specific Gravity and Absorption of Coarse Aggregate," *Annual Book of ASTM Standards*, Section 4, Construction, Vol. 4.02 Concrete and Aggregates, American Society of Testing and Materials, West Conshohocken, PA.

ASTM D 854 (2001), "Standard Test Method for Specific Gravity of Soil Solids by Water Pycnometer," *Annual Book of ASTM Standards*," Section 4, Construction, Vol. 4.08 Soil and Rock, American Society of Testing and Materials, West Conshohocken, PA.

ASTM D 1556 (2000), "Standard Test Method for Density and Unit Weight of Soil in Place by the Sand-Cone Method," *Annual Book of ASTM Standards*," Section 4, Construction, Vol. 4.08 Soil and Rock, American Society of Testing and Materials, West Conshohocken, PA.

ASTM D 2167 (1994), "Standard Test Method for Density and Unit Weight of Soil in Place by the Rubber Balloon Method," *Annual Book of ASTM Standards*," Section 4, Construction, Vol. 4.08 Soil and Rock, American Society of Testing and Materials, West Conshohocken, PA.

ASTM D 2922 (2001), "Standard Test Methods for Density of Soil and Soil-Aggregate in Place by Nuclear Methods (Shallow Depth)," *Annual Book of ASTM Standards*, Section 4, Construction, Vol. 4.08 Soil and Rock, American Society of Testing and Materials, West Conshohocken, PA.

ASTM D 2950 (2001) "Standard Test Methods for Density of Bituminous Concrete in Place by Nuclear Methods," *Annual Book of ASTM Standards,* Section 4, Construction, Vol. 4.08 Soil and Rock, American Society of Testing and Materials, West Conshohocken, PA.

ASTM D 3080 (2004), "Standard Test Method for Direct Shear Test of Soils Under Consolidated Drained Conditions," *Annual Book of ASTM Standards*, Section 4, Construction, Vol. 4.08 Soil and Rock, American Society of Testing and Materials, West Conshohocken, PA.

ASTM D 4318 (2005), "Standard Test Methods for Liquid Limit, Plastic Limit, and Plasticity Index of Soils," *Annual Book of ASTM Standards*, Section 4, Construction, Vol. 4.08 Soil and Rock, American Society of Testing and Materials, West Conshohocken, PA.

ASTM D 4767 (2004), "Standard Test Method for Consolidated Undrained Triaxial Compression Test for Cohesive Soils", *Annual Book of ASTM Standards*, Section 4, Construction, Vol. 4.08 Soil and Rock, American Society of Testing and Materials, West Conshohocken, PA.

ASTM D 4972 (2001), "Standard Test Method for pH of Soils," *Annual Book of ASTM Standards*, Section 4, Construction, Vol. 4.08 Soil and Rock, American Society of Testing and Materials, West Conshohocken, PA.

ASTM D 5030 (2001), "Standard Test Methods for Density of Soil and Rock in Place by the Water Replacement Method in a Test Pit," *Annual Book of ASTM Standards*, Section 4, Construction, Vol. 4.08 Soil and Rock, American Society of Testing and Materials, West Conshohocken, PA.

ASTM D 5084 (2001), "Standard Test Method for Measurement of Hydraulic Conductivity of Saturated Porous Materials Using a Flexible Wall Permeameter," *Annual Book of ASTM Standards*," Section 4, Construction, Vol. 4.08 Soil and Rock, American Society of Testing and Materials, West Conshohocken, PA.

ASTM D 5333 (2001) "Standard Test Method for Measurement of Collapse Potential of Soils," *Annual Book of ASTM Standards*," Section 4, Construction, Vol. 4.08 Soil and Rock, American Society of Testing and Materials, West Conshohocken, PA.

Augustesen, A., Liingaard, M., and Lade, P. V. (2004), "Evaluation of time-dependent behavior of soils," *International Journal of Geomechanics*, Vol. 4, Issue 3, pp. 137-156.

Ayoub, N. F. (1983), "Evaluation of Long Term Behavior of Cold-recycled Asphalt Pavement Using the Creep Test," M.S. Thesis, *The State University of New York at Buffalo*, 79 pp.

Barksdale, R. D., Itani, S. Y., and Swor, T. E. (1992), "Evaluation of recycled concrete, opened-graded aggregate, and large top-size aggregate bases," *Transportation Research Record*, Vol. 1345, Transportation Research Board, National Research Council, Washington, D.C., pp.92-105.

Black, D. K. and Lee, K. L. (1973), "Saturating Laboratory Samples by Back Pressure," *Journal of Soil Mechanics and Foundations Division*, ASCE, Vol. 99, No. SM1, pp. 75-93.

Black, K. N. (1995), "The Nuclear Asphalst Content Gauge," *Public Roads*, Winter, Vol. 58, No. 3, pp. 8-13.

British Standard 1377 (1990), "Methods of Test for Soils for Civil Engineering Purposes," as a standard laboratory compaction test, *BSI British Standards*, London, United Kingdom.

Bruinsma, J. E., Peterson, K. R., and Snyder, M. B. (1997), "Chemical Approach to Formation of Calcite Precipitate from Recycled Concrete Aggregate Base Layers," *Transportation Research Record*, No. 1577, pp. 10-17.

Bruinsma, J. E. and Snyder, M. B. (1995), "Measurement and Mitigation of Precipitate from Crushed Concrete Base Material," Final Report, *Michigan Concrete Paving Association*, Lansing.

Buck, A. D. (1973), "Recycled concrete," *Highway Research Record*, Issue 430, Highway Research Board, pp.1-8.

Burati, J. L., and Elzoghbi, G. B. (1987), "Correlation of Nuclear Density Results with Core Densities," *Transportation Research Record*, Vol. 1126, Transportation Research Board, National Research Council, Washington, D.C., pp. 53-67.

Campanella, R. G. and Vaid, Y. P. (1974), "Triaxial and plane strain creep rupture of an undisturbed clay," *Canadian Geotechnical Journal*, 11(1), pp. 1-10.

Casagrande, A. (1936), "The Determination of the Pre-Consolidation Load and Its Practical Significance," Discussion D-34, *Proceedings of the First International Conference on Soil Mechanics and Foundation Engineering*, Cambridge, Vol. III, pp. 60-64.

Casagrande, A. and Fadum, R. E. (1940), "Notes on soil testing for engineering purposes," *Harvard Univ. Grad. School of Engineering Publ. 268*, 74 pp.

Christensen, R. W. and Wu, T. H. (1964), "Analysis of Clay Deformation as a Rate Process," *Journal of the Soil Mechanics and Foundations Division*, ASCE, Proc. Paper, pp. 125-157.

Clescerl, L. S., Greenberg, A. E., and Eaton, A. D. (1999), "Standard Methods for the Examination of Water and Wastewater," 20th Edition, *American Public Health Association*, Washington, D.C., 1325 pp.

Cosentino, P. J. and Kalajian, E. H. (2001), "Developing Specifications for Using Recycled Asphalt Pavement as Base, Subbase or General Fill Materials," Final Report, *Florida Department of Transportation*, Gainesville, Florida, 277 pp.

Cuttell, G. D., Snyder, M. B., Vandenbossche, J. M., and Wade, M. J. (1997), "Performance of rigid pavements containing recycled concrete aggregates," *Transportation Research Record*, Vol. 1574, Transportation Research Board, National Research Council, Washington, D.C., pp. 89-98.

Eighmy, T. T. and Magee, B. J. (2001), "The Road to Reuse," *Civil Engineering*, American Society of Civil Engineers, Reston, VA, Vol. 71, No. 9, pp. 66-71.

Elias, V. and Christopher, B. R. (1996), "Mechanically stabilized earth walls and reinforced soil slopes design and construction guidelines," *FHWA Demonstration Project 82*, Report No. FHWA SA-96-071, Federal Highway Administration, Washington, D.C., 371 pp.

Elias, V., Christopher B. R., and Berg, R. R. (2001), "FHWA construction guidelines: Mechanically Stabilized Earth Walls and Reinforced Soil Slopes Design and Construction Guidelines," Report No. FHWA-NHI-00-043, *Federal Highway Administration*, 394 pp.

Esfeller, M. (2006), "Electrochemical Assessment and Service-life Prediction of Mechanically Stabilized Earth Walls Backfilled with Crushed Concrete and Recycled Asphalt Pavement," M.S. Thesis, *Texas A&M University*.

Estakhri, C. K. and Button, J. W. (1992), "Routine Maintenance Uses for Milled Reclaimed Asphalt Pavement (RAP)," TTI Report 1272-1, *Texas Transportation Institute*, College Station, Texas.

Eyring, H. (1936), "Viscosity, plasticity, and diffusion as examples of absolute reaction rates," *Journal of Chemical Physics*, Vol. 4, No. 4, pp. 283-291.

Febres-Cordero, E. and Mesri, G. (1974), "Influence of Testing Conditions on Creep Behavior of Clay," *Report No. FRA-ORD&D-75-29*, Department of Transportation, Washington, D.C., 232 pp.

Feda, J. (1992), "Creep of Soils and Related Phenomena," *Elsevier Science Publishing Company*, Inc., New York, 422 pp.

Feldmann, R. M. (1981), "Tufa Precipitation and Its Effect on Drainage of Highways," *Ohio Department of Transportation*, Federal Highway Administration, Report No. FHWA/OH-81/010, 147 pp.

Federal Highway Administration (FHWA) (2000), "User guidelines: Reclaimed asphalt pavement, reclaimed concrete material," http://www.tfhrc.gov//////hnr20/recycle/waste/, accessed October 1, 2000.

Federal Highway Administration (FHWA) (2004), "Transportation Applications of Recycled Concrete Aggregate," *FHWA State of the Practice National Review*, September, 2004, Washington, DC, 47 pp.

Finnie I. and Heller W.R. (1959), "Creep of Engineering Materials," McGraw-Hill Book Co. Inc., New York.

Ford, G. R. (1987), "Geotextile/Crushed Concrete Study – Preliminary Summary," *Minnesota Department of Transportation,* Maplewood, M.N.

Glasstone, S., Laidler, K., and Eyring, H. (1941), "The Theory of Rate Process," McGraw Hill Book Co., Inc., New York.

Guilloux, A., Schlosser, F., and Long, N. T. (1979), "Etude du frottement sable – armature en laboratoire," *Proc. Int. Conf. Soil Reinforcement*, Paris, Vol. 1, pp. 35-40.

Gupta, J. D., Kneller, W.A., Tamirisa, R., and Skrzypczak-Jankun, E. (1994), "Characterization of Base and Subbase Iron and Steel Slag Aggregates Causing Deposition of Calcareous Tufa in Drains," *Transportation Research Record,* No. 1434.

Halm, H. J. (1980), "Concrete recycling," *Transportation Research News*, Issue 89, Transportation Research Board, National Research Council, Washington, D.C, pp.6-10.

Herrin, M. and Jones, G. (1963), "Behavior of Bituminous Materials from the Viewpoint of Absolute Rate Theory," *Proceedings of the Association of Asphalt Paving Technologists*, Vol. 32, pp. 82-105.

Houston, W. N., Mahmoud, H. H., and Houston, S. L. (1993), "A Laboratory Procedure for Partial-Wetting Collapse Determination," *Geotechnical Special Publication No. 39*, ASCE, pp. 54-63.

Hsieh, T. W. (2003), "Hydraulic Conductivity of Recycled Asphalt Pavement and Crushed Concrete," Master's Report, *The University of Texas at Austin*, 62 pp.

Hurd, J. O. (1988), "Effect of Slag Type on Tufa Precipitate Formation," *Transportation Research Record*, No. 1192, pp. 79-84.

Jain, A. (2004), "Evaluation of Pullout Capacity of Ribbed Metallic Strip Reinforcement in Crushed Concrete and Recycled Asphalt," M.S. Thesis, *Univ. of Texas at Austin.*

Jones, C. J. F. P. (1984), "Earth Reinforcement and Soil Structures," *Butterworth and Co. Ltd.*, 183 pp.

Kennedy, T. W. and Perez, I. (1977), "Preliminary mixture design procedure for recycled asphalt materials," *Recycling of Bituminous Pavements*, ASTM Special Technical Pub. No. 662, pp. 47-67.

Kennedy, T. W., Tahmoressi, M., and Solaimanian, M. (1989), "Evaluation of a Thin-Lift Nuclear Gauge," *Transportation Research Record*, Vol. 1217, Transportation Research Board, National Research Council, Washington, D.C., pp. 9-19.

Kuhn, M. R. and Mitchell, J. K. (1993), "New Perspectives on Soil Creep," *Journal of Geotechnical Engineering*, ASCE, Vol. 119, No. 3, pp. 507-524.

Lambe, T. W. and Whitman, R. V. (1979), "Soil Mechanics," John Wiley & Sons, New York, NY.

Lawton, E. C., Fragaszy, R. J., and Hetherington, M. D. (1992), "Review of Wetting-Induced Collapse in Compacted Soil," *Journal of Geotechnical Engineering*, Vol. 118, No. 9, pp. 1376-1394.

Lutenegger, A. J. and Saber, R. T. (1988), "Determination of Collapse Potential of Soils," *Geotechnical Testing Journal*, American Society of Testing and Materials, Vol. 11, No. 3, pp. 173-178.

Mack, J. W., Solberg, C. E., and Voigt, G. F. (1993), "Recycling concrete pavements," *Concrete Construction*, Vol. 38, No. 7, p.470-473.

Maher, M. H., Gucunski, N., and Papp, W. J., Jr. (1997), "Recycled asphalt pavement as a base and sub-base material," Testing Soil Mixed with Waste or Recycled Materials, ASTM Special Technical Publication No. 1275, pp. 42-53.

Malhotra, V. M. (1978), "Recycled concrete-a new aggregate," *Canadian Journal of Civil Engineering*, Vol. 5, No. 1, pp. 42-52.

Mamlouk, M. S. (1988), "Nuclear Density Testing of Granular Materials: State of the Art," Research Report No. FHWA-AZ88-839, *Federal Highway Administration*, 62 pp.

Marx, E. (2001), "Influence of Compaction Conditions on the Settlement Due to Wetting of Fine Uniform Sands," M.S. Thesis, *The University of Texas at Austin*, 126 pp.

Mesri, G., Febres-Cordero, E., Shields, D.R., and Castro, A. (1981), "Shear Stress-Strain-Time Behavior of Clays," *Geotechnique*, Vol. 31, No. 4, pp. 537-552.

Mitchell, J. K. (1964), "Shearing Resistance of Soils as a Rate Process," *Journal of the Soil Mechanics and Foundations Division*, ASCE, Vol. 90, No. SM1, pp. 29-61.

Mitchell, J. K., Campanella, R. G., and Singh, A. (1968), "Soil Creep as a Rate Process," *Journal of Soil Mechanics and Foundations Division*, ASCE, Vol. 94, No. SM1, pp. 231-253.

Mitchell, J. K. (1993), "Fundamentals of Soil Behavior," *John Wiley and Sons*, New York.

Monkman, F. C. and Grant, N. J. (1956), "An Empirical Relationship between Rupture Life and Minimum creep rate in creep-rupture Tests," *Proc. Amer. Soc. Test. Material*, Philadelphia, PA., Vol. 56, pp. 593-620.

Morris, D. V. and Delphia, J. G. (1999), "Specifications for Backfill of Reinforced-Earth Retaining Walls," FHWA/TX-99/1431-S, *Texas Transportation Institute*, 189 pp.

Muethel, R. W. (1989), "Calcium Carbonate Precipitate from Crushed Concrete," Research report R-1297, *Michigan Department of Transportation*, Materials and Technology Division, Lansing, 19 pp.

Murayama, S. and Shibata, T. (1958), "On the Rheological Characters of Clay," Part 1, Bulletin of Disaster Prevention Research Inst., *Kyoto University*, No. 26.

Murayama, S. and Shibata, T. (1961), "Rheological Properties of Clays," *Proc., 5th Int. Conf. on Soil Mechanics and Foundation Engineering*, Vol. 1, pp. 269–274.

Murayama, S. and Shibata, T. (1964), "Flow and Stress Relaxation of Clays," *Proc., IUTAM Symposium on Rheology and Soil Mechanics*, Grenoble, Springer Verlag, pp. 99-129.

Nagi, M. and Whiting, D. (1999), "Evaluation of Precision of a Nuclear Gauge for Measurement of Water and Cement Content of Fresh Concrete," *Cement, Concrete, and Aggregates*, CCAGDP, Vol. 21, No. 1, June 1999, pp. 1-11.

Najjar, S. S. and Rauch, A. F. (2003), "Data Report: Standard Laboratory Test Soils," Department of Civil Engineering, *The University of Texas at Austin*.

Nicholson, P. G., Russell, P. W., and Fujii, C. F. (1996), " Soil Creep and Creep Testing of Highly Weathered Tropical Soils," *Geotechnical Special Publication*, No. 61, Measuring and Modeling Time Dependent Soil Behavior, pp. 195-213.

Ogolla, M. A. (2002), "Durability of Recycled Crushed Concrete and Recycled Asphalt Pavements in Mechanically Stabilized Earth Retaining Walls," Master's Thesis, *The University of Texas at Austin*, 130 pp.

O'Mahony, M. M. (1997), "An Analysis of the Shear Strength of Recycled Aggregates," *Material and Structures,* Vol. 30, pp. 599-606.

O'Mahony, M. M., and Milligan, G. W. E. (1991), "Use of recycled materials in subbase layers," *Transportation Research Record*, Vol. 1310, Transportation Research Board, National Research Council, Washington, D.C., pp. 73-80.

Palossy, L., Scharle, P., and Szalatkay, I. (1993), "Earth Walls," Ellis Horwood, West Sussex, England, 246 pp.

Pao, Y. H. and Marin, J. (1952), "Prediction of Creep Curves from Stress-Strain Data," *Proc. Amer. Soc. Test. Material*, Philadelphia, PA, Vol. 52, pp. 51-57.

Petrarca, R. W. and Galdiero, V. A. (1984), "Summary of testing of recycled crushed concrete." *Transportation Research Record*, Vol. 989, Transportation Research Board, National Research Council, Washington, D.C, pp.19-26.

Polivka, M. and Best, C. (1960), "Investigation of the problem of creep in concrete by Dorn's method," *University of California*, Department of Civil Engineering.

Popova, S. N., Popov, B. N., White, R. E., Petrou, M. F., and Morris, D. (1998), "Corrosion effects of stabilized backfill on steel reinforcement," *ACI Structural Journal*, Vol. 95, No. 5, pp. 570-577.

Rashwan, S., and Abourizk, S. (1997), "The properties of recycled concrete," *Concrete International*, Vol. 19, pp.56-60.

Rathje, E. M., Rauch, A. F., Folliard, K. F., Viyanant, C., Ogolla, M, Trejo, D., Little, D., and Esfeller, M. (2001), "Recycled Asphalt Pavement and Crushed Concrete Backfill: State-of-the-Art Review and Material Characterization," Research Report No. FHWA/TX-0-4177-1, *Center for Transportation Research*, Austin, TX, 116 pp.

Regimand, A. and Gilbert, A. B. (1999), "Apparatus and Method for Field Calibration of Nuclear Surface Density Gauges," *Field Instrumentation for Soil and Rock*, ASTM STP 1358, G.N. Durham and W.A. Marr, Eds., American Society for Testing and Materials, West Conshohocken, PA, pp. 135-147.

Ripple, C. D. and Day, P. R. (1966), "Suction responses due to shear of dilute montmorillonite-water pastes, *Clays and Clay Minerals*, Vol. 14, pp. 307-316.

Rubeler, R. C. (1989), "Soil corrosion evaluation of screw anchors," Effects of Soil Characteristics on Corrosion, *ASTM Special Technical Pub. No. 1013*, V. Chaker and J.D. Palmer, Eds., American Society for Testing and Materials.

Saeed, A., Hudson, W. R., and Anaejionu, P. (1995), "Location and availability of waste and recycled materials in Texas and evaluation of their utilization potential in roadbase," Research Report 1348-1, *Center for Transportation Research*, The University of Texas at Austin, 40 pp.

Saeed, A. and Hudson, W. R. (1996), "Evaluation and the use of waste and reclaimed materials in roadbase construction," Research Report 1348-2F, *Center for Transportation Research*, The University of Texas at Austin, 189 pp.

Saito, M. and Uezawa, H. (1961), "Failure of Soil Due to Creep," *Proc. 5th ICSMFE*, Paris, Vol. 1, pp. 315-318.

Sanders, S. R., Rath, D., and Parker Jr., F. (1994), "Comparison of Nuclear and Core Pavement Density Measurements," *Journal of Transportation Engineering*, Vol. 120, Issue 6, pp. 953-966.

Sawicki, A. (1999), "Creep of geosynthetic reinforced soil retaining walls," *Geotextiles and Geomembranes*, Vol. 17, pp.51-65.

Schlosser, F. and Delage, P. (1988), "The application of polymeric reinforcement in soil retaining structures," NATO ASI Series, *Applied Sciences*, Vol. 147, pp. 3-65.

Schlosser, F. (1990), "Mechanically Stabilized Earth Retaining Structures in Europe," *Geotechnical Special Publication*, No. 25, pp. 347-378.

Senior, S. A., Szoke, S. I., and Rogers, C. A. (1994), "Ontario's experience with reclaimed materials for use in aggregates," *International Road Federation Conference*, Calgary, Alberta.

Singh, A. and Mitchell, J.K. (1968), "General stress-strain-time function for soils," *Journal of Soil Mechanics and Foundations Division*, Proceedings of the ASCE, Vol. 94, No. SM1, pp. 21-46.

Singh, A. and Mitchell, J.K. (1969), "Creep Potential and Creep Rupture of Soils," *Proceedings of the 7th International Conference on Soil Mechanics and Foundation Engineering*, Vol. 1, pp. 379-384.

Snead, D. E. (1970), "Creep Rupture of Saturated Undisturbed Clays," Ph.D. thesis, *University of British Columbia*, Vancouver, British Columbia.

Snoeyink, V. L. and Jenkins, D. (1980), "Water Chemistry," John Wiley & Sons, Inc., New York, 463 pp.

Snyder M. B. (1995), "Use of Crushed Concrete Products in Minnesota Pavement Foundations," Report No. MN/RC-96/12, *Minnesota Department of Transportation*, St. Paul, M.N., 52 pp.

Snyder M. B. and Bruinsma, J. E. (1996), "Review of Studies Concerning Effects of Unbound Crushed Concrete Bases on PCC Pavement Drainage," *Transportation Research Record*, No. 1519, pp. 51-58.

Tamirisa, R. (1993), "Study of Highway Base/Subbase Aggregates That Cause Depositions of Calcareous "Tufa" in Drains," M.S. thesis, *University of Toledo*, Ohio.

Texas Department of Transportation (TxDOT) (1999). "Year of the recycled roadway materials - January: Crushed concrete." http://www.dot.state.tx.us/insdtdot/orgchart/gsd/recycle/mat.htm, accessed October 1, 2000, 17 pp.

Troxler Electronics, Inc. (2001), "Manual of Operation and Instruction: Model 3440 Surface Moisture-Density Gauge," *Troxler Laboratories*, Research Triangle Park, North Carolina, 220 pp.

Vaid, Y. P. and Campanella, R. G. (1977), "Time-Dependent Behavior of Undisturbed Clay," *Journal of the Geotechnical Engineering Division*, ASCE, Vol. 103, No. 7, pp. 693-709.

Vita

Born on May 22, 1975, in Bangkok, Thailand, Chirayus Viyanant is a son of Prof. Dr. Vithoon Viyanant and Assoc. Prof. Jaruporn Viyanant. After completion of his study at St. Gabriel's College, Bangkok, in 1993, he began his university education at Kasetsart University, Bangkok, where he was conferred the degree of Bachelor of Engineering in 1997. He began his graduate study in January 1998 at The University of Texas at Arlington where he received the Master degree of Science in 2000. Following his Master's degree completion, he was subsequently admitted to the Graduate School of The University of Texas at Austin where he commenced his Ph.D. study in Geotechnical Engineering in August 2000. He is currently a doctoral candidate at The University of Texas at Austin, and also is a geotechnical engineer at Bechtel Corporation. After six years of study and research, he will be awarded in summer 2006 with the degree of Doctor of Philosophy with a major in Civil Engineering.

Permanent address: 109 Soi Charansanitwong 71
Bangplad, Bangkok 10700
THAILAND

This dissertation was typed by the author.